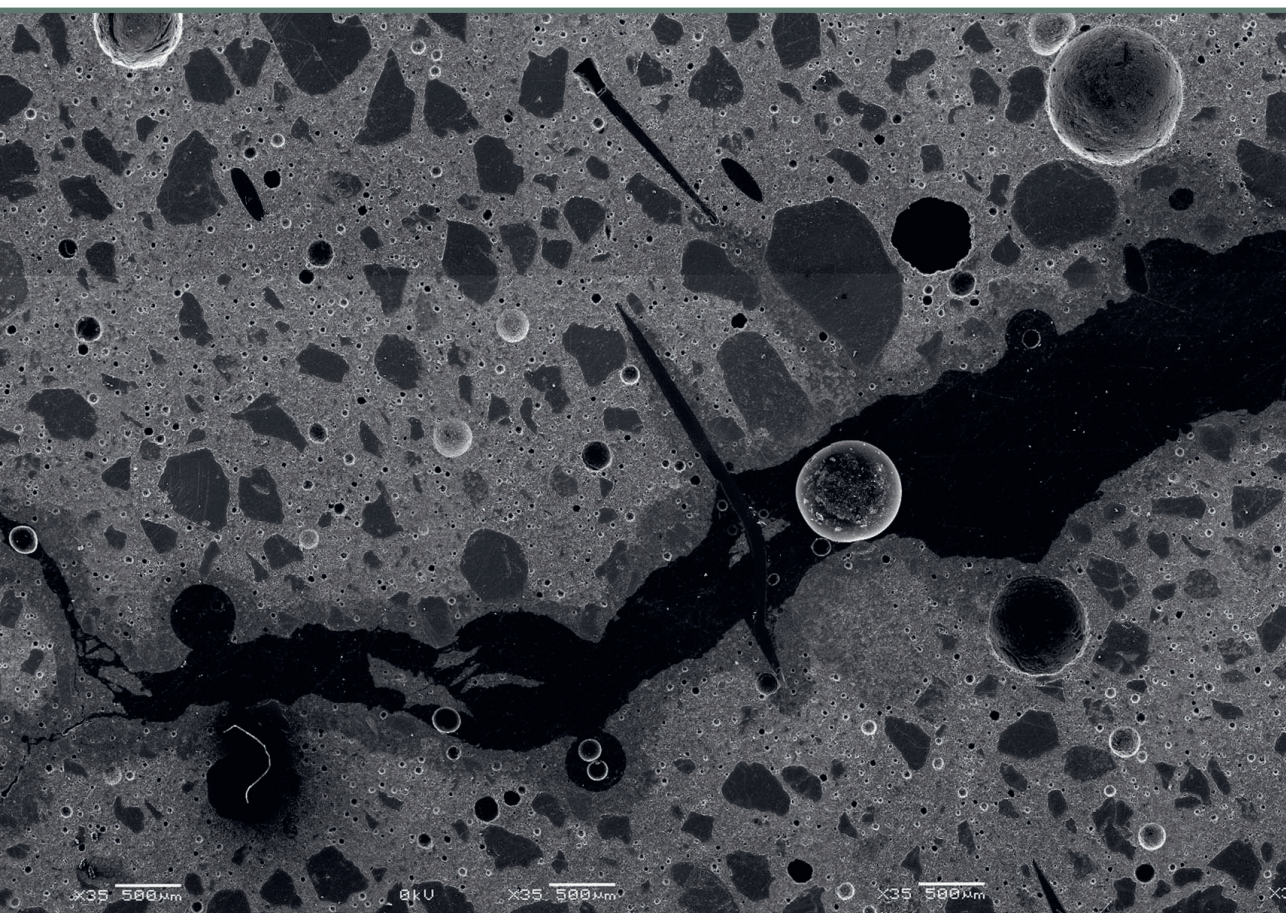


Rihards Gailītis

**METHODOLOGY FOR ASSESSING LONG-TERM
DEFORMATION INFLUENCE ON GEOPOLYMER
COMPOSITE MICROSTRUCTURE**

Doctoral Thesis



RIGA TECHNICAL UNIVERSITY

Faculty of Civil Engineering
Institute of Structural Engineering

Rihards Gailītis

Doctoral Student of the Study Programme “Civil Engineering”

**METHODOLOGY FOR ASSESSING LONG-
TERM DEFORMATION INFLUENCE ON
GEOPOLYMER COMPOSITE
MICROSTRUCTURE**

Doctoral Thesis

Scientific supervisors

Associate Professor Dr. sc. ing.

ANDĪNA SPRINCE

Professor Dr. sc. ing.

LEONĪDS PAKRASTIŅŠ

RTU Press

Riga 2023

Gailītis, R. Methodology for Assessing Long-Term Deformation Influence on Geopolymer Composite Microstructure. Doctoral Thesis. Riga: RTU Press, 2023. 168 p.

Published in accordance with the decision of the Promotion Council “RTU P-06” of 16th of June 2023, Minutes No. 04030–9.6.2/5.

DOCTORAL THESIS PROPOSED TO RIGA TECHNICAL UNIVERSITY FOR THE PROMOTION TO THE SCIENTIFIC DEGREE OF DOCTOR OF SCIENCE

To be granted the scientific degree of Doctor of Science (Ph. D.), the present Doctoral Thesis has been submitted for the defence at the open meeting of RTU Promotion Council on 10th of November 2023 at 14.15 at the Faculty of Civil Engineering of Riga Technical University, Ķīpsalas 6a, Room 342.

OFFICIAL REVIEWERS

Senior Researcher Dr. sc. ing. Sandris Ručevskis,
Riga Technical University

Associate Professor Ph. D. Barbara Kucharczykova,
Brno University of Technology, Czech Republic

Associate Professor Dr. habil. sc. ing. Marek Hebda,
Cracow University of Technology, Poland

DECLARATION OF ACADEMIC INTEGRITY

I hereby declare that the Doctoral Thesis submitted for review to Riga Technical University for promotion to the scientific degree of Doctor of Science (Ph. D.) is my own. I confirm that this Doctoral Thesis has not been submitted to any other university for promotion to a scientific degree.

Rihards Gailītis (signature)

Date:

The Doctoral Thesis has been written in English as a summary of scientific publications. It consists of a summary and nine scientific publications. Seven of the publications are in English, and their total length is 65 pages. Two of the publications are Latvian national patents and are in Latvian, and their total length is 34 pages. The Bibliography contains 185 titles.

Acknowledgement

This Doctoral Thesis was written from 2018 till 2023 at the Institute of Structural Engineering of Faculty of Civil Engineering of Riga Technical University.

I would like to thank the personnel of the departments of the Faculty of Civil Engineering of Riga Technical University – the Department of Structural Engineering, Department of Building Materials and Products, Department of Structural Mechanics, Department of Composite Materials and Structures – as well as the employees of the Faculty of Material Engineering and Physics of the Cracow University of Technology.

Huge thanks to Thesis supervisors Dr. sc. ing. Andīna Sprince and Dr. sc. ing. Leonīds Pakraстиņš for supporting and encouraging me in the field of science. Also, big thanks to Dr. ing. Kinga Korniejenko, who initiated my research interest in the field of geopolymers and to B. sc. ing. Tomass Kozlovskis who has been of great support in the test preparation and issue resolvment. Furthermore, my gratitude goes to Dr. sc. ing. Līga Gaile, Ph. D. Līva Pupure, Dr. sc. ing. Gita Šakale, Ph. D. Atis Degro, Dr. sc. ing. Andrejs Pupurs, and M. sc. ing. Laura Vītola, who have always given advice, criticism, and knowledge in the field of science. Undoubtedly huge thanks to all of my bachelor's and master's students.

Big thanks to my family – to Patrīcija, mom Agnese, dad Arturs and sister Dace, who had to bear with my unsatisfactory behaviour due to unpleasing results in the Thesis development. Also, huge thanks to my grandpa Kārlis, who has been my greatest opponent and has been questioning my every move in the field of science, therefore motivating me to prove myself and never stop the development.

The Thesis research has been supported by:

- Riga Technical University's Doctoral Grant programme (DOK.BIF/19, DOK.BIF/20, DOK.BIF/21).
- The Latvian Council of Science grant to the scientific project "Long-term deformations of innovative cement composite materials under different stress states" No. lzp-2018/2-0249.
- The European Social Fund project No. 8.2.2.0/20/I/008 "Strengthening of PhD students and academic staff of Riga Technical University and Banking Graduate School in areas of strategic specialization".



NACIONĀLAIS
ATTĪSTĪBAS
PLĀNS 2020



EIROPAS SAVIENĪBA
Eiropas Sociālais
fonds

IEGULDĪJUMS TAVĀ NĀKOTNĒ

TABLE OF CONTENTS

Abbreviations	7
General description of the thesis	8
The aim of the work	8
Tasks.....	8
Scientific novelty.....	8
Practical novelty	8
Structure of the Thesis.....	9
Approbation and publications	9
List of papers.....	9
National patents.....	11
Results of the research were presented at the following conferences.....	11
Declaration of the authorship for the papers	12
Thesis to defend	16
1. Introduction	17
2. Geopolymer composites	20
2.1. Constituents.....	21
2.1.1. Aluminosilicates.....	21
2.1.1.1. Fly ash.....	21
2.1.2. Reinforcement	22
2.1.2.1. Steel fibers.....	25
2.1.2.2. Inorganic fibers	25
2.1.2.3. Carbon fibers.....	25
2.1.2.4. Polymeric fibers	26
2.1.2.5. Natural fibers.....	26
2.2. Geopolymer composite properties	26
2.2.1. Mechanical properties	26
2.2.2. Geopolymer composite durability.....	30
2.2.3. Geopolymer composite's thermal endurance.....	31
2.2.4. Time dependent properties of geopolymer composite	31
2.2.4.1. Creep properties	31
2.2.4.2. Shrinkage properties	35

3. Geopolymer microstructure.....	37
3.1. Characteristics and processes of alkali-activating reaction.....	37
3.2. Pore structure of the fly ash-based geopolymer.....	37
3.3. Geopolymer and OPC composite microstructure differences.....	39
3.4. Microstructure development of geopolymer composite incorporating lime and silica	40
4. Geopolymer composite application in civil engineering.....	41
4.1. Geopolymer application in soil stabilization.....	41
4.2. Geopolymer application in buildings and infrastructure.....	41
4.3. Geopolymer application as mortars	43
4.4. Geopolymer application as fire resistant layer.....	43
4.5. Geopolymer application as insulating layer.....	44
5. Geopolymer composite long-term environmental influence.....	45
5.1. Environmental assessment of geopolymer long-term impact on the environment based on life cycle assessment	45
Conclusions	48
References	50
Annex / publications.....	59
Annex I: Article I:	60
Annex II: Article II:.....	70
Annex III: Article III:	79
Annex IV: Article IV:	88
Annex V: Article V:	97
Annex VI: Article VI:	110
Annex VII: Article VII:	117
Annex VIII: Patent I:.....	132
Annex IX: Patent II:	151

ABBREVIATIONS

ADPF – abiotic depletion of fossil fuels
BA – bottom ash
BFA – biomass fly ash
Ca(OH)₂ – calcium hydroxide
CAC – calcium aluminate cement
CaCO₃ – calcium carbonate
CT – curing time
EFC – Earth Friendly Concrete
FA – fly ash
FS – ferrochrome slag
GBFS – granulated blast furnace slag
GGBFS – ground granulated blast furnace slag
GLSS – granulated lead smelter slag
GP – geopolymer
GPC – geopolymer concrete
IOT – iron ore tailing
KHFA – ultra-fine kaolite high-performance ash
KL – kaolin
LS – limestone
LWA – lightweight aggregate
M – molarity
MK – metakaolin
NaCl – sodium chloride
NaOH – sodium hydroxide
NS – Nano-silica
OPC – Ordinary Portland cement
PAN – polyacrylonitrile
PE – polyethylene
PET – polyethylene terephthalate
PCFA – powder coal fly ash
POFA – palm oil fuel ash
PP – polypropylene
PVA – polyvinyl alcohol
RHA – rice husk ash
SD –sawdust
SEM – scanning electron microscope
SF – silica fume
SiO₂/Al₂O₃ – silicon dioxide / aluminium oxide
SMF – silico-manganese fume
SSD – saturated surface dry

GENERAL DESCRIPTION OF THE THESIS

The aim of the work

1. Evaluate mechanical and long-term properties of geopolymer composite reinforced with different fibers in compression, tension and three-point bending.
2. Determine fiber reinforced geopolymer composite long-term deformation influence on microstructure in compression, tension and three-point bending.

Tasks

1. Develop geopolymer composites that have their properties enhanced by:
 - a) polyvinyl alcohol fibers;
 - b) steel fibers;
 - c) polypropylene fibers;
 - d) carbon fibers;
 - e) waste steel fibers from car tire recycling.
2. Determine the developed composites' properties:
 - a) compressive, tensile and bending strength;
 - b) creep and drying shrinkage.
3. Develop a method for the long-term load application effect assessment on cement composites in various stress-strain states.
4. Determine possible links between the specimen cross-section microstructure composition and the long-term deformations.

Scientific novelty

1. A new methodology has been developed and patented for long-term property determination in compression, tension and three-point bending for concrete and cement composites.
2. Patent application The Technique for Outside Effect Determination on Concrete and Cement Composite Microstructure in Various Stress-Strain States has been developed and filed.
3. The effect of fiber reinforcement effect on geopolymer composite mechanical and long-term properties has been tested and analysed.
4. Long-term load effect on geopolymer composite microstructure in compression, tension and three-point bending has been assessed.

Practical novelty

1. A new method of long-term property determination in laboratory conditions has been developed for concrete and cement composites that further leads to increased

information about novel concrete and cement composites and their application in civil engineering.

2. A patent was developed and filed for a new technique for outside effect determination on concrete and cement composite microstructure in various stress-strain states by testing polished section specimens in a scanning electron microscope. It allows to increase information regarding long-term load application effect on concrete and cement composite microstructure.
3. Compositions of geopolymer composites have been developed to whom mechanical and long-term properties have been determined and can be used for structure development for application in civil engineering.
4. Increased information is provided on fly ash-based geopolymer composite mechanical and long-term properties and fiber reinforcement influence on their long-term properties, thus increasing application of these composites in civil engineering.

Structure of the Thesis

The Thesis is a summary of scientific publications focused on long-term and mechanical property assessment of plain and fiber reinforced geopolymer composites and the determination of long-term deformation effect on geopolymer composite microstructure.

Approbation and publications

The results of the Thesis have been published in 22 SCI journals and conference proceedings (13 of them are published in conference proceedings and 2 are patents) and have been presented in 15 international conferences.

List of papers

1. **Gailitis, R.**, Pudans, P., Ziemelis, K., Bumanis, G., Sprince, A. Early-Age Creep and Shrinkage Properties of Printed and Cast Cement Composite. (2023). *Materials Proceedings*. 13(1) 35.
2. **Gailitis, R.**, Sprince, A., Kozlovskis, T., Pakrastins, L., Volkova, V. Impact of Polypropylene, Steel, and PVA Fibre Reinforcement on Geopolymer Composite Creep and Shrinkage Deformations. (2023) *Journal of Physics: Conference Series*, 2423 (1).
3. Radina, L., Sprince, A., Borodinecs, A., Pakrastins, L., **Gailitis, R.**, Sakale, G. Foamed Geopolymers: A Review of Recent Studies. (2023) *Journal of Physics: Conference Series*, 2423 (1).
4. **Gailitis, R.**, Pakrastins, L., Sprince, A., Radina, L., Sakale, G., Miernik, K. Different Fiber Reinforcement Effect on Fly Ash Based Geopolymer Long-Term Deflection in Three-Point Bending and Microstructure. (2022) *Materials*, 15 (23).
5. Pupure, L., Varna, J., **Gailitis, R.**, Al-Maqdasi, Z., Pakrastins, L. Development of Methodology for Experimental Parameter Identification for Inelastic 3D Material

- Model (2022) ECCM 2022 – Proceedings of the 20th European Conference on Composite Materials: Composites Meet Sustainability, 6, pp. 282–289.
6. **Gailitis, R.**, Figiela, B., Abelkalns, K., Sprince, A., Sahmenko, G., Choinska, M., Guigou, M. D. Creep and shrinkage behaviour of disintegrated and non-disintegrated cement mortar. (2021) *Materials*, 14 (24).
 7. Sprince, A., Kozlovskis, T., **Gailitis, R.**, Valivonis, J., Korniejenko, K., Castel, A. Tensile creep of cement and concrete composites: Monitoring by means of 2D-digital image correlation. (2021) *Applied Sciences (Switzerland)*, 11 (18).
 8. Kozub, B., Bazan, P., **Gailitis, R.**, Korniejenko, K., Mierzwiński, D. Foamed geopolymer composites with the addition of glass wool waste. (2021) *Materials*, 14 (17).
 9. **Gailitis, R.**, Sprince, A., Kozlovskis, T., Radina, L., Pakrastins, L., Vatin, N. Long-term properties of different fiber reinforcement effect on fly ash-based geopolymer composite. (2021) *Crystals*, 11 (7).
 10. Sprince, A., **Gailitis, R.**, Pakrastins, L., Kozlovskis, T., Vatin, N. Long-term properties of cement mortar under compression, tension, and 3-point bending. (2021) *Magazine of Civil Engineering*, 105 (5).
 11. **Gailitis, R.**, Sprince, A., Pakrastins, L., Bazan, P., Korniejenko, K. Plain and PVA fibre-reinforced geopolymer compact tension specimen critical area surface composition assessment. (2021) *Vide. Tehnologija. Resursi – Environment, Technology, Resources*, 3, pp. 72–77.
 12. **Gailitis, R.**, Sprince, A., Pakrastins, L., Korniejenko, K., Kozlovskis, T. Plain Geopolymer Concrete Cross-Section Surface Analysis After Creep and Shrinkage Tests in Compression and Tension. (2021) *RILEM Book series*, 31, pp. 13–24.
 13. **Gailitis, R.**, Sprince, A., Pakrastins, L., Korniejenko, K., Kozlovskis, T. Reinforced and Plain Geopolymer Concrete Specimen Cross-section Composition Influence on Creep Strains. (2021) *Proceedings of 4th International RILEM conference on Microstructure Related Durability of Cementitious Composites (Microdurability2020)* (Indexation pending).
 14. **Gailitis, R.**, Korniejenko, K., Sprince, A., Pakrastins, L. Comparison of the long-term properties of foamed concrete and geopolymer concrete in compression. (2020) *AIP Conference Proceedings*, 2239.
 15. **Gailitis, R.**, Sliseris, J., Korniejenko, K., Mikula, J., Łach, M., Pakrastins, L., Sprince, A. Long-Term Deformation Properties of a Carbon-Fiber-Reinforced Alkali-Activated Cement Composite. (2020) *Mechanics of Composite Materials*, 56 (1), pp. 85–92.
 16. Sprince, A., Pakrastins, L., **Gailitis, R.** Long-Term Parameters of New Cement Composites. (2020) *RILEM Book series*, 24, pp. 85–94.
 17. **Gailitis, R.**, Korniejenko, K., Łach, M., Sliseris, J., Morán, J., Rodriguez, E., Mikula, J. Mechanical Properties of Geopolymer Concretes Reinforced with Waste Steel Fibers. (2019) *IOP Conference Series: Materials Science and Engineering*, 660 (1).

18. **Gailitis, R.**, Sprince, A., Pakrastins, L., Sahmenko, G., Kozlovskis, T. Drying Shrinkage Deformation Comparison between Foam Concrete, Geopolymer Concrete, Disintegrated, and Non-disintegrated Cement Mortar. (2019) IOP Conference Series: Materials Science and Engineering, 660 (1).
19. **Gailitis, R.**, Sprince, A., Pakrastins, L., Shakhmenko, G., Kozlovskis, T., Radina, L. Long-Term Properties of Foamed Concrete. (2019) Proceeding of 13th International Conference Modern Building Materials, Structures and Techniques (MBMST 2019) (Indexation pending).
20. **Gailitis, R.**, Sprince, A., Pakrastins, L., Shakhmenko, G., Kozlovskis, T. Comparison of the long-term properties in compression of different size foamed concrete (2019) Vide. Tehnologija. Resursi – Environment. Technology. Resources, 3, pp. 41–44.

National patents

1. Sprince, A., Pakrastins, L., Radina, L., **Gailitis, R.**, Kozlovskis T. Paņēmiens betona un cementa kompozītu ilglaicīgo īpašību noteikšanai dažādos sprieguma stāvokļos/ Method for Determination of Long-Term Properties of Concrete and Cement Composites in Various Stress Conditions/ Latvian patent No. **15659B**.
2. **Gailitis, R.**, Sprince, A., Pakrastins, L. Paņēmiens ārējo iedarbju ietekmes noteikšanai uz betonu un cementa kompozītmateriālu mikrostruktūru dažādos sprieguma stāvokļos/ Technique for Outside Effect Determination on Concrete and Cement Composite Microstructure in Various Stress-Strain States/ Latvian patent application No. **LVP2023000039 (Filed for patent)**.

Results of the research were presented at the following conferences

1. 10th Scientific-Technical Conference on Material Problems in Civil Engineering MatBud'2023, Cracow, Poland, 19–21 April 2023.
2. 5th International Conference on Innovative Materials, Structures and Technologies, IMST 2022, Riga, Latvia, 28–30 September 2022.
3. 2022 Global Conference on Polymers, Plastics and Composites (PPC2022), Budapest, Hungary, March 21–22, 2022.
4. RTU 62. starptautiskā zinātniskā konference apakšsekcija “Būvniecība”, tiešsaiste, 28. oktobris 2021.
5. World Symposium on Mechanical-Materials Engineering & Science (WMMES2021) Prague, Czech Republic, 9–11 September 2021.
6. 13th International Scientific and Practical Conference. Environment. Technology. Resources, online, 17–18 June 2021.
7. The Biot-Bažant Conference on Engineering Mechanics and Physics of Porous Materials (A One-time Fusion of Concreep and the Biot Conference on Poromechanics), online, 1–3 June 2021.
8. 4th International RILEM conference on Microstructure Related Durability of Cementitious Composites (Microdurability2020), online, 29 April – 25 May 2021.
9. International RILEM Conference on Early-age and Long-term Cracking in RC Structures (CRC2021), online, 9–10 April 2021.

10. RTU 61. starptautiskā zinātniskā konference apakšsekcija “Būvniecība”, tiešsaiste, 22. Oktobris, 2020.
11. 1st International Scientific Conference Advanced Construction and Architecture 2020 (ACA2020), online, 23–25 September 2020.
12. 4th International Conference on Innovative Materials, Structures and Technologies, IMST 2019, Riga, Latvia, 25–27 September 2019.
13. 4th Polish Congress of Mechanics, PCM 2019 and the 23rd International Conference on Computer Methods in Mechanics, CMM 2019, Cracow, Poland, 8–12 September 2019.
14. 12th International Scientific and Practical Conference “Environment. Technology. Resources”, RTA, Rezekne, June 20–22, 2019 (Plenary Session).
15. 13th International Conference “Modern Building Materials, Structures and Techniques”, Vilnius, Lithuania, May 16–17, 2019.

Declaration of the authorship for the papers

Rihards Gailitis has conducted a major part of the experimental work, evaluated the results, and written all of the appended papers and Patent II. In general, the co-authors contributed with experiment planning, provision of materials, SEM internship arranging, specific specimen preparation, and constructive criticism/advice on the obtained results and their representation in the publications, which further increased the scientific quality of the publications.

Paper No.	Reference	Corresponding author	R. Gailitis' contribution
Paper I	Gailitis, R. , Korniejenko, K., Łach, M., Sliseris, J., Morán, J., Rodriguez, E., Mikuła, J. Mechanical Properties of Geopolymer Concretes Reinforced with Waste Steel Fibers. (2019) IOP Conference Series: Materials Science and Engineering, 660 (1), art. no. 012007, Open Access, SNIP 0.344.	R. Gailitis	95 % of the mechanical property testing and evaluation, test result formatting and assessment, manuscript preparation.
Paper II	Gailitis, R. , Sliseris, J., Korniejenko, K., Mikuła, J., Łach, M., Pakrastins, L., Sprince, A. Long-Term Deformation Properties of a Carbon-Fiber-Reinforced Alkali-Activated Cement Composite. (2020) Mechanics	R. Gailitis	95 % of specimen preparation for the long-term and mechanical property tests and the tests, result evaluation preparation of the manuscript, and structure of SEM micro analysis.

	of Composite Materials, 56 (1), pp. 85–92, SNIP 0.832.		
Paper III	Gailitis, R. , Sprince, A., Kozlovskis, T., Radina, L., Pakrastins, L., Vatin, N. Long-term Properties of Different Fiber Reinforcement Effect on Fly Ash-based Geopolymer Composite. (2021) Crystals, 11 (7), art. no. 760, Open Access, SNIP 0.821.	R. Gailitis	Preparation of the geopolymer composite specimens, 80 % of the experimental work that includes their adaptation to creep and shrinkage tests, all the mechanical property assessment, creep and shrinkage test result assessments, result formatting, and manuscript preparation and revision.
Paper IV	Gailitis, R. , Sprince, A., Pakrastins, L., Korniejenko, K., Kozlovskis, T. Reinforced and Plain Geopolymer Concrete Specimen Cross-section Composition Influence on Creep Strains. (2021) Proceedings of 4th International RILEM Conference on Microstructure Related Durability of Cementitious Composites (Microdurability2020), Open Access.	R. Gailitis	Specimen preparation, 85 % of the long-term testing, development, and adaptation of microstructure specimen preparation and investigation, and further specimen investigation with SEM and result quantitative analysis, preparation, and presentation of the scientific paper and findings.
Paper V	Gailitis, R. , Sprince, A., Pakrastins, L., Korniejenko, K., Kozlovskis, T. Plain Geopolymer Concrete Cross-Section Surface Analysis After Creep and Shrinkage Tests in Compression and Tension (2021) RILEM Book series, 31, pp. 13–24. SNIP 0.320.	R. Gailitis	The specimen preparation, 65 % of the long-term mechanical property testing, mechanical property assessment and creep and shrinkage test result assessment, the polished section preparation and analysis specifically adapted for the geopolymer composite testing purposes, result formatting, and manuscript preparation and revision.

Paper VI	Gailitis, R. , Sprince, A., Pakrastins, L., Bazan, P., Korniejenko, K. Plain and PVA Fibre-reinforced Geopolymer Compact Tension Specimen Critical Area Surface Composition Assessment. (2021) Vide. Tehnologija. Resursi/ Environment. Technology. Resources, 3, pp. 72–77, Open Access.	R. Gailitis	80 % of the specimen preparation, 80 % of the testing of the long-term properties, 100 % of the microstructure tests, preparation of the manuscript, revision, and presenting in the conference.
Paper VII	Gailitis, R. , Pakrastins, L., Sprince, A., Radina, L., Sakale, G., Miernik, K. Different Fiber Reinforcement Effect on Fly-Ash Based Geopolymer Long-Term Deflection in Three-Point Bending and Microstructure (2022) Materials, 15 (23), Open Access, SNIP 1.137.	R. Gailitis	100 % of the specimen preparation, 60 % of the specimen long-term testing, 100 % of the microstructure specimen preparation and testing, and 100 % of the manuscript preparation and all the revision cycles.
Patent I	Sprince, A., Pakrastins, L., Radina, L., Gailitis, R. , Kozlovskis, T., Paņēmiens betona un cementa kompozītu ilglaicīgo īpašību noteikšanai dažādos sprieguma stāvokļos/ Method for Determination of Long-Term Properties of Concrete and Cement Composites in Various Stress Conditions/ Latvian patent No. 15659B.	A. Sprince	Testing in the laboratory environment for method validation of the developed methods for long-term property determination in compression, tension, and 3-point bending of the cement composites.
Patent II	Gailitis, R. , Sprince, A., Pakrastins, L. Paņēmiens ārējo iedarbju ietekmes noteikšanai uz betonu un cementa kompozītmateriālu mikrostruktūru dažādos sprieguma stāvokļos/	R. Gailitis	R. Gailitis developed the methods for polished section preparation and surface analysis and assessment procedures of specimens that have been subject to long-term testing. Also, methodology

	<p>Technique for Outside Effect Determination on Concrete and Cement Composite Microstructure in Various Stress-Strain States/ Latvian patent application No. LVP2023000039</p>		<p>has been tested, and the results were published in conference proceedings as well as full-text publications. He prepared the patent application together with the RTU patent specialist.</p>
--	---	--	---

Thesis to defend

1. Polypropylene fiber with an amount of 1–5 % and 5 % waste steel cord fiber incorporation into the geopolymer matrix reduces creep in compression, and 1 % steel fiber incorporation reduces creep in three-point bending in contrast to creep exhibited of the plain geopolymer specimens. In the cases of 1 % carbon fiber or 1 % steel fiber incorporation for creep in compression, 1 % PVA fiber incorporation for specimens tested in tension and 0.5 % PVA/0.5 % steel, and 1 % PVA fiber introduction for specimens tested in three-point bending raises creep strains. This is mainly due to the significantly higher specific surface area of polypropylene fibers and bonding properties between the geopolymer matrix and steel fibers.
2. Fiber incorporation into geopolymer composite does reduce shrinkage strains only in the cases of 1–5 % polypropylene fiber, 1 % steel fiber, and 5 % waste steel cord fiber incorporation in compression and 1 % polyvinyl alcohol fiber introduction in tension. By adding 1 % carbon fibers, shrinkage is not reduced significantly. This is because of increased air entrapment due to fiber incorporation and increased micro crack amount in the specimen.
3. Developed and validated new methodology “Method for Determining the Long-Term Properties of Concrete and Cement Composites in Various Stress-strain Conditions” No. 15659B.
4. Developed and validated a new methodology “Technique for Outside Effect Determination on Concrete and Cement Composite Microstructure in Various Stress-Strain States”, No. LVP2023000039.
5. As a result of the creep specimen, tested in a linear state, and shrinkage specimen microstructure analysis, it is determined that in tension, micro cracks have a significant influence on long-term properties. The amount of them in creep and shrinkage specimens is similar. The same results are visible in specimens subjected to three-point bending. For the specimens meant for long-term testing in compression, micro cracks have not been discovered. The amount of micro cracks differs due to the specimen surface area and size differences.

1. INTRODUCTION

Ordinary Portland cement (OPC) is used as a common binder in most of the conventional concrete structures. The buildings and infrastructure made from concrete have been safe and durable. Furthermore, properties and their development for regular OPC-based concrete are well known [1]. This makes the demand for OPC high, and it is expected to rise in the coming years due to rapid urbanization and the high demand for residential units [2]. Annual OPC production in the next 30-year period is expected to increase by 50 % [3], [4]. Despite all the advantages that OPC provides, the biggest drawback is OPC’s energy intensity that further means high CO₂ emissions during the manufacturing process.

Carbon dioxide and other pollutants are the main cause of global warming. In Fig. 1, where CO₂ emissions worldwide are presented, it is visible that the main source of CO₂ emissions from a usage perspective is energy production, which produces twice as much CO₂ than industry. If we compare each country’s contribution to CO₂ emission, we see that the biggest pollutant is China, that emits 1/3 greater amount of CO₂ than the USA and nearly twice as much as EU. The United States Geological Survey (see Fig. 2) shows unbalanced OPC production in the world. The largest producers are based in Eastern Asia [5].

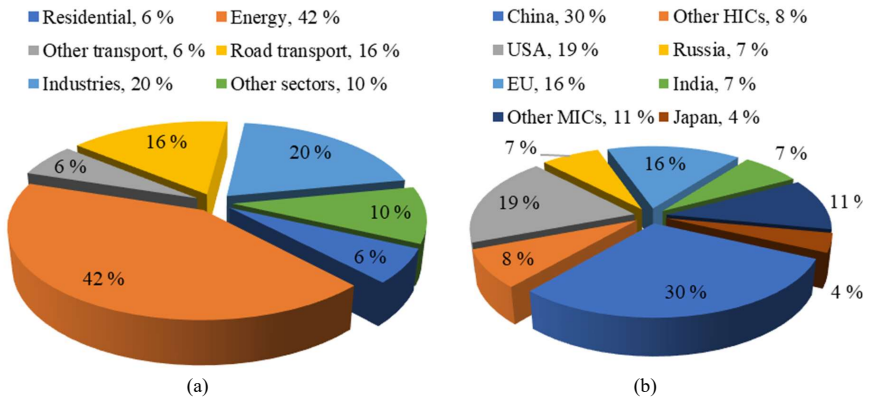


Fig. 1. CO₂ emissions worldwide (a); by sectors (b) by countries [6].

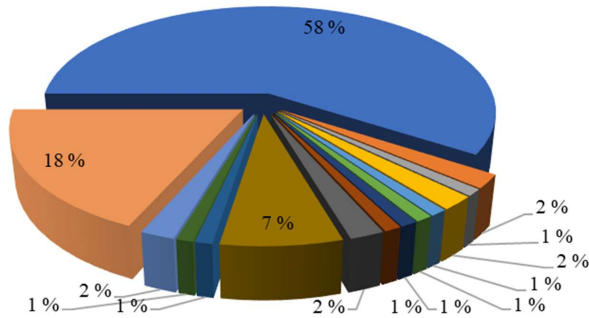


Fig. 2. OPC production around the world [5].

Depending on the source, the cement production contribution to CO₂ emission is reported to be 5–30 %. In [7], it was reported that cement production contributes 5 % of all CO₂ emissions, others estimated that cement clinker production was responsible for 8 % of the world CO₂ emissions in 2017 [8], [9] that dropped to 4 % in 2019 [10]. Others claim that all in all, concrete production is responsible for up to 30 % of all CO₂ emissions [11].

The calcination process and raw material burning are pointed out as the main sources of greenhouse gas emission sources [12], [13]. Emission amounts of CO₂ are alarming, and recent reductions in them are mainly caused by the COVID-19 pandemic and further disruption in worldwide supply chains not by demand reduction or novel material application introduction in the building environment. Therefore, it is a high priority to take measures and drastically reduce CO₂ emissions, taking meaningful actions when choosing building materials.

CO₂ emissions from the production of concrete and OPC can be reduced by different approaches:

- cement replacement by secondary raw materials and/or secondary cementitious materials;
- use of alternative fuel and energy resources in clinker cement production;
- use of alternative binders in the manufacturing of cement;
- changes in manufacturing processes and techniques [14].

One of the possible solutions is geopolymeric material that can be produced from recycled materials such as fly ash, silica fume, various slags, meta-kaolin, and others that would totally or in part replace the cement in concrete [15], [16]. It is known that alkali activated concrete has up to 60 % lower energy consumption than the Portland cement concrete [17]. Furthermore, it is claimed that geopolymer composites have the same or even better mechanical properties than OPC composites. Even though a lot of research for the purposes of geopolymer wider commercial application has been done, there is a need for more investigations on long-term behavior and durability [18]. It has been determined that geopolymer composites have higher

shrinkage while polymerized as well as the creep values in elevated temperatures and other specific situations [19]–[27]. But there is a lack of information about the creep and shrinkage properties of the polymerized geopolymer composite elements, and it is not known if they have similar long-term property decrease as the OPC based composites.

2. GEOPOLYMER COMPOSITES

In 1978, a new reaction of solid aluminosilicate with alkali solution was found by Davidovits to produce a geopolymer (GP). Geopolymer is a binder that is created in the reaction of aluminium oxide (Al_2O_3) and silicon dioxide (SiO_2). This binder, in its basic form, has a low Ca amount, unlike OPC. This binder has a tetrahedral framework that is connected with long-range covalent bonds [28]. It has been found that the efficiency and rate of GP forming are greatly affected by hydroxide or hydroxide base plus silicate [29]. To this day, various silicate and aluminate silicate materials have been used to create GPs, for instance, red mud, rice husk ash, ground granulated blast furnace slag, fly ash, and metakaolin [30]–[32].

In the literature regarding geopolymer it is claimed that in most cases, geopolymer composites show the same or superior properties as the OPC based composites. General property differences between geopolymer concrete and ordinary Portland cement are shown in Table 1.

Table 1

Differences in the Properties of GPC and OPC [1], [33]–[41]

Properties	Geopolymer concrete	Ordinary Portland cement concrete	Comments
Compressive strength	Higher	Lower	At an early age. GPC gains higher strength compared to OPC. The main factors influencing GPC strength are aluminosilicate source, type of activator, curing conditions and length, and reactivity of the precursors
Water absorption	Moderate	Slightly lower	Internal porosity in the GPC matrix slightly increases its water absorption in contrast to OPC
Setting time	Faster	Slower	In general, GPC is considered to have a short setting time, but unlike the OPC setting time, it is more affected by the factors such as activator type, source material properties, and exposure to temperature
Shrinkage	Moderate	Lower	Curing conditions and the mixture's moisture content affect shrinkage-related crack development to GPC
Tensile strength	Higher	Lower	GPC shows higher tensile strength and compressive strength
Durability	Higher	Lower	Presence of silicate and alumina products provides better durability of GPC
Resistance to acids	Higher resistance	Lower resistance	Alumino-silicates in GPC contribute to better acid resistance than in OPC
Fire resistance	Typically, higher	Limited	Due to its chemical composition, GPC degrades less in fire, while OPC shows less fire resistance
Freezing and thawing cycles	Less susceptible	More susceptible	GPC shows greater resistance to aggressive environments and to rapid temperature changes in the environment
CO ₂ emissions	Low	High	Overall, GPC poses smaller potential CO ₂ emissions than OPC during the life cycle
Porosity	Moderate	Lower	GPC shows a greater number of pores in the cross-section
Insulating properties	Higher	Limited	Depending on the curing condition, precursor and activator types of GPC show better insulating properties than OPC

In the next sections, geopolymer properties and its microstructure and environmental influence will be discussed. In the subsections, geopolymer constituents, properties, microstructure, and its influence and life cycle assessment will be discussed in detail.

2.1.Constituents

2.1.1. Aluminosilicates

Aluminosilicates, or in other words, materials that are composed of aluminium, silicone, and oxygen, are the base constituent of GP materials. They are sourced from waste utilization and are indispensable in making the GP matrix. Fly ash (FA) is a primarily used waste product for manufacturing GP. Other aluminosilicate sources and individuals in combination with each other and as standalone aluminosilicates have also been reported. The aluminosilicate materials as well as additives for the creation of GPs are shown in Table 2.

Table 2

Aluminosilicates as Source Materials for Geopolymer Composites [42]

Type	Abbreviation
(a) Aluminosilicate as source material	
Fly ash	FA
Bottom ash	BA
Granulated blast furnace slag	GBFS
Metakaolin	MK
Natural zeolites	
Kaolin	KL
Palm oil fuel ash	POFA
Granulated lead smelter slag	GLSS
Rice husk ash	RHA
Ferrochrome slag	FS
Ultra-fine kaolite high-performance ash	KHFA
Biomass fly ash	BFA
Silico-manganese fume	SMF
(b) Additives as source material	
Calcium aluminate cement	CAC
Nano-silica	NS
Calcium hydroxide	Ca(OH) ₂
Ordinary Portland cement	OPC
Silica fume	SF

2.1.1.1. Fly ash

Fly ash is generated during the burning process by industries that consume coal as an energy source or manufacturing ingredients. Mainly, these are power plants and metallurgic plants. The scheme of coal power plant operating, where fly ash is obtained, is shown in Fig. 3.

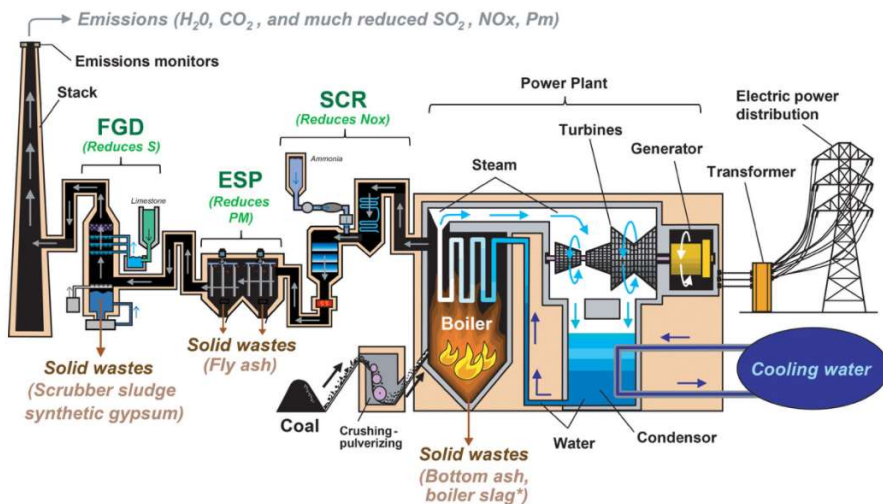


Fig. 3. Coal power plant's operational scheme [43].

For power plant application, the coal is crushed and introduced into the ignition chamber together with air. Here the crushed coal combusts generating heat and molten minerals. Boiler tubes remove all the heat from the kiln. As a result, fuel gas gets cooler and mineral residue hardens and forms ash. Coarse ash drops to the bottom of the ignition chamber and is further characterized as slag. Fly ash particles are retained in the fuel gas. As the gas rises, fly ash particles are captured in electrostatic precipitators or fabric filters that are placed for particle emission requirements.

Fly ash contains Al_2O_3 and SiO_2 that are key ingredients to form cementitious substances. Fly ash reacts with lime $Ca(OH)_2$ in the presence of water to form compounds identical to cement. Its usage in concrete has a significant effect, and it is found that it has high potential as a supportive material to GP. Fly ash containing concrete has greater strength and is more durable as compared to conventional concrete. By using fly ash, the cost of concrete is reduced and sulphate resistance is increased [44].

Using fly ash, landfill areas can be conserved and even reduced, water consumption and energy needs reduced, and greenhouse gas emissions minimized. Using fly ash, the needed amount of OPC is reduced and therefore CO_2 emissions are greatly reduced as well. Per ton fly ash used the CO_2 emissions are reduced by a ton. Utilizing a whole year's supply of fly ash in concrete is equivalent to 25 % disposal of CO_2 released by vehicles worldwide [45].

In the author's research, described in **Papers I–VII** [46]–[52], fly ash from the coal power plant located in Skawina, Poland, was used. It was determined that this fly ash is particularly suitable for geopolymer due to high SiO_2 (47.81 %) and Al_2O_3 (22.80 %) content.

2.1.2. Reinforcement

In field practice, fibers are added to concrete to reduce or even altogether avoid early age cracking caused by shrinkage creep. Fibers also increase the concrete's tensile strength and

crack resistance in the later stages of its life [53]. Often the material properties of fibers are more dominant than the binder properties in altering the performance of fiber reinforced geopolymer composite [54]. A good example is poly-propylene fibers that regardless of the binder type (OPC- based or geopolymer) would show weak binder and fiber interaction that further contributes to reduced compressive strength of the composite [55]–[59]. The physical and mechanical properties of the fibers used as reinforcement are compiled in Table 3.

Table 3

Reinforcement Fiber's Physical and Mechanical Properties [60]–[65]

Material category		Density (g/cm ³)	Tensile strength (MPa)	Modulus of elasticity (GPa)	Ultimate elongation (%)	
Metallic		Steel	7.65–7.85	345–2850	200–210	0.5–3.5
Carbon based	Synthetic	PAN	1.8–1.9	2500–7000	250–500	0.6–2.5
		Rayon	1.4–1.7	500–1500	35–60	2.5
		Mesophase patch	1.6–2.2	1500–3500	200–900	0.3–0.9
		Graphene		130000	1000	
		Carbon nanotube		11000–63000	1000–1800	
		Polyvinyl alcohol	1.2–1.3	800–2500	29–42	5.7–7
		Polypropylene	0.9–0.95	240–760	1.5–10	15–80
		Polyethylene	0.92–0.97	80–3500	5–113	3–100
		Aramid	1.38–1.47	2300–3500	63–120	2–4.5
		Acrylic	1.16–1.18	270–1000	13.8–19.3	
		Polyethylene terephthalate	1.3–1.4	420–450	3.1–10	11.2
	Polyester	1.22–1.38	580–1100	15	35.0	
	Nylon	1.13–1.41	440–1000	4.1–5.2	16–20	
	Natural	Jute	1.3–1.5	250–350	26–32	1.5–1.9
		Sisal	1.34–1.45	280–750	13–26	3.0–5.0
		Coconut	0.87–1.4	120–200	19–26	10.0–25.0
		Bamboo	0.6–1.1	140–800	11–32	2.5–3.7
		Cotton	1.5–1.6	390–600	5.8–11	6.0–10.0
		Palm	1.3–1.46	21–60	0.6	
		Wool	1.3	160	3.5	
		Hemp	1.4–1.5	270–900	23.5–90	1–3.5
		Kenaf	1.4	223–930	14.5–53	1.5–2.7
		Coir	1.15–1.46	95–230	2.8–6	15–51.4
Banana		1.4	500	12.0	1.5–9	
Flax fabric		1.5	500–1500	50–70		
Bagasse	1.3	222–290	17–27	1.1		
Abaca	1.5	400–980	6.2–20	1–10		
Inorganic	E-glass	2.5–2.62	3100–3800	72.4	4.8	
	S-glass	2.46–2.49	4020–4650	86.9	5.4	
	C-glass	2.6	3310	69	4.8	
	AR-glass	2.7	3240	73	4.4	
	Basalt	2.65–2.80	3000–4840	89–110	3.00–3.15	
	Asbestos	2.55	620	160		
	Alumina	3.3–3.95	1700–2000	300–380	0.4	
	Alumina-silica	3.4	1590–2550	200–248	0.8–1	
	Silicone Nitride		2500–4800	195–300		
	Silicone Carbide	2.5–2.7	2200–3450	221–250		
	Boron nitride	7.65–7.85	2100	345		

In further subsections, the most commonly industrially used fibers are described.

2.1.2.1. Steel fibers

Steel fibers are used mainly due to their high mechanical strength, flexibility and availability. According to ASTM A820-16 steel fibers can be arranged into 5 groups depending on their usage and purposes. They are: (1) pieces of smooth or deformed cold-draw wire; (2) smooth or deformed cut sheet; (3) melt-extracted; (4) mill cut; and (5) modified cold-drawn wire steel fibers. These fibers have a wide range of tensile strength (310–2850 MPa) and ultimate elongation (0.5–3.5 %) that differs according to the material and fabrication process [66]–[68].

The main disadvantage of steel fiber application is corrosion. To limit the corrosion's effect, mainly two solutions are applied: (1) usage of stainless steel alloys, for example, austenitic, ferritic, martensitic, duplex, and precipitation hardenable steels [69], or (2) sacrificial coating on fibers like copper and zinc [70], [71].

In **Papers I, III, IV, and VII** [46], [48], [49], [52], steel fibers were used. In **Papers I and IV** [46], [49], waste steel fibers from car tyre recycling were used. As steel chords from tyres are not useful for metallurgical application, they mostly end up in the landfill. In specimen preparation, it was observed that due to the different chord cross-section dimensions and length, it was hard or, in the case of cylindrical specimen preparation, nearly impossible to incorporate tyre chords into the geopolymer composition while mixing, like for regular steel fiber reinforcement. Therefore, a more suitable way of incorporation of waste steel fiber reinforcement is putting it into the mold and then fill and vibrate the matrix into it. In **Papers III and VII** [48], [52], steel fibers La Gramigna gold (0.3 x 20 mm) were used. It was observed that low amounts of steel fiber addition do not significantly affect geopolymer composite flowability and consistency.

2.1.2.2. Inorganic fibers

Inorganic fibers consist of a mixture of silica and alumina. Those fibers have a high melting point that makes them suitable for thermal application. These fibers have low cost, high tensile strength and chemical stability, and good insulating properties [60]. Silica fibers, aluminosilicate, alumina fibers, and basalt fibers are the most widely used inorganic fibers.

2.1.2.3. Carbon fibers

Reinforcement fibers, known for having the highest specific strength and lightness, are carbon fibers. Carbon fibers show outstanding tensile strength and modulus at high temperatures, chemical and thermal stability, low thermal expansion, and high electrical and thermal conductivity. Also, carbon fibers show good elastic properties that are not affected by fatigue deformations while loading and unloading are happening. According to fiber geometric characteristics, they can be divided into two groups: (1) fibers that are continuous in length and (2) carbon nanofibers [72], [73].

In **Paper II**, mechanical and long-term properties of carbon fiber reinforced geopolymer specimens were examined [47]. It was observed that 1 % of carbon fiber reinforcement introduction into the matrix slightly increases thickness of the geopolymer composite but does not significantly affect its flowability.

2.1.2.4. Polymeric fibers

As it is known, polymers are long chains of repeating monomers. They are held together through strong intermolecular bonds [74]. Depending on the chain order, polymers are divided into crystalline (over 80 % crystallinity), semi-crystalline (crystallinity between 10 % and 80 %), and amorphous (crystallinity is less than 10 %) polymers [64], [75]. When crystallinity is increased it also can enhance the polymer's mechanical properties, rigidity, environmental stability, and surface roughness. Based on the source material and the specifics of the production process, polymer fibers can be categorized as synthetic or natural.

Synthetic polymer fibers can be manufactured from raw material or recycled plastic waste. It has been claimed that the usage of recycled fibers in construction is a good solution for such widely used plastic disposal as polyethylene terephthalate (PET) and polypropylene (PP) [74]. For reinforcement of cementitious materials, the most widely used fibers are based on PP, polyvinyl alcohol (PVA), polyethylene (PE), and PET [76]. The main advantages of PP fibers are low cost, inert characteristics at high pH environment of the cement composite, ability to control plastic shrinkage-caused cracking in the concrete, and easy dispersion [77]. The downside for these fibers are low thermal resistance, low modulus of elasticity, and poor interfacial contact with cementitious matrixes due to their inherent hydrophobic characteristics [59], [78]–[80]. PET has similar mechanical properties as PP and nylon fibers. In contrast to previously mentioned fibers, PET fiber manufacturing is more cost effective and environmentally friendly. Recent developments in PET bottle recycling to produce PET fibers show promise for the construction industry [81]. The PVA fibers have higher tensile strength and modulus of elasticity than the abovementioned fibers. Those fibers also show stronger chemical bonding with cementitious matrix due to hydroxyl groups in its molecular chains [82], [83].

In **Papers III, IV, and VII**, PP and PVA fiber reinforced geopolymer composite's mechanical and long-term properties are researched [48], [49], [52].

2.1.2.5. Natural fibers

It is considered that jute, hemp, kenaf, bagasse and sisal are natural fibers. These fibers are common, widely available, and have low price. Furthermore, they have low density, reduced thermal conductivity, and good mechanical properties. The main drawbacks of these fibers are their low durability. At high fiber concentration, fibers significantly reduce the workability of the mix, and are the cause of inconsistent material properties and poor bonding/interaction with matrix [84]–[86].

2.2. Geopolymer composite properties

2.2.1. Mechanical properties

One of the most important and preliminary defining property of concrete is compressive strength. High initial compressive strength is of immense importance for construction materials. Therefore, flexural strength, tensile strength, and modulus of elasticity are closely linked with compressive strength. Mechanical properties are greatly affected by the properties of the utilized source material. It has been found that the compressive strength of GPC is significantly

influenced by the composition of the mix, the surface area, and particle shape of the fly ash [87]. The strength of GP composites is affected by many factors. The main factors are calcium content, molarity of alkali solution (NaOH, KOH), binder/aggregate ratio, solution/binder ratio, and silicate/hydroxide ratio. Furthermore, the development of strength is equally affected by the source material's properties, curing conditions, and filler particle size distribution [88]. It has been reported that heat cured fly ash-based GP composite achieves its complete compressive strength within one day. Other reports say that nearly 90 % of compressive strength can be achieved within a couple of hours if it is cured at temperatures around 80 °C to 90 °C. In **Paper II**, the geopolymer composite modulus of elasticity development was evaluated throughout the testing time. The specimens were polymerized for 24 hours at 75 °C. The alkali solution had 12 mol concentration. It was determined that as the tested specimens' age was 28 days, the modulus of elasticity from the 28th day till the 62nd day on average increased by 0.8 % each day and dropped the development to 0.4 % per day from the 62nd till the 150th day. Furthermore, the compressive strength had increased by 7 % and 27 % (for plain and carbon fiber reinforced specimens, respectively) from the beginning of the tests till the end. It was also determined that if the geopolymer specimen is subjected to water saturation for 24 hours, then its compressive strength decreases significantly. Compressive strength decreased by 2.2 % for plain specimens and 14.3 % to 35.1 % for carbon fiber reinforced specimens [47]. The strength development of GPC cured in ambient temperature is very close to OPC strength development. Nevertheless, all of the curing conditions result in long-term strength, and the additional heat to ambient temperature just speeds up the strength development and achieving of ultimate compressive strength for the specific GPC mix.

Some researchers have found that using 8-12M NaOH activation solutions and curing samples at 85 °C for 1 day results in specimens showing compressive strength from 35 MPa to 40 MPa. The compressive strength can be significantly increased if sodium silicate is added to NaOH ($\text{SiO}_2/\text{Na}_2\text{O} = 1.23$), reaching up to 90 MPa [89]. In **Papers IV and V**, the compressive strength values for the cylindrical specimens, made using 10M NaOH solution and cured for 24 hours in 75 °C, were from 30.37MPa to 36.33 MPa for plain specimens and 44.52 MPa for waste steel cord reinforced specimens [49], [50]. With the same NaOH solution and curing conditions, in **Paper III**, the compressive strength at the age of 28 days is 52.5 MPa, 55.1 MPa, 33.9 MPa, and 48.4 MPa for plain geopolymer composite, geopolymer composite with 1 % and 5 % PP fiber reinforcement and 1 % steel fiber reinforcement, respectively [48]. Specimens, made with the 12M NaOH solution, at the age of 28 days showed 48.16 MPa and 45.48 MPa for specimens with 1 % carbon fiber and without them (see **Paper II**). The curing procedure for these specimens was done for 24 hours at 75 °C [47]. The cubic geopolymer composite specimens mentioned in **Paper I** exhibit compressive strength values of 113.97 MPa, 81.07 MPa, and 85.2 MPa for 3.5 %, 2 % steel cord reinforced and plain geopolymer composites. These specimens were made using 10M NaOH solution. They were cured for 24 hours at 75 °C [46].

Water/binder ratio also plays a significant role in GPC compressive strength. It has been found that in order to gain the maximum compressive strength of fly ash-based GP composite, the optimal $\text{SiO}_2/\text{Al}_2\text{O}_3$ ratio has to be 15.9 [90]. It was also found that compressive strength

was affected by the molarity of the activation solution. An increase was observed in compressive strength after 7, 14, 28 and 56 days when using 12–14 M activation solutions. The decrease in compressive strength was observed using activation solutions with molarities of 14 M and higher. The relations are showed in Fig. 4 [91].

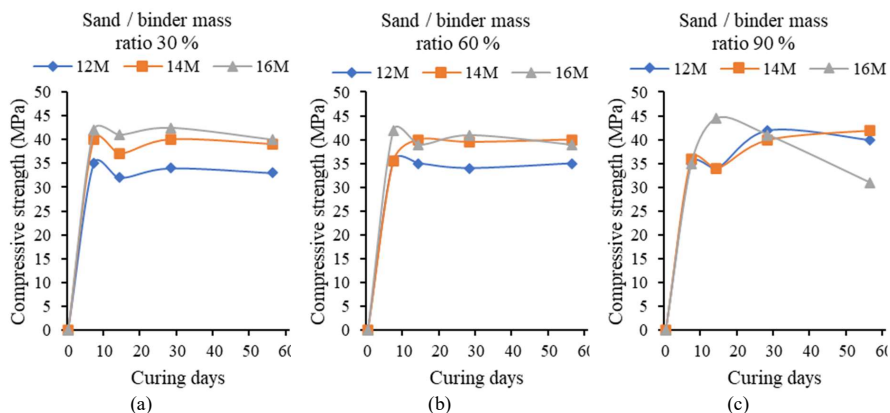


Fig. 4. Geopolymer mortar's compressive strength according to curing days, sodium hydroxide concentration, and sand/binder ratio [91].

In the early days of the GP composite research, tests were done with GP based on kaolinite, fly ash, NaOH, water and sodium silica mix. It was found that compressive strength was affected not only by the curing time but also by the curing temperature. Specimens cured at 60 °C for 48 hours had the highest strength (see Fig. 5) [92].

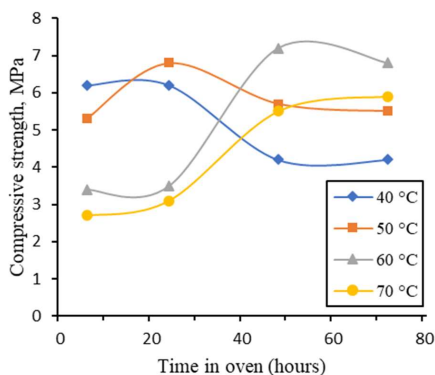


Fig. 5. Compressive strength development of fly ash-based geopolymer composite cured at different temperatures [92].

In Table 4, the important effect of variable parts on compressive strength on paste, mortar and concrete are summarized.

Table 4

Geopolymer Composite's Compressive Strength Variation Due to Different Variables [42]

Category	Source materials	Molarity	t (°C)	Curing time (h)	Compressive strength (MPa)
Paste	FA	12	70	24	65.0
	Fluidized bed FA-MK	10	40	24	72.0
	FA and SD	10	40	24	67.0
	RHA and WTS	10	60	24	24.0
	FA and coir fiber	8	75	24	31.4
	FA-MK-Sepiolite	10	20	24	52.0
	FA and POFA	14	65	48	72.7
	Nano TiO ₂ in fluidized bed FA-MK	10	40	72	77.0
FA and IOT	10	7 thermal cycles at 200	N/A	36.0	
Mortar	MK with CG	N/A	22	24	97.0
	GGBFS, MK and RHA	14	65	24	47.9
	FA	16	65	24	56.0
Concrete	FA	14	75	22	80.0
	FA	12	75	24	62.3
	FA	15	80	24	48.7
	FA	16	60	24	53.6
	FA	14	25	24	34.3
	BA	14	25	24	0.6
	FA and BA	14	25	24	8.4
	FA	14	46	24	42.5
	FA	14	46	24	40.6
	FA and LWA	12	70	24	17.0
	FA and KL	14	100	72	54.0
	FA and SF	14	100	72	51.2
	FA and nano-silica	12	25	24	46.4
	FA and nano-silica	8	80	24	47.0
	FA and LS	8	60	24	32.0
	FA and GGBFS	12	75	18	53.2
	FA with SSD	8	60	24	62.0
	FA, POFA, and OPS	14	65	48	30.1
	PCFA, GGBFS, and LWA	3	20	24	9.0
	POFA, MK, OPS, and steel fiber	14	65	48	31.9
	POFA, GGBFS, and MK	14	65	24	41.5

As for the tensile strength of geopolymer composites, in **Papers V and VI**, plain and 1 % PVA fiber reinforced specimens achieved 5.13 MPa and 4.95 MPa. These specimens were made using a 10 M NaOH solution and were cured at 75 °C for 24 hours [49], [51].

Regarding fly ash-based geopolymer bending strength with and without various fibers, similar as in **Paper VII** [52], plain and polymer fiber reinforced specimens show the best bending strength in contrast to specimens reinforced with low amount of steel fibers or with the combination of steel and PVA fibers. The bending strength for plain GP is 8.07 MPa and is followed by the 1 %PVA fiber, 0.5 % PVA/0.5 %steel fiber, and 1 % steel fiber reinforced specimens with a bending strength of 7.32 MPa, 6.93 MPa, and 6.20 MPa, respectively. Previously mentioned GP compositions with the best initial bending strength also have the largest deterioration of bending strength throughout the long-term deflection test. For the plain and 1 % PVA fiber reinforced, the flexural strength deterioration after the long-term test is 13 % and 15.15 %, respectively. For the remaining composites the reduction of bending strength is less than 1 %. Furthermore, the measurement errors of plain and 1 % PVA fiber reinforced GP are the largest. The errors vary from ± 0.49 MPa to ± 0.86 MPa for plain GP and ± 0.50 MPa to ± 0.70 MPa for 1 % PVA fiber reinforced GP.

2.2.2. Geopolymer composite durability

The resistance to weathering, degradation, abrasion, and chemical resistance are essential to any structural element. Absorption capability, noticeable volume of pours, water and chloride absorption, sulfate and/or other acid influence are important parameters that show GPC stability and suitability for structural use. GP composites usually show higher endurance to aggressive environment impact than OPC.

The highest durability issue arises from water absorption. High water absorption greatly reduces the compressive strength of GP composite [93]. Acid attacks, liquid absorption, strength degradation and weight loss, chloride ingress, discontinuous pores and voids, and wetting-drying cycles have relatively less impact on durability. GP composites are considered acid resistant. Nevertheless, acids can have a significant effect on GP composites, their durability, and composition stability. GP resistance to acids mainly relies on the acid properties and GPC specimen physical state and chemical composition [94]. Absorption ratios are highly important because the higher they become, the higher the capillary water level in GPC mix [95]. Strength loss mainly would be generated by imperfections in the chemical composition of the GP and reduced compactness that leads to reduced split tensile strength, flexural strength, and compressive strength [96]. Significant weight loss of specimens leads to durability loss mainly while specimens are submerged in solutions that hold sulphates from sodium and magnesium, sulphuric acid, and NaCl. In the beginning, it appears that the specimen's weight increases as the chemicals penetrate into a structure. Afterward, it is observed that absorption of the solutions have also led to the expansion of the specimen that further causes a significant amount of micro cracks that further reduce the durability [97]. Chloride penetration into the specimen would create the same results as weight loss. As the specimen is subjected to chloride solution, it would penetrate specimen and would expand in the specimen that leads to micro and macro cracks that further significantly reduce the durability of the specimen [98]. Discontinuous pores increase GPC workability and resilience under sever environmental conditions [99]. Heating and cooling and exposure to moisture cycles influence the microstructure of the specimen and further affect mechanical properties. The higher the weight loss during these cycles, the greater reduction in durability of this specimen [100].

Shrinkage-introduced cracks in most cases have less impact on durability than the previously stated situations. They can be introduced during the polymerization process and through moisture cycles. In most cases, shrinkage would not cause a high amount of cracks, but if a high amount of shrinkage cracks are present, then the durability of the specimen can be significantly impacted and mechanical properties reduced [101].

2.2.3. Geopolymer composite's thermal endurance

Unlike OPC that would lose 20–30 % of strength if it is heated at 800 °C to 1000 °C, GPC shows different thermal properties in elevated temperatures. Geopolymer composites exhibit decent fire resistance properties at high temperatures due to nano-pore presence in the microstructure. The melting temperature of GP composites is about 1200 °C with no signs of spalling [102]. Micro-pores allow evaporation and migration of water vapor in the structure of GP without posing harm to the aluminosilicate network. While elevated temperatures are applied to specimens, various processes are happening, for instance, water that has been absorbed by N-A-S-H gel evaporates, water-free products are formed, melting and crystallization of stable water free phases that leads to further GP matrix destruction. It has been observed that if GP paste that contains fly ash is exposed to 800 °C, the residual strength is increased by 6 %, but metakaolin containing GP paste would show 34 % decrease in residual strength [103].

2.2.4. Time dependent properties of geopolymer composite

Creep and shrinkage can cause a significant increase in strain with time. Thus, for material's use in the long-term, it is of high importance that these properties are studied. Often creep and shrinkage are considered as independent phenomena, but there are some studies that claim that these phenomena have strong poromechanical (studies of porous material permeated by interconnected network of pores) couplings [104]–[106].

Nevertheless, there is still lack of information and research regarding creep and shrinkage behavior of geopolymer composites in various stresses, especially in tension and three-point bending.

Methodology for determining the long-term properties of concrete and cement composites in various stress-strain conditions (**Patent I**) was developed and verified not only for the purpose to measure creep strains but also to record shrinkage and modulus of elasticity changes [107]. It also regulates how to carry long-term tests in compression, tension and three-point bending. The developed method regulates the specimen's preparation, loading and unloading procedures, and length and environmental necessities for long-term property laboratory testing.

2.2.4.1. Creep properties

Creep is defined as a phenomenon where strain increases in time while the applied stress remains constant [108]. Creep is a very important factor in any cement-based composite. Creep affects stress distribution and deformations throughout the specimen's or the structural element's cross-section. A survey on concrete bridges in 2011 [109] showed the importance of reliable estimation of the basic creep compliance function of concrete to accurately predict the long-term deflection of the bridge over a 20-year period. Basic creep characterization of concrete is also important in the prediction of relaxation of prestressed cables to nuclear vessels [110].

Creep for hardened concrete most often is divided into two occurrences:

- (1) basic creep that happens while the specimen has constant moisture; this process is irreversible;
- (2) drying creep (also called Pickett effect or stress-induced shrinkage) happens due to drying and is partially reversible [111].

Furthermore, drying creep is attributed to a micro cracking effect due to the shrinkage strain gradient between the external and internal layers of specimen upon drying [112]. Basic creep can be divided into short-term and long-term creep, referencing it to different kinetics [112]–[114]. It has been reported that the main factors effecting creep for OPC based materials are mixture proportions, curing age, temperature and humidity of the surrounding environment, and the level of applied stress [115]. For geopolymer composites, it is expected that the same factors are affecting creep development. Creep curve is generally divided into the transient elastic deformation stage (instant creep), primary creep stage (decelerating creep), steady creep stage (secondary creep or isokinetic creep), and accelerated creep stage (tertiary creep or creep failure). They are dependent from creep rate and creep time relations, as it is shown in Fig. 6 [116]. Due to the nature of geopolymer polymerization process, the factors that affect OPC composite creep would have different effects on geopolymer composites.

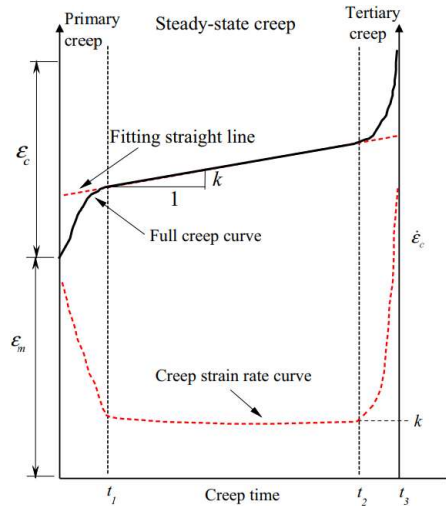


Fig. 6. Schematic diagram of a usual creep curve and creep strain rate [116].

As geopolymer binder is a fairly recently developed material, there has been increased interest in creep properties of geopolymer in recent years. It has been showed that fly ash-based geopolymer concrete exhibits low creep values over a 12-week testing period [19]. Furthermore, it has been found that fly ash-based geopolymer has lower specific creep (creep strain normalized with applied stress) [20] and creep coefficient (the ratio between creep strain and elastic strain) [20], [21] than OPC concrete. This matches with the results in **Papers II–**

VII [47]–[52], where it was observed that creep properties for plain specimens are low, and in **Paper II** [47] it was shown that they are lower than for OPC by around 13 % to 23 %. It was further concluded in **Papers II and III** [47], [48] that insufficient amount of fiber incorporation into geopolymer composite would lead to higher creep strains. Still, if the reinforcement is in sufficient amount and has the necessary properties for the specific service state, the creep is limited. In **Paper IV** [49], recycled tyre cord reinforcement decreases creep strains by 30 %. It has been claimed [22] that this low creep is attributed to a micro aggregation effect of unreacted fly ash in the binder.

Most of the studies that have looked into the creep properties of the geopolymer composites have determined creep in compression [23]–[25], [101]. In general, the fly ash-based GP composite would have a lower creep than OPC based concrete. It has been claimed that GP concrete cured at 60 °C for 24 hours has up to 50 % less compressive creep than OPC based concrete [22]. Similar creep properties have been observed for the specimens cured for 6 hours at 60 °C [101]. There have been creep measurements for GP composites cured from 40 °C to 80 °C for different durations. It was observed that GPs that have been cured at 40 °C for three days have insignificant or the same creep properties as OPC based specimens, but compressive creep strains of GP specimens that have been cured for 7 days at 80 °C have been significantly reduced and got negligible [20]. In **Paper II**, up to 23 % reduction in creep strains was observed for the geopolymer composite that has been cured for 24 hours at 75 °C [47].

The creep in tension has a different manner than creep in compression. Tensile creep has a critical role in assessment of the early age cracking risk [117]. Tensile creep shows more linear behavior throughout time than creep in compression. The development rate of creep strain in compression throughout time would decrease. Some researchers claim that creep coefficients measured for compressive stresses can be multiplied by factor 1 to 3 to get creep coefficient in tension [118]. The mechanisms of creep in tension are different to those in compression. The tensile creep strain rate does not reduce at the same rate as the creep strains in the compression [119]. Tensile creep determination for concrete at early age can be done using the direct tension experiment or the indirect tension test [120], [121]. The ring test is a simplified indirect tension method that is quite popular to determine tensile creep and restrained shrinkage cracking risk [122].

Some researchers [123] claim that at an early age, creep in compression for cement composites would be bigger than creep in tension, while others [124] claim the opposite. In **Paper V** [50], it was determined that creep strain for plain geopolymer composite in compression is around 35.8 % higher than in tension. Furthermore, creep strains in compression develop and increase throughout testing time, the creep strains in tension do not exhibit significant increases throughout test. As for the specific creep values, here significantly, specimens that have been tested in tension show higher values. They have, on average, 85.92 % higher specific creep than the specimens tested in compression, as shown in Fig. 7.

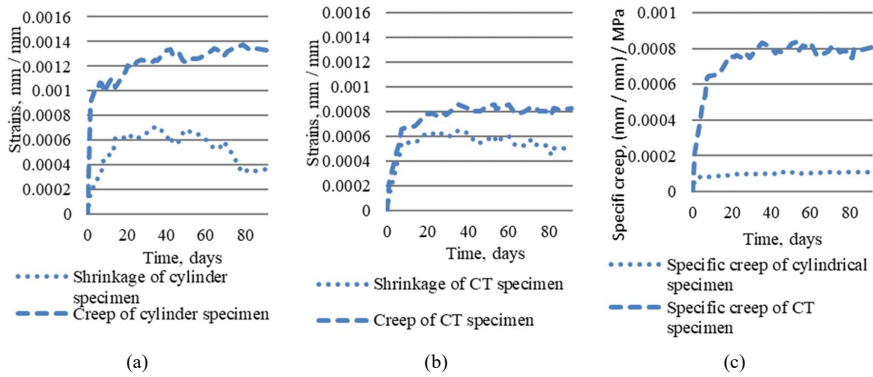


Fig. 7. Creep and shrinkage curves of compression (a) and tension (b), and specific creep (c) of compression and tension of specimens [50].

In **Paper VI** [51], it was determined that 1 % PVA fiber reinforced geopolymer composites exhibit similar creep strains as plain GP. Tensile strength also is similar. It also has to be mentioned that the 1 % PVA fiber reinforced GP specimens have larger creep strains in the early stage, but after 40 days of testing, creep strains are equal to the plain and 1 % PVA fiber reinforced specimens.

Just like the OPC based concrete, also GP concrete shows low tensile capacity. The authors claim that for reinforced GP structures it is inevitable to show cracking in service life [119]. At the early stage of structure's life, a restrained shrinkage is one of the factors that induces early age cracking. The evolution of restrained shrinkage in the first few days would introduce time dependent tensile stress development in concrete [125]. In the concrete member that has been restrained by reinforcement, the shrinkage increases the tensile stress while tensile creep is relaxing tensile stress. All of the previously referred studies are focusing on quantitative analysis of experimental data but information regarding creep and shrinkage in GP is limited.

The long-term deflection properties of geopolymer composites are not widely studied. Some of the studies [126], [127] that looked into long-term properties of specimens tested in deflection show that geopolymer composites have close correlation with the Portland cement based composite long-term deflection properties. **Paper VII** [52] shows similarities with [126] the acquired deflection characteristics. As for the quantitative comparison, it is impossible to compare the results presented in **Paper VII** with other results, for instance, the results published in [126] where the deflection strain graphs are represented using absolute strain measurements not relative (measurements not dependent from the measured specimen's size and applied load impact) strains. From the results in **Paper VII** [52] it becomes clear that the usage of steel fibers is beneficial in contrast to the PVA fiber or combined PVA and steel fiber usage. Furthermore, while creep properties of geopolymer composites reinforced with 1 % steel fibers in compression and tension show the highest creep and specific creep properties in long-term deflection, they show the lowest long-term deflection that is 39 % less than the next GP composition.

In **Patent I**, the test setup and procedures necessary for creep testing in compression, tension and bending are described.

2.2.4.2. Shrinkage properties

Shrinkage of concrete materials in general comes from the shrinkage of the paste (matrix). It is due to high dimensional stability of the aggregates [128], [129]. The shrinkage of materials can be divided into groups based on mechanisms that influence shrinkage development. These are plastic shrinkage, carbonation shrinkage, autogenous or chemical shrinkage and drying shrinkage. Plastic shrinkage happens instantly when mixture is poured into mould. Carbonation shrinkage happens due to CO_2 from the environment penetration into the outer surface of the specimen and reaction with $\text{Ca}(\text{OH})_2$ from the hydration products. That further produces CaCO_3 and water molecules. Autogenous shrinkage is caused by self-desiccation of the composites. It is an unavoidable process that reduces volume of the element and is very likely to happen to composites with low water/cement ratio [130]. Drying shrinkage is the volume reduction of the specimen that is caused by water evaporation from the gel pore surface. Most of it happens in the hardening process of the specimens [131]. For geopolymer composites and alkali activated composites in general, the main shrinkage comes from autogenous and drying shrinkage. For geopolymers, autogenous shrinkage means loss of internal water during polymerization that further creates capillary stress. Drying shrinkage happens due to water evaporation into the environment, and it is proportional to the moisture loss from the composite [128], [132]–[134]. In contrast to autogenous shrinkage, drying shrinkage is more affected by alkali concentration and outside environment effects. The tests done in [26] showed that the geopolymer binder drying shrinkage increased with the increase of alkali concentration (Na_2O). In the meantime, autogenous shrinkage stayed relatively constant, as is shown in Fig. 8.

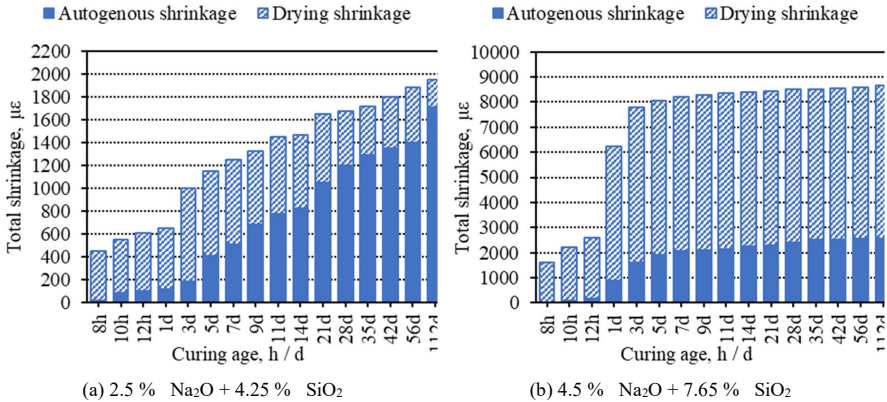


Fig. 8. Autogenous and drying shrinkage of alkali activated composites with different alkali concentration [26].

Other researchers state that it is hard to accurately determine the level of autogenous and drying shrinkage from one another for the composites mainly due to the fact that autogenous and drying shrinkage happen simultaneously if the specimen is not sealed. Therefore, measured

drying shrinkage often has a fraction of autogenous shrinkage as well. The shrinkage, especially for alkali activated composites, is closely linked to polymerization process and used raw material properties that greatly influence the moisture loss and the pore structure development of the composites [27], [128], [135].

In **Papers II–VI** [47]–[51], drying shrinkage strains were measured. It was determined that fiber reinforcement plays a significant role in shrinkage reduction for specimens tested in compression and tension. For instance, in **Paper IV**, specimens that have been reinforced with recycled tyre steel cords show on average 50 % less shrinkage than plain geopolymer composites [49]. Furthermore, in **Paper VI**, the 1 % PVA fiber reinforced specimen tested in tension showed on average 54.21 % lower shrinkage than plain specimens [51]. Also, in **Paper V**, shrinkage strains were determined in compression and tension [50]. There shrinkage strains between compression and tension specimens on average were 15.8 % less for the specimens meant for testing in tension.

The mechanisms that influence shrinkage can be divided into four groups: capillary stress, interlayer water loss, disjoining pressure, and surface energy [133]. These shrinkage mechanisms influence cement-based materials and alkali activated cement-based composites. While mechanisms are the same, the shrinkage values for the OPC based and geopolymer composites differ, mainly due to differences in hardening reaction mechanisms [136]. In general, the alkali activated cement composites, slag-based composites in particular, show larger shrinkage than OPC based composites. This geopolymer shrinkage increase is mainly due to the differences in pore size distribution and reaction products in the paste mix. These results of the previously mentioned research are based on quantitative analysis of experimental data.

In **Patent I**, the test setup and procedures necessary for drying shrinkage testing in compression, tension and bending are described.

3. GEOPOLYMER MICROSTRUCTURE

3.1.Characteristics and processes of alkali-activating reaction

Some studies have shown that the alkali-activated reaction of fly ash-based GP is affected by certain factors, such as the fineness of fly ash particles, curing conditions, and alkali activation solution concentration [137]–[141]. The dissolution process of Al and Si happens when fly ash is subjected to alkali solution. Larger molecules condense into a gel (polymerization and nucleation), and as the alkali effect on fly ash continues, larger spheres open to reveal smaller spheres inside. Smaller spheres then would be dissolved almost fully with the formation of reaction products inside and outside the large spheres. The AlO_4 and SiO_4 formation by silicon and aluminium-rich fly ash dissolution forms three types of monomers by combining with oxygen atoms. Then, these three types of monomers form a gel with a simple structure. After that, the gel is restructured and then polymerized and hardened in the disordered structure with high mechanical strength and forms an alkali-activated cementitious material [142]–[147]. The polymerization process is shown in the scheme in Fig. 9.



Fig. 9. Fly ash-based geopolymer cement/concrete chemical development scheme[148].

The influence of the fly ash particle size on the polymerization reaction shows significance when the reaction temperature is low. Fly ash with a smaller particle size has higher solubility and stronger reactivity.

3.2.Pore structure of the fly ash-based geopolymer

In general terms pore structure in fly ash-based GP composites is affected by curing conditions. Geopolymer pores are mainly within the small pore size range. This is unlike OPC

based composites. There the hydration products do not have a filling or optimizing effect on the pores. Some researchers [149] observed fly ash-based GP gel pores and capillary pores that have been cured for 7 and 28 days and concluded that pores were concentrated in the small pore size range. That differs from OPC composites. Furthermore, in the fly ash based GP, the C-A-S-H gel was distributed uniformly, and no capillary pores were found in it. Nevertheless, a small amount of large cavities from partial fly ash particle dissolution were observed. In OPC based composites, C-S-H gel was concentrated, and capillary pores were formed. In other studies [150] it was observed that the pore volume increased and morphology varied significantly when the setting time was increased for OPC composites. It was determined that the main factor could be the expansion of the basic silica gel and the merging of pores. Fly ash based composites showed the filling effect of the fly ash particles and gel. This contributes to negligible variations in pore volume and morphology. Furthermore, variations in micropore diameter and volume were linked to the polymerization level of fly ash during curing.

Also, silicon content in the alkali activator plays a crucial role in the pore structure development of fly ash-based GP. A larger quantity of silicone contributes to the larger quantity of gel and contributes to the uniform distribution of the gel with the pore filling effect at the micro scale [151], [152]. An alkali activator with high silicon content contributes to the formation of uniform and dense microstructure [149]. Despite this, in [153] it was determined that high silicon content in alkali solution does not influence the refinement of pore structure of fly ash-based GP. It was pointed out that the pore size distribution was concentrated within the sub-mesoporous region (0.22–3.6 nm), and the pore network was more refined when the silicon content in alkali solution was low. Pore distribution in mesoporous region was from 3.6 nm to 50 nm, and the pore refinement degraded when the silicon amount in alkali solution was high. Furthermore, longer curing time can promote formation of the N-A-S-H gel with pore filling effect and even more reduce porosity [154], [155]. To a certain extent the volume of capillary pores decreases with the increase of curing temperature [155].

There are many possibilities to measure the porosity of the material. The most often used ones are [156]:

- mercury porosimetry,
- helium pycnometry,
- image analysis,
- water absorption.

To determine porosity, in **Papers IV–VII**, a technique for outside effect determination on concrete and cement composite microstructure in various stress-strain states (**Patent II**) [157] was developed and used. The technique is based on polished section specimens that are examined in the scanning electron microscope (SEM) or optical microscope with a specific image recording equipment. The acquired images from polished sections are compiled and rendered and quantitative image analysis is done. This technique (**Patent II**) can be used not only for porosity determination but also for the specimen cross section characterization purposes. It details and regulates the acquiring and storage of specimens. It also regulates the specimen preparation procedures and image acquiring sequence and recommends the best ways to render and quantitatively analyse images and their composition.

In **Papers IV–VI**, it was determined that fiber incorporation into geopolymer composite leads to increased porosity. Porosity was increased by 0.61 % and 2.26 % in the specimens reinforced by the steel fibers from recycled car tyres [49]. Also, it was determined that specimens that have been subjected to load (tested for creep properties) had around 1.17 % less air voids than the specimens that had not been subjected to load. For the specimens without reinforcement, no significant reduction of air voids due to loading was established. In **Paper V**, it was determined that the specimens meant for testing in tension had a significantly higher air void amount than the specimens used in compression tests [50]. The specimens used in tension have a 2.14 % and 3.01 % higher amount of air voids than the compression specimens. Also, as these are plain specimens, the difference between the specimens meant for compression testing and those that have or have not been subjected to load has not been established. For the specimens used in tension testing there is a difference in porosity. There is a 0.69 % reduction for specimens subjected to load. Furthermore, in **Paper VI**, it is determined that for the specimens used in tension, the testing fiber introduction significantly increases the air void amount [51]. In specimens with a 1 % PVA fibers, the air void amount is increased by 1.88 % and 2.50 %. In a three-point bending for the long-term deflection tested specimens, the differences in air voids between plain, 1 % PVA, 0.5 % PVA/0.5 % steel and 1 % steel fiber reinforced specimens is within a 1.37 % difference, as it is shown in **Paper VII** [52]. The highest air voids are found in plain specimens with 5.02 % of analysed surface area, and lowest in 0.5 % PVA/0.5 % steel fiber reinforced specimens with 3.65 % of the analysed surface area consisting of air voids. Significant differences become apparent when the specimen's cross section surface analysis is done for the specimens tested for bending strength. Then the air void and crack area differ from 14.50 % and 16.48 % for 0.5 % PVA/0.5 % steel and 1 % steel fiber reinforced specimens up to 18.57 % and 22.00 % for plain and 1 % PVA fiber reinforced specimens. This leads to the conclusion that for thin specimens with large surface area, fiber incorporation allows an entrapped air release.

3.3. Geopolymer and OPC composite microstructure differences

As it was mentioned in the previous section, hardened GP shows a denser structure than the cured OPC composite. In GP system, C-A-S-H matrix chains have been found to be longer than the C-S-H gel chains in OPC systems. It is mainly because of Al^{3+} substituting Si^{4+} in bridging positions. C-A-S-H gels showed a lower amount of Ca/Si ratio and a higher ratio of Al/Si than C-S-H. There were indications of tobermorite 1.4 nm existence with a chain length of 11 nm and tobermorite 1.1 nm with a chain length of 14 nm tetrahedra. Furthermore, the modulus of elasticity for tobermorite 1.1 nm was 77.3 MPa and for tobermorite 1.4 nm – 49.9 MPa. This is because of higher interlayer cohesion of bonding between bridging tetrahedral of conservative layers [158].

If the differences in gel composition of GP and OPC composite systems are compared, the main difference is that the C-S-H forming in OPC composite shows lower Al and higher Ca content than the formation of C-A-S-H in slag-based GP composites. If the fly ash is introduced

in the system of GP, N-(C)-A-S-H can be identified with low Ca content, but N-A-S-H can only be stable at pH lower than 12 [159], [160].

The slag-based GP pore size varies in the field of mesopores (pore size <50 nm). These GPs also show lower porosity than OPC based composites. If the pore size distribution is compared to OPC based paste and slag based GP paste, it becomes apparent that most of the pores for the OPC based paste are within a range of 10 nm to 100 nm, while for the GP paste, most of the pores were below 20 nm [161]–[163].

3.4. Microstructure development of geopolymer composite incorporating lime and silica

As fly ash stocks in the future can be exhausted and necessity of elevated temperatures for such GP polymerization can be an overwhelming boundary, other alternative source materials have been tested as more suitable base materials for GPs. By introducing lime and silica fume in the GP matrix [164], compressive strength and microstructure for 7-, 14-, and 28-year old specimens were determined. The researchers replaced fly ash partially with lime and silica fume within the range of 5–10 % and 1–3 %, respectively. It was found that by partially replacing fly ash with lime, the setting time and workability of such material would be reduced, while the usage of silica fume would increase these properties. The compressive strength for these specimens increases if 7.5 % lime and 2 % silica fume is used. It was also observed that at the age of 7 days specimens show a less homogeneous microstructure with some unreacted fly ash particles. It was deduced that fly ash reacted throughout time as polymerization continued. At the age of 28 days the microstructure appeared homogeneous and compact. Microstructure appearance directly contributed to the compressive strength values.

4. GEOPOLYMER COMPOSITE APPLICATION IN CIVIL ENGINEERING

High compressive strength, higher durability to acid attacks and thermal durability, low carbon emissions and low processing energy consumption and others are the properties that justify the GP application in civil engineering in contrast to conventional Portland cement and other cement-like materials that have lime in them.

4.1. Geopolymer application in soil stabilization

It has been claimed that GP usage in soil stabilization is feasible especially on sites where there are soft or weak soils [165]. Some authors [166] have found that very effective in the stabilization of deep soil are fly ash slurry. It has to be pointed out that these slurries are calcium-based GPs. Others [167] have deduced that alkali activated metakaolin shows promising results in soil stabilization in contrast to cement-stabilized soil. It was found that in an unconfined compressive strength test at the age of 28 days metakaolin (15 %) stabilized soil had 4 MPa, while the cement (5 %) stabilized soil strength was 3.5 MPa and non-treated soil showed 0.5 MPa strength. Soils that have been stabilized using metakaolin appear more ductile [168]. These soils show lower shrinkage. It is significant at 11 % metakaolin concentration.

Researchers have used Class F fly ash (with low Ca content) together with alkali solution (with sodium hydroxide and sodium silicate). The alkali solution was prepared in 10 M, 12.5 M, and 15 M concentrations. At the early age, the 15 M solution showed higher strength, but at the age of 90 days and 365 days, 12.5 M concentration was much higher. Alkali solutions with concentration of 15 M handled several times were too viscous to handle and crystallized at lower temperatures. Furthermore, as the sodium silicate and sodium hydroxide are quite expensive, the 12.5 M solution seems more suitable from this standpoint [166].

It has been concluded that the usage of alkali activated compound in jet grouting is suitable for soil stabilization and comparable to traditional cementitious grouting methods, however the strength development has to be researched further [169].

4.2. Geopolymer application in buildings and infrastructure

There have been various claims of the first building in the world that would have its structure entirely made from GP. Some authors claim that it is the Global Change Institute of the University of Queensland building (Fig. 10) that was constructed in 2013 by HASSEL in conjunction with Bligh Tanner and Wagners [170]. The building is made from precast elements. They were made from slag/fly ash-based GP, called earth friendly concrete (EFC) that is the Wagners brand name for their commercial form of GP concrete.

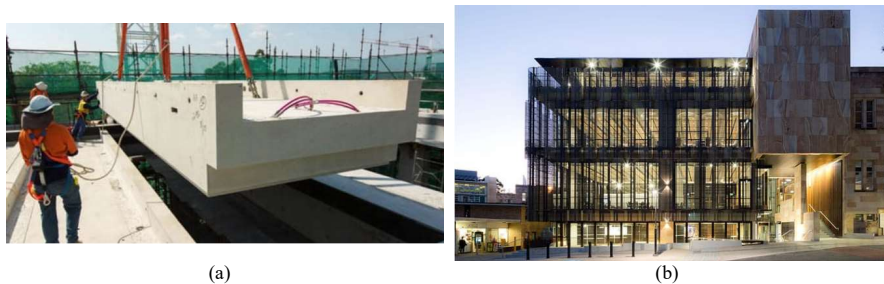


Fig. 10. The Global Change Institute of the University of Queensland building: (a) one of 33 floor panel montage and (b) finished building [170].

Other researchers claim that the first two buildings were built in the 1960s in Ukraine, Mariupol. Two 9-storey residential buildings were constructed from alkali activated material developed by the Ukrainian scientist Glukhovsky. This material had some Portland cement in it. The first building made from alkali-activated concrete without Portland cement was built in 1989 in Lipetsk, Russia, and it had 20 floors [171].

Besides the previously mentioned cases there have not been any claims of other residential buildings made from GP composites.

In contrast to applications in residential buildings, the use of GP composites for infrastructure purposes is much more common. For instance, in Australia, the Rocla Research Center has produced and successfully implemented sewer pipes, railway sleepers, cemetery crypts, box culverts, and wall panels [172]. In 2015, Wagners Australia and Glasby documented large scale commercial application of GP concrete at the Brisbane West Wellcamp Airport. Approximately 40000 cubic meters of fly ash-based GP concrete was used to make 435 mm thick heavy duty pavements in the northern end of the runway, aircraft turning areas, taxiway on the western side, and hangars on the eastern side of the runway [169]. In India, there has been a successful experience with pavement stone development and usage on paved road surfaces [173]. It was concluded that the fresh properties of GP composite (slump value and spread) were equivalent to the concrete guidelines. Additionally, strength values were greater than the target values.

Dense microstructure of GP composites results in low permeability that further reduces and inhibits penetration of seawater, thus making GP composites suitable for marine applications [174]. The authors of [175] have claimed that aluminosilicate geopolymeric gels are chemically stable in sea water and can be a sustainable alternative to Portland cement based marine structures. Some researchers [176] have proposed the use of fly ash and steel furnace slag as source materials for high density GP composite for coastal protection structures. The composites achieved a compressive strength value up to 37 MPa and a size reduction of breakwater structures by 30 % to 40% was proposed without compromising the structural performance. This resulted in the reduction of material requirements that further reduces overall carbon footprint. The authors of [177] have had similar reports on enhanced properties of fly ash-based GP composites exposed to harsh environments such as sea water and acidic environments.

Also, in India they have had success with GP concrete road creation. In 2017, at the Council of Scientific and Industrial Research in the Central Building of the Research Institute in Roorkee, a 50-meter long and 3-meter wide road segment was laid. In Uttar Pradesh, at NTPC Energy Technology Research Alliance, a 100-meter long and 6.5-meter wide road segment was laid. In 2017, several haul roads were laid for heavy load carrying from the mines in Bhubaneswar. In Lanjigarh, Sesa Sterlite Ltd in cooperation with IMMT laid a 40-meter long GP road. In late 2019, in Ramagundam, NTPC in association with NETRA laid a 500-meter long fly ash based GP concrete road [178].

All in all, the GP technology is more advanced and technically more applicable in precast state. The main factor is that GP is quite sensitive while it is setting (polymerizing). It is easier to provide a high temperature curing environment and safe alkali processing environment in specific location than on a building site and have all of the necessary technological means moveable. This can be concluded for the developed and tested geopolymer compositions in **Papers I–VII**. As all of the tested geopolymer specimens were developed, prepared and tested in laboratory conditions, the acquired properties are only possible in certain conditions. These conditions are molded structures and polymerized in a controlled environment. Therefore, the developed geopolymer composite compositions in previously mentioned papers would be suitable for precast structure development. Also, it would be significantly easier to abide health and environment requirements in a precast element factory than on site, as the alkali solution is caustic and hazardous to the environment.

If today's GP manufacturing technology had to be made mobile, the on-site GP construction cost would be unaffordable and GP usage financially unreasonable. The only place where low calcium GP composite usage on building sites seems feasible is in the countries and at time when the average daily temperature is high to sustain the polymerization reaction of the GP composite.

4.3. Geopolymer application as mortars

Geopolymer mortars possess similar properties as natural rocks like granite and marble. Geopolymer composite's durability characteristics, especially in harsh environments, poses it as an alternative to conventional cement mortars in building restoration. Researchers [179] have reported that metakaolin based GP with calcium carbonate (CaCO_3) and calcium hydroxide (Ca(OH)_2) in it can be used as mortar for the restoration purposes of historical buildings.

In 2012, Zeobond reported the use of a commercial GP concrete ready mix with steel reinforcement for the creation of slabs and footpaths in Melbourne (Australia). In 2011 and 2012, Zeobond and Rocla produced and tested according to Australian standards precast pipes, railway sleepers, and pavers and installed them in several construction projects [169].

4.4. Geopolymer application as fire resistant layer

In recent research, scientists investigated GP performance under elevated temperatures and compared it with OPC concrete specimens. They used Class C fly ash that was activated with

the solution consisting of sodium hydroxide and sodium silicate. Both GP and OPC concrete specimens were exposed to temperatures up to 1200 °C. The OPC based specimens showed severe cracking at temperatures above 800 °C while GP specimens showed an insignificant amount of visible cracks and no spalling even at high temperatures. The residual compressive strength for OPC based specimens (49 MPa) was lower than for GP specimens (54 MPa). From these results it was concluded that GP is suitable to be used as fire resistant coating or as whole material for structures where fire resistance and structural performance are crucial [38].

4.5. Geopolymer application as insulating layer

Researchers [180] have found that when metakaolin-based GP matrix is mixed together with sawdust, the resulting material can act as effective insulation material for buildings. If the water to biomass ratio is up to 2, then the material exhibits low heat conductivity (0.118–0.125 W/mK). This material poses potential for practical application as building insulation.

As all of the geopolymer compositions that have been subjected to microstructure assessments (**in Papers IV–VII**) have porosity and air void amount less than 10 % in uncracked state, they would not be suitable to be applied as an insulating material. Thus, there have been various studies with similar base compositions with the addition of foaming agent that have found it suitable for insulation purposes.

5. GEOPOLYMER COMPOSITE LONG-TERM ENVIRONMENTAL INFLUENCE

5.1. Environmental assessment of geopolymer long-term impact on the environment based on life cycle assessment

Life cycle assessment has been the main analytical mechanism that till today has supported valid claims that GP is an environmentally friendlier material than OPC based composites. A research done in Australia [181] looked into the hybrid life cycle assessment (hLCA) of greenhouse gas emissions from cement, concrete, and GP concrete.

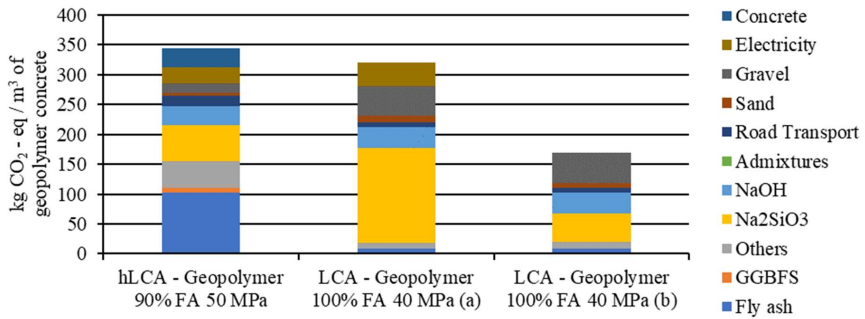


Fig. 11. Comparison of fly ash geopolymer concrete carbon footprint intensities of hLCA and LCA, made by the authors in [7] and [182], based on [7].

The researchers concluded that unlike life cycle assessment research that had previously been conducted by Davidovits and Grant hLCA (Fig. 12) shows an increase in greenhouse gas emissions for 50 MPa OPC concrete: 25 MPa OPC concrete, 25 MPa blended cement concrete, and 50 MPa GP concrete by 29 %, 22 %, 11–50 %, and 48–103 % (depending on emission allocation with sourcing of FA), respectively (Fig. 12).

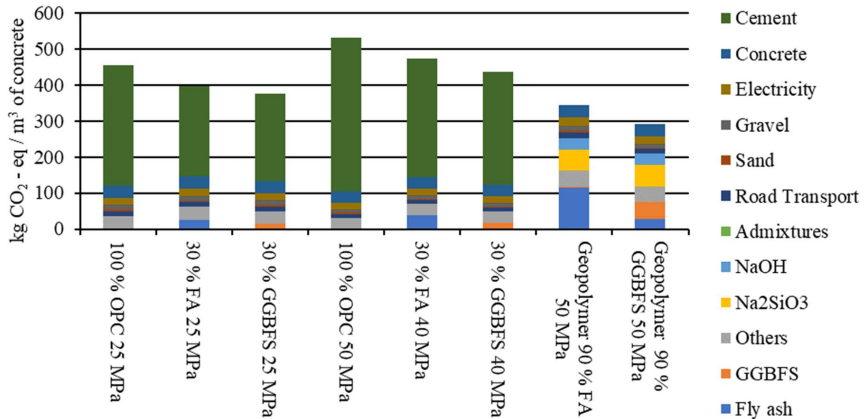


Fig. 12. Carbon footprint of 8 types of concrete according to hLCA [181].

Furthermore, it was concluded that the findings go hand in hand with other life cycle assessment research findings. In other words, GP concrete has the greatest potential to reduce greenhouse gas emissions in comparison to OPC and blended cement-based concrete. Fly ash and ground granulated blast furnace slag-based GP concrete can substantially reduce greenhouse gas emissions by 32 % and 43 %, respectively, as compared to OPC concrete with no loss in compressive strength using the economic allocation method. When compared with blended cement concrete, ground granulated blast furnace slag-based GP (16 %) has a higher reduction of greenhouse gas emissions than fly ash based GP (just 9 %). Other research [183] has a similar conclusion – GP has a 37 % lower global warming potential than OPC. It was also concluded that GP concrete shows worse results regarding energy requirements for its production. GP concrete shows a 287 % greater use of fossil fuel resources than OPC based concrete. It has to be mentioned that in this regard the literature is not consistent because some authors [184] claim that energy consumption related to GP concrete production is 48 % higher than for OPC concrete production, others [40] report that abiotic depletion of fossil fuels (ADPF) for GP concrete is 26 % lower than for OPC based concrete.

The authors in [185] have made similar life cycle assessment evaluations of GP concrete and OPC concrete usage impact on the environment. They concluded that considering factors such as ecosystem, human health and resources GP concrete shows less negative impact on the environment than cement-based concrete. The whole situation is represented in Fig. 13. Cement in concrete makes the greatest impact (76.42 %) of all ingredients in the concrete, while sodium hydroxide and sodium silicate in GP have only a combined impact of 59.97 % of all GP ingredients. If the sodium silicate is replaced with silica fume, then the impact is even more reduced. The global warming potential for GP concrete is reduced to 148 kg, 135 kg, and 133 kg of CO₂-e for GP without silica fume, GP with silica fume, and GP with silica fume and 47.61 % reduction of sodium silicate, respectively. In the meantime, cement-based concrete has 597.54 kg of CO₂ impact. It was also found that the impact of GP concrete on the environment is more affected by the transportation of raw materials than of ordinary cement concrete. For GP concrete it varies from 20.83–29.01 %, while for cement-based concrete it is 9.71 %. Researchers also claim that replacing cement with GP in concrete can reduce the costs of concrete by 10.87–17.77 %.

All in all, the environment gains from using GP composites instead of OPC composites lie in material location. The GP, researched in **Papers I–VII**, would be less environmentally damaging if they were used near the source of fly ash and alkali manufacturing facilities. Otherwise, all the gains from fly ash utilization in GP are lost by shipping impact on the environment. As fly ash is considered a waste material, it has to be used in areas where this waste is located or as close to the location as possible. The only way that the GP composite usage would be justified would be in the structures where extra resistance to the acidic or harsh outside environment impact is necessary. Otherwise, GP composites usage would have a higher negative impact on the environment than that of OPC based composites.

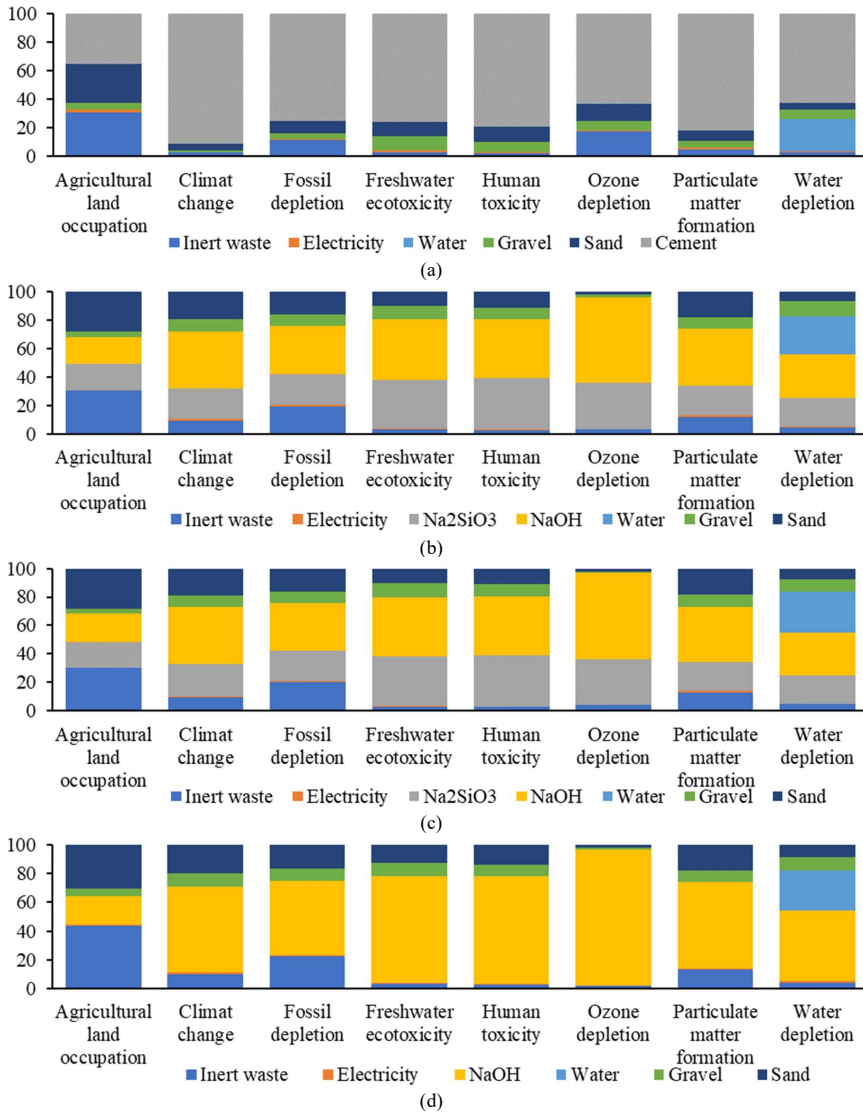


Fig. 13. Environmental impact from the ingredients of cement-based concrete (a), geopolymers concrete (b), geopolymers concrete with silica fume and sodium silicate (c), and geopolymers concrete with silica fume and without sodium silicate (d) [185].

CONCLUSIONS

The Thesis focuses on methodology development for long-term deformation influence assessment on innovative cement composite microstructure. The main conclusions are:

1. Geopolymer composites based on fly ash show remarkable mechanical properties. Plain geopolymer composites at the age of 7 days show compressive strength equal to C30/37 class Portland cement concrete. At the age of 28 days, plain geopolymer composites exhibit compressive strength not lower than C40/45 class Portland cement concrete, reaching up to 61.44 MPa for cylindrical specimens and 92.0 MPa for cube specimens.
2. Fiber reinforcement introduction into geopolymer composite is not beneficial in all cases. For compact tension specimens, the 1 % PVA fiber introduction led to 3.7 % lower tensile strength. In three-point bending, 1 % PVA fiber, 0.5 % PVA/0.5 % steel fiber and 1 % steel fiber reinforcement introduction led to 9 %, 14.2 %, and 23.2 % flexural strength reduction, respectively.
3. Fiber reinforcement introduction to geopolymer composite for creep strain reduction is beneficial in the case of flexural stress. Geopolymer composites with 1 % steel and 0.5 % PVA/0.5 % steel fiber reinforcement show 51.7 % and 2.7 % creep reduction in contrast to plain specimens. Creep strains for compact tension specimens do not decrease significantly when 1 % PVA fibers are introduced. In compression, 1 % and 5 % PP fiber introduction reduces creep strains by 21.2 % and 49.7 % in contrast to plain geopolymer.
4. The specific creep of geopolymer composites in compression is on average 85.92 % less than in tension. It shows that in tension, geopolymer composites have 7.5 higher specific creep than in compression that indicates that in tension, geopolymer composites are more prone to creep. In three-point bending, the 1 % steel fiber amount shows 37.1 % less specific creep than the plain geopolymer composite. Geopolymer composites in three-point bending show 99.18 % less specific creep than in compression and 99.88 % less than in tension. Furthermore, in compression, geopolymer composites show 13 % to 23 % lower specific creep than ordinary Portland cement-based composites.
5. Fiber introduction shows benefits in shrinkage strain reduction. For compact tension geopolymer composites, the 1 % PVA fiber reduces shrinkage strains by 54.21 %.
6. Regarding long-term property results, the methodology of long-term property determination in various stress-strain conditions was developed (**Patent I**) and patented.
7. Microstructure analysis of specimens that were exposed to long-term compressive load showed that fiber incorporation into the geopolymer matrix significantly increases the amount of air void into the mix. Fiber addition of 1 % would increase air entrapment by 0.61 % to 2.26 % in steel fibers, 1.88 % in 2.50 % PVA fibers, and 1 % to 2.26 % in waste steel fiber reinforced specimens. It also shows that air

entrapment throughout the specimen cross section decreases from 4.7 % to 10.3 % in contrast to the outer layers of cross section.

8. Air inclusion for compact tension specimens is on average 5.15 % higher than for the compression specimens. Furthermore, for PVA fiber reinforced compact tension specimens, it is on average 19.85 % to 26.29 % higher than for the plain geopolymer composites.
9. There are clear indications that the long-term properties of geopolymer composites are linked with microstructure composition – shrinkage cracks play a huge role, and in this case, fiber reinforcement improves the mechanical and long-term properties and reduces shrinkage effects.
10. Regarding the loading effect on the specimen cross section composition and further interaction with creep strains, at least with the applied load amount of 20 % from ultimate load, in compression, no indications of specimen cross section disintegration or rupture were found. In tension and three-point bending, cracks were observed for the loaded specimens. It further leads to conclusions that specimen shape, especially for heat cured geopolymer composite, leads to inner stresses that due to shrinkage, create micro cracks, and while in compression, micro cracking would not have an immediate visible effect on the long-term property amount in tension and three-point bending, where some part or all cross section is subjected to tensile stress, the long-term properties are influenced immediately.
11. Regarding the results of quantitative image analysis of the polished sections of long-term tested geopolymer composites, the method for determining the outside factor impact on concrete and cement composite microstructure in various stress-strain states (**Patent II**) was developed and applied in the patent.

REFERENCES

- [1] Z. Li, B. Delsaute, T. Lu, A. Kostiuchenko, S. Staquet, and G. Ye, "A comparative study on the mechanical properties, autogenous shrinkage and cracking proneness of alkali-activated concrete and ordinary Portland cement concrete," *Constr. Build. Mater.*, vol. 292, p. 123418, 2021, doi: 10.1016/j.conbuildmat.2021.123418.
- [2] B. A. Tayeh, D. M. A. Saffar, and R. Alyousef, "The Utilization of Recycled Aggregate in High Performance Concrete: A Review," *J. Mater. Res. Technol.*, vol. 9, no. 4, pp. 8469–8481, 2020, doi: 10.1016/j.jmrt.2020.05.126.
- [3] B. Singh, G. Ishwarya, M. Gupta, and S. K. Bhattacharyya, "Geopolymer concrete: A review of some recent developments," *Constr. Build. Mater.*, vol. 85, pp. 78–90, 2015, doi: 10.1016/j.conbuildmat.2015.03.036.
- [4] D. Suescum-Morales, D. Cantador-Fernández, J. R. Jiménez, and J. M. Fernández, "Mitigation of CO₂ emissions by hydrotalcites of Mg₃Al-CO₃ at 0 °C and high pressure," *Appl. Clay Sci.*, vol. 202, no. December 2020, 2021, doi: 10.1016/j.clay.2020.105950.
- [5] J. A. Ober, "Mineral commodity summaries 2018," Reston, VA, 2018, doi: 10.3133/70194932.
- [6] Y. H. M. Amran, R. Alyousef, H. Alabduljabbar, and M. El-Zeadani, "Clean production and properties of geopolymer concrete; A review," *J. Clean. Prod.*, vol. 251, p. 119679, 2020, doi: 10.1016/j.jclepro.2019.119679.
- [7] L. K. Turner and F. G. Collins, "Carbon dioxide equivalent (CO₂-e) emissions: A comparison between geopolymer and OPC cement concrete," *Constr. Build. Mater.*, vol. 43, pp. 125–130, 2013, doi: 10.1016/j.conbuildmat.2013.01.023.
- [8] J. G. J. Olivier, K. M. Schure, and J. A. H. W. Peters, "TRENDS IN GLOBAL CO₂ AND TOTAL GREENHOUSE GAS EMISSIONS Summary of the 2017 report," no. 2983, 2017, [Online]. Available: <http://www.pbl.nl/sites/default/files/cms/publicaties/pbl-2017-summary-trends-in-global-co2-and-total-greenhouse-gas-emissions-2983.pdf>
- [9] R. M. Andrew, "Global CO₂ emissions from cement production," *Earth Syst. Sci. Data*, vol. 10, no. 1, pp. 195–217, 2018, doi: 10.5194/essd-10-195-2018.
- [10] J. G. . Olivier and J. A. H. w. Peters, "TRENDS IN GLOBAL CO₂ AND TOTAL GREENHOUSE GAS: 2020 Report," *PBL Netherlands Environ. Assess. Agency, Hague.*, no. December, 2020.
- [11] H. Li, Q. Deng, J. Zhang, B. Xia, and M. Skitmore, "Assessing the life cycle CO₂ emissions of reinforced concrete structures: Four cases from China," *J. Clean. Prod.*, vol. 210, no. 38, pp. 1496–1506, 2019, doi: 10.1016/j.jclepro.2018.11.102.
- [12] A. Josa, A. Aguado, A. Cardim, and E. Byars, "Comparative analysis of the life cycle impact assessment of available cement inventories in the EU," *Cem. Concr. Res.*, vol. 37, no. 5, pp. 781–788, 2007, doi: 10.1016/j.cemconres.2007.02.004.
- [13] C. Valderrama, R. Granados, J. L. Cortina, C. M. Gasol, M. Guillem, and A. Josa, "Implementation of best available techniques in cement manufacturing: A life-cycle assessment study," *J. Clean. Prod.*, vol. 25, pp. 60–67, 2012, doi: 10.1016/j.jclepro.2011.11.055.
- [14] A. R. G. Azevedo *et al.*, "Analysis of the compactness and properties of the hardened state of mortars with recycling of construction and demolition waste (CDW)," *J. Mater. Res. Technol.*, vol. 9, no. 3, pp. 5942–5952, 2020, doi: 10.1016/j.jmrt.2020.03.122.
- [15] P. Zhang, Y. Zheng, K. Wang, and J. Zhang, "A review on properties of fresh and hardened geopolymer mortar," *Compos. Part B Eng.*, vol. 152, no. June, pp. 79–95, 2018, doi: 10.1016/j.compositesb.2018.06.031.
- [16] B. A. Tayeh, A. M. Zeyad, I. S. Agwa, and M. Amin, "Effect of elevated temperatures on mechanical properties of lightweight geopolymer concrete," *Case Stud. Constr. Mater.*, vol. 15, no. August, p. e00673, 2021, doi: 10.1016/j.cscm.2021.e00673.
- [17] B. C. Lippiatt and S. Ahmad, *Measuring the Life-Cycle Environmental and Economic Performance of Concrete: the Bees Approach*. 2004.
- [18] P. Duxson, S. W. Mallicoate, G. C. Lukey, W. M. Kriven, and J. S. J. van Deventer, "The effect of alkali and Si/Al ratio on the development of mechanical properties of metakaolin-based geopolymers," *Colloids Surfaces A Physicochem. Eng. Asp.*, vol. 292, no. 1, pp. 8–20, 2007, doi: 10.1016/j.colsurfa.2006.05.044.
- [19] S. E. W. Djwanto Hardjito Dody M. J. Sumajouw, and B. Vijaya Rangan, "On the Development of Fly Ash-Based Geopolymer Concrete," *ACI Mater. J.*, vol. 101, no. 6, doi: 10.14359/13485.
- [20] A. Castel, S. J. Foster, T. Ng, J. G. Sanjayan, and R. I. Gilbert, "Creep and drying shrinkage of a blended slag and low calcium fly ash geopolymer Concrete," *Mater. Struct. Constr.*, vol. 49, no. 5, pp. 1619–1628, 2016, doi: 10.1617/s11527-015-0599-1.
- [21] K. Sagoe-Crentsil, T. Brown, and A. Taylor, "Drying shrinkage and creep performance of geopolymer

- concrete,” *J. Sustain. Cem. Mater.*, vol. 2, no. 1, pp. 35–42, 2013, doi: 10.1080/21650373.2013.764963.
- [22] W. S.E., “Creep Behaviour of Fly Ash-Based Geopolymer Concrete,” *Civ. Eng. Dimens.*, vol. 12, no. 2, 2010, doi: 10.9744/ced.12.2.73-78.
- [23] S. E. Wallah and B. V. Rangan, “Low-Calcium Fly Ash Based,” pp. 1–107, 2006, [Online]. Available: <https://espace.curtin.edu.au/handle/20.500.11937/34322>
- [24] S. Chen, C. Wu, and D. Yan, “Binder-scale creep behavior of metakaolin-based geopolymer,” *Cem. Concr. Res.*, vol. 124, no. July, p. 105810, 2019, doi: 10.1016/j.cemconres.2019.105810.
- [25] I. Khan, T. Xu, A. Castel, R. I. Gilbert, and M. Babae, “Risk of early age cracking in geopolymer concrete due to restrained shrinkage,” *Constr. Build. Mater.*, vol. 229, p. 116840, 2019, doi: 10.1016/j.conbuildmat.2019.116840.
- [26] A. A. Melo Neto, M. A. Cincotto, and W. Repette, “Drying and autogenous shrinkage of pastes and mortars with activated slag cement,” *Cem. Concr. Res.*, vol. 38, no. 4, pp. 565–574, 2008, doi: 10.1016/j.cemconres.2007.11.002.
- [27] F. Puertas, T. Amat, A. Fernández-Jiménez, and T. Vázquez, “Mechanical and durable behaviour of alkaline cement mortars reinforced with polypropylene fibres,” *Cem. Concr. Res.*, vol. 33, no. 12, pp. 2031–2036, 2003, doi: 10.1016/S0008-8846(03)00222-9.
- [28] K. Pimraksa, P. Chindaprasirt, A. Rungchet, K. Sagoe-crentsil, and T. Sato, “Lightweight geopolymer made of highly porous siliceous materials with various,” *Mater. Sci. Eng. A*, vol. 528, no. 21, pp. 6616–6623, 2011, doi: 10.1016/j.msea.2011.04.044.
- [29] M. T. Marvila, A. R. G. de Azevedo, and C. M. F. Vieira, “Reaction mechanisms of alkali-activated materials,” *Rev. IBRACON Estruturas e Mater.*, vol. 14, no. 3, pp. 1–26, 2021, doi: 10.1590/s1983-41952021000300009.
- [30] J. He, Y. Jie, J. Zhang, Y. Yu, and G. Zhang, “Synthesis and characterization of red mud and rice husk ash-based geopolymer composites,” *Cem. Concr. Compos.*, vol. 37, no. 1, pp. 108–118, 2013, doi: 10.1016/j.cemconcomp.2012.11.010.
- [31] U. Rattanasak and P. Chindaprasirt, “Influence of NaOH solution on the synthesis of fly ash geopolymer,” *Miner. Eng.*, vol. 22, no. 12, pp. 1073–1078, 2009, doi: 10.1016/j.mineng.2009.03.022.
- [32] J. Temuujin, W. Rickard, M. Lee, and A. Van Riessen, “Preparation and thermal properties of fire resistant metakaolin-based geopolymer-type coatings,” *J. Non. Cryst. Solids*, vol. 357, no. 5, pp. 1399–1404, 2011, doi: 10.1016/j.jnoncrysol.2010.09.063.
- [33] M. L. Kumar and V. Revathi, “Microstructural Properties of Alkali-Activated Metakaolin and Bottom Ash Geopolymer,” *Arab. J. Sci. Eng.*, vol. 45, no. 5, pp. 4235–4246, 2020, doi: 10.1007/s13369-020-04417-6.
- [34] S. Pilehvar *et al.*, “Effect of freeze-thaw cycles on the mechanical behavior of geopolymer concrete and Portland cement concrete containing micro-encapsulated phase change materials,” *Constr. Build. Mater.*, vol. 200, pp. 94–103, 2019, doi: 10.1016/j.conbuildmat.2018.12.057.
- [35] R. H. Haddad and O. Alshbuol, “Production of geopolymer concrete using natural pozzolan: A parametric study,” *Constr. Build. Mater.*, vol. 114, pp. 699–707, 2016, doi: 10.1016/j.conbuildmat.2016.04.011.
- [36] M. Olivia and H. Nikraz, “Properties of fly ash geopolymer concrete designed by Taguchi method,” *Mater. Des.*, vol. 36, pp. 191–198, 2012, doi: 10.1016/j.matdes.2011.10.036.
- [37] A. E. Kurtoglu *et al.*, “Mechanical and durability properties of fly ash and slag based geopolymer concrete,” *Advances in Concrete Construction*, vol. 6, no. 4, pp. 345–362, 2018, doi: 10.12989/acc.2018.6.4.345.
- [38] X. Jiang, R. Xiao, M. Zhang, W. Hu, Y. Bai, and B. Huang, “A laboratory investigation of steel to fly ash-based geopolymer paste bonding behavior after exposure to elevated temperatures,” *Constr. Build. Mater.*, vol. 254, p. 119267, 2020, doi: 10.1016/j.conbuildmat.2020.119267.
- [39] S. Luhar, I. Luhar, and R. Gupta, “Durability performance evaluation of green geopolymer concrete,” *Eur. J. Environ. Civ. Eng.*, vol. 0, no. 0, pp. 1–49, 2020, doi: 10.1080/19648189.2020.1847691.
- [40] D. A. Salas, A. D. Ramirez, N. Ulloa, H. Baykara, and A. J. Boero, “Life cycle assessment of geopolymer concrete,” *Constr. Build. Mater.*, vol. 190, pp. 170–177, 2018, doi: 10.1016/j.conbuildmat.2018.09.123.
- [41] A. Hassan, M. Arif, and M. Shariq, *Influence of microstructure of geopolymer concrete on its mechanical properties – A review*, vol. 35. Springer Singapore, 2020, doi: 10.1007/978-981-13-7480-7_10.
- [42] F. Farooq *et al.*, “Geopolymer concrete as sustainable material: A state of the art review,” *Constr. Build. Mater.*, vol. 306, no. March, p. 124762, 2021, doi: 10.1016/j.conbuildmat.2021.124762.
- [43] “Coal Combustion Byproducts, Kentucky Geological Survey, University of Kentucky.” <https://www.uky.edu/KGS/coal/coal-for-combustionbyproducts.php> (accessed Feb. 03, 2022).
- [44] G. Couto Mantese and D. Capaldo Amaral, “Comparison of industrial symbiosis indicators through agent-based modeling,” *J. Clean. Prod.*, vol. 140, pp. 1652–1671, 2017, doi: 10.1016/j.jclepro.2016.09.142.
- [45] P. Poudenx, “The effect of transportation policies on energy consumption and greenhouse gas emission from urban passenger transportation,” *Transp. Res. Part A Policy Pract.*, vol. 42, no. 6, pp. 901–909, 2008, doi: 10.1016/j.tra.2008.01.013.

- [46] R. Gailitis *et al.*, “Mechanical Properties of Geopolymer Concretes Reinforced with Waste Steel Fibers,” *IOP Conf. Ser. Mater. Sci. Eng.*, vol. 660, no. 1, 2019, doi: 10.1088/1757-899X/660/1/012007.
- [47] R. Gailitis *et al.*, “Long-Term Deformation Properties of a Carbon-Fiber-Reinforced Alkali-Activated Cement Composite,” *Mech. Compos. Mater.*, vol. 56, no. 1, pp. 85–92, 2020, doi: 10.1007/s11029-020-09862-w.
- [48] R. Gailitis, A. Sprince, T. Kozlovskis, L. Radina, and L. Pakrastins, “Long-Term Properties of Different Fiber Reinforcement Effect on Fly Ash-Based Geopolymer Composite,” pp. 1–8, 2021.
- [49] R. Gailitis, A. Sprince, L. Pakrastins, K. Korniejenko, and T. Kozlovskis, “REINFORCED AND PLAIN GEOPOLYMER CONCRETE SPECIMEN CROSS-SECTION COMPOSITION INFLUENCE ON CREEP STRAINS,” no. 1, pp. 739–746.
- [50] R. Gailitis, A. Sprince, L. Pakrastins, K. Korniejenko, and T. Kozlovskis, *Plain Geopolymer Concrete Cross-Section Surface Analysis After Creep and Shrinkage Tests in Compression and Tension*, vol. 31. Springer International Publishing, 2021, doi: 10.1007/978-3-030-72921-9_2.
- [51] R. Gailitis, A. Sprince, L. Pakrastins, P. Bazan, and K. Korniejenko, “Plain and PVA fibre-reinforced geopolymer compact tension specimen critical area surface composition assessment,” *Vide. Tehnol. Resur. – Environ. Technol. Resour.*, vol. 3, pp. 72–77, 2021, doi: 10.17770/str2021vol3.6569.
- [52] R. Gailitis, L. Pakrastins, A. Sprince, L. Radina, G. Sakale, and K. Miernik, “Different Fiber Reinforcement Effects on Fly Ash-Based Geopolymer Long-Term Deflection in Three-Point Bending and Microstructure,” *Materials (Basel)*, vol. 15, no. 23, 2022, doi: 10.3390/ma15238512.
- [53] W. Meng and K. H. Khayat, “Mechanical properties of ultra-high-performance concrete enhanced with graphite nanoplatelets and carbon nanofibers,” *Compos. Part B Eng.*, vol. 107, pp. 113–122, 2016, doi: 10.1016/j.compositesb.2016.09.069.
- [54] N. Ranjbar and M. Zhang, “Fiber-reinforced geopolymer composites: A review,” *Cem. Concr. Compos.*, vol. 107, no. February 2019, p. 103498, 2020, doi: 10.1016/j.cemconcomp.2019.103498.
- [55] M. Mastali, A. Dalvand, A. R. Sattarifarid, Z. Abdollahnejad, and M. Illikainen, “Characterization and optimization of hardened properties of self-consolidating concrete incorporating recycled steel, industrial steel, polypropylene and hybrid fibers,” *Compos. Part B Eng.*, vol. 151, no. May, pp. 186–200, 2018, doi: 10.1016/j.compositesb.2018.06.021.
- [56] P. Sukontasukkul, P. Pongsopha, P. Chindaprasirt, and S. Songpiriyakij, “Flexural performance and toughness of hybrid steel and polypropylene fibre reinforced geopolymer,” *Constr. Build. Mater.*, vol. 161, pp. 37–44, 2018, doi: 10.1016/j.conbuildmat.2017.11.122.
- [57] A. Bhutta, P. H. R. Borges, C. Zanotti, M. Farooq, and N. Banthia, “Flexural behavior of geopolymer composites reinforced with steel and polypropylene macro fibers,” *Cem. Concr. Compos.*, vol. 80, pp. 31–40, 2017, doi: 10.1016/j.cemconcomp.2016.11.014.
- [58] M. Farooq, A. Bhutta, and N. Banthia, “Tensile performance of eco-friendly ductile geopolymer composites (EDGC) incorporating different micro-fibers,” *Cem. Concr. Compos.*, vol. 103, no. January, pp. 183–192, 2019, doi: 10.1016/j.cemconcomp.2019.05.004.
- [59] N. Ranjbar *et al.*, “A comprehensive study of the polypropylene fiber reinforced fly ash based geopolymer,” *PLoS One*, vol. 11, no. 1, 2016, doi: 10.1371/journal.pone.0147546.
- [60] T. F. Cooke, “Inorganic Fibers – A Literature Review,” *J. Am. Ceram. Soc.*, vol. 74, no. 12, pp. 2959–2978, 1991, doi: 10.1111/j.1151-2916.1991.tb04289.x.
- [61] L. Yan, B. Kasal, and L. Huang, “A review of recent research on the use of cellulosic fibres, their fibre fabric reinforced cementitious, geo-polymer and polymer composites in civil engineering,” *Compos. Part B Eng.*, vol. 92, pp. 94–132, 2016, doi: 10.1016/j.compositesb.2016.02.002.
- [62] R. F. Zollo, “Fiber-reinforced concrete: an overview after 30 years of development,” *Cem. Concr. Compos.*, vol. 19, no. 2, pp. 107–122, 1997, doi: [https://doi.org/10.1016/S0958-9465\(96\)00046-7](https://doi.org/10.1016/S0958-9465(96)00046-7).
- [63] S. Chand, “Carbon fibers for composites,” *J. Mater. Sci.*, vol. 35, no. 6, pp. 1303–1313, 2000, doi: 10.1023/A:1004780301489.
- [64] M. Mehrali *et al.*, “Blending Electronics with the Human Body: A Pathway toward a Cybernetic Future,” *Adv. Sci.*, vol. 5, no. 10, 2018, doi: 10.1002/advs.201700931.
- [65] A. Bentur and S. Mindess, *Fibre reinforced cementitious composites*. CRC Press, 2006.
- [66] R. S. Olivito and F. A. Zuccarello, “An experimental study on the tensile strength of steel fiber reinforced concrete,” *Compos. Part B Eng.*, vol. 41, no. 3, pp. 246–255, 2010, doi: 10.1016/j.compositesb.2009.12.003.
- [67] M. H. Al-Majidi, A. Lampropoulos, and A. B. Cundy, “Steel fibre reinforced geopolymer concrete (SFRGC) with improved microstructure and enhanced fibre-matrix interfacial properties,” *Constr. Build. Mater.*, vol. 139, pp. 286–307, 2017, doi: 10.1016/j.conbuildmat.2017.02.045.
- [68] R. Wang, X. Gao, J. Zhang, and G. Han, “Spatial distribution of steel fibers and air bubbles in UHPC cylinder determined by X-ray CT method,” *Constr. Build. Mater.*, vol. 160, pp. 39–47, 2018, doi: 10.1016/j.conbuildmat.2017.11.030.

- [69] A. J. Sedriks, "Corrosion of stainless steel, 2," 1996.
- [70] C. A. Schunemann, "Copper coated steel." Google Patents, Mar. 28, 1967.
- [71] N. C. Hosking, M. A. Ström, P. H. Shipway, and C. D. Rudd, "Corrosion resistance of zinc-magnesium coated steel," *Corros. Sci.*, vol. 49, no. 9, pp. 3669–3695, 2007, doi: 10.1016/j.corsci.2007.03.032.
- [72] D. D. L. Chung, *Carbon composites: composites with carbon fibers, nanofibers, and nanotubes*. Butterworth-Heinemann, 2016.
- [73] A. Piretti, M. Traina, and A. Bunsell, "Handbook of tensile properties of textile and technical fibers." Cambridge: Woodhead Publishing Limited) p, 2009.
- [74] R. Siddique, J. Khatib, and I. Kaur, "Use of recycled plastic in concrete: A review," vol. 28, pp. 1835–1852, 2008, doi: 10.1016/j.wasman.2007.09.011.
- [75] Y. Ko, "Investigation of Polymorphism for Amorphous and Semi-Crystalline Poly (-Ethylene Terephthalate-) Using High-Pressure Brillouin Spectroscopy," vol. 70, no. 4, pp. 382–388, 2017, doi: 10.3938/jkps.70.382.
- [76] J. P. M. Mwangi, *Flexural behavior of sisal fiber reinforced concrete beams*. University of California, Davis, 2001.
- [77] A. Larena and G. Pinto, "The Effect of Surface Roughness and Crystallinity on the Light Scattering of Polyethylene Tubular Blown Films *," vol. 33, no. 12, 1993.
- [78] B. Mu, C. Meyer, and S. Shimanovich, "Improving the interface bond between fiber mesh and cementitious matrix," vol. 32, no. January 2001, pp. 783–787, 2002.
- [79] A. E. Richardson, "Compressive strength of concrete with polypropylene fibre additions," 2006, doi: 10.1108/02630800610666673.
- [80] N. Banthia and R. Gupta, "Influence of polypropylene fiber geometry on plastic shrinkage cracking in concrete," vol. 36, pp. 1263–1267, 2006, doi: 10.1016/j.cemconres.2006.01.010.
- [81] T. Ochi, S. Okubo, and K. Fukui, "Development of recycled PET fiber and its application as concrete-reinforcing fiber," vol. 29, pp. 448–455, 2007, doi: 10.1016/j.cemconcomp.2007.02.002.
- [82] C. Redon, V. C. Li, C. Wu, H. Hoshiro, T. Saito, and A. Ogawa, "Measuring and modifying interface properties of PVA fibers in ECC matrix," *J. Mater. Civ. Eng.*, vol. 13, no. 6, pp. 399–406, 2001, doi: 10.1061/(ASCE)0899-1561(2001)13:6(399).
- [83] V. C. Li, C. Wu, S. Wang, A. Ogawa, and T. Saito, "Interface tailoring for strain-hardening polyvinyl alcohol-engineered cementitious composite (PVA-ECC)," *ACI Mater. J.*, vol. 99, no. 5, pp. 463–472, 2002, [Online]. Available: <https://www.scopus.com/inward/record.uri?eid=2-s2.0-0036767230&partnerID=40&md5=241b9eb0215ca919c93679653a6baed4>
- [84] J. Claramunt, R. Dias, and T. Filho, "Cellulosic fiber reinforced cement-based composites : A review of recent," vol. 79, pp. 115–128, 2015, doi: 10.1016/j.conbuildmat.2015.01.035.
- [85] Z. N. Azwa, B. F. Yousif, A. C. Manalo, and W. Karunasena, "A review on the degradability of polymeric composites based on natural fibres," *Mater. Des.*, vol. 47, pp. 424–442, 2013, doi: 10.1016/j.matdes.2012.11.025.
- [86] R. Chen, S. Ahmari, and L. Zhang, "Utilization of sweet sorghum fiber to reinforce fly ash-based geopolymer," pp. 2548–2558, 2014, doi: 10.1007/s10853-013-7950-0.
- [87] M. M. Al-mashhadani, O. Canpolat, Y. Aygörmez, M. Uysal, and S. Erdem, "Mechanical and microstructural characterization of fiber reinforced fly ash based geopolymer composites," *Constr. Build. Mater.*, vol. 167, pp. 505–513, 2018, doi: 10.1016/j.conbuildmat.2018.02.061.
- [88] L. N. Assi, E. Eddie Deaver, and P. Ziehl, "Effect of source and particle size distribution on the mechanical and microstructural properties of fly Ash-Based geopolymer concrete," *Constr. Build. Mater.*, vol. 167, pp. 372–380, 2018, doi: 10.1016/j.conbuildmat.2018.01.193.
- [89] A. Palomo, M. W. Grutzeck, and M. T. Blanco, "Alkali-activated fly ashes: A cement for the future," *Cem. Concr. Res.*, vol. 29, no. 8, pp. 1323–1329, 1999, doi: 10.1016/S0008-8846(98)00243-9.
- [90] S. Songpiriyakij, T. Kubprasit, C. Jaturapitakkul, and P. Chindaprasit, "Compressive strength and degree of reaction of biomass- and fly ash-based geopolymer," *Constr. Build. Mater.*, vol. 24, no. 3, pp. 236–240, 2010, doi: 10.1016/j.conbuildmat.2009.09.002.
- [91] E. Vasconcelos, S. Fernandes, B. De Aguiar, and F. Pacheco-Torgal, "Concrete retrofitting using CFRP and geopolymer mortars," *Mater. Sci. Forum*, vol. 730–732, pp. 427–432, 2013, doi: 10.4028/www.scientific.net/MSF.730-732.427.
- [92] C. a. Strydom and J. C. Swanepoel, "Utilisation of fly ash in a geopolymeric material," *Appl. Geochemistry*, vol. 17, no. 8, pp. 1143–1148, 2002.
- [93] G. Lavanya and J. Jegan, "Durability Study on High Calcium Fly Ash Based Geopolymer Concrete," *Adv. Mater. Sci. Eng.*, vol. 2015, 2015, doi: 10.1155/2015/731056.
- [94] T. Bakharev, "Resistance of geopolymer materials to acid attack," *Cem. Concr. Res.*, vol. 35, no. 4, pp. 658–670, 2005, doi: 10.1016/j.cemconres.2004.06.005.
- [95] D. W. Law, A. A. Adam, T. K. Molyneaux, I. Patnaikuni, and A. Wardhono, "Long term durability

- properties of class F fly ash geopolymer concrete,” *Mater. Struct. Constr.*, vol. 48, no. 3, pp. 721–731, 2014, doi: 10.1617/s11527-014-0268-9.
- [96] H. J. Zhuang, H. Y. Zhang, and H. Xu, “Resistance of geopolymer mortar to acid and chloride attacks,” *Procedia Eng.*, vol. 210, pp. 126–131, 2017, doi: 10.1016/j.proeng.2017.11.057.
- [97] O. F. Nnaemeka and N. B. Singh, “Durability properties of geopolymer concrete made from fly ash in presence of Kaolin,” *Mater. Today Proc.*, vol. 29, pp. 781–784, 2019, doi: 10.1016/j.matpr.2020.04.696.
- [98] C. Tennakoon, A. Shayan, J. G. Sanjayan, and A. Xu, “Chloride ingress and steel corrosion in geopolymer concrete based on long term tests,” *Mater. Des.*, vol. 116, pp. 287–299, 2017, doi: 10.1016/j.matdes.2016.12.030.
- [99] C. Gunasekara, D. W. Law, and S. Setunge, “Long term permeation properties of different fly ash geopolymer concretes,” *Constr. Build. Mater.*, vol. 124, pp. 352–362, 2016, doi: 10.1016/j.conbuildmat.2016.07.121.
- [100] W. H. Lee, J. H. Wang, Y. C. Ding, and T. W. Cheng, “A study on the characteristics and microstructures of GGBS/FA based geopolymer paste and concrete,” *Constr. Build. Mater.*, vol. 211, pp. 807–813, 2019, doi: 10.1016/j.conbuildmat.2019.03.291.
- [101] K. Sagoe-Crentsil, T. Brown, and A. Taylor, “Drying shrinkage and creep performance of geopolymer concrete,” *J. Sustain. Cem. Mater.*, vol. 2, no. 1, pp. 35–42, Mar. 2013, doi: 10.1080/21650373.2013.764963.
- [102] Z. Zhang, J. L. Provis, A. Reid, and H. Wang, “Mechanical, thermal insulation, thermal resistance and acoustic absorption properties of geopolymer foam concrete,” *Cem. Concr. Compos.*, vol. 62, pp. 97–105, 2015, doi: 10.1016/j.cemconcomp.2015.03.013.
- [103] D. L. Y. Kong, J. G. Sanjayan, and K. Sagoe-Crentsil, “Comparative performance of geopolymers made with metakaolin and fly ash after exposure to elevated temperatures,” *Cem. Concr. Res.*, vol. 37, no. 12, pp. 1583–1589, 2007, doi: 10.1016/j.cemconres.2007.08.021.
- [104] R. L’Hermite, *What do we know about plastic deformation and creep of concrete?* Waterways Experiment Station, 1960.
- [105] C. Hua, *Analyses et modélisations du retrait d’autodessiccation de la pâte de ciment durcissante*, no. OA15. 1995.
- [106] R. Le Roy, R. L. E. Roy, and P. Acker, “Déformations instantanées et différées des bétons à hautes performances,” 2010.
- [107] A. Sprince, L. Pakraštīņš, L. Radiņa, R. Gailītis, and T. Kozlovskis, “Paņēmiens betona un cementa kompozītu ilglaicīgo īpašību noteikšanai dažādos sprieguma stāvokļos/Method for Determination of Long-Term Properties of Concrete and Cement Composites in Various Stress Conditions,” 15659B, 2023
- [108] W. Liu, H. Zhou, S. Zhang, and S. Jiang, “Constitutive model of concrete creep damage considering the deterioration of creep parameters,” *Constr. Build. Mater.*, vol. 308, no. October, p. 125047, 2021, doi: 10.1016/j.conbuildmat.2021.125047.
- [109] Z. P. Bazant, M. H. Hubler, and Q. Yu, “Excessive Creep Deflection: An Awakening,” *Concr. Int.*, vol. 33, no. 8, pp. 44–46, 2011.
- [110] J. M. Torrenti and R. Le Roy, “Analysis of some basic creep tests on concrete and their implications for modeling,” *Struct. Concr.*, vol. 19, no. 2, pp. 483–488, 2018, doi: 10.1002/suco.201600197.
- [111] J. Baronet, L. Sorelli, J. P. Charron, M. Vandamme, and J. Sanahuja, “A two-scale method to rapidly characterize the logarithmic basic creep of concrete by coupling microindentation and uniaxial compression creep test,” *Cem. Concr. Compos.*, vol. 125, no. November 2019, p. 104274, 2022, doi: 10.1016/j.cemconcomp.2021.104274.
- [112] S. A. Altoubat and D. A. Lange, “The Pickett effect at early age and experiment separating its mechanisms in tension,” *Mater. Struct.*, vol. 35, no. 4, pp. 211–218, 2002, doi: 10.1007/BF02533082.
- [113] J. Sanahuja and L. Dormieux, “Creep of a C-S-H gel: A micromechanical approach,” *An. Acad. Bras. Cienc.*, vol. 82, no. 1, pp. 25–41, 2010, doi: 10.1590/s0001-37652010000100004.
- [114] L. Dormieux, J. Sanahuja, and S. Maghous, “Influence of capillary effects on strength of non-saturated porous media,” *Comptes Rendus - Mec.*, vol. 334, no. 1, pp. 19–24, 2006, doi: 10.1016/j.crme.2005.11.004.
- [115] S. Liang and Y. Wei, “Methodology of obtaining intrinsic creep property of concrete by flexural deflection test,” *Cem. Concr. Compos.*, vol. 97, no. April 2018, pp. 288–299, 2019, doi: 10.1016/j.cemconcomp.2019.01.003.
- [116] Y. Zhao *et al.*, “Creep Behavior of Intact and Cracked Limestone Under Multi-Level Loading and Unloading Cycles,” *Rock Mech. Rock Eng.*, vol. 50, no. 6, pp. 1409–1424, 2017, doi: 10.1007/s00603-017-1187-1.
- [117] L. Li, A. G. P. Dabarera, and V. Dao, “Basic tensile creep of concrete with and without superabsorbent polymers at early ages,” *Constr. Build. Mater.*, vol. 320, no. July 2020, p. 126180, 2022, doi: 10.1016/j.conbuildmat.2021.126180.
- [118] R. I. Gilbert and G. Ranzi, *Time-Dependent Behaviour of Concrete Structures*. 2010. doi:

- 10.1201/9781482288711.
- [119] Z. Q. Cheng, R. Zhao, Y. Yuan, F. Li, A. Castel, and T. Xu, "Ageing coefficient for early age tensile creep of blended slag and low calcium fly ash geopolymer concrete," *Constr. Build. Mater.*, vol. 262, p. 119855, 2020, doi: 10.1016/j.conbuildmat.2020.119855.
- [120] K. Kovler, S. Igarashi, and A. Bentur, "Tensile creep behavior of high strength concretes at early ages," *Mater. Struct. Constr.*, vol. 32, no. 219, pp. 383–387, 1999, doi: 10.1007/bf02479631.
- [121] S. A. Altoubat and D. A. Lange, "Tensile basic creep: Measurements and behavior at early age," *ACI Mater. J.*, vol. 98, no. 5, pp. 386–393, 2001, doi: 10.14359/10728.
- [122] A. B. Hossain and J. Weiss, "Assessing residual stress development and stress relaxation in restrained concrete ring specimens," *Cem. Concr. Compos.*, vol. 26, no. 5, pp. 531–540, 2004, doi: 10.1016/S0958-9465(03)00069-6.
- [123] P. Rossi, J. L. Tailhan, and F. Le Maou, "Comparison of concrete creep in tension and in compression: Influence of concrete age at loading and drying conditions," *Cem. Concr. Res.*, vol. 51, pp. 78–84, 2013, doi: 10.1016/j.cemconres.2013.04.001.
- [124] D. S. Artrushi, "Tensile and Compressive Creep of Early Age Concrete : Testing and Modelling," *Sci. Technol.*, no. 3377, p. 314, 2003.
- [125] I. Khan, T. Xu, A. Castel, and R. I. Gilbert, "Early-age tensile creep and shrinkage-induced cracking in internally restrained concrete members," *Mag. Concr. Res.*, vol. 71, no. 22, pp. 1167–1179, 2019, doi: 10.1680/jmacr.18.00038.
- [126] C. H. Un, J. G. Sanjayan, R. San Nicolas, and J. S. J. Van Deventer, "Predictions of long-term deflection of geopolymer concrete beams," *Constr. Build. Mater.*, vol. 94, pp. 10–19, 2015, doi: 10.1016/j.conbuildmat.2015.06.030.
- [127] M. T. Junaid, A. Elbana, and S. Altoubat, "Flexural response of geopolymer and fiber reinforced geopolymer concrete beams reinforced with GFRP bars and strengthened using CFRP sheets," *Structures*, vol. 24, no. January, pp. 666–677, 2020, doi: 10.1016/j.istruc.2020.02.003.
- [128] R. J. Thomas, D. Lezama, and S. Peethamparan, "On drying shrinkage in alkali-activated concrete: Improving dimensional stability by aging or heat-curing," *Cem. Concr. Res.*, vol. 91, pp. 13–23, 2017, doi: 10.1016/j.cemconres.2016.10.003.
- [129] B. Zhang, H. Zhu, Y. Cheng, G. F. Huseien, and K. W. Shah, "Shrinkage mechanisms and shrinkage-mitigating strategies of alkali-activated slag composites: A critical review," *Constr. Build. Mater.*, vol. 318, no. November 2021, p. 125993, 2022, doi: 10.1016/j.conbuildmat.2021.125993.
- [130] M. N. Amin, J. S. Kim, T. T. Dat, and J. K. Kim, "Improving test methods to measure early age autogenous shrinkage in concrete based on air cooling," *IES J. Part A Civ. Struct. Eng.*, vol. 3, no. 4, pp. 244–256, 2010, doi: 10.1080/19373260.2010.522314.
- [131] Z. Abdollahnejad, M. Mastali, B. Woof, and M. Illikainen, "High strength fiber reinforced one-part alkali activated slag/fly ash binders with ceramic aggregates: Microscopic analysis, mechanical properties, drying shrinkage, and freeze-thaw resistance," *Constr. Build. Mater.*, vol. 241, p. 118129, 2020, doi: 10.1016/j.conbuildmat.2020.118129.
- [132] D. P. Bentz, "A review of early-age properties of cement-based materials," *Cem. Concr. Res.*, vol. 38, no. 2, pp. 196–204, 2008, doi: 10.1016/j.cemconres.2007.09.005.
- [133] H. Ye and A. Radlińska, "A Review and Comparative Study of Existing Shrinkage Prediction Models for Portland and Non-Portland Cementitious Materials," *Adv. Mater. Sci. Eng.*, vol. 2016, pp. 10–14, 2016, doi: 10.1155/2016/2418219.
- [134] C. Song, Y. C. Choi, and S. Choi, "Effect of internal curing by superabsorbent polymers – Internal relative humidity and autogenous shrinkage of alkali-activated slag mortars," *Constr. Build. Mater.*, vol. 123, pp. 198–206, 2016, doi: 10.1016/j.conbuildmat.2016.07.007.
- [135] Z. Y. Qu, Q. Yu, Y. D. Ji, F. Gauvin, and I. K. Voets, "Mitigating shrinkage of alkali activated slag with biofilm," *Cem. Concr. Res.*, vol. 138, no. September, 2020, doi: 10.1016/j.cemconres.2020.106234.
- [136] E. Adesanya, A. Aladejare, A. Adediran, A. Lawal, and M. Illikainen, "Predicting shrinkage of alkali-activated blast furnace-fly ash mortars using artificial neural network (ANN)," *Cem. Concr. Compos.*, vol. 124, no. August, p. 104265, 2021, doi: 10.1016/j.cemconcomp.2021.104265.
- [137] S. K. Nath and S. Kumar, "Reaction kinetics of fly ash geopolymerization: Role of particle size controlled by using ball mill," *Adv. Powder Technol.*, vol. 30, no. 5, pp. 1079–1088, 2019, doi: 10.1016/j.apt.2019.03.003.
- [138] S. K. Nath and S. Kumar, "Role of alkali concentration on reaction kinetics of fly ash geopolymerization," *J. Non. Cryst. Solids*, vol. 505, no. September 2018, pp. 241–251, 2019, doi: 10.1016/j.jnoncrysol.2018.11.007.
- [139] Y. Ling, K. Wang, X. Wang, and S. Hua, "Effects of mix design parameters on heat of geopolymerization, set time, and compressive strength of high calcium fly ash geopolymer," *Constr. Build. Mater.*, vol. 228, p. 116763, 2019, doi: 10.1016/j.conbuildmat.2019.116763.

- [140] Z. Xie and Y. Xi, "Hardening mechanisms of an alkaline-activated class F fly ash," *Cem. Concr. Res.*, vol. 31, no. 9, pp. 1245–1249, 2001, doi: 10.1016/S0008-8846(01)00571-3.
- [141] M. Criado, A. Palomo, and A. Fernández-Jiménez, "Alkali activation of fly ashes. Part 1: Effect of curing conditions on the carbonation of the reaction products," *Fuel*, vol. 84, no. 16, pp. 2048–2054, 2005, doi: 10.1016/j.fuel.2005.03.030.
- [142] P. Duxson, A. Fernández-Jiménez, J. L. Provis, G. C. Lukey, A. Palomo, and J. S. J. Van Deventer, "Geopolymer technology: The current state of the art," *J. Mater. Sci.*, vol. 42, no. 9, pp. 2917–2933, 2007, doi: 10.1007/s10853-006-0637-z.
- [143] V. D. Glukhovskiy, G. S. Rostovskaja, and G. V. Rumyna, "High strength slag-alkaline cements," in *Proceedings of the seventh international congress on the chemistry of cement*, 1980, vol. 3, pp. 164–168.
- [144] J. Davidovits, "Geopolymer chemistry and properties," in *Proceedings of the 1st International Conference on Geopolymer*, 1988, vol. 88, pp. 25–48.
- [145] J. G. S. Van Jaarsveld, J. S. J. Van Deventer, and L. Lorenzen, "Factors affecting the immobilization of metals in geopolymerized flyash," *Metall. Mater. Trans. B Process Metall. Mater. Process. Sci.*, vol. 29, no. 1, pp. 283–291, 1998, doi: 10.1007/s11663-998-0032-z.
- [146] A. Fernández-Jiménez and A. Palomo, "Alkali-activated fly ashes: properties and characteristics," in *11th International Congress on the Chemistry of Cement (Durban, South Africa)*, 2003, vol. 3, pp. 1332–1340.
- [147] J. Davidovits, "Properties of geopolymer cements," in *First international conference on alkaline cements and concretes*, 1994, vol. 1, pp. 131–149.
- [148] X. Y. Zhuang *et al.*, "Fly ash-based geopolymer: Clean production, properties and applications," *J. Clean. Prod.*, vol. 125, pp. 253–267, 2016, doi: 10.1016/j.jclepro.2016.03.019.
- [149] Y. Ma, J. Hu, and G. Ye, "The pore structure and permeability of alkali activated fly ash," *Fuel*, vol. 104, pp. 771–780, 2013, doi: 10.1016/j.fuel.2012.05.034.
- [150] M. Yang, S. R. Paudel, and E. Asa, "Comparison of pore structure in alkali activated fly ash geopolymer and ordinary concrete due to alkali-silica reaction using micro-computed tomography," *Constr. Build. Mater.*, vol. 236, p. 117524, 2020, doi: 10.1016/j.conbuildmat.2019.117524.
- [151] A. Fernández-Jiménez, A. Palomo, and M. Criado, "Microstructure development of alkali-activated fly ash cement: A descriptive model," *Cem. Concr. Res.*, vol. 35, no. 6, pp. 1204–1209, 2005, doi: 10.1016/j.cemconres.2004.08.021.
- [152] P. Duxson, J. L. Provis, G. C. Lukey, S. W. Mallicoat, W. M. Kriven, and J. S. J. Van Deventer, "Understanding the relationship between geopolymer composition, microstructure and mechanical properties," *Colloids Surfaces A Physicochem. Eng. Asp.*, vol. 269, no. 1–3, pp. 47–58, 2005, doi: 10.1016/j.colsurfa.2005.06.060.
- [153] Sindhunata, J. L. Provis, G. C. Lukey, H. Xu, and J. S. J. Van Deventer, "Structural evolution of fly ash based geopolymers in alkaline environments," *Ind. Eng. Chem. Res.*, vol. 47, no. 9, pp. 2991–2999, 2008, doi: 10.1021/ie0707671.
- [154] G. Fang and M. Zhang, "The evolution of interfacial transition zone in alkali-activated fly ash-slag concrete," *Cem. Concr. Res.*, vol. 129, no. December 2019, p. 105963, 2020, doi: 10.1016/j.cemconres.2019.105963.
- [155] P. Steins *et al.*, "Effect of aging and alkali activator on the porous structure of a geopolymer," *J. Appl. Crystallogr.*, vol. 47, no. 1, pp. 316–324, 2014, doi: 10.1107/S160057671303197X.
- [156] F. Andreola, C. Leonelli, M. Romagnoli, and P. Miselli, "Techniques used to determine porosity," *Am. Ceram. Soc. Bull.*, vol. 79, no. 7, pp. 49–52, 2000.
- [157] R. Gailitis, A. Sprince, and L. Pakrastiņš, "Paņēmiens ārējo iedarbju ietekmes noteikšanai uz betonu un cementa kompozītmateriālu mikrostruktūru dažādos sprieguma stāvokļos/ Technique for Outside Effect Determination on Concrete and Cement Composite Microstructure in Various Stress-Strain States," LVP2023000029, 2023
- [158] F. Puertas, M. Palacios, H. Manzano, J. S. Dolado, A. Rico, and J. Rodríguez, "A model for the C-A-S-H gel formed in alkali-activated slag cements," *J. Eur. Ceram. Soc.*, vol. 31, no. 12, pp. 2043–2056, 2011, doi: 10.1016/j.jeurceramsoc.2011.04.036.
- [159] I. Garcia-Lodeiro, A. Palomo, A. Fernández-Jiménez, and D. E. MacPhee, "Compatibility studies between N-A-S-H and C-A-S-H gels. Study in the ternary diagram Na₂O-CaO-Al₂O₃-SiO₂-H₂O," *Cem. Concr. Res.*, vol. 41, no. 9, pp. 923–931, 2011, doi: 10.1016/j.cemconres.2011.05.006.
- [160] J. S. J. van Deventer, R. S. Nicolas, I. Ismail, S. A. Bernal, D. G. Brice, and J. L. Provis, "Microstructure and durability of alkali-activated materials as key parameters for standardization," *J. Sustain. Cem. Mater.*, vol. 4, no. 2, pp. 116–128, 2014, doi: 10.1080/21650373.2014.979265.
- [161] F. Collins and J. G. Sanjayan, "Effect of pore size distribution on drying shrinkage of alkali-activated slag concrete," *Cem. Concr. Res.*, vol. 30, no. 9, pp. 1401–1406, 2000, doi: 10.1016/S0008-8846(00)00327-6.
- [162] E. J. Garboczi, "Permeability, diffusivity, and microstructural parameters: A critical review," *Cem. Concr. Res.*, vol. 20, no. 4, pp. 591–601, 1990, doi: 10.1016/0008-8846(90)90101-3.

- [163] T. Häkkinen, "The influence of slag content on the microstructure, permeability and mechanical properties of concrete Part I Microstructural studies and basic mechanical properties," *Cem. Concr. Res.*, vol. 23, no. 2, pp. 407–421, 1993, doi: 10.1016/0008-8846(93)90106-J.
- [164] S. K. Das *et al.*, "Fresh, strength and microstructure properties of geopolymer concrete incorporating lime and silica fume as replacement of fly ash," *J. Build. Eng.*, vol. 32, no. September, p. 101780, 2020, doi: 10.1016/j.jobte.2020.101780.
- [165] C. Phetchuay, S. Horpibulsuk, A. Arulrajah, C. Suksiripattanapong, and A. Udomchai, "Strength development in soft marine clay stabilized by fly ash and calcium carbide residue based geopolymer," *Appl. Clay Sci.*, vol. 127–128, pp. 134–142, 2016, doi: 10.1016/j.clay.2016.04.005.
- [166] N. Cristelo, S. Glendinning, and A. T. Pinto, "Deep soft soil improvement by alkaline activation," *Proc. Inst. Civ. Eng. Gr. Improv.*, vol. 164, no. 2, pp. 73–82, 2011, doi: 10.1680/grim.900032.
- [167] L. Zhang, S. Ahmari, and J. Zhang, "Synthesis and characterization of fly ash modified mine tailings-based geopolymers," *Constr. Build. Mater.*, vol. 25, no. 9, pp. 3773–3781, 2011, doi: 10.1016/j.conbuildmat.2011.04.005.
- [168] M. Zhang, H. Guo, T. El-Korchi, G. Zhang, and M. Tao, "Experimental feasibility study of geopolymer as the next-generation soil stabilizer," *Constr. Build. Mater.*, vol. 47, pp. 1468–1478, 2013, doi: 10.1016/j.conbuildmat.2013.06.017.
- [169] M. Nawaz, A. Heitor, and M. Sivakumar, "Geopolymers in construction - recent developments," *Constr. Build. Mater.*, vol. 260, p. 120472, 2020, doi: 10.1016/j.conbuildmat.2020.120472.
- [170] "World's first public building with structural Geopolymer Concrete – Geopolymer Institute." <https://www.geopolymer.org/news/worlds-first-public-building-with-structural-geopolymer-concrete/> (accessed Jan. 24, 2022).
- [171] A. L. Almutairi, B. A. Tayeh, A. Adesina, H. F. Isleem, and A. M. Zeyad, "Potential applications of geopolymer concrete in construction: A review," *Case Stud. Constr. Mater.*, vol. 15, no. August, p. e00733, 2021, doi: 10.1016/j.cscm.2021.e00733.
- [172] J. T. Gourley, "Geopolymers in Australia," *J. Aust. Ceram. Soc.*, vol. 50, no. 1, pp. 102–110, 2014.
- [173] K. K. S. and R. R. Girish M. G., "Geopolymer Friendly Alternative Cement Paving Grade," *Int. J. Civ. Eng. Technol.*, vol. 8, no. 7, p. 886, 2017, [Online]. Available: <http://http://www.iaeme.com/ijciet/issues.asp?JType=IJCIET&VType=8&IType=7http://www.iaeme.com/IJCIET/issues>.
- [174] A. Hassan, M. Arif, and M. Shariq, "A review of properties and behaviour of reinforced geopolymer concrete structural elements- A clean technology option for sustainable development," *J. Clean. Prod.*, vol. 245, p. 118762, 2020, doi: 10.1016/j.jclepro.2019.118762.
- [175] I. Ismail and S. A. Bernal, "Microstructural changes in alkali activated fly ash / slag geopolymers with sulfate exposure," pp. 361–373, 2013, doi: 10.1617/s11527-012-9906-2.
- [176] A. Hasan, S. J. Foster, and A. Castel, "Development of high-density geopolymer concrete with steel furnace slag aggregate for coastal protection structures," *Constr. Build. Mater.*, vol. 248, p. 118681, 2020, doi: 10.1016/j.conbuildmat.2020.118681.
- [177] F. Fan, Z. Liu, G. Xu, H. Peng, and C. S. Cai, "Mechanical and thermal properties of fly ash based geopolymers," *Constr. Build. Mater.*, vol. 160, pp. 66–81, 2018, doi: 10.1016/j.conbuildmat.2017.11.023.
- [178] S. T., K. R. P.R., S. M., S. A., and J. R., "A state-of-the-art on development of geopolymer concrete and its field applications," *Case Stud. Constr. Mater.*, vol. 16, no. September 2021, p. e00812, 2022, doi: 10.1016/j.cscm.2021.e00812.
- [179] Y. H. M. Amran, N. Farzadnia, and A. A. A. Ali, "Properties and applications of foamed concrete; A review," *Constr. Build. Mater.*, vol. 101, pp. 990–1005, 2015, doi: 10.1016/j.conbuildmat.2015.10.112.
- [180] S. Zou *et al.*, "Experimental research on an innovative sawdust biomass-based insulation material for buildings," *J. Clean. Prod.*, vol. 260, p. 121029, 2020, doi: 10.1016/j.jclepro.2020.121029.
- [181] S. H. Teh, T. Wiedmann, A. Castel, and J. de Burgh, "Hybrid life cycle assessment of greenhouse gas emissions from cement, concrete and geopolymer concrete in Australia," *J. Clean. Prod.*, vol. 152, pp. 312–320, 2017, doi: 10.1016/j.jclepro.2017.03.122.
- [182] "# 24 False CO2 Values Published in Scientific Papers – Geopolymer Institute." <http://www.geopolymer.org/library/technical-papers/false-co2-values-published-in-scientific-papers/> (accessed Feb. 03, 2022).
- [183] J. I. T. Garces, I. J. Dollente, A. B. Beltran, R. R. Tan, and M. A. B. Pomentilla, "Life cycle assessment of self-healing geopolymer concrete," *Clean. Eng. Technol.*, vol. 4, no. May, p. 100147, 2021, doi: 10.1016/j.clet.2021.100147.
- [184] A. Mellado, C. Catalán, N. Bouzón, M. V. Borrachero, J. M. Monzó, and J. Payá, "Carbon footprint of geopolymeric mortar: Study of the contribution of the alkaline activating solution and assessment of an alternative route," *RSC Adv.*, vol. 4, no. 45, pp. 23846–23852, 2014, doi: 10.1039/c4ra03375b.
- [185] R. Bajpai, K. Choudhary, A. Srivastava, K. S. Sangwan, and M. Singh, "Environmental impact assessment

of fly ash and silica fume based geopolymer concrete,” *J. Clean. Prod.*, vol. 254, p. 120147, 2020, doi: 10.1016/j.jclepro.2020.120147.

ANNEX / PUBLICATIONS

Annex I: Paper I:

Gailitis R., Korniejenko K., Łach M., Sliseris J., Moran J., Rodriguez E., Miķuła J.
Mechanical Properties of Geopolymer Concretes Reinforced with Waste Steel Fibers
IOP Conference Series: Materials Science and Engineering, 660 (1)

PAPER • OPEN ACCESS

Mechanical Properties of Geopolymer Concretes Reinforced with Waste Steel Fibers

To cite this article: R Gailitis *et al* 2019 *IOP Conf. Ser.: Mater. Sci. Eng.* **660** 012007

View the [article online](#) for updates and enhancements.

You may also like

- [A laser-based sensor system for tire tread deformation measurement](#)
Yi Xiong and Ari Tuononen
- [Direct strain energy harvesting in automobile tires using piezoelectric PZT-polymer composites](#)
D A van den Ende, H J van de Wiel, W A Groen *et al.*
- [Hybrid and electric vehicle tribology: a review](#)
Hemanth G, Suresha B and Ananthapadmanabha



The Electrochemical Society
Advancing solid state & electrochemical science & technology

242nd ECS Meeting

Oct 9 – 13, 2022 • Atlanta, GA, US

Extended abstract submission deadline: April 22, 2022

Connect. Engage. Champion. Empower. Accelerate.

MOVE SCIENCE FORWARD



Submit your abstract



Mechanical Properties of Geopolymer Concretes Reinforced with Waste Steel Fibers

R Gailitis², K Korniejenko¹, M Łach¹, J Sliseris², J Morán³, E Rodriguez³ and J Mikula¹

¹ Institute of Materials Engineering, Faculty of Mechanical Engineering, Cracow University of Technology, Jana Pawła II 37, 31-864 Cracow, Poland.

² Faculty of Civil Engineering, Riga Technical University, 1 Kalku Street, LV-1658, Riga, Latvia.

³ Area de Materiales Compuestos Estructurales (CET), Instituto de Investigaciones en Ciencia y Tecnología de Materiales (INTEMA), Facultad de Ingeniería, UNMDdP-Conicet, Diagonal J. B. Alberdi 2695, 7600 Mar del Plata, Argentina.

E-mail: kinga.korniejenko@mech.pk.edu.pl

Abstract. The article presents the research that try to determinate the possibilities of utilization the waste came from used tires to create the composites based on geopolymer matrix. The tire is multicomponent construction. It mainly consists of elastomer (rubber), metal and textile fibres such called textile cord. A lot of components causes difficulties in the tire recycling process. The main aim of the research was determinate the possibilities of recycling the waste steel from used tires in geopolymer composites and develop the eco-friendly material for construction industry. The matrix based on fly ash from power station located in city named Skawina (Poland) and fine sand at a ratio of 1:1. The process of activation was made by 10M sodium hydroxide solution combined with the sodium silicate solution. In order to manufacture these composites the addition of 2% and 3.5% of waste steel fibres by mass was applied. Also specimen without steel fiber reinforcement were made to get reference specimens. The waste steel fibres came from recycling company from Argentina – ‘Regomax’. The specimens were prepared according to the methodology described in the standard EN 12390-1. The research methods used were: microstructure research, tensile strength and compressive strength tests as well as analysis of breakthroughs.

1. Introduction

Cement is categorized as indispensable material in the construction industry all over world, special in developing countries. Due to this increased cement consumption there are intense negative effects, such as release of carbon dioxide into the atmosphere [1]. In comparison to the traditional materials, such as Portland concrete, geopolymers have a number of advantages, especially connected with reduction of footprint and eco-friendly character. Manufacturing of this class of materials compared to the traditional concretes is economically more beneficial including the low energy consumption.

Additional environmental benefit is connected with using to production process waste materials: for example, fly ashes and mine tailings. Coal power stations contributes to 25-30% of world's energy production. Consequences to this is 800 million tons of fly ash generated worldwide every year by power stations. Only half of this amount is recycled. This recycled amount can be increased by manufacturing



environmentally friendly binders such as geopolymers [2]. Also it has to be acknowledged that production of Portland cement causes significant amount of CO₂ emissions. Portland cement production every year causes around 5-7% of the total CO₂ anthropogenic emissions. Cement production reached a distressing value of about 4200 million tons in 2016 that contributes approximately to 3570 million tons of CO₂ [3].

Geopolymer is comparable in performance to ordinary Portland cement [4]. Geopolymer concrete main advantage is its contribution to the environment. It is estimated that carbon footprint made by geopolymer concrete manufacturing is 26 to 46% less than Portland cement concrete if in concrete mix Portland cement is replaced completely [4, 5]. It is reckoned that production of 1 tonne of caolin geopolymer contributes to 0.180 tonnes of CO₂, that is 6 times less than manufacturing of Portland cement concrete [6].

Geopolymer belongs to a group of novel three-dimensional inorganic materials. This novel material got multiple beneficial properties such as low density, low cost, environmentally friendly nature and high mechanical performance. However like traditional brittle materials, geopolymer shows poor tensile and flexural properties and appalling fracture behavior [7]. As a composite material geopolymer concrete is two or more constituent material arrangement. A continuous called matrix and the dispersed phase or phases, either fibers or particulates, in order to develop another material with desired combination of properties [5, 8]. A significant increase of tensile strength fracture energy can be achieved by adding fibers to geopolymer matrix [9, 10].

In terms of sustainable raw material management, it is crucial to recycle industrial waste as much as possible and also to develop new technologies that not only reduces industrial waste landfills but also produce materials with new added value [2, 11]. Contemporary, every year approximately 17 million tons of waste tires, which have no further use [12, 13]. This waste is categorized as serious contaminant to environment, therefore, recycling of tires is extremely important [14, 15].

This study shows how two secondly used components interacts with each other and what kind of properties has got developed material. The aim of this study is to show how different amount of reused steel fiber reinforcement can improve or disapprove material properties in compression and tensile loads.

2. Materials and methods

Cubic (70x70x70 mm) and prismatic (50x50x200 mm) specimens were prepared with 2% and 3,5% by mass steel fibers from recycled car tire cords and without steel fiber reinforcement. The matrix was based on fly ash from power plant located in Skawina city (Poland). This kind of fly ash is suitable for manufacturing geopolymers because of proper physical properties and chemical composition. The fly ash contains of spherical aluminosilicate particles in different sizes: > 0.0039 in. [$>100\ \mu\text{m}$] – ca.3%, 0.0028 – 0.0039 in. [$71-100\ \mu\text{m}$] – ca. 12%, 0.0025 – 0.0028 in. [$63-71\ \mu\text{m}$] – ca. 10%, 0.0022 – 0.0025 in. [$56-63\ \mu\text{m}$] – ca. 15% and <0.0022 in. [$<56\ \mu\text{m}$] – ca. 60%. This fly ash is rich in oxides such as SiO₂ (47.81%), Al₂O₃ (22.80%). High value of SiO₂ and Al₂O₃ is advantageous for geopolymerization.

Steel fibers were obtained from Argentinian company “Regomax”, that recycles old tires to get milled rubber for synthetic grass and other rubber produce production. Steel cords from tires are recycling process byproduct that has no particular market as reusable material so they have scrap value - <http://www.regomax.com/>.

Specimens were prepared using sodium promoter, fly ash, sand (ratio sand and fly ash – 1:1) and steel fibers (2% and 3.5%). The process of activation has been made by 10M sodium hydroxide solution combined with the sodium silicate solution (liquid glass at a ratio of 1:2.5). In order to manufacture the composites the technical sodium hydroxide in flakes were used and water solution of sodium silicate R-145 (modulus 2.5, density 0.052 lb/in.³ - 1.45 g/cm³). Tap water was used instead of the distilled one. The alkaline solution was prepared by means of pouring the aqueous solution of sodium silicate and water over solid sodium hydroxide. The solution was mixed and left until its temperature became stable and the concentrations equalized about 2 hours. The fly ash, sand, alkaline solution and steel fibers were mixed about 15 minutes by using low speed mixing machine (to receive the homogenous paste). Next, it was poured into two sets of plastic molds. The specimens were hand-formed and then subjected to

vibratory removal of air bubbles. Tightly closed molds were heated in the laboratory dryer for 24h at 75 °C. Then, the specimens were unmolded. The prepared specimens had following dimensions: per each testing batch 3 cubes 70x70x70 mm and prisms 50x50x200 mm.

3. Results and discussion

3.1. Microstructure research

The SEM observations were made for plain samples (figure 1) as well as for composition reinforced by fibres (figure 2 and figure 3). The images were made at various magnifications - between 20 – 220x. The different magnification allows to observe of microstructure of composites, including fibres distribution as well as it gives a preliminary information about the coherency of fibres (reinforcement) with the geopolymer matrix.

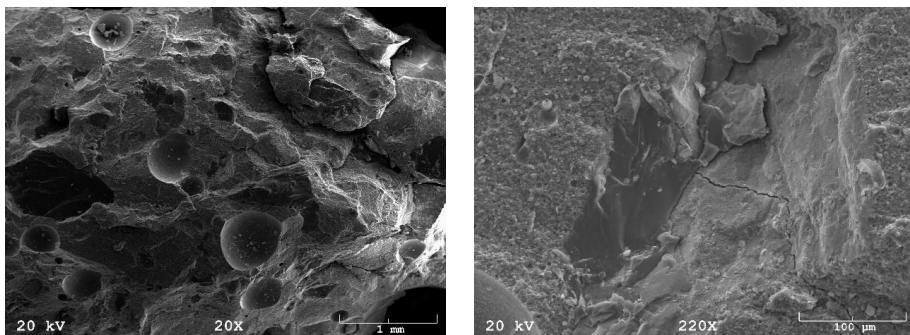


Figure 1. SEM scan of non-reinforced geopolymer sample.

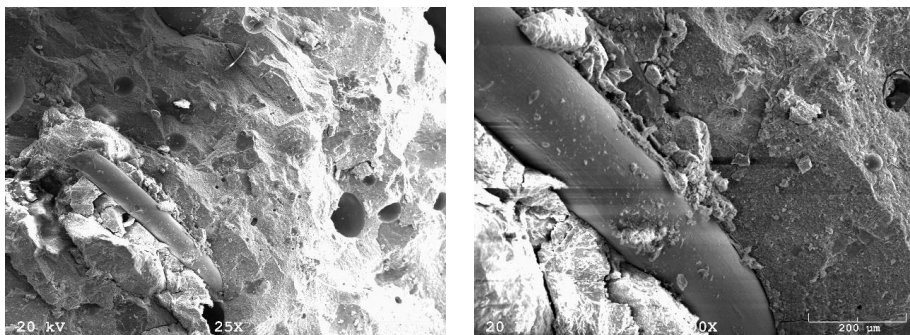


Figure 2. SEM scan of geopolymer sample reinforced with 2% steel fibers.

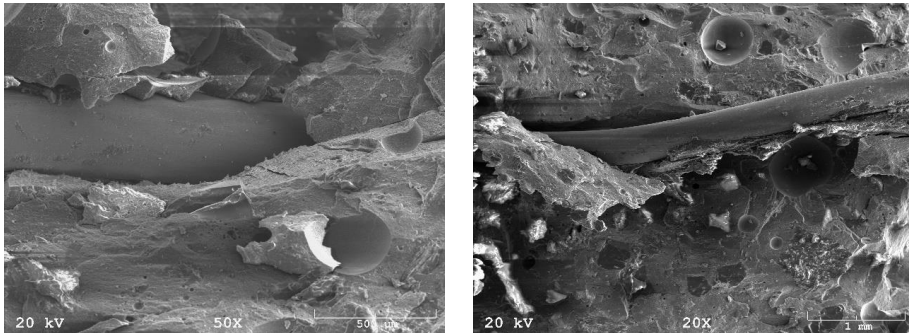


Figure 3. SEM scan of geopolymer sample reinforced with 3.5% steel fibers.

The microstructural observation allow to notice that the structure is coherent - good adhesion the steel fibres to the matrix. The contact zone are visible on figure 3.

3.2. Compressive strength

Table 1 and figure 4 show the compressive strength for geopolymer concrete cubes 28 days after they were made.

Table 1. Compressive strength of geopolymer concrete.

Specimen type	Specimen number	Specimen size			Compressive strength, kN	Compressive strength, MPa
		Width, mm	Height, mm	Length, mm		
Geopolymer with 3.5% steel fibers	1	71.55	71.20	70.86	581.7	114.7
	2	72.17	71.42	71.38	605.0	117.4
	3	71.19	71.26	71.98	562.7	109.8
Geopolymer with 2% steel fibers	1	71.54	71.53	71.15	398.0	78.2
	2	71.48	71.18	71.30	407.6	80.0
	3	71.44	71.65	71.16	431.9	85.0
Geopolymer without steel fibers	1	70.22	71.58	71.12	362.0	72.5
	2	72.38	71.08	71.34	475.2	92.0
	3	71.62	71.20	71.70	467.7	91.1

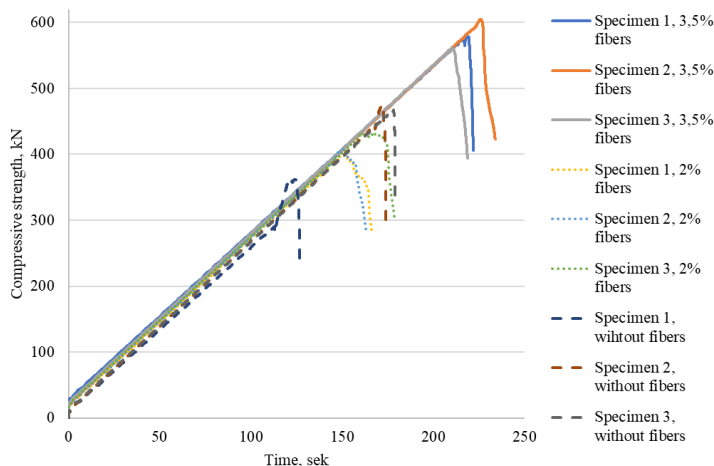


Figure 4. Geopolymer cubic specimen compressive strength loading graph.

For specimens with largest amount of steel fiber reinforcement compressive strength is considerably higher than all other specimens. Furthermore it is interesting that compressive strength of specimens without steel fiber reinforcement is not the lowest.

3.3. Tensile strength

Table 2 shows the tensile strength for geopolymer concrete spherical specimens 28 days after they were made. For specimens with largest amount of steel fiber reinforcement compressive strength is considerably higher than all other specimens. As well as in for cubes the tensile strength of specimens without steel fiber reinforcement is not the lowest.

Also in figure 5 it is shown that specimens with 3.5% steel fiber reinforcement after first crack development in bended part still holds and increases load capacity after it breaks.

Table 2. Tensile strength of geopolymer concrete.

Specimen type	Specimen number	Specimen size			Compressive strength, kN	Compressive strength, MPa
		Width, mm	Height, mm	Length, mm		
Geopolymer with 3,5% steel fibers	1	50.46	50.03	206.67	5.8	10.2
	2	50.56	50.37	203.33	5.9	10.4
	3	50.21	51.56	206.67	6.5	11.3
Geopolymer with 2% steel fibers	1	50.84	50.14	210.00	4.7	8.4
	2	51.45	50.16	205.00	4.3	7.5
	3	50.23	50.21	210.00	3.6	6.4
Geopolymer without steel fibers	1	50.08	50.22	210.00	4.2	7.5
	2	49.69	50.25	208.30	4.8	8.6
	3	49.54	50.22	208.30	5.6	10.1

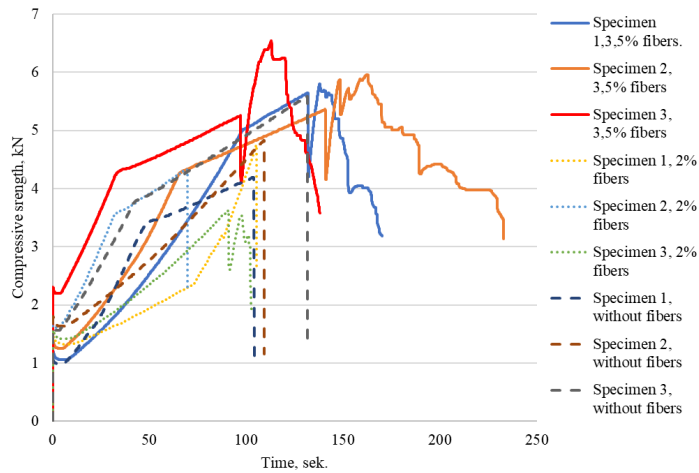


Figure 5. Geopolymer spherical specimens tensile loading graph.

As it is visible in figure 6, figure 7 and figure 8 only specimens with 3.5% steel fiber reinforcement keeps carrying load after crack appearance. All other specimens (with 2% fiber reinforcement and without fibers) fail after crack appearance.

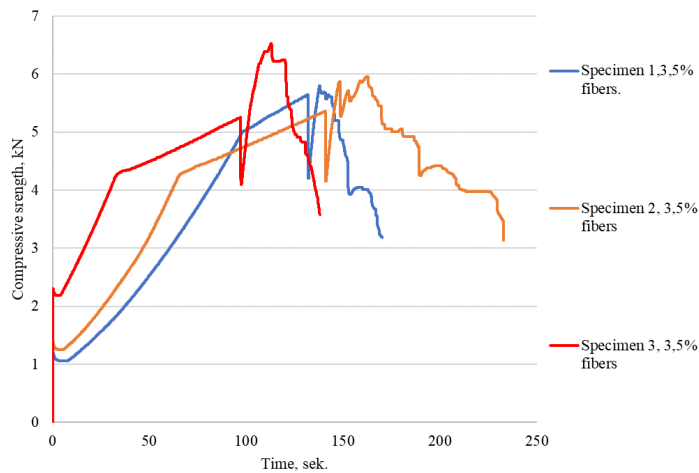


Figure 6. Geopolymer spherical specimens with 3.5% steel fiber reinforcement tensile loading graph.

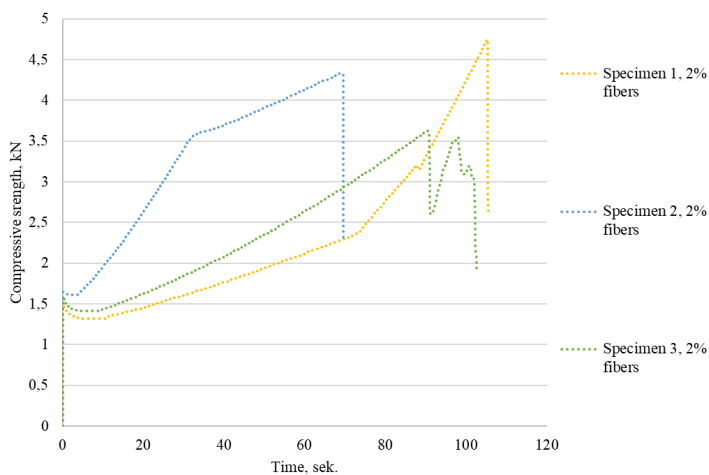


Figure 7. Geopolymer spherical specimens with 2% steel fiber reinforcement tensile loading graph.

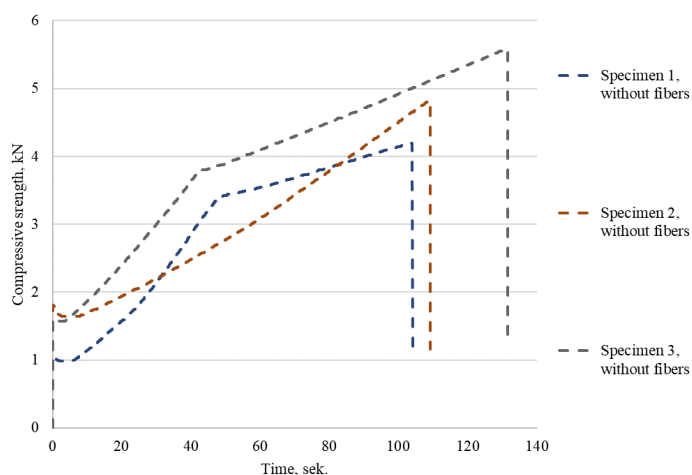


Figure 8. Geopolymer spherical specimens without steel fiber reinforcement tensile loading graph.

4. Conclusions

Regarding tensile strength specimens with fiber reinforcement of 3.5% has further load capacity even if some of geopolymer matrix has failed in stretched part of specimen. For specimens with 2% fiber reinforcement there are not enough fibers in stretched part so they could not carry all the load and specimen fails. In compressive strength cubic specimens with steel fiber reinforcement fails without significant late increase in load capacity as the specimens without fiber reinforcement do.

The load-bearing capacity of geopolymer cubes with 3.5% steel fiber reinforcement is 29% higher than specimens with 2% steel fiber reinforcement and 26% higher than specimens without reinforcement. Furthermore it can be acknowledge that for geopolymer cubes steel reinforcement gives

increase in compressive strength when steel reinforcement is 3.5%. For less reinforcement amount there is decrease in specimen compressive strength.

For tensile strength there is similar conclusion. Specimens with 3.5% steel fiber reinforcement has got 30% higher tensile strength than specimens with 2% steel fiber reinforcement and 18% higher tensile strength than specimens without fibers. Furthermore specimens without fibers has got 15% higher tensile strength than specimens with 2% steel fiber reinforcement. It could only mean, that for geopolymer matrix reinforced with waste tire steel cord fibers has to be at least 3.5% from mass of the mix to contribute to specimen strength increase.

The decrease in tensile and compression strength for geopolymer concrete with 2% steel fiber reinforcement can be because the fibers could be surfaced to specimens top not bottom side where tensile loads are. Due to this the reinforcement has not worked as it should have and most on tensile load was carried by geopolymer matrix not steel fiber reinforcement with geopolymer matrix together. Furthermore, the collapse of specimens with 2% steel fiber reinforcement and specimens without reinforcement (Fig.5, Fig.7 and Fig.8) is similar and could indicate, that for specimen with 2% steel fiber reinforcement the steel fibers have not been arranged evenly through the cross section of specimen.

Acknowledgments

1. This work has been supported by the Latvian Council of Science within the scope of the project 'Long-term properties of innovative cement composites in various stress-strain conditions' No. Izp-2018/2-0249.
2. This work has been supported by the ERANet-LAC 2nd Joint Call (<http://www.eranet-lac.eu>) and funded by Ministry of Science, Technology and Productive Innovation (MINCYT) in Argentina and the National Centre for Research and Development in Poland, within the framework of the grant: 'Development of eco-friendly composite materials based on geopolymer matrix and reinforced with waste fibers'.

References

- [1] Celik A, Yilmaz K, Canpolat O, Al-Mashhadani MM, Aygörmöz Y and Uysal M 2018 *Constr Build Mater* **187**, 1190
- [2] Mucsi G, Szenczi A and Nagy S 2018 *Journal of Cleaner Production* **178**, 429
- [3] Novais RM, Carvalheiras J, Seabra MP, Pullar RC and Labrincha JA 2017 *Journal of Cleaner Production* **166**, 343
- [4] Luna-Galiano Y, Leiva C, Villegas R, Arroyo F, Vilches L and Fernández-Pereira C 2018 *Materials Letters* **233**, 1
- [5] Lokuge W, Wilson A, Gunasekara C, Law DW and Setunge S 2018 *Constr Build Mater* **166**, 472
- [6] Nguyen KT, Le TA and Lee K 2018 *Constr Build Mater* **169**, 462
- [7] Yan S, He P, Jia D, Wang J, Duan X, Yang Z, Wang S and Zhou Y 2017 *Composites Part B* **114**, 289
- [8] Sprince A, Pakrastinsh L and Vatin N 2016 *IOP Conf. Ser.: Mater. Sci. Eng.* **123** (1), 012050
- [9] Sliseris J 2018 *Mechanics of Composite Materials* **5** (5), 1
- [10] Nikolenko SD, Sushko EA, Sazonova SA, Odnolko AA and Manokhin VY 2017 *Magazine of Civil Engineering* **7**, 3
- [11] Vishwakarma V and Ramachandran D 2018 *Constr Build Mater* **162**, 96
- [12] Łach M, Kiszka A, Korniejenko K and Mikula J 2018 *IOP Conf. Ser.: Mater. Sci. Eng.* **416**, 012089
- [13] Smithers Rapra 2017 *The Future of Tire Manufacturing to 2022*, <https://www.smithersrapra.com/market-reports/tire-industry-market-reports/the-future-of-tire-manufacturing-to-2022> (access: 23.03.2018)
- [14] Molanorouzi M, Mohaved SO 2016 *Polymer Degradation and Stability* **128**, 115
- [15] ETRMA, *Statistics - Edition 2017 2017 The European Tyre and Rubber Industry in figures*, <http://www.etrma.org/library-2> (access: 23.03.2018)

Annex II: Paper II:

Gailitis, R., Sliseris, J., Korniejenko, K., Miķūla, J., Łach, M., Pakrastins, L., Sprince,
*Long-Term Deformation Properties of a Carbon-Fiber-Reinforced Alkali-Activated
Cement Composite*
Mechanics of Composite Materials, 56 (1), pp. 85-92.

LONG-TERM DEFORMATION PROPERTIES OF A CARBON-FIBER-REINFORCED ALKALI-ACTIVATED CEMENT COMPOSITE

R. Gaillitis,^{1*} J. Sliseris,¹ K. Korniejenko,² J. Mikula,² M. Lach,² L. Pakrastins,¹ and A. Sprince¹

Keywords: creep of geopolymer concrete, shrinkage deformations

The aim of this study was to experimentally determine the creep and shrinkage properties of plain geopolymer and carbon-fiber-reinforced geopolymer concretes. The creep properties of concrete specimens were determined by loading them by 20% of their ultimate stress. The specific creep of the geopolymer concrete was in the same range as that of the ordinary Portland cement — 0.00065 1/MPa. New information on the time-dependent elastic modulus of the concretes was also obtained. The elastic modulus of the plain geopolymer concrete reached, on the average, 32.03 GPa on day 30, 36.29 GPa on day 62, and 45.73 GPa on day 158, but that of the carbon-fiber-reinforced one — 30.12 GPa on day 30, 37.79 GPa on day 62, and 53.35 GPa on day 158 after the production of their specimens.

1. Introduction

Alkali-activated concrete has been known for about 100 years. The first scholar to conduct research into an alkali-activated cement concrete was Purdon, who mixed slag with NaOH to create a new material. In 1979, after years of research, the French scientist Davidovits patented the term geopolymer, which refers to a low-calcium alkali-activated cement concrete. [1]

The mechanism of geopolymer formation includes a silicon and aluminum reaction, which is released by hydroxide silicates from sodium and potassium as an alkali activating solution. As a result, a strong aluminosilicate polymer structure is created. [2]

¹Faculty of Civil Engineering, Riga Technical University, Kalku 1, Riga, Latvia

²Cracow University of Technology, Warszawska 24, 31-155 Cracow, Poland

*Corresponding author; tel.: +371 28361105; e-mail: rihards.gaillitis@edu.rtu.lv

The main advantage of geopolymer concrete (GPC) is that it is environment-friendly. The carbon footprint of the manufacture of geopolymer concrete, in terms of CO₂ emissions, is by 26 to 46% less than that for Portland cement if the Portland cement in the concrete mix is replaced completely. [3] It has been estimated that 1 ton of kaolin geopolymer cement generates 0.180 tons of CO₂, which is six times less than that in the case of Portland cement [4].

Creep strains of GPCs at high temperatures were investigated in [5]. Owing to its low density and porous structure, GPC can be used as a heat insulation material [6]. A significant increase in its tensile properties and fracture energy can be achieved by adding fibers to it [7–9]. This effect is mostly observed in bent members, such as beams [10–11]. The introduction of a disperse fiber reinforcement can also be used to reduce its shrinkage deformations [12–13]. Additional viscoelastic properties of concrete can be achieved by adding petroleum products to the concrete mixture [14]. Special structural design procedures, for example, neural-network-based methods, have been created to predict the mechanical properties of cement-based structural elements [15–17]. Many experimental results have shown that the GPC in compression has stress–strain relationships similar to those of the Portland cement [18–19]. Thus, there are many indications that the ordinary Portland cement can be replaced by a GPC in structural designs [20].

Although the strength and creep properties of GPC in various environmental conditions have already been determined, its long-term properties under a load have been explored inadequately. Therefore, in this work, its creep shrinkage, compression strength, and time-dependent elastic modulus are investigated.

2. Methods

2.1. Preparation of specimens

Specimens with 1 wt.% of short carbon fibers and plain specimens (without fiber additives) were investigated. The matrix was based on the fly ash from a power station located in Skawina (Poland). This kind of fly ash was suitable for manufacturing geopolymers because of its appropriate physical properties and chemical composition. The oxygen composition of the fly ash was determined, and its sew analysis was performed. The ash contained spherical aluminosilicate particles in different sizes: > 0.0039 in. [$>100\ \mu\text{m}$] — ca. 3%, 0.0028–0.0039 in. [71–100 μm] — ca. 12%, 0.0025–0.0028 in. [63–71 μm] — ca. 10%, 0.0022–0.0025 in. [56–63 μm] — ca. 15% and <0.0022 in. [$<56\ \mu\text{m}$] — ca. 60%. The ash was rich in oxides, such as SiO₂ (47.81%), and Al₂O₃ (22.80%). The content of SiO₂ and Al₂O₃ was advantageous to geopolymerization.

The specimens were prepared using a sodium promoter, fly ash, sand (sand to fly ash ratio — 1:1) and carbon fibers (1 wt.% or without fibers as a geopolymer concrete (GPC). The activation process was generated by a 12-M sodium hydroxide solution combined with a sodium silicate solution (liquid glass at a ratio of 1:2.5). In order to manufacture the composites, a technical sodium hydroxide in flakes was used, together with a water solution of an R–145 sodium silicate (elastic modulus 2.5 MPa and density 1.45 g/cm³). Tap water was used instead of distilled one. An alkaline solution was prepared by pouring the aqueous solution of sodium silicate and water over the solid sodium hydroxide. The solution was mixed and left to stand until its temperature became stable and the concentrations equalized — for about 2 h. The fly ash, sand, alkaline solution, and fibers were mixed for about 15 min using a low-speed mixing machine (to produce a homogenous paste). Next, the solution was poured into two sets of plastic molds. The specimens were hand-formed and then subjected to the vibratory removal of air bubbles. Tightly closed molds were heated in a laboratory dryer for 24 h at 75°C. Then, the specimens were unmolded. The cylindrical specimens had a diameter of 46 mm and length of 190 mm.

Unmolded specimens were tested by SEM to determine their micro- and nanostructures (see Fig. 1)

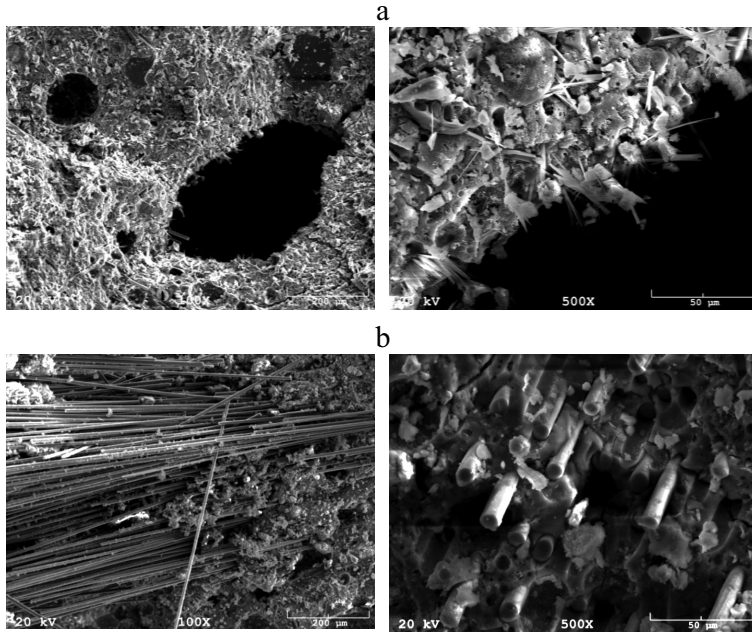


Fig. 1. Micro- and nanostructures of GPC without (a) and with a carbon-fiber reinforcement (b).



Fig. 2. Test setup for creep and elastic modulus tests.

2.2. Experimental testing of creep deformations

The compression strength was determined according to standard EN 12390-3:2009. A compression machine with a loading accuracy of $\pm 1\%$ was used, and the loading rate was 0.7 MPa/s. The tests were performed after 30, 62, and 150 days after the preparation of specimens. The tensile strength was determined in a tensile-split strength test on the same machine at a loading rate of 0.7 MPa/s. These tests were performed after 62 and 150 days after the preparation of specimens. The



Fig. 3. Water-soaked and air-dried GPC specimens.



Fig. 4. Compressed dry and wet GPC specimens.

elastic modulus was obtained 30, 62 and 150 days after specimens had been made. These tests were performed both before and after creep tests.

For creep and shrinkage tests, six aluminum plates (10×15 mm) were glued to each specimen in pairs. Then, strain indicators were attached to the plates (see Fig. 2).

The creep strains were measured on GPC specimens subjected to a uniform constant compressive load. At the same time, shrinkage was measured for the same specimens, in the same room and at the same temperature and moisture content, without loading.

Tests for the elastic modulus were performed before creep tests. Specimens were subjected to a load 40% of the ultimate compressive strength. The load was applied and removed gradually in five steps. After each loading and unloading step, deformations were measured.

In creep tests, specimens were subjected to a load 20% of its ultimate compression strength, which had been determined in compression strength tests. Two groups of specimens were tested (Group 1 – 30 days old and Group 2 – 62 days old). They were kept loaded under a constant load for 88 and 120 days. The loading was carried out in creep lever test stands designed for creep tests (see Fig. 2)

After the creep tests, specimens were cut in two and placed in water for 24 h for optimum moisture absorption (see Fig. 3).

Afterwards, all specimens were pressed to determine their compression strength depending on whether they had been loaded or not and whether they had been soaked in water or not (see Fig. 4 and Table 1).

TABLE 1. Specimen Water Absorption

Test type	Sample	Average weight, g		Average moisture absorption, g
			after 24 h in water	
Creep 1	GPC without a reinforcement	2872.5	3116.3	243.8
	GPC with a reinforcement	2895.0	3050.0	155.0
Creep 2	GPC without a reinforcement	2890.0	3106.7	216.7
	GPC with a reinforcement	2877.5	3025.0	147.5
Shrinkage	GPC without a reinforcement	2865.0	3105.0	240.0
	GPC with a reinforcement	2902.5	3080.0	177.5

TABLE 2. Compressive Strength of 28-Day-Old GPCs

Specimen type	Specimen size, mm		Average weight, kg	Average compressive load, kN	Average compressive strength, MPa
	Diameter	Height			
GPC with carbon fibers	46	95	0.3002	80.0	48.162
GPC without fibers	46	95	0.3000	75.6	45.483

TABLE 3. Compressive Strength of 150-Day-Old GPCs

Test type	Sample	Average weight, g	Average height, mm	Average compressive load, kN	Average compressive strength, MPa
Creep 1	GPC without a reinforcement	2.822	92.5	80.6	48.49
	GPC with a reinforcement	2.850	93.5	108.6	65.38
Creep 2	GPC without a reinforcement	2.830	93.0	79.8	48.02
	GPC with a reinforcement	2.808	92.0	89.1	53.61
Shrinkage	GPC without a reinforcement	2.845	93.0	54.7	32.93
	GPC with a reinforcement	2.800	92.5	53.9	32.42

The ability of concrete to creep is usually evaluated by the specific creep, which shows how much the material is going to creep under the stress applied [21] and is calculated by the formula

$$\chi_{cr}(t, t_0) = \frac{\varepsilon_{cr}(t, t_0)}{\sigma} = \frac{\varepsilon_{tot}(t) - \varepsilon_{sh}(t) - \varepsilon_{el}(t, t_0)}{\sigma} = \frac{1}{E_{cr}(t, t_0)}, \quad (1)$$

where $\chi_{cr}(t, t_0)$ is the specific creep, $\varepsilon_{cr}(t, t_0)$ is the creep strain, $\varepsilon_{tot}(t)$ is the total strain, $\varepsilon_{sh}(t)$ is the shrinkage strain, $\varepsilon_{el}(t, t_0)$ is the elastic strain, σ is the compressive stress, and $E_{cr}(t, t_0)$ is the creep modulus.

3. Results and Discussion

On GPC specimens, tests to determine its compression and tensile strength, elastic modulus, creep deformation, creep coefficient, and shrinkage were conducted.

The results obtained are shown in Tables 2, 3, and 4.

The elastic modulus was determined before and after creep tests. Its ultimate value after seven days from preparation had not yet been reached (see Fig. 5).

The total creep and shrinkage strains ε are given in Fig. 6.

TABLE 4. Compressive Strength of Moist 150-Day-Old GPCs

Test type	Sample	Average weight, g	Average height, mm	Average compressive load, kN	Average compressive strength, MPa
Creep 1	Geopolymer without a reinforcement	3.116	93.8	79.7	48.0
	Geopolymer with a reinforcement	3.050	94.5	70.6	42.5
Creep 2	Geopolymer without a reinforcement	3.107	93.7	80.9	48.7
	Geopolymer with a reinforcement	3.025	93.5	76.4	46.0
Shrinkage	Geopolymer without a reinforcement	3.105	93.0	60.6	36.5
	Geopolymer with a reinforcement	3.080	94.5	58.2	35.0

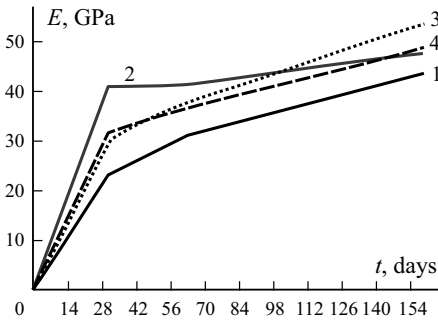


Fig. 5. Elastic moduli E of unreinforced Group 1 (—) and Group 2 (---) and reinforced (····) GPC specimens and their average value (- · -) as functions of time t .

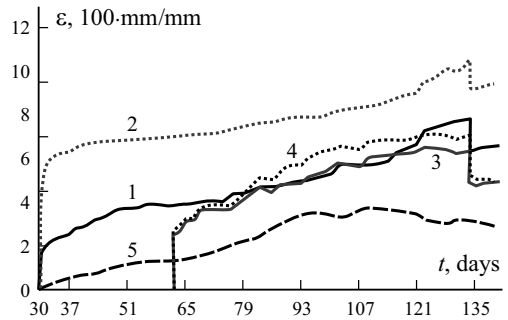


Fig. 6. Creep strains ε of unreinforced (—, ---) and reinforced (····, ···) Group 1 (—, ···) and Group 2 (---, ···) specimens and their shrinkage strains (- - -).

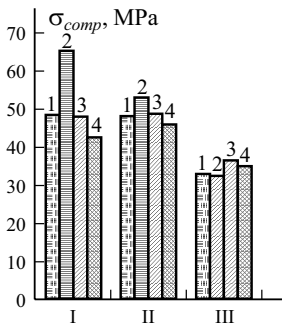


Fig. 7. Compressive strength of unreinforced (■, ▨) and reinforced (×, ◊) dry (■, ×) and moist (▨, ◊) GPC specimens of Groups 1 and 2.

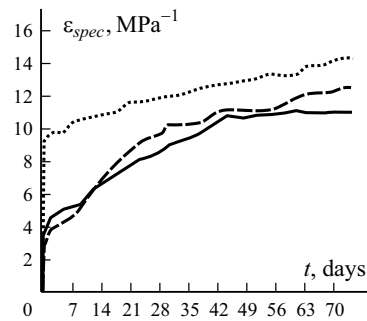


Fig. 8. Specific creep strain ε_{spec} of unreinforced (—) and reinforced (- - -) GPCs and of the ordinary Portland cement concrete (ET-1) (····).

After creep and shrinkage tests, all specimens were crushed in compression tests. The results of compression tests are shown in Fig. 7. As is seen, the compression strength of unreinforced GPC was significantly affected by moisture — it was by up to 15% lower than that of dry ones. It is also evident that the specimens with the longest loading time (Group 1) had a higher compressive strength than the nonloaded specimens (shrinkage specimens) or those loaded later.

One of the objective measurements in creep is the specific creep strain of a material [21]. In Fig. 8 are shown differences between the ordinary Portland cement concrete and GPC.

4. Conclusions

The long-term deformation properties of GPCs were obtained by performing 150-day creep-shrinkage experiments. On the basis of our results, the following conclusions can be drawn.

1. The compressive strength of the unreinforced GPC were similar to that of the classic Portland cement of strength class C40/45. The GPC reinforced by 1 wt.% of carbon fibers had a little higher compressive strength than plain GPC (on the average, 45.48 MPa for plain GPC and 48.16 MPa for the carbon-fiber-reinforced GPC before creep tests);

2. In the 130-day test, the strength of plain GPC specimens increased from 7 to 27%. A higher increase in the compressive strength was observed for the carbon-fiber-reinforced GPC (increase by 27% in contrast to 7% for plain GPC specimens).

3. The moist specimens had by about 15% lower compressive strength than the dry ones. Also, water absorption had a greater effect on the specimens with a carbon fiber reinforcement. The decrease in the compressive strength of plain GPC specimens was about 2.2%, but for carbon-fiber-reinforced GPC specimens, it decreased by 14.3 to 35.1%.

4. For the water-saturated GPC specimens which had not been subjected to loads during creep tests (shrinkage specimens), no decrease in the compressive strength was observed. On the contrary, it even increased slightly — by 9.7% for the plain GPC specimens and by 7.6% for the carbon-fiber-reinforced ones.

5. The elastic modulus of specimens did not reach the ultimate value in the first 28 days after casting. From days 28 to 62, the modulus increased by 0.8% per day, on the average, from days 62 to 150 increased by 0.4% a day, on the average.

6. The plane GPC specimens tested showed a 13% to 23% lower specific creep strain than the ordinary Portland cement concrete, which means that GPC could be used effectively in many structural applications. The specific creep strain was higher for the reinforced GPC. The specific creep strain of specimens with a carbon fiber reinforcement was by 12% higher than that of plain GPC specimens. This indicates that the 1% carbon fiber reinforcement did not affect the long-term properties of GPC positively. In the contrast, the specimens tended to creep.

7. The specimens tested in creep (loaded) from day 30 after manufacture had a compressive strength by about 8% higher than the specimens creep-tested from day 62. The compressive strength of creep-tested specimens was by 40% higher than that of specimens that were used to determine the shrinkage strain. This effect can be partly explained by microstructural changes and densification of GPC during long-term loading.

Further research is needed to develop practical recommendations for estimation of the long-term properties of GPC structures.

Acknowledgments. This study was supported by the ERANet-LAC 2nd Joint Call (<http://www.eranet-lac.eu>) and funded by the Latvian State Education Development Agency (VIAA in Latvian) and the National Centre for Research and Development, Poland, within the framework of the grant “Development of eco-friendly composite materials based on a geopolymer matrix and reinforced with waste fibers.”

It was also funded by the Latvian Council of Science, project “Long-term properties of innovative cement composites in various stress-strain conditions” project No. lzp-2018/2-0249 and supported by the European Regional Development Fund within the Activity 1.1.1.2 “Post-doctoral Research Aid” of the Specific Aid Objective 1.1.1 “To increase the research and innovative capacity of scientific institutions of Latvia and the ability to attract external financing, investing in human resources and infrastructure” of the Operational Program “Growth and Employment” (No.1.1.1.2/VIAA/3/19/401)

REFERENCES

1. F. Pacheco-Torgal, J. Castro-Gomes, and S. Jalali, "Alkali-activated binders: A review Part 1. Historical background, terminology, reaction mechanisms and hydration products," *Constr. Build. Mater.*, **22**, 1305–1314 (2008).
2. A. Mehta and R. Siddique, "Sulfuric acid resistance of fly ash based geopolymer concrete," *Constr. Build. Mater.*, **146**, 136–143 (2017).
3. W. Lokuge, A. Wilson, C. Gunasekara, D. W. Law, and S. Setunge, "Design of fly ash geopolymer concrete mix proportions using multivariate adaptive regression spline model," *Constr. Build. Mater.*, **166**, 472–481 (2018).
4. K. T. Nguyen, T. A. Le, and K. Lee, "Evaluation of the mechanical properties of sea sand-based geopolymer concrete and the corrosion of embedded steel bar," *Constr. Build. Mater.*, **169**, 462–472 (2018).
5. Z. Pan, J. G. Sanjayan, and F. Collins, "Effect of transient creep on compressive strength of geopolymer concrete for elevated temperature exposure," *Cem. Concr. Res.*, **56**, 182–189 (2014).
6. M. Łach, K. Korniejenko, and J. Mikuła, "Thermal insulation and thermally resistant materials made of geopolymer foams," *Procedia Eng.*, **151**, 410–416 (2016).
7. K. Korniejenko, E. Frączek, E. Pytlak, and M. Adamski, "Mechanical properties of geopolymer composites reinforced with natural fibers," *Procedia Eng.*, **151**, 388–393 (2016).
8. J. Sliseris, "Numerical estimation of mechanical properties of steel fiber reinforced geopolymer composite," *Mech. Comp. Mat.*, **54**, No. 5, 621–634 (2018).
9. S. D. Nikolenko, E. A. Sushko, S. A. Sazonova, A. A. Odnolko, and V. Ya. Manokhin, "Behaviour of concrete with a disperse reinforcement under dynamic loads," *Mag. Civil Eng.*, **75**, No. 7, 3–14 (2017).
10. V. I. Travush, D. V. Konin, and A. S. Krylov, "Strength of reinforced concrete beams of high-performance concrete and fiber reinforced concrete," *Mag. Civil Eng.*, **77**, No. 1, 90–100 (2018).
11. A. I. Kirsanov and O. N. Stolyarov, "Mechanical properties of synthetic fibers applied to concrete reinforcement," *Mag. Civil Eng.*, **80**, No. 4, 15–23 (2018).
12. T. A. Nizina and A. S. Balykov, "Experimental-statistical models of the properties of modified dispersed-reinforced fine-grained concrete," *Mag. Civil Eng.*, **62**, No. 2, 13–26, (2016).
13. Yu. G. Barabanshchikov, A. A. Arkharova, and M. V. Ternovskii, "On the influence on the efficiency of anti-shrinkage additives superplasticizer," *Mag. Civil Eng.*, **51**, No. 7, 23–30 (2014).
14. A. P. Svintsov, Yu. V. Nikolenko, M. I. Kharun, and A. S. Kazakov, "Effect of viscosity of petroleum products on deformation properties of concrete," *Mag. Civil Eng.*, **51**, No. 7, 16–22 (2014).
15. A. I. Grishchenko, A. S. Semenov, S. G. Semenov, and B. E. Melnikov, "Influence of structural parameters of the masonry on effective elastic properties and strength," *Mag. Civil Eng.*, **49**, No. 5, 95–106 (2014).
16. A. S. Gorshkov and N. I. Vatin, "Properties of the wall structures made of autoclaved cellular concrete products on the polyurethane foam adhesive," *Mag. Civil Eng.*, **40**, No. 5, 5–19 (2013).
17. M. Lazarevska, M. Cvetkovska, M. Knezevic, A. Trombeva Gavriloska, M. Milanovic, V. Murgul, and N. Vatin, "Neural network prognostic model for predicting the fire resistance of eccentrically loaded RC columns," *App. Mech. Mat.*, **627**, 276–282 (2014).
18. V. Korsun, N. Vatin, A. Korsun, and D. Nemova, "Physical-mechanical properties of the modified fine-grained concrete subjected to thermal effects up to 200°C," *Appl. Mech. Mat.*, **633–634**, 1013–1017 (2014).
19. I. Garanzha and N. Vatin, "Analytical methods for determination a load capacity of concrete-filled tubes under axial compression," *Appl. Mech. Mat.*, **633–634**, 965–971 (2014).
20. M. Łach, D. Mierzwiński, K. Korniejenko, J. Mikuła, and M. Hebda, "Geopolymers as a material suitable for immobilization of fly ash from municipal waste incineration plants," *J. Air Waste Manage. Assoc.*, **68**, No 11, 1190–1197 (2018).
21. A. Sprince, "Methodology for Determination of Long-Term Properties and Crack Development Research in Extra Fine Aggregate Cement Composites," PhD Thesis, Riga, [RTU], 70–77 (2015).

Annex III: Paper III:


Gailitis, R., Sprince, A., Kozlovskis, T., Radina, L., Pakrastins, L., Vatin, N.

Long-term properties of different fiber reinforcement effect on fly ash-based geopolymer composite

Crystals, 11 (7), art. no. 760

Article

Long-Term Properties of Different Fiber Reinforcement Effect on Fly Ash-Based Geopolymer Composite

Rihards Gailitis ^{1,*}, Andina Sprince ¹, Tomass Kozlovskis ¹, Liga Radina ¹, Leonids Pakrastins ¹ and Nikolai Vatin ² 

¹ Faculty of Civil Engineering, Riga Technical University, LV-1658 Riga, Latvia; andina.sprince@rtu.lv (A.S.); tomass.kozlovskis@rtu.lv (T.K.); liga.radina@rtu.lv (L.R.); leonids.pakrastins@rtu.lv (L.P.)

² Peter the Great St. Petersburg Polytechnic University, 195251 St. Petersburg, Russia; vatin@mail.ru

* Correspondence: rihards.gailitis@edu.rtu.lv

Abstract: Geopolymer composites have been around only for 40 years. Nowadays, they are used in buildings and infrastructures of various kinds. A geopolymer's main benefit is that it is a green material that is partially made by utilizing waste products. The carbon footprint from geopolymer matrix manufacturing is at least two times less than Portland cement manufacturing. Due to the nature of the geopolymer manufacturing process, there is a high risk of shrinkage that could develop unwanted micro-cracks that could reduce strength and create higher creep strains. Because of this concern, a common strategy to reduce long-term strains of the material, such as shrinkage and creep, is to add fiber reinforcement that would constrain crack development in the material. This article aims to determine how various kinds and amounts of different fiber reinforcement affect fly ash-based geopolymer composites' creep strains in compression. Specimen mixes were produced with 1% steel fibers, 1% polypropylene fibers, 5% polypropylene fibers, and without fibers (plain geopolymer). For creep and shrinkage testing, cylindrical specimens $\text{Ø}46 \times 190$ mm were used. The highest creep resistance was observed in 5% polypropylene fiber specimens, followed by 1% polypropylene fiber, plain, and 1% steel fiber specimens. The highest compressive strength was observed in 1% polypropylene fiber specimens, followed by plain specimens, 1% steel fiber specimens, and 5% polypropylene fiber-reinforced specimens. The only fiber-reinforced geopolymer mix with improved long-term properties was observed with 1% polypropylene fiber inclusion, whereas other fiber-introduced mixes showed significant decreases in long-term properties. The geopolymer composite mix with 1% polypropylene fiber reinforcement showed a reduction in creep strains of 31% compared to the plain geopolymer composite.

Keywords: fly ash-based geopolymer composite; long-term properties; fiber-reinforced geopolymer



check for updates

Citation: Gailitis, R.; Sprince, A.; Kozlovskis, T.; Radina, L.; Pakrastins, L.; Vatin, N. Long-Term Properties of Different Fiber Reinforcement Effect on Fly Ash-Based Geopolymer Composite. *Crystals* **2021**, *11*, 760. <https://doi.org/10.3390/cryst11070760>

Academic Editors: Michele Iafisco and Helmut Cölfen

Received: 6 May 2021

Accepted: 24 June 2021

Published: 29 June 2021

Publisher's Note: MDPI stays neutral with regard to jurisdictional claims in published maps and institutional affiliations.



Copyright: © 2021 by the authors. Licensee MDPI, Basel, Switzerland. This article is an open access article distributed under the terms and conditions of the Creative Commons Attribution (CC BY) license (<https://creativecommons.org/licenses/by/4.0/>).

1. Introduction

In recent years, there has been increased interest in geopolymer composites. A geopolymer composite (GP/GPC) is a three-dimensional inorganic material with multiple beneficial qualities, such as a significantly reduced carbon footprint caused by its manufacturing, increased resistance to high-temperature exposure, and resistance to various kinds of acid exposure [1–4]. It is reckoned that the manufacturing of 1 ton of kaolin-based geopolymer cement production generates 0.180 tons of CO₂, unlike ordinary Portland cement (OPC) concrete, which has a carbon footprint that is up to 6 times greater. At the same time, the cost margin varies from 7% lower to 39% higher than OPC [5,6].

The creep behavior of cementitious binders significantly affects the durability and serviceability of concrete structures. There have been several studies focused on the creep in compression. Most of them have found that, in most cases, the creep of a geopolymer composite is less than OPC [7–10].

Drying shrinkage is also a factor that influences long-term strains. According to capillary tension theory, it has been claimed that shrinkage strains are caused by capillary

pressure in the pore walls. For a geopolymer composite, the ways to reduce the pore amount include the modification of pore structure or reduction of water loss during curing, or the inclusion of inert or reactive fillers and fibers [11–13]. In certain cases, the addition of fibers can significantly reduce or even eliminate shrinkage strains. It has been claimed that 0.5 vol% of polypropylene fibers or steel fibers reduce the shrinkage significantly, but the inclusion of 2 vol% of steel fibers results in almost no shrinkage [14–16].

To enhance mechanical properties and, therefore OPC structural applications, fiber reinforcement is used. Two groups of fibers are used: (i) fibers with a low modulus of elasticity and high elongation properties (such as polypropylene, nylon, polyethylene, etc., fibers) and (ii) fibers with a high modulus of elasticity (such as carbon, steel, and glass fibers). In general, the first group does not improve the strength. Instead, they improve fracture toughness and resistance to impact and explosion loads. The second group does effectively enhance the strength and stiffness properties [17].

Polypropylene fibers (PPFs) are the most often used commercial fibers due to their cost compared to steel fibers as well as their corrosion resistance [18]. They also have many advantages over other synthetic fibers, mostly due to their lightweight properties, cost efficiency, low thermal conductivity, and resistance to acid and alkali attacks [17]. Furthermore, the plain polypropylene fibers have the ecological benefit of decomposing in the natural environment, unlike polypropylene fiber fabric [19]. According to previous studies, PPF incorporation improves splitting tensile strength and flexural strength, creep behavior, tensile strength, and shrinkage reduction. It has been claimed that the incorporation of 1% PPF results in the optimum performance enhancement to splitting and flexural strength performance increases. Still, the fiber incorporation above 3% leads to a decrease in workability [17].

Steel fibers (SFs) are increasingly used as auxiliary reinforcement for temporary load cases, partial substitution of conventional reinforcement, and a total replacement of traditional reinforcement in overall compression. Due to SF-reinforced concrete structure having good overall durability and mechanical performance, it has gained popularity, and the conventional reinforcement has been partially or completely replaced in statically indeterminate structures [20]. Steel fiber increases mechanical properties such as the strength and stiffness of concrete [17]. They are used in structural applications where it is important to control the cracking processes, such as industrial pavements and tunnel linings and ultra-high performance steel fiber-reinforced structures, such as cooling towers, silos, sewage, and industrial wastewater tunnels and treatment plants. The addition of SF increases deformation and ductility capacity in cases where the maximum flexural load is exceeded [20,21]. It has been revealed that the distribution and orientation of SF significantly affect the strengthening effect of concrete. Also, the aggregate should not exceed three-quarters of the length of fiber or 25 mm [22].

Due to the previously stated environmental concerns and the apparent benefits of geopolymer composite and fiber incorporation in OPC, it is necessary to evaluate the fiber influence on creep and shrinkage strain development in geopolymer composites.

2. Materials and Methods

A geopolymer cylindrical specimen matrix was based on fly ash sourced from the local power plant in Skawina city (Poland). This kind of fly ash is suitable for geopolymers because of its physical properties and chemical composition. The fly ash contains spherical aluminosilicate particles and is rich with oxides such as SiO₂ (47.81%) and Al₂O₃ (22.80%). The high value of SiO₂ and Al₂O₃ provides advantages for geopolymerization.

Geopolymer specimens were prepared using sodium promoter, fly ash, and sand (the ratio of sand to fly ash was 1:1). The activation solution was made using a 10-molar (10 M) NaOH solution combined with the sodium silicate R-145 solution (with a molar module of 2.5 and a density of around 1.45 g/cm³, with a ratio of NaOH and Na₂O + SiO₂ of 1:2.5). The technical NaOH in flake form and tap water was used instead of distilled water to make NaOH solution. The alkaline solution was prepared by pouring sodium silicate

and water over solid sodium hydroxide into the aqueous solution of sodium silicate and water. The solution was mixed and left over night until its temperature stabilized and the concentrations were equalized. The fly ash, sand, and alkaline solution were mixed for about 15 min using a low-speed mixing machine in order to create a homogenous paste. A quarter of the specimens were reinforced with 1% (by mass) of short PPFs (approximately 3 mm in length), another quarter of the specimens were reinforced with 5% of the same PPFs, another quarter of the specimens were reinforced with 1% steel fibers (approximately 18 mm in length), and last quarter of the specimens were plain geopolymer. Next, the mixes were poured into the plastic molds, as shown in Figures 1 and 2. The specimens were hand-formed, and then the air bubbles were removed by vibrating. The molds were heated in the laboratory dryer for 24 h at 75 °C. After the geopolymerization process, specimens were unmolded [23,24]. All of the geopolymer specimens were prepared at Cracow University of Technology (CUT).



Figure 1. Geopolymer composite mixes, which were reinforced with 1% (a) and 5% (b) polypropylene fibers.



Figure 2. Geopolymer composite mixes, which were reinforced with 1% steel fibers reinforced (a) and plain (b).

For creep strain tests in compression, specimens were prepared according to RILEM TC 107-CSP recommendations [25]. All specimens were shaped to dimensions of $\text{Ø}46 \times 190$ mm or approximately 1:4 diameter to height ratio. For strain gauge attachment, 6 aluminum plates (10×15 mm) were glued in pairs to each specimen. Afterwards, strain gauges were attached to those plates, as is shown in Figure 3a. Two aluminum plates were glued to the specimens to determine the shrinkage—one to the top and one to the bottom part of it. Hereupon, shrinkage specimens were placed in the measuring stand to determine the shrinkage strains throughout testing time, as is shown in Figure 3b. All the specimen preparatory work was done at Riga Technical University (RTU). Creep and shrinkage tests were carried out in a room with controlled atmosphere conditions: temperature 24 ± 1 °C and relative humidity $30\% \pm 3\%$.



Figure 3. Prepared creep test specimens (a) and shrinkage specimens (b).

Shrinkage and creep strains were monitored every day for the first two weeks, after which they were monitored every other day. A constant load was applied throughout the whole creep testing period. The specimens were loaded with a load equivalent to 20% of the ultimate compressive strength, which was determined in compressive strength tests. Specimens were loaded gradually by 25% of the determined load in a short period (within 5 min). A creep test was carried out on tests stands, as is shown in Figure 4.

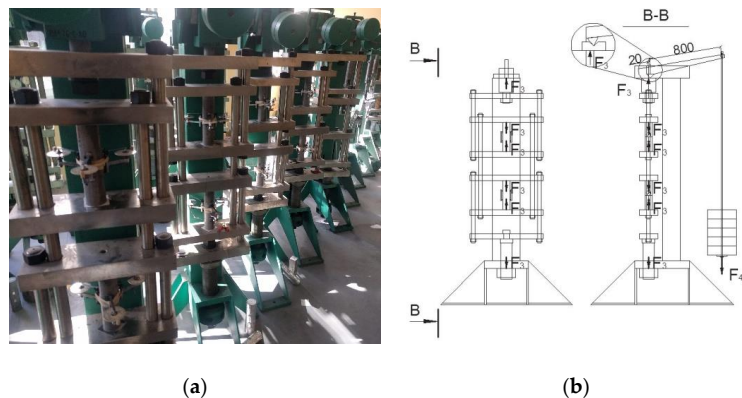


Figure 4. Creep test specimens set up in stands (a) and the test stand scheme (b) [26].

3. Results and Discussion

The compressive strength was determined before the creep tests. For each mix type, four specimens were used to determine compressive strength values. The specimen's age at the time of testing was 28 days. The compressive strength values are shown in Table 1 and Figure 5.

The applied load and counterweight amount necessary for creep test stands were calculated, considering the compressive strength values represented in Table 1. As Moradikhous states [27], the compressive strength improvement due to fiber incorporation is slight. However, with 5% PPF and 1% SF incorporation, the compressive strength is significantly lower. Ravinder et al. claimed that when fiber dosage increased from 0% to 0.3%, the compressive strength increased by 6% [28]. From Figure 5, it is clear that 1% PPF inclusion into the mix has improved the compressive strength of the composite. The compressive strength has increased by 4.9% in contrast to OGP. Other authors have observed that the compressive strength went up with a certain fiber inclusion amount, and when this amount is exceeded, the compressive strength drops significantly [29,30]. The compressive strength increased up until the fiber amount reached 0.60% by volume. Afterwards, the compressive

strength of the tested high-strength concrete specimens drops significantly down to the compressive strength level of a plain high-strength concrete specimen (PPF reinforcement 0.9% by volume). Similarly, it is with geopolymer composites where specimens with 5% PPF incorporation show an 18.62 MPa or a 35.5% drop from OGP compressive strength. Furthermore, the error amount in the compressive strength tests for the 5% PPF reinforced composites are twice as big as those for plain geopolymer specimens; therefore, it seems that a higher amount of fiber incorporation into the composite does not only affect the mouldability of it but also an inner structure that significantly affects compressive strength.

Table 1. Compressive strength values of different types of specimens.

Test Specimen Type	Average Compressive Strength, MPa
Plain geopolymer composite (OGP)	52.5
Geopolymer composite with 1% polypropylene fibers (GP with 1% PPF)	55.1
Geopolymer composite with 5% polypropylene fibers (GP with 5% PPF)	33.9
Geopolymer composite with 1% steel fibers (GP with 1% SF)	48.4

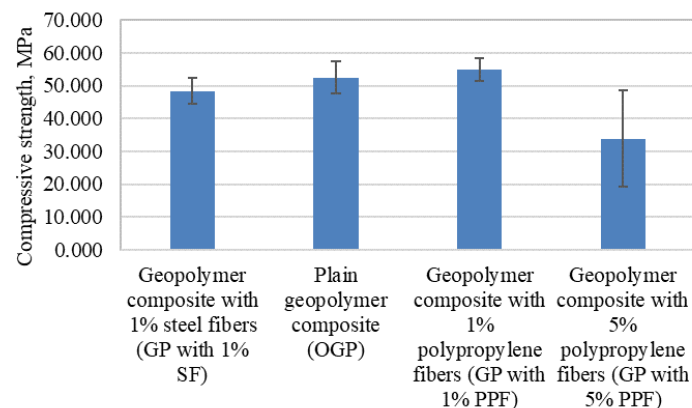


Figure 5. Geopolymer composite compressive strength values with measurement errors.

The creep and shrinkage tests were started after the first compressive strength test. Creep and shrinkage tests were carried out for 67 days.

The total strains and creep strains (total strains without shrinkage strains) are shown in Figure 6.

Figure 6a,b show that the shrinkage strain amount is around 20% to 25% of all of the long-term total strain amount for all of the tested specimens. Notably, the shrinkage strains for the specimens with 1% steel fiber-reinforced geopolymer meaningfully decrease, unlike the other geopolymer specimens. It is also visible that the creep strain curves have much slower strain, gaining capacity in the first 14 days without shrinkage strain. It is apparent that the geopolymer composite with 5% polypropylene fibers has the least amount of total strains and creep strains. Furthermore, the 1% steel fiber incorporation into the mix seems to not give any gains regarding creep strains and shrinkage strain reduction. Steel fiber incorporation has made it even worse than plain geopolymer. The creep strains for the 1% steel fiber geopolymer composite is, on average, 40% higher than the plain geopolymer. Additionally, a significant amount of elastic strains are observed in the curves of Figure 6. To evaluate creep strain amount, more thoroughly elastic strains were taken away (please see Figure 7).

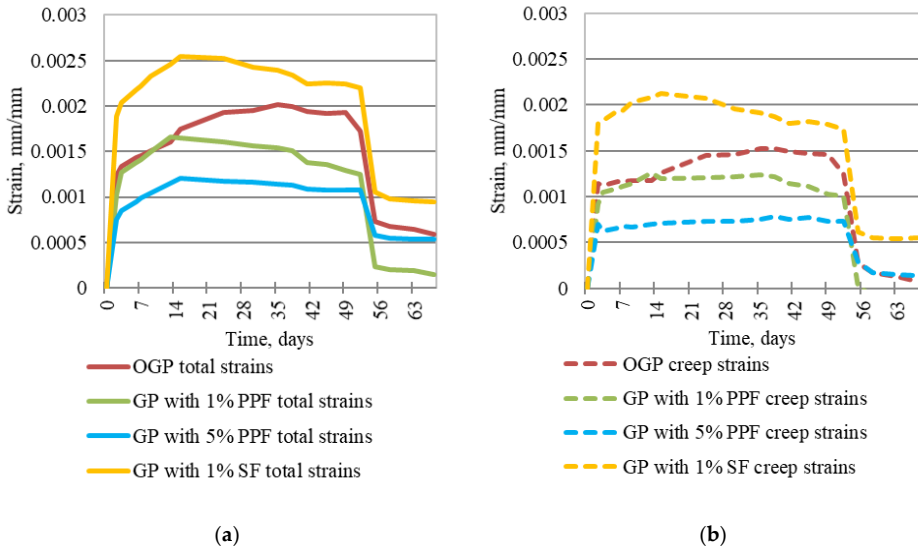


Figure 6. Reinforced and plain geopolymer composite total strains (a) and creep strains (b).

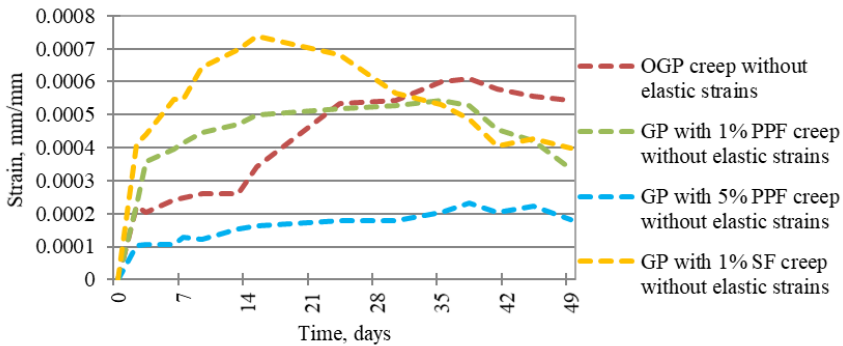


Figure 7. Creep strains without elastic strains of reinforced and plain geopolymer composite.

If the elastic strains are taken away, the relation of Figure 6b for the first 28 days is still visible in Figure 7. It is apparent from reviewing Figures 6b and 7 that the amount of elastic strains for the tested specimens varies from 68.5% to 80.9%. The elastic strains for tested geopolymer composites are 80.9%, 77.6%, 75.0%, and 68.5% for specimens with 5% PPF, 1% SF, OGP, and 1% PPF, respectively. The highest creep strain was observed in the specimens that were reinforced with 1% steel fibers. The lowest creep strains were observed for the specimens that were reinforced with 5% polypropylene fiber.

Obtained results from long-term property tests and compressive strength tests lead to thinking that only a geopolymer composite with 1% PPF incorporation could be used for engineering purposes, such as repairing mortar or the prefabrication of plates. The 1% SF-reinforced geopolymer composite did not reach intended amount of load-bearing capacity, most likely due to an insufficient amount of fiber incorporation. The 5% PPF-reinforced geopolymer composite specimens showed the lowest creep strains. However, the compressive strength for these composites was the lowest and the greatest margin of error within the tested specimens. Additionally, these specimens had the highest elastic strain of all the tested specimens. Therefore, it is apparent that reinforcement amount for the 5% PPF

reinforced geopolymer composite specimens was too much, and the reinforcement amount of 3% could represent a sufficient amount of PPF reinforcement. As for the shrinkage, the 1% PPF and 5% PPF showed the lowest values, followed by the 1% SF and OGP. The 5% PPF-reinforced composite showed, on average, a 27.27%, 60.33%, and 63.20% lower shrinkage strains than the 1% PPF-reinforced geopolymer composite, the 1% SF-reinforced composite, and the OGP composite, respectively.

4. Conclusions

Long-term properties of fly ash-based geopolymer composite with various amounts and kinds of reinforcement were determined by performing 67-day creep and shrinkage tests. Additionally, compressive strength was determined before the long-term testing. Results of the research showed the following findings:

- The geopolymer composite with 5% polypropylene fiber incorporation had the highest creep resistance of all types of specimens, followed by specimens with 1% polypropylene fiber reinforcement, the plain geopolymer, and specimens with 1% steel fiber reinforcement. At the peak, the geopolymer with 1% polypropylene fiber had 1.40 times higher creep strains. In comparison, the geopolymer without reinforcement and with 1% steel fiber had values that were 1.99 and 2.44 times higher, respectively.
- If the elastic strains are exempt, then the 5% polypropylene fiber reinforced geopolymer showed the smallest amount of creep strains, followed by the 1% polypropylene fiber-reinforced specimen, the 1% steel fiber-reinforced specimen, and the plain geopolymer specimen. The creep deformation differences were 1.84, 2.19, and 2.99 times, respectively.
- The specimens with 5% polypropylene had the least elastic strains, followed by the 1% polypropylene-reinforced specimen, the plain specimen, and the 1% steel fiber-reinforced geopolymer composite specimen. The difference were 1.25, 1.67, and 2.52 times, respectively.
- Each type of reinforcement was observed to have its own optimal amount that contributes to increased material mechanical and long-term properties. A 10-M geopolymer composite incorporating 1% polypropylene fibers was observed to improve the compressive strength, providing low creep and shrinkage strains. Specimens with 5% polypropylene fiber reinforcement were observed to have the lowest creep and second lowest shrinkage strains. They also were observed to have the lowest compressive strength of all of the tested specimens.

Author Contributions: Data curation, R.G. and T.K.; Formal analysis, R.G.; Resources, L.R.; Supervision, A.S. and L.P.; Writing—original draft, R.G.; Writing—review & editing, A.S., T.K. and N.V. All authors have read and agreed to the published version of the manuscript.

Funding: This research was partially funded by the Ministry of Science and Higher Education of the Russian Federation as part of World-class Research Center program: Advanced Digital Technologies (contract No. 075-15-2020-934 dated 17 November 2020). This work was supported by the European Regional Development Fund within the Activity 1.1.1.2 “Post-doctoral Research Aid” of the Specific Aid Objective 1.1.1 “To increase the research and innovative capacity of scientific institutions of Latvia and the ability to attract external financing, investing in human resources and infrastructure” of the Operational Programme “Growth and Employment” (No.1.1.1.2/VIAA/3/19/401). This publication was supported by Riga Technical University’s Doctoral Grant programme.

Conflicts of Interest: The authors declare no conflict of interest.

References

1. Yan, S.; He, P.; Jia, D.; Wang, J.; Duan, X.; Yang, Z.; Wang, S.; Zhou, Y. Effects of high-temperature heat treatment on the microstructure and mechanical performance of hybrid Cf-SiCf-(Al₂O₃)₃ reinforced geopolymer composites. *Compos. Part B Eng.* **2017**, *114*, 289–298. [[CrossRef](#)]
2. Lokuge, W.; Wilson, A.; Gunasekara, C.; Law, D.W.; Setunge, S. Design of fly ash geopolymer concrete mix proportions using Multivariate Adaptive Regression Spline model. *Constr. Build. Mater.* **2018**, *166*, 472–481. [[CrossRef](#)]

3. Galiano, Y.L.; Leiva, C.; Villegas, R.; Arroyo, F.; Vilches, L.; Fernández, C.L. Carbon fiber waste incorporation in blast furnace slag geopolymer-composites. *Mater. Lett.* **2018**, *233*, 1–3. [CrossRef]
4. Pan, Z.; Sanjayan, J.G.; Collins, F. Effect of transient creep on compressive strength of geopolymer concrete for elevated temperature exposure. *Cem. Concr. Res.* **2014**, *56*, 182–189. [CrossRef]
5. Nguyen, K.; Le, T.A.; Lee, K. Evaluation of the mechanical properties of sea sand-based geopolymer concrete and the corrosion of embedded steel bar. *Constr. Build. Mater.* **2018**, *169*, 462–472. [CrossRef]
6. Sele, L.; Bajare, D.; Bumanis, G.; Dembovska, L. Alkali Activated Binders Based on Metakaolin. *Environ. Technol. Resour. Proc. Int. Sci. Pract. Conf.* **2015**, *1*, 200–204. [CrossRef]
7. Wallah, S.E.; Rangan, B.V. Low-Calcium Fly Ash Based. 2006, pp. 1–107. Available online: <https://espace.curtin.edu.au/handle/20.500.11937/34322> (accessed on 6 May 2021).
8. Sagoe-Crentsil, K.; Brown, T.; Taylor, A. Drying shrinkage and creep performance of geopolymer concrete. *J. Sustain. Cem. Mater.* **2013**, *2*, 35–42. [CrossRef]
9. Chen, S.; Wu, C.; Yan, D. Binder-scale creep behavior of metakaolin-based geopolymer. *Cem. Concr. Res.* **2019**, *124*, 105810. [CrossRef]
10. Khan, I.; Xu, T.; Castel, A.; Gilbert, R.I.; Babae, M. Risk of early age cracking in geopolymer concrete due to restrained shrinkage. *Constr. Build. Mater.* **2019**, *229*, 116840. [CrossRef]
11. Nizina, T.; Balykov, A. Experimental-statistical models of properties of modified fiber-reinforced fine-grained concretes. *Mag. Civ. Eng.* **2016**, *62*, 13–25. [CrossRef]
12. Lee, N.; Jang, J.; Lee, H. Shrinkage characteristics of alkali-activated fly ash/slag paste and mortar at early ages. *Cem. Concr. Compos.* **2014**, *53*, 239–248. [CrossRef]
13. Kuenzel, C.; Li, L.; Vandeperre, L.; Boccaccini, A.; Cheeseman, C. Influence of sand on the mechanical properties of metakaolin geopolymers. *Constr. Build. Mater.* **2014**, *66*, 442–446. [CrossRef]
14. Ranjbar, N.; Talebian, S.; Mehrali, M.; Kuenzel, C.; Metselaar, H.S.C.; Jumaat, M.Z. Mechanisms of interfacial bond in steel and polypropylene fiber reinforced geopolymer composites. *Compos. Sci. Technol.* **2016**, *122*, 73–81. [CrossRef]
15. Ranjbar, N.; Mehrali, M.; Mehrali, M.; Alengaram, U.J.; Jumaat, M.Z. High tensile strength fly ash based geopolymer composite using copper coated micro steel fiber. *Constr. Build. Mater.* **2016**, *112*, 629–638. [CrossRef]
16. Ranjbar, N.; Zhang, M. Fiber-reinforced geopolymer composites: A review. *Cem. Concr. Compos.* **2020**, *107*, 103498. [CrossRef]
17. Das, C.S.; Dey, T.; Dandapat, R.; Mukharjee, B.B.; Kumar, J. Performance evaluation of polypropylene fibre reinforced recycled aggregate concrete. *Constr. Build. Mater.* **2018**, *189*, 649–659. [CrossRef]
18. Xin, C.; Wang, Z.; Zhou, J.; Gao, B. Shaking table tests on seismic behavior of polypropylene fiber reinforced concrete tunnel lining. *Tunn. Undergr. Space Technol.* **2019**, *88*, 1–15. [CrossRef]
19. Qin, Y.; Zhang, X.; Chai, J.; Xu, Z.; Li, S. Experimental study of compressive behavior of polypropylene-fiber-reinforced and polypropylene-fiber-fabric-reinforced concrete. *Constr. Build. Mater.* **2019**, *194*, 216–225. [CrossRef]
20. Marcos-Meson, V.; Fischer, G.; Edvardsen, C.; Skovhus, T.; Michel, A. Durability of Steel Fibre Reinforced Concrete (SFRC) exposed to acid attack—A literature review. *Constr. Build. Mater.* **2019**, *200*, 490–501. [CrossRef]
21. Ruiz, G.; de la Rosa, Á.; Poveda, E. Relationship between residual flexural strength and compression strength in steel-fiber reinforced concrete within the new Eurocode 2 regulatory framework. *Theor. Appl. Fract. Mech.* **2019**, *103*, 102310. [CrossRef]
22. Han, J.; Zhao, M.; Chen, J.; Lan, X. Effects of steel fiber length and coarse aggregate maximum size on mechanical properties of steel fiber reinforced concrete. *Constr. Build. Mater.* **2019**, *209*, 577–591. [CrossRef]
23. Korniejenko, K. Geopolymers for Increasing Durability for Marine Infrastructure. *Spec. Publ.* **2018**, *326*, 20.1–20.10.
24. Łach, M.; Mikula, J.; Hebda, M. Thermal analysis of the by-products of waste combustion. *J. Therm. Anal. Calorim.* **2016**, *125*, 1035–1045. [CrossRef]
25. Acker, P.; Agullo, L.; Auperin, M.; Carol, I.; Carreira, D.J.; Catarino, J.M. Rilem tc 107-csp: Creep and shrinkage prediction models: Principles of their formation recommendation measurement of time-dependent strains of concrete. *Mater. Struct.* **1998**, *31*, 507–512.
26. Sprince, A.; Pakrastinsh, L.; Baskers, B.; Gaile, L. Crack Development Research in Extra Fine Aggregate Cement Composites. *Environ. Technol. Resour. Proc. Int. Sci. Pract. Conf.* **2015**, *1*, 205–208. [CrossRef]
27. Moradikhou, A.B.; Esparham, A.; Avnaki, M.J. Physical & mechanical properties of fiber reinforced metakaolin-based geopolymer concrete. *Constr. Build. Mater.* **2020**, *251*, 118965. [CrossRef]
28. Ravinder, R.; Kumar, V.; Kumar, C.; Prakash, A.; Krishna, P.V. Strength Characteristics of Fibrous Self Curing Concrete Using Super Absorbent Polymer. In Proceedings of the National Conference on Recent Advances in Civil Engineering, Coimbatore, India, 8–9 May 2019.
29. Ahmed, T.W.; Ali, A.A.M.; Zidan, R.S. Properties of high strength polypropylene fiber concrete containing recycled aggregate. *Constr. Build. Mater.* **2020**, *241*, 118010. [CrossRef]
30. Yap, S.P.; Bu, C.H.; Alengaram, U.J.; Mo, K.H.; Jumaat, M.Z. Flexural toughness characteristics of steel–polypropylene hybrid fibre-reinforced oil palm shell concrete. *Mater. Des.* **2014**, *57*, 652–659. [CrossRef]

Annex IV: Paper IV:

Gailitis R., Sprince A., Pakrastins L., Korniejenko K., Kozlovskis T.

Reinforced and Plain Geopolymer Concrete Specimen Cross-section Composition

Influence on Creep Strains

Proceedings of 4th International RILEM conference on Microstructure Related Durability of
Cementitious Composites (Microdurability2020)

REINFORCED AND PLAIN GEOPOLYMER CONCRETE SPECIMEN CROSS-SECTION COMPOSITION INFLUENCE ON CREEP STRAINS

R. Gailitis (1), A. Sprince (1), L. Pakrastins (1), K. Korniejenko (2) and T. Kozlovskis (1)

(1) Riga Technical University Riga, Latvia

(2) Cracow University of Technology, Cracow, Poland

Abstract

Low calcium alkaline solution activated cement composite, or geopolymer concrete has been around for about 40 years. The main benefit of this material - it is partially made by utilising waste products, such as fly-ash, slags and others. It has been claimed that the manufacturing of various geopolymer binder produces up to 6 times less CO₂ than the production of Portland cement. Because of the nature of the binding process of the geopolymer concrete, there are some differences in the cause of the shrinkage. Because of this aspect, the long-term property development mechanism is slightly different, and the microstructure of the specimen could be different than for ordinary Portland cement.

Although the researches regarding the geopolymer concrete composition and mechanical properties have significantly been reviewed in the previous couple of years, there has been a lack of investigations regarding the long-term properties and the conditions affecting and influencing long-term properties of the geopolymer concrete.

Two geopolymer concrete mixes are the test subject for this article - plain geopolymer and reinforced geopolymer with 1% waste steel fibers that have been subjected to creep and shrinkage tests. Waste steel fibers are the by-product of the car tire recycling process. The steel industry is not willing to take them, but if recycle these products they can be used as fiber reinforcement. The microstructure analyses with SEM were done by analysing specimens polished sections. Afterward acquired images of specimen cross-sections were analysed by determining the amount of fiber, geopolymer binder, filler, and air void amount in analysed cross-section. The results were cross-referenced with creep and shrinkage test results of analysed specimens.

The aim of this article is to determine the loading influence and geopolymer concrete microstructure influence on long-term properties by evaluating polished specimen sections.

Keywords: Geopolymer concrete, polished section micro-analysis, long-term properties

1. INTRODUCTION

In recent years there has been increased interest in low carbon footprint materials such as geopolymer concrete. Geopolymer concrete is a novel three-dimensional inorganic material that

is formed due to a silicon and aluminium reaction that is activated by hydroxide silicates from sodium and potassium alkali activating solution. There are several beneficial properties such as low CO₂ emissions, low cost, low density and remarkable mechanical properties [1–4]. As the mechanical properties are similar to Portland cement concrete geopolymer concrete main advantage in this scope is its environmental contribution. If geopolymer matrix fully replaces the Portland cement the carbon emission for this material drops from 26 to 46% and reduction in costs varies from 7% less up to 39 % higher than for material with Portland cement as a binder [4, 5].

In terms of sustainable and effective resource management, it is critical to recycle and reuse industrial waste as much as possible so that the fraction of recycled material that goes to landfills is as little as possible. Furthermore, produced materials from recycled products should have new added value [6, 7]. Every year approximately 17 million tons of old tires are created, that have no further use [8]. This waste is a serious contaminant to the environment, so it is extremely important to recycle them.

Creep is an essential factor in human-made materials, especially to concrete and similar materials. Stress and deformation distribution throughout the cross-section of the specimen is affected by creep. The main creep affecting factors are the temperature of the surrounding environment, relative humidity, and applied stress level [9, 10].

As the shrinkage strains appear simultaneously to creep strains, it is crucial to measure shrinkage throughout the time of creep testing. Geopolymer shrinkage appears mainly due to water loss while curing reaction and evaporation and pore structure relevant factors, for example, alkaline activator, water content, binder material, and curing conditions. The pores develop during the polymerisation process [11].

This study shows the microstructure difference of waste steel cord reinforced and plain geopolymer concrete that has/has not been subjected to load.. And further, the microstructure composition results have been tried to link to achieved creep strains.

2. MATERIALS AND METHODS

Geopolymer cylindrical specimen matrix was based on fly ash sourced from the power plant in Skawina city (Poland). This fly ash is suitable for geopolymers because of its physical and chemical properties. The fly ash contains spherical aluminosilicate particles as well as it is rich with oxides such as SiO₂ (47.81%), Al₂O₃ (22.80%). The high value of SiO₂ and Al₂O₃ gives advantages for polymerisation [12].

Geopolymer specimens were prepared using sodium promoter, fly ash, sand (ratio sand and fly ash – 1:1). The process of activation has been made by 10M NaOH solution combined with the sodium silicate solution (at a ratio of 1:2.5). To make the composite the technical NaOH as flakes were used and water solution of sodium silicate R-145. Tap water was used instead of the distilled one. The alkaline solution was prepared by pouring the aqueous solution of sodium silicate and water over solid sodium hydroxide. The solution was mixed and leftover the night until its temperature is stabilised, and the concentrations equalised. The fly ash, sand, and alkaline solution were mixed for about 15 minutes by using a low-speed mixing machine (to receive the homogenous paste). Then half of the specimens were reinforced with 5% by mass of steel cords from recycled car tires. Then the mix was poured into the plastic moulds as it is shown in Fig.1. The specimens were hand-formed and then the air bubbles were removed by vibrating them. Moulds were heated in the laboratory dryer for 24h at 75 °C. Then, the

specimens were unmolded. All the geopolymer specimen preparation was done at Cracow University of Technology (CUT), Poland.



Figure 1: Plain geopolymer (a) and recycled tire steel cord reinforced geopolymer (b) concrete

All specimens were prepared according to RILEM recommendations [13]. The dimensions of the specimens were $\varnothing 46 \times 190$ mm or $\frac{1}{4}$ diameter to height ratio respectfully.

For creep deformation tests, 6 aluminium plates (10 x 15 mm) were glued to each specimen in pairs. Afterward, strain gauges were attached to those plates. For the shrinkage specimens, 1 aluminium plate was glued to the top and bottom part of the specimen. Afterward, shrinkage specimens were placed in the measuring stand to measure the shrinkage throughout testing time. All the specimen preparatory work was done at Riga Technical University (RTU), Latvia.

Creep and shrinkage strains were monitored for the first two weeks every day, afterward every two days. During creep tests, specimens were subjected to constant load throughout the whole creep testing period. The load that specimens were subjected to was equivalent to 20% of the ultimate compressive strength, which was determined in compressive strength tests. Specimens were loaded gradually by 25% of the determined load in a short period (within 5 minutes). Creep test was carried out on tests stands shown in Fig.2.

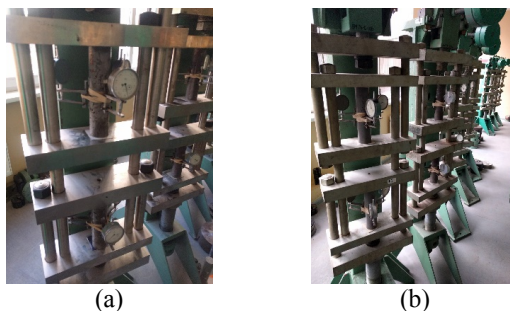


Figure 2: Specimen testing to creep strains

After creep and shrinkage tests cylinders middle parts (where the creep strain measurements were recorded) cut to disc shape specimens with a thickness of 5mm. The surfaces of specimens

were saturated with polyester resin to make specimens more durable for surface polishing cycles.

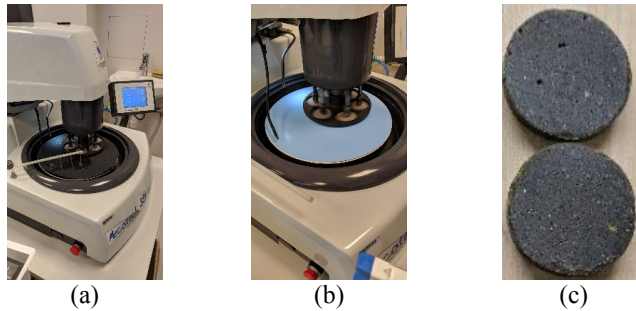


Figure 3: Specimen polishing stages (a, b) and the result (c)

Afterward, for all specimens, their surfaces were polished by various grade sandpapers and polishing compounds. The process is shown in Fig.3. Polishing was done according to the sequences shown in Table 1.

Table 1: Specimen surface polishing steps

Polishing stage number	Polishing compound (sandpaper or paste grade) type	Polishing cycle time, minutes	Compression force to specimen polishing surface, daN
1.	P180	2	2.5
2.	P320	2	2.5
3.	P600	2	2.5
4.	P1000	2	2.5
5.	3 μ m	4	2.5

Afterward, specimens were delivered to Cracow University of Technology (CUT) where they were carbon plated and surface images at 25-time magnification made.

To get the optimal amount of the specimen cross-section data and images, the reviewed cross-section is divided into zones that represent the centre, middle and outside areas of the specimen. The adopted principle is shown in Fig.4.



Figure 4: Specimen cross-section division into zones

The achieved SEM images from each examined specimen’s cross-section were joined together in Adobe Photoshop CC to get a full cross-section image. The next step was cross-section image dividing into layers based on what partition of cross-section (matrix, filler, air voids or reinforcement) is visible in it and RGB tone allocation. The process is shown in Fig. 5. The process step order is shown by the numbers. The layer dividing starts with the filler layer, then void layer, reinforcement fiber layer and finished with the matrix layer.

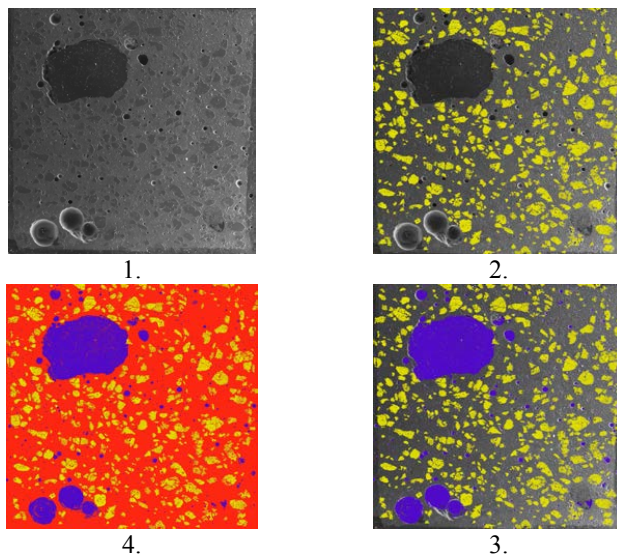


Figure 5: Image dividing sequence in layers and tone allocation

When the image was divided into layers, and the RGB tone allocated the specific tone pixel amount was divided by the number of image pixels. In doing so, the amount of particular partition of the cross-section was achieved.

3. RESULTS AND DISCUSSION

The compressive strength of the tested specimens at the beginning of the test is shown in Table 2. The specimens in the creep test were subjected to a load that was calculated from Table's 2 compressive strength values.

Table 2: Compressive strength values of 7days old cylinder specimen

Specimen material	Average compressive strength, MPa
Plain geopolymer concrete	30.37
Tire steel cord reinforced geopolymer concrete	44.52

After the initial compressive strength test, the creep and shrinkage tests were carried out for 90 days (approximately 3 months). The creep and shrinkage strain measurements are shown in Fig. 6.

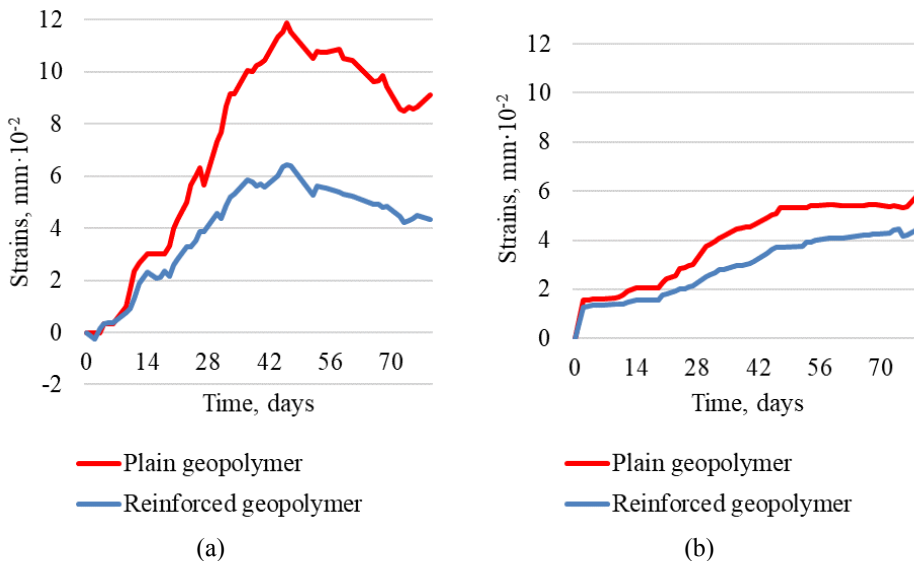


Figure 6: Shrinkage (a) and creep (b) strains

Figure 6 has shown shrinkage and creep strain curves. It is easy to determine that geopolymer concrete specimens reinforced with steel cords have significantly (~50%) less shrinkage and a bit smaller (~30%) creep properties than plain geopolymer concrete. Furthermore, it is visible that cord reinforced specimens have a slight delay in shrinkage strains to plain geopolymer specimens. That leads to thinking that steel cords from old tires have a significant restraining quality to shrinkage introduced strains.

The cross-section composition values of plain and waste steel cord reinforced geopolymer concrete is shown in Table 3.

Table 3: Average values of specimen cross-section composition

Test type	Geopolymer concrete type	Matrix amount in cross-section, %	Filler amount in cross-section, %	Air void amount in cross-section, %	Steel cord amount in cross-section, %
Shrinkage	Plain	78.96	16.91	4.13	-
	Reinforced	77.11	13.81	6.39	2.69
Creep	Plain	76.17	19.22	4.61	-
	Reinforced	77.79	15.43	5.22	1.56

From the cross-section composition values presented in Table 3, it is clear that specimens reinforced with waste tire steel cords have a significantly larger amount of air voids than plain geopolymer specimens. Also, filler distribution to creep and shrinkage specimens is uneven for both geopolymer types. For plain geopolymer, the difference is 2.31% and for reinforced specimens 1.62%. The filler amount difference in specimen cross-section composition depending on specimen type on average is 3.45% in favour of plain geopolymer. The difference is up to 2.26% for specimens that have not been subjected to load and 0.61% for those that have been loaded. This result leads to the conclusion that relatively large fiber incorporation into a geopolymer mix leads to foaming up process.

It is also apparent that the void amount for steel cord reinforced specimens that have been loaded is 19% lower than those that have not been loaded. The reason for this can be because steel cord reinforced specimens in contrast to plain ones have 32% higher compressive strength and they carried by the same amount greater load during creep tests than plain geopolymer concrete keeping the load value 20% from compressive strength load value. Therefore, the reinforcement is restraining the deformations but matrix and voids in it in this instance is the subject that is deformed for these specimens.

4. CONCLUSIONS

- The quantitative image analysis of the plain and recycled tire steel cord reinforced geopolymer concrete cross-sections shows that on average the plain geopolymer concrete specimens have from 1% up to 2.26% less amount of air voids than steel cord reinforced specimens.
- Further analysis shows that if the reviewed cross-section part is more to the centre of the specimen, then the level of the air voids decreases from 4.2% to 5.4% for plain geopolymer and from 4.7% up to 10.3% for steel cord reinforced geopolymer concrete. This could be due to insufficient vibrating to the specimens.
- Examining shrinkage and creep strain curves and cross-referencing them to achieved specimen cross-section composition, there is no direct link that cross-sections of specimens have significant flaws that would affect creep properties.
- For shrinkage strains, it is determined that for reinforced specimen greater porosity, the shrinkage strain remains lower mainly because reinforcement is restraining and delaying the strains to happen.

- Further testing and analysis are needed for specimen upper and lower parts to determine what loading influence is to specimen parts where the stress distribution is not homogeneous.

ACKNOWLEDGEMENTS

1. This work has been supported by the Latvian Council of Science within the scope of the project ‘Long term properties of innovative cement composites in various stress-strain conditions’ No. lzp-2018/2-0249.
2. This publication was supported by Riga Technical University's Doctoral Grant programme.
3. This work has been supported by the European Regional Development Fund within the Activity 1.1.1.2 “Post-doctoral Research Aid” of the Specific Aid Objective 1.1.1 “To increase the research and innovative capacity of scientific institutions of Latvia and the ability to attract external financing, investing in human resources and infrastructure” of the Operational Programme “Growth and Employment” (No.1.1.1.2/VIAA/3/19/401).

REFERENCES

- [1] A. Mehta and R. Siddique, “Sulfuric acid resistance of fly ash based geopolymer concrete,” *Constr. Build. Mater.*, vol. 146, pp. 136–143, 2017.
- [2] S. Yan *et al.*, “Effects of high-temperature heat treatment on the microstructure and mechanical performance of hybrid C f -SiC f -(Al₂O₃) reinforced geopolymer composites,” *Compos. Part B Eng.*, vol. 114, pp. 289–298, 2017.
- [3] M. Łach, D. Mierzwiński, K. Korniejenko, and J. Mięka, “Geopolymer foam as a passive fire protection,” *MATEC Web Conf.*, vol. 247, pp. 1–6, 2018.
- [4] E. Linul *et al.*, “Quasi-Static Mechanical Characterization of Lightweight Fly Ash-Based Geopolymer Foams,” *IOP Conf. Ser. Mater. Sci. Eng.*, vol. 416, no. 1, 2018.
- [5] L. Sele, D. Bajare, G. Bumanis, and L. Dembovska, “Alkali Activated Binders Based on Metakaolin,” vol. 1, pp. 200–204, 2015.
- [6] G. Mucsi, A. Szenczi, and S. Nagy, “Fiber reinforced geopolymer from synergetic utilization of fly ash and waste tire,” *J. Clean. Prod.*, vol. 178, pp. 429–440, 2018.
- [7] V. Vishwakarma and D. Ramachandran, “Green Concrete mix using solid waste and nanoparticles as alternatives – A review,” *Constr. Build. Mater.*, vol. 162, pp. 96–103, 2018.
- [8] M. Łach, A. Kiszka, K. Korniejenko, and J. Mięka, “The Mechanical Properties of Waste Tire Cords Reinforced Geopolymer Concretes,” *IOP Conf. Ser. Mater. Sci. Eng.*, vol. 416, 2018.
- [9] S. Liang and Y. Wei, “Methodology of obtaining intrinsic creep property of concrete by flexural deflection test,” *Cem. Concr. Compos.*, vol. 97, no. April 2018, pp. 288–299, 2019.
- [10] A. Sprince, L. Pakrastins, and R. Gailitis, “Long-Term Parameters of New Cement Composites BT - 3rd International Conference on the Application of Superabsorbent Polymers (SAP) and Other New Admixtures Towards Smart Concrete,” 2020, pp. 85–94.
- [11] Y. Ling, K. Wang, and C. Fu, “Shrinkage behavior of fly ash based geopolymer pastes with and without shrinkage reducing admixture,” *Cem. Concr. Compos.*, vol. 98, no. October 2018, pp. 74–82, 2019.
- [12] K. Korniejenko, M. Łach, M. Hebdowska-Krupa, and J. Mięka, “The mechanical properties of flax and hemp fibres reinforced geopolymer composites,” *IOP Conf. Ser. Mater. Sci. Eng.*, vol. 379, no. 1, 2018.
- [13] P. Acker *et al.*, “RILEM TC 107-CSP: CREEP AND SHRINKAGE PREDICTION MODELS: PRINCIPLES OF THEIR FORMATION Recommendation Measurement of time-dependent strains of concrete,” *Mater. Struct.*, vol. 31, pp. 507–512, Oct. 1998.

Annex V: Paper V:

Gailitis, R., Sprince, A., Pakrastins, L., Korniejenko, K., Kozlovskis, T.

*Plain Geopolymer Concrete Cross-Section Surface Analysis After Creep and Shrinkage
Tests in Compression and Tension*

RILEM Bookseries, 31, pp. 13-24.

Plain Geopolymer Concrete Cross-Section Surface Analysis After Creep and Shrinkage Tests in Compression and Tension

Rihards Gailitis¹, Andina Sprince¹, Leonids Pakrastins¹, Kinga Korniejenko² and Tomass Kozlovskis¹

¹ Riga Technical University, Riga, Latvia

² Cracow University of Technology, Cracow, Poland
rihards.gailitis@edu.rtu.lv

Abstract. Low calcium alkali-activated cement composite known as geopolymer has been around for more than 40 years. The main benefit of geopolymer based composites is the environmental aspect - it is partially made by utilizing waste products, such as fly-ash, slags, and others. It has been estimated that geopolymer binder production makes up to 6 times less CO₂ than the production of Portland cement. Due to the polymerization or in other words nature of the geopolymer binding process, there are some differences in creep and shrinkage development. Because of this microstructure of the specimen could be dissimilar to ordinary Portland cement. There has been an absence of investigations regarding the geopolymer composite long-term properties and micro-analysis. Also, the conditions affecting the long-term properties of the geopolymer composites have been little studied.

The subject of the research is geopolymer concrete that has been tested for creep and shrinkage in compression and tension. The specimens for microstructure analysis were acquired from the cylindrical shape (compression) and compact tension (tension) specimens. Polished sections were used for SEM microanalysis. Acquired polished section image cross-sections were analyzed by determining the amount of geopolymer binder, filler, and air void in the analyzed cross-section. The results were cross-referenced with creep and shrinkage test results. After creep and shrinkage tests in compression and tension specimen cross-section zones that have been subjected to the highest stresses were chosen and analyzed. The article's main aim is to determine the geopolymer composite microstructure and applied load influence on long-term properties.

Keywords: Geopolymer concrete, polished section microanalysis, long-term properties, compression, tension

1. Introduction

Alkali activated cement composites based on industrial waste products such as fly ash, blast furnace slag, etc., have been considered a cement for the future [1], [2]. As the cement consumption, year by year, goes up and now is responsible for 1.5 billion tonnes of CO₂ emissions annually. It becomes a significant issue around 36% of global energy consumption to research viable alternatives for less polluting binder usage with comparable properties regarding workability [3]. The use of alkali-activated materials is beneficial to CO₂ reduction. It is positive from a sustainable environment standpoint as it incorporates such industrial by-products as fly ash and slag [4]. The issue regarding wide usage of geopolymer is mainly due to the binder hardening or the polymerization process. This process requires heat; the temperature can vary from 40 to 100°C (depending on fly ash or slag type and alkali activator) and the polymerization time from 12 to 48 hours and more, therefore, excluding on-site construction works due to difficulties in achieving satisfactory structural performance [5].

Geopolymer is a low calcium alkali-activated cement composite. It is formed due to a silicon and aluminium reaction activated by hydroxide silicates from sodium and potassium alkali activating solution [6], [7].

Geopolymer concrete has similar compressive strength to regular Portland cement (PC) based composites. Unlike regular PC, geopolymer composites 85% of their final compressive strength can reach in 48 hours [8]. Long-term property wise geopolymer composites have 78% less shrinkage and 50% less creep strains than foamed regular concrete and a bit worse than regular PC composites [9].

Creep and shrinkage are well-known phenomena for cement and cement-like based composite materials, and it may influence the lifetime of structures. Most of the creep and shrinkage effects develop in the first ten years after construction. It is expected that the creep and shrinkage development after the first ten years are not significant and have a small impact on the performance of the structure [10]–[12]. Concrete and similar materials are considered to insufficient strain capacity and low tensile strength. And, consequently, they are brittle and susceptible to cracking. For cementitious composites under compression damages first happen in the paste-aggregate interface. The tensile stresses are necessary to determine long-term tensile properties for these materials [13]. Furthermore, because of the difficulties of performing tensile creep tests and differences in creep mechanisms in tension and compression, it is equally important to determine the factors that influence creep properties in compression and tension [14].

The paper focuses on the microstructure differences in specimens that have been used in creep tests in compression, tension, and shrinkage tests. Therefore, microstructure images were acquired and analysed. Results of image analysis were cross-referenced with the creep and shrinkage curves to determine whether there are notable correlations.

2. Materials and Methods

2.1. Geopolymer mix preparation

Geopolymer specimen matrixes were based on fly ash sourced from the power plant based in Skawina city (Poland). The fly ash contains spherical aluminosilicate particles and contains oxides such as SiO_2 (47.81%), Al_2O_3 (22.80%). The high value of SiO_2 and Al_2O_3 allows polymerization [15].

Geopolymer specimens were prepared using sodium promoter, fly ash, and sand (sand and fly ash ratio – 1:1). The geopolymer activation process has been made by 10M NaOH solution and the sodium silicate solution (at a rate of 1:2.5). The technical NaOH in flake form and tap water with sodium silicate R–145 solution is used to make the composite solution. The alkaline solution was prepared by pouring sodium silicate and water over solid sodium hydroxide into sodium silicate and water aqueous solution. The solution was mixed, and the temperature was stabilized. The fly ash, sand, and alkaline solution were mixed for about 15 minutes using a low-speed mixing machine (to achieve homogenous paste). Then the geopolymers were poured into the plastic moulds, as is shown in Fig.1. The specimens were hand-formed, and then the air bubbles were removed by vibrating the mass. Moulds were heated in the laboratory dryer for 24h at 75 °C. Then, the specimens were unmoulded. All the geopolymer specimen preparation was done at Cracow University of Technology (CUT), Poland.

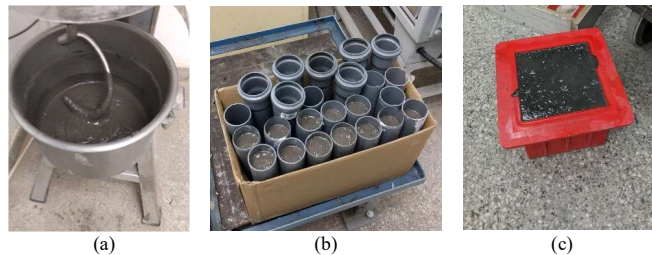


Fig. 1. Geopolymer composite preparation (a) and moulding process (b and c), CUT lab.

2.2. Test specimen preparation

For creep testing in compression, specimens were prepared according to RILEM TC 107-CSP recommendations [16]. All of the specimens were $\text{Ø} 46 \times 190$ mm or approximately 1:4 diameter to height ratio. For the dial gauge attaching six aluminium plates were glued on specimens intended for creep testing in compression. Afterward, dial gauges were attached to those plates. For shrinkage specimens one aluminium plate was glued at the bottom and top part of each specimen. After that, shrinkage specimens were placed in a stand for shrinkage measurements.

For creep measuring in tension, compact tension (CT) shaped specimens were used [17]. Specimens were cut out from a cube that was 150x150x150mm. Each cut CT specimen was 15mm thick. Afterward, the notch was cut as well as two bore holes were made (for attaching within a loading rig), as shown in Figure 2.

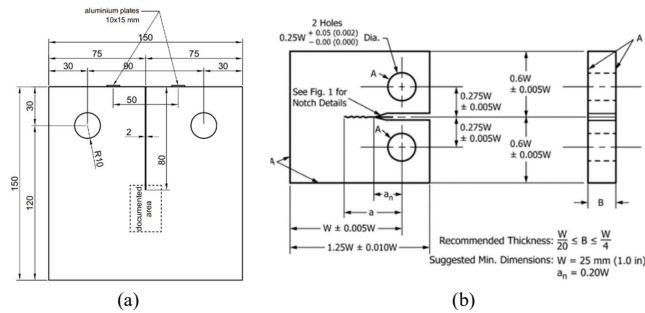


Fig. 2. Geometry of the Compact Tension (CT) specimen [17], [18].

The 2 mm wide notch in the CT specimen was sawn using a Proxxon MICRO MBS 240/E bandsaw. According to Figure 2 (a), the aluminium plates were glued to specimens intended for creep and shrinkage tests. Plates were glued 25mm to each side from the notch center. There were prepared 12 cylinders and 12 CT specimens.

2.3. Experimental setup

When the specimens' preparation was done, compressive strength and tensile strength ultimate values were determined. The procedure is shown in Figure 3.

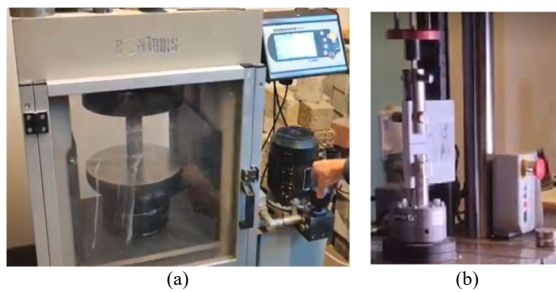


Fig. 3. Compressive (a) and tensile (b) strength determination, RTU lab.

The ultimate compressive load was determined using Controls Mod. Nr C56G2 press with a speed of 0.8 MPa/sec. The ultimate tensile load was determined using INSTRON 3000 All-Electric Dynamic Test Instrument with speed 0.15mm/sec. Determined strength values were compiled in Table 2. Following strengths determination, creep specimens were placed into lever test stands and were loaded with a constant static load equal to 20% of the ultimate load values (see Figure 4). With these stands, it is possible to apply constant loading to the specimens and to keep it uniform over a long period. Strains were measured using mechanical dial gauges “ИЧ” with a scale interval of 1/100 mm and maximum measuring range of 10 mm.

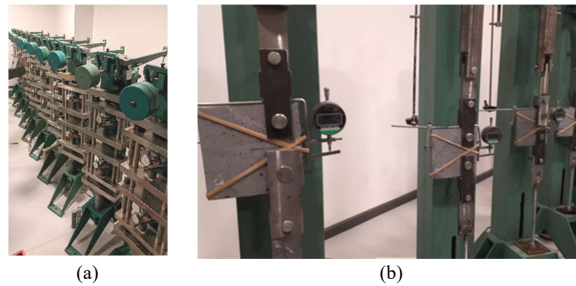


Fig. 4. Creep specimen placement into compression (a) and tension (b) test stands, RTU lab.

To determine basic creep behavior, similarly shaped shrinkage specimens were placed in equivalent environmental conditions, and their strain changes were monitored (no load applied to the shrinkage specimens). Conclusions were made based on subtracting shrinkage strain values from the creep values. Figure 5 shows the test setups for shrinkage tests. All specimens were kept in a dry atmosphere of controlled relative humidity in standard conditions: temperature $20\pm 1^{\circ}\text{C}$ and relative humidity $48\pm 3\%$. The geopolymer specimen preparation and strength, long-term tests were done at Riga Technical University (RTU), Latvia.

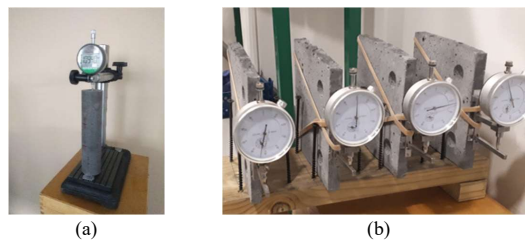


Fig. 5. Shrinkage test setup for compression (a) and tension (b) specimens, RTU lab.

2.4. Microstructure composition specimen preparation

After all long-term tests, specimen cross-section parts for the scanning electron microscope (SEM) were prepared for microstructure composition determination. Figure 6 shows prepared compression and tension specimen samples for microstructure analysis.

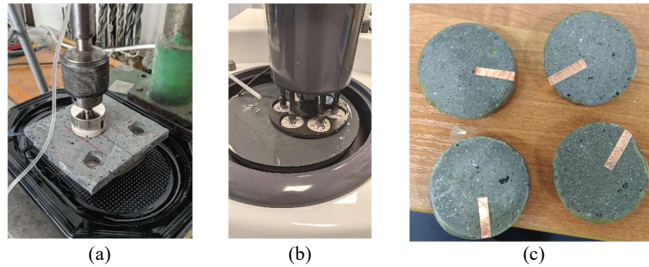


Fig. 6. SEM samples preparation (a) SEM samples polishing (b) and prepared samples before the gold plating (c), RTU lab.

For the specimens that have been subjected to compression tests, cylinders middle parts were cut into disc shape samples with a thickness of 15mm. Compact tension specimens (CT) middle part where notch ends were drilled. The drilled samples were with \varnothing 48mm and 15mm thickness. Afterward, all samples were polished according to the sequence described in Table 1.

Table 1. Specimen surface polishing sequence.

Polishing stage number	Polishing compound (sandpaper or paste grade) type	Polishing cycle time, minutes	Compression force to specimen polishing surface, daN
1.	P180	2	2.5
2.	P320	2	2.5
3.	P600	2	2.5
4.	P1000	2	2.5
5.	P1200	2	2.5
6.	3 μ m	4	2.5

When the microanalysis samples were prepared, they were delivered to Cracow University of Technology (CUT) and covered with gold. For each sample, the characteristic cross-section areas were chosen and marked. The characteristic cross-section areas were analyzed. These sample areas were shown in Figure 7.

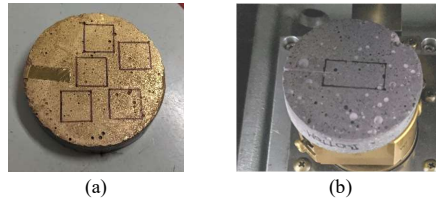


Fig. 7. Compression (a) and tension (b) SEM samples, CTU lab.

For specimens that have been subjected to compression testing, the cross-section was divided into five squared (10x10mm) section parts distributed into the central and peripheral part of the specimen cross-section. Still, for the specimens subjected to tensile loads (CT specimens), the microanalysis is done to the cross-section part near the notch and deeper into the specimen.

The SEM microanalysis was done in JEOL JSM-820. The achieved SEM images afterward were compiled together and divided into layers using Adobe Photoshop CC. The division into layers was based on partition type within cross-section (matrix, filler, air voids). For each of these partitions, the RGB tone was allocated. The process is shown in Figure 8. The layer dividing process begins with filler layer separation that was continued with the void layer.

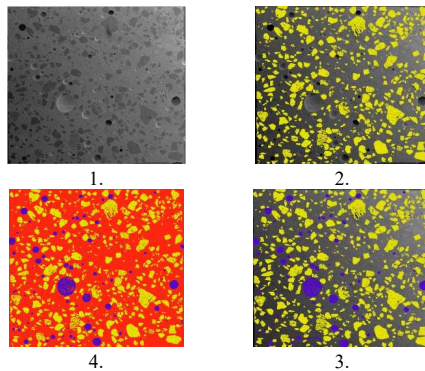


Fig. 8. Image dividing sequence in layers and tone allocation.

When the image dividing and RGB tone allocation was done, the specific tone image pixels were counted and registered. By doing so, the composition amount of the studied cross-section was acquired.

3. Results and Discussion

The compressive and tensile strength of the tested specimens is compiled in Table 2. Specimens intended for creep tests were subjected to a load equal to 20% of the load values shown in Table 2.

Table 2. Compressive and tensile ultimate load values.

Specimen type	Ultimate load value, average (kN)	Average compressive and tensile strength, MPa
Cylinders, plain geopolymer	60.35	36.33
CT, plain geopolymer	0.28	5.13

After the compression and tension ultimate load tests, the creep and shrinkage tests were carried out for 91 days (more than three months). Tests were started on the 7th day since the preparation of the specimens. The creep and shrinkage curves for compression and tension specimens are shown in Figure 9.

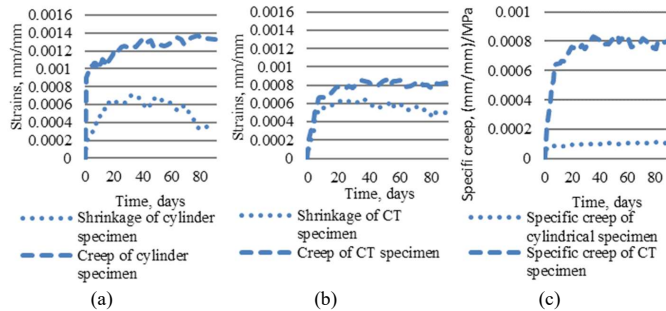


Fig. 9. Creep and shrinkage curves of compression (a) and tension (b) specimens and specific creep (c) of compression and tension specimens.

The curves in Figure 9 (a) and (b) show that throughout testing time creep strains for CT specimens are almost half of the creep strains in compression. The difference on average is 46%. It is also apparent that the amount of elastic strain at the beginning of the tests and further strain development characteristics are different for specimens in compression and tension. Furthermore, specific creep in tension (Figure 9 (c)) is more than 7 times greater than in compression. It leads to a conclusion that there are significant microstructural differences to the microstructural development of the specimens tested in compression and tension, and also, plain geopolymer composite has similar creep properties as the regular Portland cement-based composites. Also, the shrinkage curve for CT specimens in Figure 9 (b) clearly shows that specimens have properly

polymerized and achieved their modulus of elasticity close to what could be considered as the final modulus of elasticity value. Therefore, the notch is opening, unlike Portland cement composites that due to hydration would close the notch.

The obtained cross-section composition results are shown in Table 3.

Table 3. Compressive and tensile ultimate load values.

Test type	Specimen type	Matrix amount in cross-section, %	Filler amount in cross-section, %	Air void amount in cross-section, %
Shrinkage	Cylinder	73.48	20.08	6.44
	CT	73.61	16.94	9.45
Creep	Cylinder	73.76	19.62	6.62
	CT	75.64	15.60	8.76

First of all, it becomes apparent that the cylinder's air void wise was much better shape than the cube used to make CT specimens. The all in all cross-section composition analysis show that porosity for CT shaped specimens on average is from 24% to 32% higher than cylinder-shaped specimens. It means that due to the cube's dimension, it is much harder for air to escape from the middle parts of the cube while it was vibrated than it is for the air in the cylinder-shaped specimens.

The notch cross-section part's analysis was done to further determine the low amount of elastic strains for CT specimens.

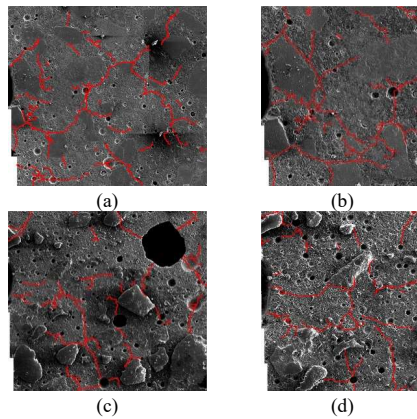


Fig. 10. Crack assessment of shrinkage specimen notch base at 100 times (a) and 200 times (b) magnification and creep specimen notch base at 100 times (c) and 200 times (d) magnification.

In Figure 10, the notch part (tip) is in the middle of the left-hand side of each image. Here it is apparent that there are a significant number of cacks in the notch area. Furthermore, the crack amount for creep specimens is close to shrinkage specimens with a slight increase to creep specimens. All that leads to thinking that due to early age testing, shrinkage plays a considerable role in the crack development, making specimens undergo larger plastic strains.

To further analyze the load impact to CT specimen cross-section notch zone (3mm from the beginning of the notch) was measured. The notch's overall general area and the notch's length and width from six equally spaced measurements along the notch length. The results are shown in Table 4.

Table 4. Notch base part analysis.

Test type	Average length of the notch, mm	Difference, %	Average width of the notch, mm	Difference, %	Average area of the notch, mm ²	Difference, %
Shrinkage	2.979	1.2	0.684	5.4	1.974	5.7
Creep	3.016		0.723		2.094	

It is clear to see that creep specimen notch basis was more deformed than shrinkage specimens. In the length of 3mm from the notch base, the notch area is average 5.7% bigger; thus, it was deformed than the notch part of the shrinkage specimens. Furthermore, while the width of the analyzed shrinkage specimens' notch part stays the same for the creep specimens, width increases on average by 0.168mm or 28.11%.

4. Conclusions

1. Compact tension (CT) specimens on average have a 5.15% higher amount of air voids than cylinder type specimens. The filler amount in the analyzed CT specimen cross-sections is 7.16% less than cylindrical specimen cross-sections, while the matrix amount stays the same. Therefore, while the cube specimens as a base of the CT specimen preparation for long-term tests are not bad, the CT specimen making directly in the right shape moulds would be considered a better practice for air void filler distribution wise.
2. The creep strain amount for the compression specimens is 35.8% higher than the creep strains for tension specimens. In contrast to ultimate load values, the difference is 99.54% in favor of the compression intended specimens.
3. Specific creep for specimens in compression is on average 85.92% less than for CT specimens. Therefore, geopolymer composites have 7.5 times larger creep strains in tension than in compression.
4. From the creep and shrinkage strain curves and notch base part cracks analysis, it is apparent that tension specimens, in this case, CT specimens, have lower elastic strain part and, in early stages, develop cracks in the base of the notch. Tension

specimen elastic strains at the beginning of tests are on average 90.9% less than compression specimens.

5. Due to early age testing and lack of fiber reinforcement, the shrinkage strains play a considerable role in the crack development into the CT specimens and, therefore, the increased amount of plastic strains of the tension specimens. Tension specimens have 0.000379 mm/mm or 47.6% higher plastic strains than was determined by creep compression specimens.

Acknowledgments

1. This work has been supported by the European Regional Development Fund within the Activity 1.1.1.2 "Post-doctoral Research Aid" of the Specific Aid Objective 1.1.1 "To increase the research and innovative capacity of scientific institutions of Latvia and the ability to attract external financing, investing in human resources and infrastructure" of the Operational Programme "Growth and Employment" (No.1.1.1.2/VIAA/3/19/401).
2. The authors acknowledge the support of the PROM programme no. PPI/PRO/2019/1/00013/U/001 which is co-financed by the European Social Fund under the Knowledge Education Development Operational Programme
3. This publication was supported by Riga Technical University's Doctoral Grant programme.

References

1. Shi, C., Jiménez, A.F., Palomo, A. New cements for the 21st century: The pursuit of an alternative to Portland cement. *Cement and Concrete Research*. 2011. 41(7). Pp. 750–763.
2. Tu, W., Zhu, Y., Fang, G., Wang, X., Zhang, M. Internal curing of alkali-activated fly ash-slag pastes using superabsorbent polymer. *Cement and Concrete Research*. 2019. 116(December 2018). Pp. 179–190.
3. Kermeli, K., Edelenbosch, O.Y., Crijns-Graus, W., van Ruijven, B.J., Mima, S., van Vuuren, D.P., Worrell, E. The scope for better industry representation in long-term energy models: Modeling the cement industry. *Applied Energy*. 2019. 240(March 2018). Pp. 964–985.
4. Rashad, A.M., Essa, G.M.F. Effect of ceramic waste powder on alkali-activated slag pastes cured in hot weather after exposure to elevated temperature. *Cement and Concrete Composites*. 2020. 111(September 2019). Pp. 103617.
5. Kang, S.H., Jeong, Y., Kim, M.O., Moon, J. Pozzolanic reaction on alkali-activated Class F fly ash for ambient condition curable structural materials. *Construction and Building Materials*. 2019. 218. Pp. 235–244.
6. Yan, S., He, P., Jia, D., Wang, J., Duan, X., Yang, Z., Wang, S., Zhou, Y. Effects of high-temperature heat treatment on the microstructure and mechanical performance of hybrid C f -SiC f -(Al₂O₃) reinforced geopolymer composites. *Composites Part B: Engineering*. 2017. 114. Pp. 289–298.

7. Linul, E., Korniejenko, K., ŞSerban, D.A., Negru, R., Marşavina, L., Łach, M., Mikula, J. Quasi-Static Mechanical Characterization of Lightweight Fly Ash-Based Geopolymer Foams. *IOP Conference Series: Materials Science and Engineering*. 2018. 416(1).
8. Assi, L.N., Carter, K., Deaver, E., Ziehl, P. Review of availability of source materials for geopolymer/sustainable concrete. *Journal of Cleaner Production*. 2020. 263. Pp. 121477.
9. Amran, M., Fediuk, R., Vatin, N., Lee, Y.H., Murali, G., Ozbakkaloglu, T., Klyuev, S., Alabduljabber, H. Fibre-reinforced foamed concretes: A review. *Materials*. 2020. 13(19). Pp. 1–36.
10. Nastic, M., Bentz, E.C., Kwon, O., Papanikolaou, V., Tchnerer, J. Shrinkage and creep strains of concrete exposed to low relative humidity and high temperature environments. *Nuclear Engineering and Design*. 2019. 352(June). Pp. 110154.
11. Boumakis, I., Di Luzio, G., Marcon, M., Vorel, J., Wan-Wendner, R. Discrete element framework for modeling tertiary creep of concrete in tension and compression. *Engineering Fracture Mechanics*. 2018. 200(July). Pp. 263–282.
12. Rossi, P., Tailhan, J.L., Le Maou, F. Comparison of concrete creep in tension and in compression: Influence of concrete age at loading and drying conditions. *Cement and Concrete Research*. 2013. 51. Pp. 78–84.
13. Ranaivomanana, N., Multon, S., Turatsinze, A. Basic creep of concrete under compression, tension and bending. *Construction and Building Materials*. 2013. 38. Pp. 173–180.
14. Cheng, Z.Q., Zhao, R., Yuan, Y., Li, F., Castel, A., Xu, T. Ageing coefficient for early age tensile creep of blended slag and low calcium fly ash geopolymer concrete. *Construction and Building Materials*. 2020. 262. Pp. 119855.
15. Korniejenko, K., Łach, M., Hebdowska-Krupa, M., Mikula, J. The mechanical properties of flax and hemp fibres reinforced geopolymer composites. *IOP Conference Series: Materials Science and Engineering*. 2018. 379(1).
16. Acker, P., Agullo, L., Auperin, M., Carol, I., J Carreira, D., M R Catarino, J., Chem, J.-C., A Chiorino, M., W Dougill, J., Huet, C., Kanstad, T., Kim, J.-K., Kfistek, V., Republic, C., S Muller, H., Byung, G., Oh, H., Ozbolt, J., Reid, S., Wittmann, F. RILEM TC 107-CSP: CREEP AND SHRINKAGE PREDICTION MODELS: PRINCIPLES OF THEIR FORMATION Recommendation Measurement of time-dependent strains of concrete. *Materials and Structures*. 1998. 31. Pp. 507–512.
17. ASTM. E647 - Standard Test Method for Measurement of Fatigue Crack Growth Rates. *ASTM Book of Standards*. 2016. 03(July). Pp. 1–49.
18. Sprince, A., Pakrastinsh, L., Baskers, B., Gaile, L. Crack development research in extra fine aggregate cement composites. *Vide. Tehnologija. Resursi - Environment, Technology, Resources*. 2015. 1. Pp. 205–208.

Annex VI: Paper VI:

Gailitis, R., Sprince, A., Pakrastins, L., Bazan, P., Kornijejenko, K.

*Plain and PVA fibre-reinforced geopolymer compact tension specimen critical area
surface composition assessment*

Vide. Tehnologija. Resursi - Environment, Technology, Resources, 3, pp. 72-77

Plain and PVA Fibre-Reinforced Geopolymer Compact Tension Specimen Critical Area Surface Composition Assessment

Rihards Gailītis

Faculty of Civil Engineering
Riga Technical University
Riga, Latvia
rihards.gailitis@edu.rtu.lv

Andina Sprince

Faculty of Civil Engineering
Riga Technical University
Riga, Latvia
andina.sprince@rtu.lv

Leonids Pakrastins

Faculty of Civil Engineering
Riga Technical University
Riga, Latvia
leonids.pakrastins@rtu.lv

Patrycja Bazan

Faculty of Materials Science and
Physics
Cracow University of Technology
Krakow, Poland
patrycja.bazan@pk.edu.pl

Kinga Korniejenko

Faculty of Materials Science and
Physics
Cracow University of Technology
Krakow, Poland
kkorniej@gmail.com

Abstract - For more than 40 years, low calcium alkali-activated cement composite, or in other words, geopolymer, has been around. In recent years there has been increased interest in this material and its properties. It is mainly due to the claim that geopolymer is the cement of the future. This claim is based on environmental factors. For instance, the CO₂ emissions for geopolymer binder can be up to 6 less than for Portland cement binder. Most of the researches regarding geopolymer composite properties examine only mechanical and long-term properties in compression. There has been a lack of long-term tests in tension due to difficulties in performing them. As the tensile stresses are an essential part of structure assessment, it is necessary to evaluate new material properties as thoroughly as possible. Due to the nature of geopolymer specimen hardening (polymerisation), there is a difference in modulus of elasticity development and shrinkage caused by binding that could have factors that regular Portland cement specimens do not.

This article aims to evaluate the surface composition of plain and 1% PVA reinforced geopolymer compact tension specimens that have been subjected to creep and shrinkage tests. Specimen cross-section images were acquired using the scanning electron microscope (SEM). Using the quantitative image analysis method, amounts of cross-section composition elements are determined. Furthermore, the amount of cracks is determined and compared between plain and PVA fiber-reinforced specimens.

It has been determined that even though 1% of PVA fibre-reinforced specimens have lower tensile strength, their creep and shrinkage strains are lower, and the number of microcracks at the notch base of the specimen. Still, it has to be acknowledged that the amount of air voids in all analysed specimens is relatively high.

Keywords - Geopolymer composite, long-term properties, creep, shrinkage, quantitative image analysis

I. INTRODUCTION

Alkali-activated materials have been known as an alternative binder to ordinary Portland cement (OPC) mainly due to environmental reasons. Year by year, cement consumption goes up and now is responsible for more than 1.5 billion tonnes of CO₂ emission annually or, in other words, 5 to 8% of global CO₂ emissions. This due to limestone decomposition to generate reactive calcium silicate and aluminate phases [1]–[4]. By using alkali-activated materials, environmental benefits are gained in two ways. One is waste material stockpile reduction because, in alkali-activated material, such materials are used like fly ash, blast furnace slag, etc., as a part of the binder. The second way is by using these industrial waste materials as binder components, the necessity for OPC is reduced, and therefore, the CO₂ is reduced. It has been estimated that by replacing OPC as a binder altogether with a geopolymer matrix, the emitted CO₂ level can be reduced

Online ISSN 2256-070X

<https://doi.org/10.17770/etr2021vol3.6569>

© 2021 Rihards Gailītis, Andina Sprince, Leonids Pakrastins, Patrycja Bazan, Kinga Korniejenko.

Published by Rezekne Academy of Technologies.

This is an open access article under the [Creative Commons Attribution 4.0 International License](https://creativecommons.org/licenses/by/4.0/).

up to 46% [5], [6]. The negative aspect of binder change from OPC to geopolymer shows in cost increase, approximately up to 39% [7].

Alkali-activated blast furnace slag cement types have been studied since the 1930s, but research in alkali-activated composites and geopolymers has increased significantly since the 1980s [1]. Geopolymer is a low calcium alkali-activated binder formed because of silicon and aluminium reactions activated by hydroxide silicates from sodium and potassium hydroxide solutions [7], [8]. The main issue regarding the wide usage of geopolymer composites in construction is mainly because there is a need for increased temperature for proper binder hardening. In fact, for sufficient polymerisation, composite has to be subjected to temperature from 40 to 100°C (depending on fly ash or slag type and alkali activator) and heated in this temperature from 12 to 48 hours and more, therefore, preventing any on-site construction works [9].

Geopolymer composites have similar compressive strength to OPC-based composites. The difference between geopolymer and OPC composites is that geopolymer composites will achieve 85% of their final compressive strength in the first 48 hours [10]. Long-term property geopolymer composites have 78% less shrinkage and 50% less creep strains than foamed OPC-based composite and a bit larger creep and shrinkage strains than OPC composite [11].

Creep and shrinkage are very well-known phenomenon for cement and similar binder-based composites. These phenomena may influence the lifetime of structures. Most creep and shrinkage happen in the first ten years of the composite's lifetime. Cement and cement-like materials are considered to have insufficient tensile strain capacity and low tensile strength. Consequently, they are brittle and susceptible to cracking. As performing creep test in tension is quite difficult and there are differences in creep and shrinkage mechanisms in compression and tension, it is necessary not only to develop and carry out these kinds of tests but also to determine factors that are influencing long-term properties in tension [12]–[16].

This article focuses on determining the differences in compact tension (CT) specimen polished section sample surface compositions after creep and shrinkage tests. The polished section's specific zone is marked. The images taken and quantitatively analysed to determine whether the 1% PVA fibre reinforcement incorporation has a significant effect on sample microstructure and, therefore, influence long-term properties.

II. MATERIALS AND METHODS

For long-term tests, two types of geopolymer composites were prepared. Geopolymer specimen matrixes were based on fly ash sourced from the power plant based in Skawina city (Poland). The fly ash contains spherical aluminosilicate particles and contains oxides such as SiO₂ (47.81%), Al₂O₃ (22.80%). The high value of SiO₂ and Al₂O₃ allows polymerisation [17].

Geopolymer specimens were prepared using sodium promoter, fly ash, and sand (sand and fly ash ratio – 1:1). The geopolymer activation process has been made by 10M NaOH solution and the sodium silicate solution (at a rate of 1:2.5). The technical NaOH in flake form and tap water with sodium silicate R–145 solution is used to make the composite solution. The alkaline solution was prepared by pouring sodium silicate and water over solid sodium hydroxide into sodium silicate and water aqueous solution. The solution was mixed, and the temperature was stabilised. The fly ash, sand, and alkaline solution were mixed for about 15 minutes using a low-speed mixing machine (to achieve homogenous paste). Then the geopolymers were poured into the plastic moulds, as is shown in Fig.1. The specimens were hand-formed, and then the air bubbles were removed by vibrating the mass. Moulds were heated in the laboratory dryer for 24h at 75 °C. Then, the specimens were unmoulded. All the geopolymer specimen preparation was done at Cracow University of Technology (CUT), Poland.

The mixes were moulded into cube moulds 150x150x150mm. The mixing procedure is shown in Fig. 1.

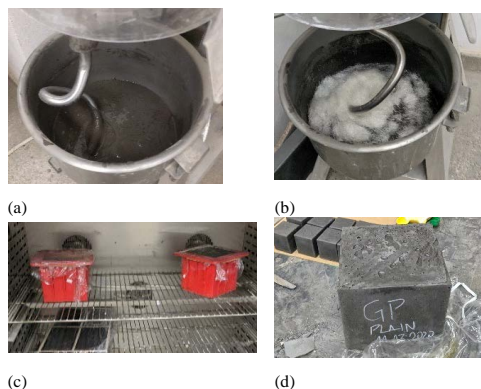


Fig. 1. Plain (a) and fibre-reinforced (b) geopolymer composite mixing and moulding (c, d) process, CUT lab

For long-term testing purposes, each of the cubes was cut to the tile-shaped CT specimens with a thickness of 15mm. Each of the tile-shaped specimens had grip 20mm holes drilled, and 2mm notch sawed according to ASTM E647 [18]. The rules of ASTM E647 for specimens preparation, please see Fig. 2 (b). The actual prepared CT dimensions are shown in Fig. 2 (a).

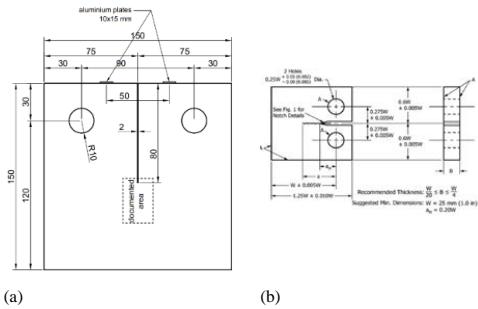


Fig. 2. Geometry of the Compact Tension (CT) specimen [18], [19]

Compact tension specimens for the creep test were loaded with 20% of their tensile strength, and shrinkage specimens were kept in the same environment as the creep specimens (*without loading). Strain readings were done simultaneously for both tests. Tests were carried out for 91 days.

When long-term testing was done, each of the CT specimens had their notch base area drilled out. In Fig. 3 (a,b,c) drilling process is shown.

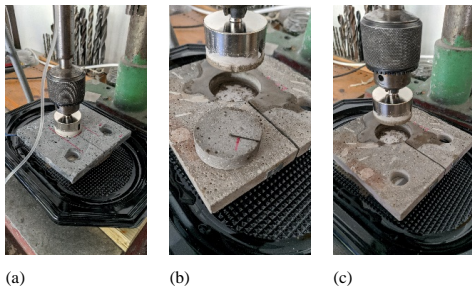


Fig. 3. CT specimen notch base sample drilling process, RTU lab

When areas for polished section samples were drilled out, they were ground and polished with various compounds at various speeds and durations. The polishing and grinding are done with Mecatech 334 automatic single station polishing machine. The polishing sequence is shown in Table 1.

TABLE 1 SAMPLE SURFACE POLISHING SEQUENCE

Polishing stage number	Polishing compound (sandpaper or paste grade) type	Polishing cycle time, minutes	Compression force to sample polishing surface, daN
1.	P180	2	2.5
2.	P320	2	2.5
3.	P600	2	2.5
4.	P1000	2	2.5
5.	P1200	2	2.5
6.	3 μ m	4	2.5

The polishing procedure is shown in Fig.4 (a,b).

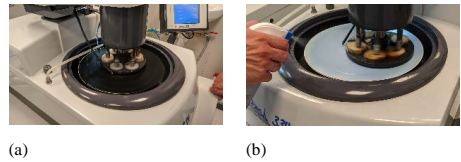


Fig. 4. Notch base samples grinding (a) and polishing (b) process, RTU lab

After grinding and polishing, samples are dried in the chamber at 40°C for 48 hours to release all the excess moisture from grinding. When samples are dried, they are placed in zip-lock bags together with silica gel so that samples stay dried for longer.

At the beginning of the samples' SEM microanalysis, the samples are covered with gold (Fig. 5 (a)). After the sample covering the specific zone on it is marked, the specific area's tracing on the polished section would be done more precisely (Fig. 5 (b)).

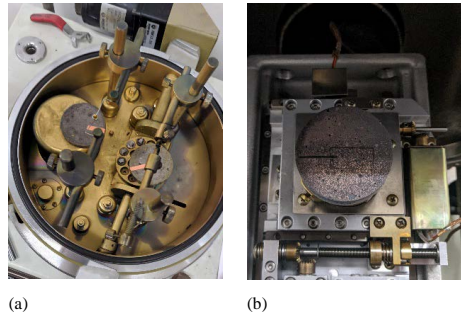


Fig. 5. CT specimen polished section sample covering with gold (a) and placement in SEM vacuum chamber (b), CUT lab

The marked zone on the sample in Fig. 5(b) is 10 x 20 mm. SEM microanalysis is done in JEOL JSM-820. Achieved images are compiled and divided into layers and analysed using Adobe Photoshop CC. Dividing into layers is based on the partition type visible within the analysed cross-section. Division layers are matrix, filler, air-voids, and reinforcement. For each specific layer, an RGB tone is allocated. The process is shown in Fig. 6(a,b,c,d).

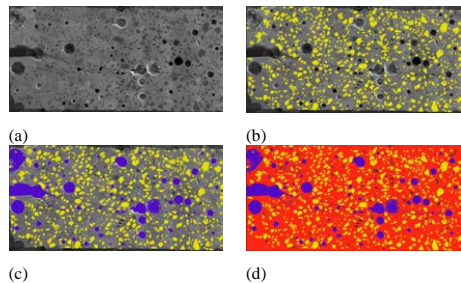


Fig. 6. Image dividing sequence into layers

When the image dividing and RGB tone selection were made, the amount of specific RGB pixels was counted. This way, the composition amount of the studied cross-section was acquired.

III. RESULTS AND DISCUSSION

The tensile strength of the CT specimens at the beginning of the long-term tests is compiled in Table 2.

TABLE 2 TENSILE STRENGTH OF CT SPECIMENS

Mix type	Ultimate tensile load value, average (kN)	Average tensile strength, MPa
Plain geopolymer composite	0.2767	5.1326
Geopolymer composite with 1% PVA	0.2667	4.9471

When the tensile strength values are determined, then load for the creep test is calculated. Creep and shrinkage tests are carried out for 91 days. The creep and shrinkage curves are shown in Fig.7.

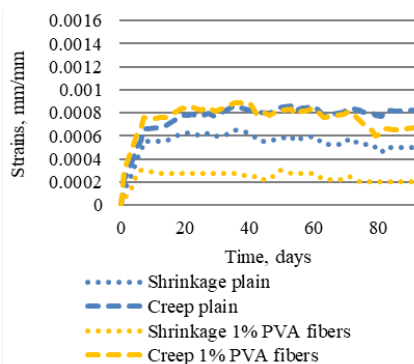


Fig. 7. Plain and fibre-reinforced geopolymer composite CT specimen creep and shrinkage strains

From Fig. 7, it is apparent that 1% PVA fibre incorporation into geopolymer composite does not bear any significant improvements in creep properties. The creep curves for plain and reinforced specimens are the same. As for the shrinkage strain curves, there is a significant difference between plain and fibre-reinforced specimens. The difference here is, on average, a 54.21% decrease in shrinkage strains for reinforced specimens in contrast to plain specimens.

Also, it is visible in Fig.7 that reinforced specimens have a significant reduction on day 70th. This leads to thinking that something has happened to one or more specimens that could have caused this reduction in strains and loss of load-bearing capability. To further elaborate on this decrease in strains, the quantitative surface composition analysis is done for the notch-based polished sections. The results of the analysis are compiled in Table 3.

TABLE 3 CROSS-SECTION COMPOSITION OF CT SPECIMENS

Test type	Mix type	Matrix amount, %	Filler amount, %	Air void amount, %	Fiber amount, %
Shrinkage	Plain	75.48	16.93	7.59	-
	Fibre-reinforced	75.75	14.07	9.47	0.71
Creep	Plain	77.39	15.60	7.01	-
	Fibre-reinforced	74.98	14.58	9.51	0.93

As shown in Table 3, the reinforced samples show higher amounts of air voids than plain samples. On average, the increase is 19.85% and 26.29% for reinforced shrinkage and creep specimens, respectively. Further analysing results, there are differences between plain and reinforced samples. For instance, plain samples that have been subjected to load (samples from creep specimens) show a lower amount of air voids than those that have not been subjected to any load. The decrease to loaded specimens on average is 7.64%. The same is not happening with fibre-reinforced samples. There is a slight visible increase of 0.42% in air void amount for loaded samples for them. This amount is negligible and leads to thinking that even specimens are tested only in tension; there is still some compression happening to specimens. As these compression strains are quite low, the fibre reinforcement does not allow compression effects to occur in the cross-section.

At the microanalysis, it was also discovered that fibre-reinforced samples have a significantly higher amount of micro-cracks that had developed a macro crack that would explain the creep curve drop in one polished section case Fig. 7 on day 70th. In Fig. 8 (a,b), the actual image is shown.

In Fig. 8 (b), there is directly visible one main crack that starts at the CT specimen base and goes throughout the sample.

Further analysing the surface microanalysis results in Table 3 shows a common trend that all of the reinforced samples have lower filler amounts than plain samples. The filler amount is relatively stable in context whether samples have or have not been subjected to any load. The difference between shrinkage and creep samples for reinforced samples is 3.51%, and for plain samples, 7.86%.

The matrix amount of all the samples is similar to all other entity amounts.

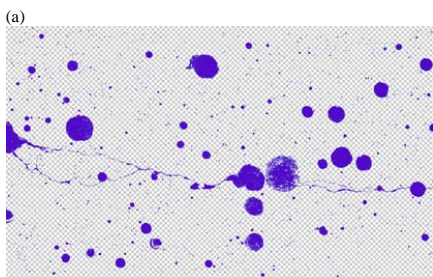
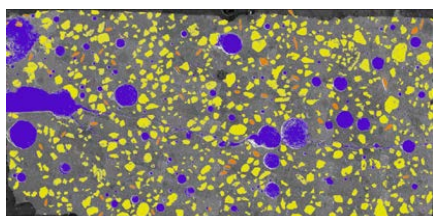


Fig. 8. Fibre-reinforced CT specimen notch base sample air void, reinforcement, filler placement (a), and air void/crack placement (b) in polished section

IV. CONCLUSIONS

Such conclusions can be drawn from the results:

1. The air inclusion amount for the fibre-reinforced samples is significantly higher and is not influenced by tension strains. It is 19.85 and 26.29% higher than plain shrinkage and creep samples correspondingly.
2. Increased air void amount and low amounts of fibre reinforcement increase the possibility of sample cracking and load-bearing capability loss. Fibre-reinforced specimens show 3.7% lower tensile strength and structural imperfections due to the small fibre reinforcement amount.
3. Reinforced samples show lower amounts of filler in them. In contrast to plain specimens, the filler amount for reinforced shrinkage and creep samples is 3.51% and 7.86%, respectively.
4. Fibre reinforcement does not significantly affect creep properties in tension but affects shrinkage strain reduction. On average, shrinkage strains are 54.21% lower for fibre-reinforced specimens than plain geopolymer CT specimens.

V. ACKNOWLEDGEMENTS

This work has been supported by the European Regional Development Fund within the Activity 1.1.1.2 "Post-doctoral Research Aid" of the Specific Aid Objective 1.1.1 "To increase the research and innovative capacity of scientific institutions of Latvia and the ability to attract external financing, investing in human resources and

infrastructure" of the Operational Programme "Growth and Employment" (No.1.1.1.2/VIAA/3/19/401).

This publication was supported by Riga Technical University's Doctoral Grant programme.

REFERENCES

- [1] N. Alharbi, B. Varela, and R. Hailstone, "Alkali-activated slag characterization by scanning electron microscopy, X-ray microanalysis and nuclear magnetic resonance spectroscopy," *Mater. Charact.*, vol. 168, no. July, p. 110504, 2020, doi: 10.1016/j.matchar.2020.110504.
- [2] C. Shi, A. F. Jiménez, and A. Palomo, "New cements for the 21st century: The pursuit of an alternative to Portland cement," *Cem. Concr. Res.*, vol. 41, no. 7, pp. 750–763, 2011, doi: 10.1016/j.cemconres.2011.03.016.
- [3] W. Tu, Y. Zhu, G. Fang, X. Wang, and M. Zhang, "Internal curing of alkali-activated fly ash-slag pastes using superabsorbent polymer," *Cem. Concr. Res.*, vol. 116, no. December 2018, pp. 179–190, 2019, doi: 10.1016/j.cemconres.2018.11.018.
- [4] K. Kermeli et al., "The scope for better industry representation in long-term energy models: Modeling the cement industry," *Appl. Energy*, vol. 240, no. March 2018, pp. 964–985, 2019, doi: 10.1016/j.apenergy.2019.01.252.
- [5] L. Sele, D. Bajare, G. Bumanis, and L. Dembovska, "Alkali Activated Binders Based on Metakaolin," vol. 1, pp. 200–204, 2015, doi: 10.17770/etr2015vol1.204.
- [6] A. M. Rashad and G. M. F. Essa, "Effect of ceramic waste powder on alkali-activated slag pastes cured in hot weather after exposure to elevated temperature," *Cem. Concr. Compos.*, vol. 111, no. September 2019, p. 103617, 2020, doi: 10.1016/j.cemconcomp.2020.103617.
- [7] E. Linul et al., "Quasi-Static Mechanical Characterization of Lightweight Fly Ash-Based Geopolymer Foams," *IOP Conf. Ser. Mater. Sci. Eng.*, vol. 416, no. 1, 2018, doi: 10.1088/1757-899X/416/1/012102.
- [8] S. Yan et al., "Effects of high-temperature heat treatment on the microstructure and mechanical performance of hybrid C f -SiC f - (Al₂O₃) reinforced geopolymer composites," *Compos. Part B Eng.*, vol. 114, pp. 289–298, 2017, doi: 10.1016/j.compositesb.2017.02.011.
- [9] S. H. Kang, Y. Jeong, M. O. Kim, and J. Moon, "Pozzolanic reaction on alkali-activated Class F fly ash for ambient condition curable structural materials," *Constr. Build. Mater.*, vol. 218, pp. 235–244, 2019, doi: 10.1016/j.conbuildmat.2019.05.129.
- [10] L. N. Assi, K. Carter, E. Deaver, and P. Ziehl, "Review of availability of source materials for geopolymer/sustainable concrete," *J. Clean. Prod.*, vol. 263, p. 121477, 2020, doi: 10.1016/j.jclepro.2020.121477.
- [11] M. Amran et al., "Fibre-reinforced foamed concretes: A review," *Materials (Basel)*, vol. 13, no. 19, pp. 1–36, 2020, doi: 10.3390/ma13194323.
- [12] M. Nastic, E. C. Bentz, O. Kwon, V. Papanikolaou, and J. Tcherner, "Shrinkage and creep strains of concrete exposed to low relative humidity and high temperature environments," *Nucl. Eng. Des.*, vol. 352, no. June, p. 110154, 2019, doi: 10.1016/j.nucengdes.2019.110154.
- [13] I. Boumakis, G. Di Luzio, M. Marcon, J. Vorel, and R. Wan-Wendner, "Discrete element framework for modeling tertiary creep of concrete in tension and compression," *Eng. Fract. Mech.*, vol. 200, no. July, pp. 263–282, 2018, doi: 10.1016/j.engfractmech.2018.07.006.
- [14] P. Rossi, J. L. Tailhan, and F. Le Maou, "Comparison of concrete creep in tension and in compression: Influence of concrete age at loading and drying conditions," *Cem. Concr. Res.*, vol. 51, pp. 78–84, 2013, doi: 10.1016/j.cemconres.2013.04.001.
- [15] N. Ranaivomanana, S. Multon, and A. Turatsinze, "Basic creep of concrete under compression, tension and bending," *Constr. Build.*

- Mater., vol. 38, pp. 173–180, 2013, doi: 10.1016/j.conbuildmat.2012.08.024.
- [16] Z. Q. Cheng, R. Zhao, Y. Yuan, F. Li, A. Castel, and T. Xu, "Ageing coefficient for early age tensile creep of blended slag and low calcium fly ash geopolymer concrete," *Constr. Build. Mater.*, vol. 262, p. 119855, 2020, doi: 10.1016/j.conbuildmat.2020.119855.
- [17] K. Korniejenko, M. Lach, M. Hebdowska-Krupa, and J. Mikula, "The mechanical properties of flax and hemp fibres reinforced geopolymer composites," *IOP Conf. Ser. Mater. Sci. Eng.*, vol. 379, no. 1, 2018, doi: 10.1088/1757-899X/379/1/012023.
- [18] ASTM, "E647 - Standard Test Method for Measurement of Fatigue Crack Growth Rates," *ASTM B. Stand.*, vol. 03, no. July, pp. 1–49, 2016, doi: 10.1520/E0647-15E01.2.
- [19] A. Sprince, L. Pakrastinsh, B. Baskers, and L. Gaile, "Crack development research in extra fine aggregate cement composites," *Vide. Tehnol. Resur. - Environ. Technol. Resour.*, vol. 1, pp. 205–208, 2015, doi: 10.17770/etr2015vol1.199.

Annex VII: Paper VII:

Gailitis, R., Pakrastins, L., Sprince, A., Radina, L., Sakale, G., Miernik, K.
*Different Fiber Reinforcement Effect on Fly Ash Based Geopolymer Long-Term
Deflection in Three-Point Bending and Microstructure*
Materials, 15 (23)

Article

Different Fiber Reinforcement Effects on Fly Ash-Based Geopolymer Long-Term Deflection in Three-Point Bending and Microstructure

Rihards Gailitis ^{1,*}, Leonids Pakrastins ¹, Andina Sprince ¹, Liga Radina ¹, Gita Sakale ¹ and Krzysztof Miernik ²

¹ Institute of Structural Engineering, Riga Technical University, Kipsalas 6A, LV-1048 Riga, Latvia

² Department of Materials Engineering, Faculty of Material Engineering and Physics, Cracow University of Technology, Jana Pawła II 37, 31-864 Cracow, Poland

* Correspondence: rihards.gailitis@rtu.lv

Abstract: This study investigated the effect of a low amount of polyvinyl alcohol (PVA) and steel fiber reinforcement on fly ash-based geopolymer composite long-term deflection and its microstructure. For testing purposes, specimens with different amounts and types of fiber reinforcement as well as plain (reference) were prepared. The long-term deflection test was performed by loading specimens with 40% of the ultimate flexural strength. A microstructure analysis was performed using polished section specimens, and images were acquired at 25-times magnification on a scanning electron microscope. The results of the flexural strength test show that all geopolymer composites with fiber reinforcement have lower flexural strength than plain geopolymer composites. The long-term deflection tests show that the highest deflections exhibit 1% PVA fiber-reinforced specimens. The lowest amount of deflection is for 1% steel fiber-reinforced specimens. Specific creep shows similar results to plain, and 1% steel fiber-reinforced specimens, while 1% PVA and 0.5% PVA/0.5% steel fiber-reinforced specimen exhibits the same properties. The quantitative microanalysis of the polished section further confirms the deflection results. Specimens with 1% PVA fiber reinforcement have significantly higher porosity than all other specimens. They are followed by plain specimens and 1% steel fiber, and 0.5% PVA/0.5 steel fiber-reinforced specimens have almost the same porosity level.

Keywords: fly ash-based geopolymer composite; long-term deflection; fiber-reinforced geopolymer



Citation: Gailitis, R.; Pakrastins, L.; Sprince, A.; Radina, L.; Sakale, G.; Miernik, K. Different Fiber Reinforcement Effects on Fly Ash-Based Geopolymer Long-Term Deflection in Three-Point Bending and Microstructure. *Materials* **2022**, *15*, 8512. <https://doi.org/10.3390/ma15238512>

Academic Editor: Mohammad Saberian

Received: 3 November 2022

Accepted: 24 November 2022

Published: 29 November 2022

Publisher's Note: MDPI stays neutral with regard to jurisdictional claims in published maps and institutional affiliations.



Copyright: © 2022 by the authors. Licensee MDPI, Basel, Switzerland. This article is an open access article distributed under the terms and conditions of the Creative Commons Attribution (CC BY) license (<https://creativecommons.org/licenses/by/4.0/>).

1. Introduction

Currently, the most popular construction material is concrete based on ordinary Portland cement (OPC). Its popularity is mainly due to the low cost of concrete. As the worldwide population grows, it is estimated that the consumption of OPC will increase so much that yearly CO₂ pollution will grow from around 7% at present to 17% [1].

Geopolymer is considered a very sustainable material, mainly because it can be produced from industrial waste materials. A significant number of studies show that geopolymer has the necessary properties to be a suitable construction material and is very likely to replace OPC concrete, completely in some cases [2–6]. There have been estimations that producing concrete-like materials by means of geopolymerization can reduce CO₂ emissions regarding OPC production by up to 86% per one ton of Portland cement [1].

Geopolymer matrix can be produced from fly ash and various slags, such as granulated blast furnace slag, kaolin, and pozzolans. Most studies have researched geopolymers based on fly ash. Fly ash is a byproduct of coal power plants. In some countries, fly ash remains 20 to 60% cheaper than Portland cement. In most cases, these countries have coal power plants [7].

According to the life cycle assessment of ordinary Portland cement concrete (OPCC) and alkali-activated binary concrete (AABC), the AABC has 44.7% less kg CO₂ eq/m³ than OPCC. These results indicate that AABC usage as an alternative to OPCC is valid [8].

As it is known, geopolymer composites have similar compressive strength to OPC-based composites. Geopolymer composite also achieves 85% of its strength in the first 48 h [9]. Moreover, its tensile and flexural strength are close to OPC but slightly more brittle. It is well known that fiber introduction into the composition of geopolymer composite in a certain amount reduces creep and shrinkage in compression and tension, further reducing cracking effects and redistributing stresses throughout the cross-section of the structure [10–13]. It is known that steel fibers have high mechanical strength, flexibility, and availability. They have many shapes and can be manufactured in different ways that further show their strength. The tensile strength of steel fibers differs from 310 to 2850 MPa [14]. The most popular polymer fibers are polyvinyl alcohol (PVA) and polypropylene (PP). Polypropylene fibers have low-cost favorable characteristics in high pH environments and the ability to control plastic shrinkage-caused cracking, but they have low thermal resistance, low modulus of elasticity, and poor interfacial contact with the cementitious matrix [15,16]. The PVA fibers have a higher modulus of elasticity and tensile strength, as well as showing higher chemical bonding with the cementitious matrix [17,18].

Tensile and flexural strength can be significantly increased by the addition of fibers. By adding 2% of sorghum fibers, the tensile strength can be increased by 36% [19]. It is claimed that the addition of 2% PVA fibers or 2% steel fibers, or hybrid fiber reinforcement consisting of 1% PVA and 1% steel fibers, leads to great flexural strength [20].

Long-term deflection assessment is of high importance for the further development of geopolymer construction structural design for serviceability. There are only a few deflection assessments under flexural stress results reported for geopolymer composites. Results from the research of [21] show a close correlation with OPCC's long-term deflection properties. Still, data are inconclusive on whether geopolymer composite is subjectable to larger long-term deflections than OPCC.

The aim of this article is to determine the long-term deflection properties of different fiber-reinforced geopolymer composites under three-point bending and the fiber reinforcement influence on specimen microstructure after long-term and mechanical tests.

2. Materials and Methods

The geopolymer composite matrix was based on fly ash from the coal-powered power plant located in Skawina, Poland. This specific fly ash is suitable for geopolymer production because it contains spherical aluminosilicate particles. It is rich in oxides such as SiO_2 (47.81%) and Al_2O_3 (22.80%). The significantly high content of SiO_2 and Al_2O_3 in this fly ash is advantageous for geopolymerization.

Geopolymer composites preparations were made according to the following steps:

1. Day 1—10 M NaOH solution preparation. Alkali solution is prepared by mixing NaOH flakes with water. As the chemical reaction is exothermic, the container with the solution after mixing is placed in cold water for one hour to reduce the temperature. Then, the R-145 sodium silicate is added to the sodium hydroxide and mixed until the solution has an even consistency. The solution is left until the next morning to settle.
2. Day 2—Geopolymer specimen preparation.
 - 2.1. Specimen dry mix is prepared by mixing quartz sand and fly ash together. The sand and fly ash content ratios are 1:1 by mass. Sand and fly ash are mixed in a mixer for 5 min at the machine's lowest speed.
 - 2.2. After dry mix preparation, the previously prepared alkali solution is added to the dry mix and mixed until the geopolymer achieves a moldable consistency. Mixing is performed for 15 min at the machine's lowest speed [22,23]. For the fiber-reinforced specimens, after the first 15 min of mixing, the previously prepared and weighed fiber reinforcement (Figure 1) is added, and the whole geopolymer composition is mixed for 5 min. Whole geopolymer mixing is shown in Figure 2.

- 2.3. The geopolymer mixture is poured into previously oiled plywood molds. The molds are vibrated to release entrapped air and covered with plastic film, then placed into a heat chamber at 75 °C for 24 h.

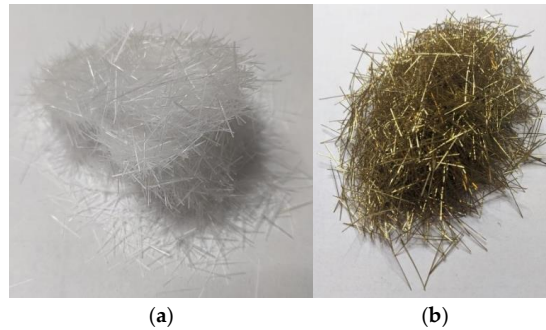


Figure 1. Used PVA (a) and steel (b) fibers.

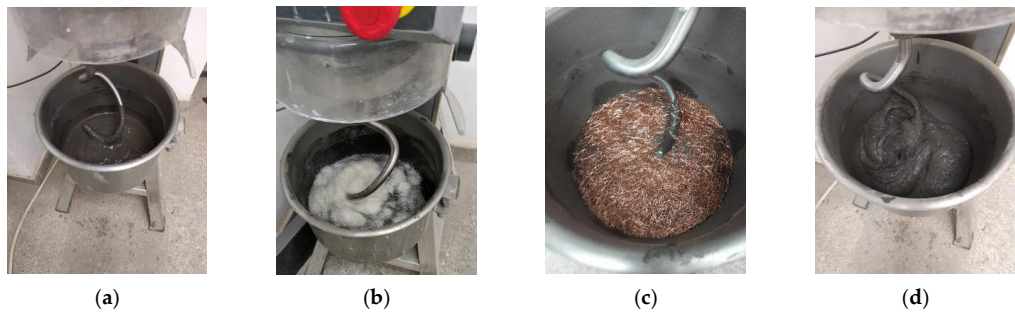


Figure 2. Geopolymer composite composition preparation procedure from geopolymer paste (a) to PVA (b) and steel (c) fiber addition and end composition (d).

The weight and weight ratios regarding geopolymer composite preparation are compiled in Table 1. The properties of the fibers used in the specific geopolymer composites are presented in Table 2.

Table 1. Used geopolymer composite alkali solution and dry mix quantitative parameters.

Alkali Solution		Dry Mix	
Constituent	Weight (g)	Constituent	Weight Ratio
NaOH flakes	400	Quartz sand	1.00
Water	1000	Fly ash	1.00
R-145 Na ₂ O + SiO ₂ solution (molar module 2.5, density 1.45 g/cm ³)	3500	Fibers	0.01

Table 2. Basic properties of the used fibers.

Fiber Parameter	PVA Mesofibers (MasterFiber 400/401)	Steel Fibers (La Graminga GOLD)
Length (mm)	18.00	20.00
Diameter (mm)	0.16	0.30
Tensile strength (MPa)	790–1160	2635–3565

After mixing, the geopolymer composite was laid in plate molds and polymerized for 24 h at 75 °C. The polymerization process is shown in Figure 3.

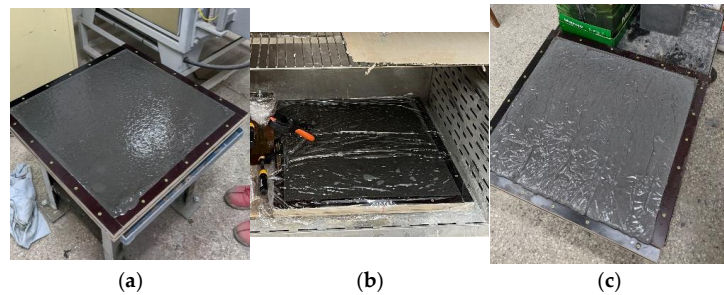


Figure 3. Geopolymer composite molding (a) and polymerization process (b,c).

After polymerization, plate shape specimens were cut into beam-shaped specimens with dimensions $20 \times 75 \times 450$ mm. Specimen cutting and preparation were performed in Riga Technical University facilities (RTU). Specimens before and after cutting are shown in Figure 4.

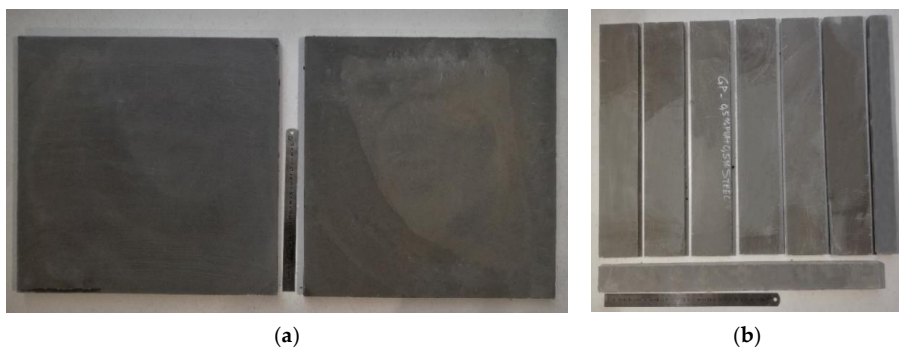


Figure 4. Geopolymer composite plate specimens before (a) and after (b) cutting.

After cutting, specimens were packed into plastic and aluminum film to prevent shrinkage. The aluminum plate was also glued to the specimen to allow accurate measurements of creep deflection. The procedure is shown in Figure 5.

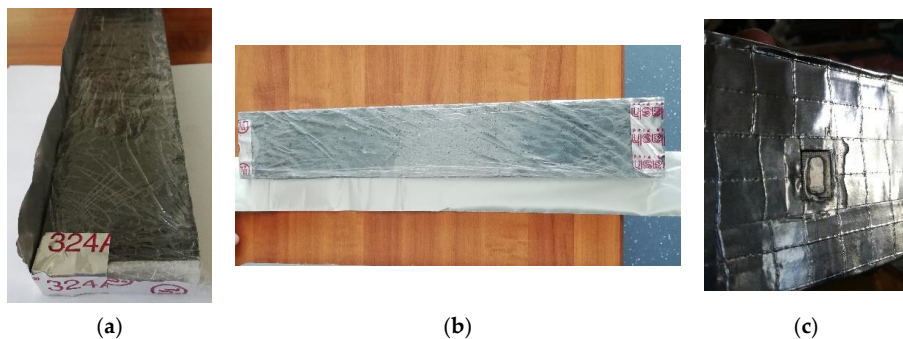


Figure 5. Geopolymer composite specimen wrapping (a,b) and plate-gluing (c) process.

After this, flexural strength was determined, and the specimens were placed on a deflection creep stand and loaded with 40% of the ultimate flexural strength value. Placement into the deflection creep stand was according to the scheme in Figure 6. The actual specimen placement into deflection creep stand is shown in Figure 7.

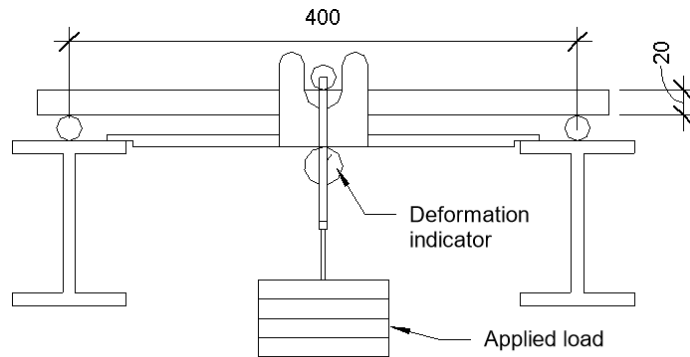


Figure 6. Specimen placement into the long-term deflection test stand.



Figure 7. Setup and testing of long-term deflection strain in three-point bending.

A creep test was carried out for 108 days in the RTU lab, and the specimens were unloaded on the 95th day of testing.

After the creep tests, three specimens were used for quantitative microstructure investigations and three to determine flexural strength after long-term testing, which were then also used for a microstructure analysis. The specimens intended for the microstructure analysis middle part where the load was applied and deflection measured were saturated with epoxy resin to develop polished section specimens for the microstructure testing purposes, as shown in Figure 8.

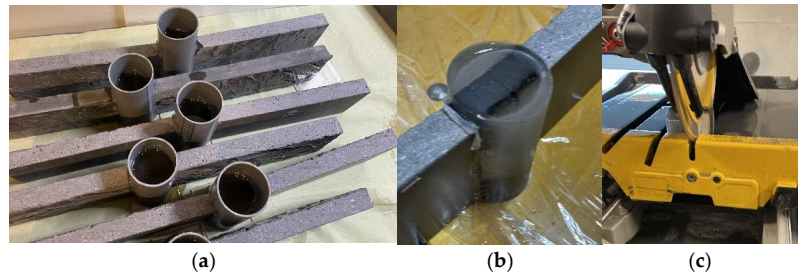


Figure 8. Geopolymer composite polished section casting into epoxy (a,b) and cutting (c) procedure.

The polished section specimen development shown in Figures 8 and 9 was performed according to the procedure mentioned in [24,25].



Figure 9. Geopolymer composite polished section specimen polishing with sandpaper (a) and polishing paste (b).

After the polishing process, the polished section specimens are examined using a scanning electron microscope JEOL IT200 (JEOL, Tokyo, Japan) to determine the loading effect on a measured zone of the beam specimens. Images of the specimens are taken at 25-times magnification.

3. Results and Discussion

The flexural strength was determined before and after the creep tests. For each mix type, three specimens were used each time to determine flexural strength values. The specimen age at the time of testing was 28 and 274 days. From the destructive deflection tests, the ultimate flexural load is determined, and the bending strength is calculated according to the equation:

$$\sigma = \frac{3FL}{2bd^2} \quad (1)$$

where:

F —Applied force;

L —Span of the specimen;

b —Width of the specimen
 d —Thickness of the specimen

The flexural strength values are shown in Figure 10 and Table 3.

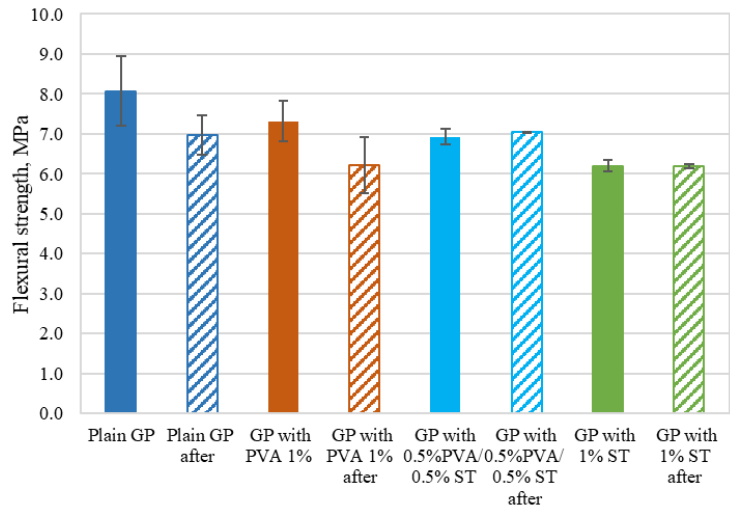


Figure 10. Geopolymer composite flexural strength values with measurement errors before and after long-term deflection tests.

Table 3. Geopolymer composite flexural strength average values and coefficient of variation values.

Geopolymer Composite Type	Age 28 Days		Age 274 Days	
	Flexural Strength (MPa)	Coefficient of Variation	Flexural Strength (MPa)	Coefficient of Variation
Plain GP	8.07	10.67	6.98	7.05
1% PVA GP	7.32	6.93	6.21	11.25
0.5% PVA/0.5% St GP	6.93	2.85	7.05	1.34
1% Steel GP	6.20	2.27	6.18	0.87

As shown in Figure 10 and Table 3, the plain geopolymer composites exhibit the highest flexural strength, followed by the 1% PVA fiber-reinforced specimens and 0.5% PVA/0.5% steel, and 1% steel fiber reinforced specimens with a 9%, 14%, and 23% reduction in flexural strength, respectively. Despite this factor, plain specimens have the highest standard deviation. For plain specimens, this is ± 0.86 MPa; ± 0.51 MPa for 1% PVA fiber-reinforced specimens; ± 0.20 MPa for 0.5% PVA/0.5% steel fiber-reinforced; and ± 0.14 MPa for 1% steel fiber-reinforced specimens. Similar flexural strength values were achieved by [26,27]. Nazari et al. studied boroaluminosilicate geopolymer with steel fiber reinforcement 2, 3, and 5% by volume, and the results show flexural strength ranging from 6.3 to 11.8 MPa. They found that this was achieved by not only increasing the fiber amount, but also by increasing the ratio of borax and sodium hydroxide ration. Still, the main influence on the flexural strength increase is the increase in fiber reinforcement. Plain geopolymer specimens exhibit flexural strength from 5.0 to 9.5 MPa [26]. Constancio Trindade et al. [27] tested geopolymer based on metakaolin reinforced with PVA and polyethylene (PE) fibers (the fiber content introduced in the geopolymers was 2% by volume). The flexural strength of the specimens that were not subjected to elevated temperatures showed significantly higher flexural strength than fly ash-based specimens. In other words, metakaolin geopolymer exhibits 19.7 MPa to PVA fiber-reinforced specimens and 23.5 MPa to PE fiber-reinforced specimens. Plain specimens have a flexural strength of 9.8 MPa. Others [28,29] report similar flexural strength with small-scale specimens

that show a bending strength of 4.6 MPa to plain and 3.5 to 4.6 MPa reinforced with steel fibers. Large-scale beam-shaped specimens with reinforcement bars have bending strength from 22.46 to 29.36 MPa to reinforced specimens and 18.96 MPa to plain specimens. Still, according to the previously mentioned research and its specimen thickness-to-span ratio, it shows that the specimens tested in this study have rather remarkable flexural strength that most likely would be at its highest amount if the steel fiber reinforcement were approximately 4 to 5%, and the PVA fibers from 3 to 4%.

Specimens that were crashed after long-term tests showed a decrease in flexural strength. For specimens reinforced with 0.5% PVA/0.5% steel and 1% steel fibers, the decrease was slight, but for plain and 1% PVA fiber-reinforced specimens, the decrease was 14% and 15.2%, correspondingly.

For all of the geopolymer composite mixes, the flexural values determined at the age of 28 days are higher than [21] the 28-day flexural strength values. Plain GP flexural strength is 14.1% higher than the highest flexural strength achieved in [21]. Still, it has to be noted that the specimen dimensions here and in [21] are different.

Based on Table 3 and the claims of Z. Junwei [30] that appropriate fiber reinforcement should improve structural defects such as micro holes and micro cracks, this further leads to increased mechanical properties. In turn, this leads to the conclusion that the fiber amount used in this study is too low.

As seen in Figure 11, the lowest creep deflection is linked to the specimens with 1% steel fiber reinforcement, followed by plain geopolymer specimens, geopolymer with 0.5% PVA/0.5% steel fibers, and 1% PVA fiber-reinforced specimens. In other words, creep deflections for the plain specimens, 0.5% PVA/0.5% steel fiber-reinforced, and 1% PVA fiber-reinforced specimens are 48.2%, 53.1%, and 59.6% larger, respectively, than the 1% steel fiber-reinforced specimens.

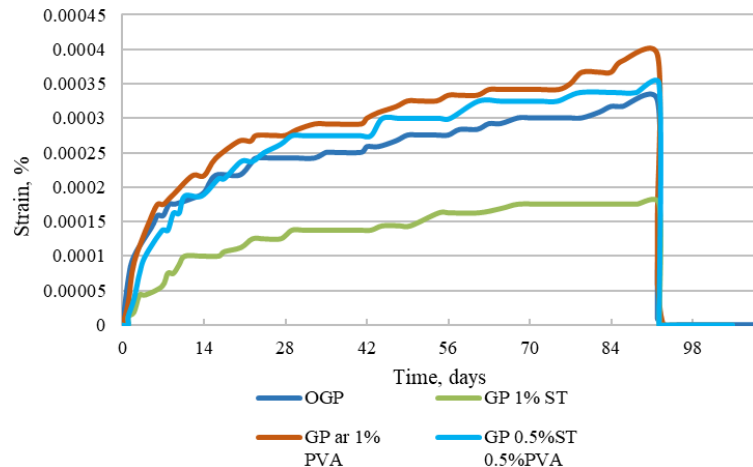


Figure 11. Plain, 1% PVA fiber-reinforced, 1% steel and 0.5% PVA/0.5% steel fiber-reinforced specimen creep deflections.

If we compare the results in Figure 11 with the long-term deflection results from [31], we can see that, unlike OPC mortar specimens that would exhibit hydration effects and show that autogenous and drying shrinkage have a leading effect over creep effects, the GP specimens do not show such an effect. Furthermore, the long-term strains for the GP are 0.8% from the flexural strength registered to OPC mortar specimens tested at an early age. In their study, Un et al. [21] presented long-term deflection of composite geopolymer beams, and there is visible close relation with the Figure 11 curves. Furthermore, it is clear

that when specimens reach the age of 100 days (in Figure 11, day 72), the creep strains stop generating and stabilize.

As flexural strength for different geopolymers compositions is different, the flexural deflections are also different. To evaluate creep deflections without different stress amount impact, the specific creep is calculated (see Figure 12). The calculation is made according to the equation:

$$\chi_{cr}(t, t_0) = \frac{\varepsilon_{cr}(t, t_0)}{\sigma} = \frac{\varepsilon_{kop}(t) - \varepsilon_{sh}(t) - \varepsilon_{el}(t, t_0)}{\sigma} = \frac{1}{E_{cr}(t, t_0)} \quad (2)$$

where:

- $\chi_{cr}(t, t_0)$ is the specific creep,
- $\varepsilon_{cr}(t, t_0)$ is the creep strain,
- $\varepsilon_{kop}(t)$ is the total strain,
- $\varepsilon_{sh}(t)$ is the shrinkage strain,
- $\varepsilon_{el}(t, t_0)$ is the elastic strain,
- σ is the compressive stress,
- $E_{cr}(t, t_0)$ is the modulus of creep.

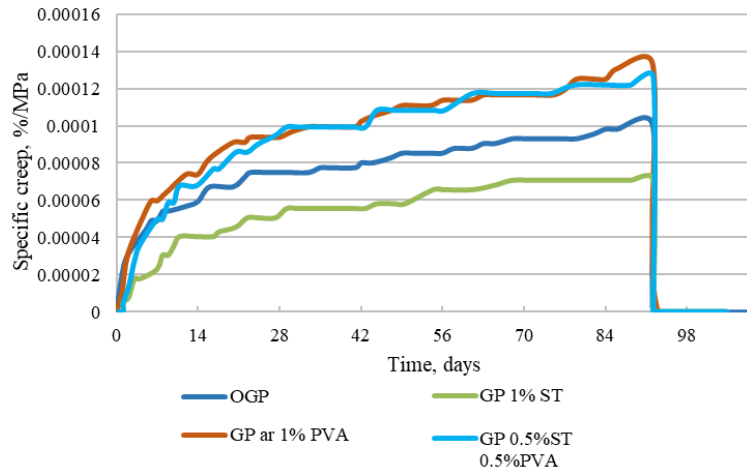


Figure 12. Plain, 1% PVA fiber-reinforced, 1% steel, and 0.5% PVA/0.5% steel fiber-reinforced specimen specific creep.

In Figure 12, the specific creep values show similar relations to the creep deflection values in Figure 11. The differences are shown in values. Specimens with 1% steel fiber reinforcement still have the lowest specific creep, followed by plain geopolymer specimens with 39.0% higher specific creep, 0.5% PVA/0.5% steel fiber-reinforced specimens with a 43.6% increase, and 1% PVA fiber-reinforced specimens with 52.2% higher specific creep. This leads to that the assumption that, even though specimens with the addition of polymer fiber—as mentioned in this study in Table 3 and other studies [26–29]—have higher flexural strength, they are more prone to creep effects and would have larger long-term deflections than steel fiber-reinforced specimens.

Further, to elaborate on the bending force influence on the specimen cross-section at which the load is applied, a SEM image quantitative analysis is carried out. In Figure 13, an acquired SEM image dividing the sequence into layers is shown on the specimen that is subjected to the flexural strength test.

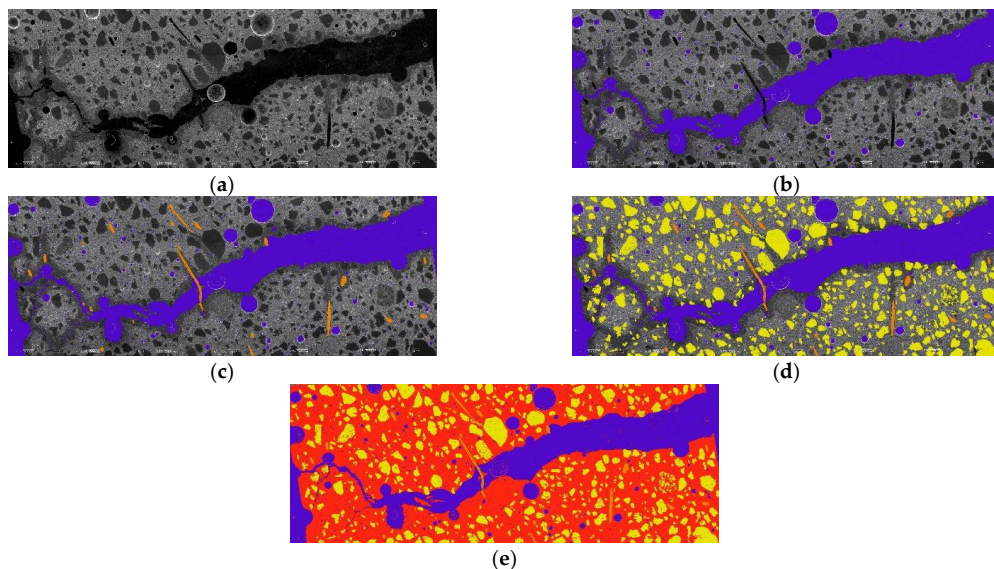


Figure 13. Geopolymer specimen reinforced with 0.5% PVA/0.5% steel fibers after long-term and bending strength test image dividing sequence from raw image (a) to air voids (b), added reinforcement (c), and filler (d) and matrix (e) in 25-times magnification. The image area is 20 mm high and 75 mm wide.

The quantitative image analysis is based on a determination of the specimen cross-section composition-parameter quantity ratio to all areas of the cross-sections. In other words, each partition of the studied cross-section is divided into a separate layer, and a specific RGB color is assigned to this layer. When all of the images of the specific cross-section are divided into layers and color codes are assigned, the number of pixels is counted for all of the raw undivided image, as well as for each of the specific color layers. Then, the acquired number of pixels linked to the specific layer is attributed to the total number of pixels in the whole image, and the quantitative amount of the specific cross-section composition partition is determined. In the case of the long-term deflection specimens, the zone viewed in this research (the location in which the load is applied) is only 75 mm thick. As each of the polished section specimens at the beginning is approximately 15 mm thick, only four specimens are made and studied. The results of the quantitative image cross-section analysis for the specimens used for long-term deflection tests are compiled in Table 4, and in Table 5, the results from the analysis of flexural strength regarding the specimen surface quantitative image are compiled.

Table 4. Results of geopolymer composite polished-section microstructure image quantitative analysis after long-term deflection test.

Geopolymer Composite Type	Matrix (%)	Filler (%)	Air Voids (%)	Fiber Reinforcement (%)
Plain GP	75.93	19.05	5.02	-
1% PVA GP	74.58	19.62	4.64	1.16
0.5% PVA/0.5% St GP	77.76	18.12	3.65	0.47
1% Steel GP	77.50	17.28	4.62	0.60

Table 5. Geopolymer composite from flexural strength test polished-section microstructure image quantitative analysis results.

Geopolymer Composite Type	Matrix (%)	Filler (%)	Air Voids, Cracks (%)	Fiber Reinforcement (%)
Plain GP	65.10	16.33	18.57	-
1% PVA GP	61.02	16.04	22.00	0.94
0.5% PVA/0.5% St GP	69.09	15.99	14.50	0.42
1% Steel GP	67.87	15.12	16.48	0.52

First, from Table 4, it is clear that the highest quantity of air voids was in the plain geopolymer composite specimens. From the fiber-reinforced specimens, it becomes apparent that the highest air void amount to the amount of fibers visible in the cross-section was from the 1% steel fiber-reinforced specimens. The smallest ratio between fiber and air void amount was linked to the specimens reinforced with 1% PVA fibers.

Furthermore, as all of the reinforced geopolymer composites were 1% reinforced from the filler and matrix mass, it is clear that the PVA fiber reinforcement amount was around three times larger than the amount of steel fibers that were used, and about two times larger than the PVA and steel fiber reinforcement mix. The previous two statements lead to the assumption that steel and PVA + steel fiber reinforcement does not have such a significant frothing capability while mixing as the PVA fibers alone. The reduction in the matrix for the PVA fiber specimens is significant.

In the microstructure images, cracks can be observed from the specimens that were destroyed during the flexural strength tests. In these cases, the fiber-bridging effect is noticeable, especially for the specimens with 1% PVA fiber incorporation. Furthermore, the crack opening for specimens reinforced with 1% PVA fibers is bigger than for all the other specimens. This correlates with the study of Y. Hiddaji et al. [32], in which SEM was used to determine the microstructure changes prior to and after high-temperature exposure in metakaolin and phosphate sludge-based geopolymer composites reinforced with glass fibers. In specimens that were not exposed to a temperature impact, they found small microcracks caused by water evaporation. They also found larger crack distribution of the glass fiber-reinforced specimens than the plain specimens that had straight cracks on the fractured surface. This shows that fiber reinforcement, due to polymerization effects and water evaporation, creates small but quantitatively more cracks than in plain specimens. Furthermore, Z. Deng et al. [33] found that PVA–fiber interaction with geopolymer composites leads to an increase in porosity. Furthermore, the authors indicated that with a higher PVA fiber content, higher porosity would be achieved. They found that when the PVA fiber amount is increased to 0.3% and up to 0.6% increases by 7.01% and 9.13% from the plain specimens. Thus, we can assume that the plate specimens used in this study had much better entrapped air release, unlike the prismatic specimens used by Z. Deng.

From Table 5, it becomes apparent that the changes in the polished section surface composition in contrast to Table 4 are significant. The specimens reinforced with 1% PVA fibers have the highest crack and air void amount and are followed by plain specimens, 1% steel fiber-reinforced specimens, and 0.5% PVA/0.5% steel fiber-reinforced specimens. Therefore, it is safe to assume that even though 1% PVA fiber-reinforced specimens have the lowest flexural strength, they retain some load-bearing capacity for the longest period, while the load is applied, and cracking of the stretched zone has begun. This is less so for 1% steel fiber-reinforced specimens, and less again for 0.5% PVA/0.5% steel fiber-reinforced specimens. This was also observed while specimens were loaded. The period between the achievement of ultimate flexural strength value and specimen collapse was longer than the 1% PVA fiber-reinforced specimens, while for 1% steel fiber-reinforced and 0.5% PVA/0.5% steel fiber-reinforced specimens, it was similar. Furthermore, it can be noted that, as expected, the plain specimens that collapsed under load were brittle, while the fiber-reinforced specimen collapse was plastic. In this case, PVA fibers that have a lower

modulus of elasticity than steel fibers show that they cannot provide stress distribution throughout the specimens. Moreover, this leads to the assumption that the material is more elastic, and it would deflect other specimens with different or no reinforcement until it reaches the ultimate bending strength. This leads to bigger cracks and empty areas in the specimen cross-section, as is visible in Table 5 and when comparing with Table 4.

4. Conclusions

The long-term deflection properties of fly ash-based geopolymer composites reinforced with PVA and steel fibers were determined in a 109-day long creep test. Flexural strength was determined before and after the deflection creep tests, and a quantitative microstructure analysis was conducted on the specimens that were exposed to both the long-term test and a flexural strength test after the long-term test. The results of the performed tests show that:

- The highest flexural strength before and after the tests is found in the plain geopolymer specimens. The 1% PVA fiber-reinforced and 0.5% PVA/0.5% steel fiber-reinforced specimens have 9% and 14.2% lower flexural strength, respectively. The 1% steel fiber-reinforced specimens have 23.2% lower flexural strength than the plain specimens. After long-term deflection tests, the flexural strength values for the plain specimens are 11.1% and 11.4% lower for 1% PVA and 1% steel fiber reinforcement and 0.9% higher for the specimens reinforced with 0.5% PVA/0.5% steel fibers;
- The lowest long-term deflection in three-point bending is linked to the 1% steel fiber reinforced specimens. The 0.5% PVA/0.5% steel fiber-reinforced, plain, and 1% PVA fiber-reinforced specimens have 49.3%, 51.7%, and 60.6% higher long-term deflection, respectively;
- Specimens reinforced with 1% steel fibers or those with the lowest specific creep are less likely to deform under three-point bending, followed by plain specimens, 0.5% PVA/0.5% steel fiber-reinforced specimens, and 1% PVA fiber-reinforced specimens, by 37.1%, 43.3%, and 53.5%, respectively;
- The microstructure quantitative analysis of long-term deflection test specimens shows that specimens with 1% PVA fiber reinforcement have two times higher detected fiber reinforcement amount than all the other fiber-reinforced specimens, while air void amounts for the 1% PVA fiber reinforced specimens are 1.51 and 1.37 times higher than 0.5% PVA/0.5% steel, and 1% steel fiber-reinforced specimens. The flexural strength test specimen microstructure quantitative analysis showed 5.52% and 7.50% lower air void and crack amount linked to 1% steel fiber and 0.5% PVA/0.5% steel fiber-reinforced specimens than to 1% PVA fiber reinforced specimens, showing that these specimens have lower plasticity than those reinforced with 1% PVA fibers;
- Overall, it is apparent that beam-shaped specimens with random fiber distribution throughout have lower deflection strength. Moreover, steel fiber incorporation into geopolymer specimens seems to be most beneficial for reducing long-term deflection. It can be concluded that for the bent specimens, not only the lowest bending strength and its reduction while exposed to the long-term load application, but also the lowest long-term deflection and specific creep is linked to the specimens with 1% steel fiber incorporation.

The next stage of this research will be to take all the data from the composition geopolymer composite long-term tests on compression, tension, and three-point bending and develop a model on long-term property assessment for this kind of geopolymer composite, as well as to identify the links and similarities between the tensile and compressive long-term properties and long-term flexural properties of these geopolymer composites.

Author Contributions: Conceptualization, R.G. and G.S.; methodology, R.G.; software, K.M. and G.S.; validation, G.S. and L.R.; formal analysis, R.G.; investigation, R.G. and K.M.; resources, L.P. and K.M.; data curation, R.G., G.S., L.R. and K.M.; writing—original draft preparation, R.G.; writing—review and editing, R.G. and A.S.; visualization, R.G.; supervision, L.P. and A.S.; funding acquisition, R.G. All authors have read and agreed to the published version of the manuscript.

Funding: This work was supported by the European Social Fund within the Project No 8.2.2.0/20/1/008 «Strengthening of PhD students and academic personnel of Riga Technical University and BA School of Business and Finance in the strategic fields of specialization» of the Specific Objective 8.2.2 «To Strengthen Academic Staff of Higher Education Institutions in Strategic Specialization Areas» of the Operational Programme «Growth and Employment».

Institutional Review Board Statement: Not applicable.

Informed Consent Statement: Not applicable.

Data Availability Statement: The authors consider that the data presented in this study are as they are. At the request raw data can be provided. Also compressive strength test results can be seen in this publication of the tested geopolymer mix <https://doi.org/10.3390/cryst11070760>.

Acknowledgments: This work was supported by the European Regional Development Fund within the Activity 1.1.1.2 “Post-doctoral Research Aid” of the Specific Aid Objective 1.1.1 “To increase the research and innovative capacity of scientific institutions of Latvia and the ability to attract external financing, investing in human resources and infrastructure” of the Operational Programme “Growth and Employment” (No.1.1.1.2/VIAA/3/19/401). This publication was supported by Riga Technical University’s Doctoral Grant programme.

Conflicts of Interest: The authors declare no conflict of interest.

References

- Villa, C.; Pecina, E.T.; Torres, R.; Gómez, L. Geopolymer synthesis using alkaline activation of natural zeolite. *Constr. Build. Mater.* **2010**, *24*, 2084–2090. [CrossRef]
- Hassan, A.; Arif, M.; Shariq, M. A review of properties and behaviour of reinforced geopolymer concrete structural elements—A clean technology option for sustainable development. *J. Clean. Prod.* **2020**, *245*, 118762. [CrossRef]
- Kong, D.L.Y.; Sanjayan, J.G.; Sagoe-Crentsil, K. Comparative performance of geopolymers made with metakaolin and fly ash after exposure to elevated temperatures. *Cem. Concr. Res.* **2007**, *37*, 1583–1589. [CrossRef]
- Sarfraz Ali, M.; Sachan, A.K. A review on the durability and applicability of Geopolymer concrete from the recent research studies. *Mater. Today Proc.* **2021**, *52*, 911–922. [CrossRef]
- Almutairi, A.L.; Tayeh, B.A.; Adesina, A.; Isleem, H.F.; Zeyad, A.M. Potential applications of geopolymer concrete in construction: A review. *Case Stud. Constr. Mater.* **2021**, *15*, e00733. [CrossRef]
- Hardjito, D.; Wallah, S.E.; Sumajouw, D.M.; Rangan, B.V. On the Development of Fly Ash-Based Geopolymer Concrete. *ACI Mater. J.* **2004**, *101*, 467–472. [CrossRef]
- Liu, M.Y.J.; Alengaram, U.J.; Santhanam, M.; Jumaat, M.Z.; Mo, K.H. Microstructural investigations of palm oil fuel ash and fly ash based binders in lightweight aggregate foamed geopolymer concrete. *Constr. Build. Mater.* **2016**, *120*, 112–122. [CrossRef]
- Robayo-Salazar, R.; Mejía-Arcila, J.; Mejía de Gutiérrez, R.; Martínez, E. Life cycle assessment (LCA) of an alkali-activated binary concrete based on natural volcanic pozzolan: A comparative analysis to OPC concrete. *Constr. Build. Mater.* **2018**, *176*, 103–111. [CrossRef]
- Assi, L.N.; Carter, K.; Deaver, E.; Ziehl, P. Review of availability of source materials for geopolymer/sustainable concrete. *J. Clean. Prod.* **2020**, *263*, 121477. [CrossRef]
- Ranjbar, N.; Zhang, M. Fiber-reinforced geopolymer composites: A review. *Cem. Concr. Compos.* **2020**, *107*, 103498. [CrossRef]
- Bhutta, A.; Borges, P.H.R.; Zanotti, C.; Farooq, M.; Banthia, N. Flexural behavior of geopolymer composites reinforced with steel and polypropylene macro fibers. *Cem. Concr. Compos.* **2017**, *80*, 31–40. [CrossRef]
- Sukontasukkul, P.; Pongsopha, P.; Chindaprasirt, P.; Songpiriyakij, S. Flexural performance and toughness of hybrid steel and polypropylene fibre reinforced geopolymer. *Constr. Build. Mater.* **2018**, *161*, 37–44. [CrossRef]
- Farooq, M.; Bhutta, A.; Banthia, N. Tensile performance of eco-friendly ductile geopolymer composites (EDGC) incorporating different micro-fibers. *Cem. Concr. Compos.* **2019**, *103*, 183–192. [CrossRef]
- Meng, Q.; Wu, C.; Hao, H.; Li, J.; Wu, P.; Yang, Y.; Wang, Z. Steel fibre reinforced alkali-activated geopolymer concrete slabs subjected to natural gas explosion in buried utility tunnel. *Constr. Build. Mater.* **2020**, *246*, 118447. [CrossRef]
- Mu, B.; Meyer, C.; Shimanovich, S. Improving the interface bond between fiber mesh and cementitious matrix. *Cem. Concr. Res.* **2002**, *32*, 783–787. [CrossRef]
- Banthia, N.; Gupta, R. Influence of polypropylene fiber geometry on plastic shrinkage cracking in concrete. *Cem. Concr. Res.* **2006**, *36*, 1263–1267. [CrossRef]
- Redon, C.; Li, V.C.; Wu, C.; Hoshiro, H.; Saito, T.; Ogawa, A. Measuring and modifying interface properties of PVA fibers in ECC matrix. *J. Mater. Civ. Eng.* **2001**, *13*, 399–406. Available online: https://deepblue.lib.umich.edu/bitstream/handle/2027.42/84898/redon_JMCE01.pdf?sequence=1 (accessed on 21 September 2022). [CrossRef]
- Li, V.C.; Wu, C.; Wang, S.; Ogawa, A.; Saito, T. Interface tailoring for strain-hardening polyvinyl alcohol-engineered cementitious composite (PVA-ECC). *ACI Mater. J.* **2002**, *99*, 463–472. Available online: <https://www.researchgate.net/profile/Victor-Li>

- 15/publication/280224066_Interface_Tailoring_for_Strain-hardening_PVA-ECC/links/58c6f9afa6fdcde55e4134d/Interface-Tailoring-for-Strain-hardening-PVA-ECC.pdf (accessed on 21 September 2022).
19. Segui, P.; Aubert, J.E.; Husson, B.; Measson, M. Characterization of wastepaper sludge ash for its valorization as a component of hydraulic binders. *Appl. Clay Sci.* **2012**, *57*, 79–85. [[CrossRef](#)]
 20. Amran, M.; Fediuk, R.; Murali, G.; Avudaiappan, S.; Ozbakkaloglu, T. Fly Ash-Based Eco-Efficient Concretes: A Comprehensive Review of the Short-Term Properties. *Materials* **2021**, *14*, 4264. [[CrossRef](#)]
 21. Un, C.H.; Sanjayan, J.G.; San Nicolas, R.; Van Deventer, J.S.J. Predictions of long-term deflection of geopolymer concrete beams. *Constr. Build. Mater.* **2015**, *94*, 10–19. [[CrossRef](#)]
 22. Korniejenko, K. Geopolymers for Increasing Durability for Marine Infrastructure. *Spec. Publ.* **2018**, *326*, 20.1–20.10.
 23. Łach, M.; Mikula, J.; Hebda, M. Thermal analysis of the by-products of waste combustion. *J. Therm. Anal. Calorim.* **2016**, *125*, 1035–1045. [[CrossRef](#)]
 24. Gailitis, R.; Sprince, A.; Pakrastins, L.; Korniejenko, K.; Kozlovskis, T. Reinforced and Plain Geopolymer Concrete Specimen Cross-Section Composition Influence on Creep Strains. In Proceedings of the 4th International Rilem Conference on Microstructure Related Durability of Cementitious Composites, Online, 29 April–25 May 2021; pp. 739–746.
 25. Gailitis, R.; Sprince, A.; Pakrastins, L.; Korniejenko, K.; Kozlovskis, T. *Plain Geopolymer Concrete Cross-Section Surface Analysis after Creep and Shrinkage Tests in Compression and Tension*; Springer International Publishing: New York, NY, USA, 2021; pp. 13–24, ISBN 9783030729219.
 26. Nazari, A.; Maghsoudpour, A.; Sanjayan, J.G. Flexural strength of plain and fibre-reinforced borosilicate geopolymer. *Constr. Build. Mater.* **2015**, *76*, 207–213. [[CrossRef](#)]
 27. Constância Trindade, A.C.; Liebscher, M.; Curosu, I.; de Andrade Silva, F.; Mechtcherine, V. Influence of elevated temperatures on the residual and quasi in-situ flexural strength of strain-hardening geopolymer composites (SHGC) reinforced with PVA and PE fibers. *Constr. Build. Mater.* **2022**, *314*, 125649. [[CrossRef](#)]
 28. Alsaif, A.S.; Abdulrahman, S.; Albidah, A. Compressive and flexural characteristics of geopolymer rubberized concrete reinforced with recycled tires steel fibers. *Mater. Today Proc.* **2022**, *65*, 1230–1236. [[CrossRef](#)]
 29. Ahmed, H.Q.; Jaf, D.K.; Yaseen, S.A. Flexural strength and failure of geopolymer concrete beams reinforced with carbon fibre-reinforced polymer bars. *Constr. Build. Mater.* **2020**, *231*, 117185. [[CrossRef](#)]
 30. Junwei, Z.; Shijie, L.; Hongjian, P. Experimental investigation of multiscale hybrid fibres on the mechanical properties of high-performance concrete. *Constr. Build. Mater.* **2021**, *299*, 123895. [[CrossRef](#)]
 31. Sprince, A.; Gailitis, R.; Pakrastins, L.; Kozlovskis, T.; Vatin, N. Long-term properties of cement mortar under compression, tension, and 3-point bending. *Mag. Civ. Eng.* **2021**, *105*, 3–12. [[CrossRef](#)]
 32. Haddaji, Y.; Majdoubi, H.; Mansouri, S.; Alomayri, T.S.; Allaoui, D.; Manoun, B.; Oumam, M.; Hannache, H. Microstructure and flexural performances of glass fibers reinforced phosphate sludge based geopolymers at elevated temperatures. *Case Stud. Constr. Mater.* **2022**, *16*, e00928. [[CrossRef](#)]
 33. Deng, Z.; Yang, Z.; Bian, J.; Lin, J.; Long, Z.; Hong, G.; Yang, Z.; Ye, Y. Advantages and disadvantages of PVA-fibre-reinforced slag-and fly ash-blended geopolymer composites: Engineering properties and microstructure. *Constr. Build. Mater.* **2022**, *349*, 128690. [[CrossRef](#)]

Annex VIII: Patent I:

Sprince A., Pakrastins L., Radina L., **Gailitis R.**, Kozlovskis T.

*Paņēmiens betona un cementa kompozītu ilglaicīgo īpašību noteikšanai dažādos
sprieguma stāvokļos/ Method for Determination of Long-Term Properties of Concrete and
Cement Composites in Various Stress Conditions*

Latvian patent No. 15659B

(11) **LV 15659 B1**(51) Starpt.pat.kl. **G01N 17/00**
G01N 3/00

Latvijas patents izgudrojumam
2007g. 15.februāra Latvijas Republikas likums

(12) **Īsziņas**

(21) Pieteikuma numurs:	LVP2020000096	(71) Īpašnieks(i):	RĪGAS TEHNISKĀ UNIVERSITĀTE, Kaļķu iela 1, Rīga, LV
(22) Pieteikuma datums:	28.12.2020	(72) Izgudrotājs(i):	Andīna SPRINCE (LV) Leonīds PAKRASTIŅŠ (LV) Līga RADIŅA (LV) Rihards GAILĪTIS (LV) Tomass KOZLOVSKIS (LV)
(43) Pieteikuma publikācijas datums:	20.07.2022	(74) Pilnvarnieks vai pārstāvis:	Jevgeņijs FORTŪNA, FORAL Intelektuālā Īpašuma aģentūra, SIA, Kalēju iela 14 - 7, Rīga, LV
(45) Patenta publikācijas datums:	20.05.2023		

(54) **Izgudrojuma nosaukums:** PAŅĒMIENS BETONA UN CEMENTA KOMPOZĪTU ILGLAICĪGO ĪPAŠĪBU NOTEIKŠANAI DAŽĀDOS SPRIEGUMA STĀVOKĻOS
METHOD FOR DETERMINATION OF LONG-TERM PROPERTIES OF CONCRETE AND CEMENT COMPOSITES IN VARIOUS STRESS CONDITIONS

(57) **Kopsavilkums:**

Izgudrojums attiecas uz būvniecību un inženierzinātņi, un tehnoloģiju, proti, uz paņēmieni betona un cementa kompozītu ilglaicīgo īpašību noteikšanai dažādos sprieguma stāvokļos. Paņēmienā piedāvāts šļūdes deformācijas stiepē noteikt, izmantojot koncentrētas stiepes (CT) paraugus, kas dod iespēju samazināt eksperimentālo rezultātu izkliedi un ir īpaši piemērots smalkgraudainu betona un cementa kompozītu deformāciju nolasišanai, izmantojot tikai vienu digitālo deformāciju.

IZGUDROJUMA APRAKSTS

Tehnikas nozare

[001] Izgudrojums attiecas uz būvniecību un inženierzinātni, un tehnoloģiju, proti, uz paņēmienu betonu un cementa kompozītu ilglaicīgo īpašību noteikšanai dažādos sprieguma stāvokļos.

Zināmais tehnikas līmenis

[002] Projektējot ēkas un inženierbūves ir nepieciešams prognozēt būvkonstrukciju elementu darbību un iespējamo seku attīstību visā kalpošanas laikā. Ilgstošas slodzes ietekmē konstrukcijās rodas šļūdes deformācijas (tās ir dimensionālās, neelastīgās izmaiņas laikā, ilgstošas slodzes iespaidā, kas norisinās pēc sākotnējām, acumirkļīgajām deformācijām. Šļūdes deformācijas varbūt vairākas reizes lielākas par sākotnējām deformācijām. Ilglaicīgās deformācijas vērtība raksturo materiāla šļūdētspēju (ACI 209.1R-05, 2005; Neville et al., 1983 u.c.), kas var izsaukt būvkonstrukciju pārmērīgu izlieci, plaisāšanu, nestabilitāti, izkļaušanos, iepriekšējā saspietuma zudumus u.c. novirzes. Ja nepilnības pamana laikus, tad visbiežāk tās tiek savlaicīgi novērstas, bet, ja bojājumus nepamana vai ignorē, tie var novest pie konstrukciju priekšlaicīgas sagrūšanas. Bieži šādas konstrukcijas sagrūst ilgi pirms paredzētā kalpošanas laika beigām. Šļūdes deformāciju lielums, galvenokārt, ir atkarīgs no slodzes lieluma, kā arī no betona un cementa kompozīta stiprības. Betona un cementa kompozīta šļūdes un rukuma deformācijas (tās ir no slodzes neatkarīgas deformācijas, kas veidojas paraugos, kuri pakļauti apkārtējās vides apstākļu ietekmei ar iespējām mitruma izmaiņām un pieļaujamu izžūšanu). Žūšanas rukums ir atkarīgs no paraugu formas un izmēriem (ACI 209.1R-05, 2005; Neville et al., 1983 u.c.). Īpašības ietekmē arī liels skaits citu faktoru, piemēram, tā sastāvs -hidratētās cementa pastas apjoms betona un cementa kompozītā; pildvielu veids, apjoms, ģeometrija un īpašības; ķīmiskās piedevas; šķiedru veids, daudzums un ģeometrija, arī apkārtējās vides apstākļi - mitrums, temperatūra, kā arī betona un cementa kompozīta elementa ģeometriskā forma un izmēri.

[003] Ir zināmi standarti betona ilglaicīgo īpašību - šļūdes deformāciju eksperimentālai noteikšanai spiedes slogojumā, bet tajos sniegtā informācija nav viennozīmīga un izstrādātās metodikas vairāk atbilst parastās stiprības betonu ilglaicīgo īpašību - šļūdes deformāciju spiedes slogojumā un rukuma deformāciju noteikšanai un prognozēšanai. Tajos šļūdes deformācijas spiedē, galvenokārt, ir ieteikts noteikt, izmantojot cilindriskus paraugus.

Piedāvāto paraugu ģeometriju attiecības svārstās no $1/2$ līdz $1/4$. Ir arī standarti, kas iesaka lietot prizmatiskas formas paraugus.

[004] Standartos deformācijas tiek ieteikts noteikt, paraugus, galvenokārt, ievietojot atspere vai hidropneimatiskajos standos, bet šiem stendiem ir būtiski trūkumi – paraugus nav iespējams pakļaut nemainīgai slodzei neierobežoti ilgu laiku, jo uzspriegums ar laiku samazinās un eksperimentu laikā ir nepieciešamas veikt spriegumu līmeņa korekcijas.

[005] Ir zināms standarts EN 12390 „*Sacietējuša betona testēšana*”, kas attiecas uz Eiropas reģionu, bet tas nesniedz informāciju par to, kā noteikt betona ilglaicīgās īpašības – šļūde un rukums.

[006] Ir arī zināms standarts ISO 1920-9:2009 „*Testing of concrete – Part 9: Determination of creep of concrete cylinders in compression*”, kurā sniegta informācija par to, kā noteikt šļūdes deformācijas spiedes slogojumā, un ISO 1920-8:2009 „*Testing of concrete – Part 8: Determination of drying shrinkage of concrete for samples prepared in the field or in the laboratory*”, kurā savukārt aprakstīts, kā noteikt žūšanas rukuma deformācijas. Bet nav izstrādāti standarti betona un cementa kompozītu šļūdes deformāciju noteikšanai stiepes un lieces sprieguma stāvokļos.

[007] Konstrukciju vai to modeļu eksperimentālo pārbaužu rezultātā var uzzināt cementa un betona kompozītu reālos dažādu īpašību raksturlielumus, piemēram, stiprību, pārvietojumus, deformācijas u.c. Ar eksperimentālo pārbaužu metodikām var novērtēt arī dažādu iekšēju un ārēju faktoru ietekmi uz konstrukcijām, ko ne vienmēr iespējams novērtēt ar teorētiskiem aprēķiniem; kā arī dažādu konstrukciju kopdarbības efektivitāti, arī atsevišķa elementa ietekmi uz būves kopējo darbību. Eksperimentālajās pārbaudēs var iegūt arī izejas datus dažādu konstruktīvo materiālu salīdzināšanai vai, ja nepieciešams, tās var izmantot, lai novērtētu esošo konstrukciju stāvokli, kā arī izmantot veicot konstrukciju pastiprināšanu, vai pārbaudot konstrukciju pie slodzes palielināšanas (veicot būvju pārbūvi vai funkcijas maiņu), tāpat tās var izmantot, lai pārbaudītu teorētisko aprēķinu precizitāti.

[008] Ir zināms būvkonstrukciju projektēšanas standarts EN 1992-1-1:2005 “*Betona konstrukciju projektēšana*”, kurā minēts, ka šis standarts lietojams normālas un augstas izturības betonam, kura kubiskā stiprība nav augstāka par 105 MPa, kā arī, ka tajā dotās šļūdes koeficients (tā ir šļūdes un momentāno, elastīgo deformāciju attiecība). Šļūdes koeficients ir bezdimensionāls lielums, kas parasti ir robežās no 0 līdz 5. Tas parāda materiāla šļūdētspēju un to izmanto, lai aprēķinātu konstruktīvo elementu pārvietojumus un iepriekš saspriegto konstrukciju sasprieguma zudumus. Šļūdes koeficientu ietekmē dažādi faktori, piemēram, slodžu līmenis, cementa kompozīta vecums u.c. (ACI 209.1R–05, 2005; Neville et.al., 1983;

Gilbert, Ranzi, 2011 u.c.) kā vērtības ir izmantojamas tikai gadījumos, kad netiek prasīta augsta precizitāte un, ja betona cilindriskā stiprība nepārsniedz 90 MPa, bet nav norādīts, kā rīkoties, ja projektā tiek prasīta augstāka precizitāte un tiek izmantoti augstākas stiprības betona un cementa kompozīti.

[009] Lai dotie EN 1992-1-1:2005 šļūdes koeficienti būtu izmantojami konstrukciju aprēķinos, ir nepieciešams atrast un pielietot būtisko ietekmes faktoru pārejas koeficientus. Bet, lai tos noteiktu, ir jāveic plaši eksperimentāli pētījumi dažādu veidu būvmateriālu (tas ir mākslīgs, akmens veida kompozītmateriāls, cementa/pildvielu daudzfāžu būvmateriāls, kas sastāv no rupjo un smalko pildvielu daļām, kuras ir iestrādātas cementa pastā ($\bar{u}/c \geq 0.45$; $f_{ck28} \approx 12 - 40 \text{ MPa}$) (Neville et al., 1983 u.c.), augstas (tas ir mākslīgs, akmens veida kompozītmateriāls ar augstu mehānisko stiprību un zemu caurlaidību ($\bar{u}/c \leq 0.4$; $f_{ck28} \approx 40 - 120 \text{ MPa}$) (Neville, 1998; Naaman, Reinhardt, 2003) un sevišķi augstas (tas ir mākslīgs, akmens veida kompozītmateriāls ar sevišķi augstu mehānisko stiprību un zemu caurlaidību ($\bar{u}/c \geq 0.2$; $\max f_{ck28} \approx 120 - 400 \text{ MPa}$) (Naaman, Reinhardt, 2003; Graybeal, 2006) stiprības betonu un cementu kompozītiem.

[010] Ir arī zināms standarts ACI 209R-92 “*Prediction of Creep, Shrinkage, and Temperature Effects in Concrete Structures*”, kurā ir apkopoti dažādi šļūdes un rukuma deformāciju ietekmējošo faktoru koeficienti. Šis standarts ir vienīgais šāda veida inženieraprēķinu palīgmateriāls, kur apkopots liels skaits dažādu autoru eksperimentālo datu rezultāti (no 1937. – 1979. gadam), kas daļēji uzskatāmi par novecojušiem, jo nav ziņu par laika posmu no 1979.gada līdz 2020.gadam. Minētajā laika posmā iegūtie dažādu faktoru ietekmes koeficienti izmantojami tikai parastas stiprības betonu un cementa kompozītiem, bet pēdējo 40 gadu laikā, kompozītu sastāvi un īpašības ir mainījušies, betonu un cementu kompozītu sastāvi nepārtraukti tiek uzlaboti un vairs nepietiek tikai ar parastas stiprības betonu īpašībām. Tātad šos ACI 209R-92 standarta faktoros ir nekorekti pielietot mūsdienu augstas un sevišķi augstas stiprības betoniem un cementa kompozītiem, atšķirīgo iekšējo un ārējo faktoru dēļ.

[011] Ir arī zināms Andīnas Sprinces promocijas darbs „*Metodoloģija īpaši smalkgraudainu cementa kompozītu ilglaicīgo īpašību noteikšanai un plaisu attīstības izpētei*”, 2015.g. 10.aprīlis, kurā izveidota metodoloģija īpaši smalkgraudainu cementa kompozītu (ISCK), kam pildvielas lielākais, ģeometriskais izmērs $\leq 5 \text{ mm}$, ilglaicīgo īpašību noteikšanai un plaisu attīstības izpētei.

[012] ISCK ilglaicīgo īpašību noteikšanas un plaisu attīstības izpētes metodoloģija nosaka cementa kompozītu sastāva, paraugu izgatavošanas un eksperimentālo pārbaužu veikšanas procedūru aprakstus, kā arī iegūto datu apstrādi un aparatūras izvēli. Metodoloģija ir lietojama

materiālu mehānisko īpašību noteikšanas laboratorijās. Metodoloģijas izstrādes gaitā ir pārveidots stends cementa kompozītu vienass šļūdes deformāciju noteikšanai stiepē un adaptēts stends vienass šļūdes deformāciju noteikšanai spiedē.

[013] Zināmais paņēmieni vispārīgā gadījumā ir iedalāms trīs daļās: pirmā – materiāla un paraugu gatavošanas apraksts; otrā – dažāda veida eksperimentālo testu procedūru apraksts, un trešā – iegūto datu apstrāde un meklējamo parametru noteikšana. Paņēmieni ietver tehnisko pamatojumu, iekārtu un mērierīču izvēles pamatprincipus, kā arī reģistrējamo parametru sarakstu.

[014] Pirmajā daļā tiek veikta dažādu cementa un betona kompozītu sastāvu projektēšana, sastāvdaļu sagatavošana, daudzumu noteikšana un sajaukšana, veidņu sagatavošana un nepieciešamo formu eksperimentālo paraugu betonēšana, kā arī paraugu pirmapstrāde pēc atveidošanas un tālāka sagatavošana eksperimentālajām pārbaudēm.

[015] Otrajā daļā tiek veikta pārbaudes iekārtu sagatavošana un eksperimentālās pārbaudes, savukārt trešajā daļā tiek veikta datu detalizēta apstrāde.

[016] Eksperimentālās pārbaudes iedalāmas trīs apakšdaļās. Pirmajā apakšdaļā veic īslaicīgos testus un nosaka cementa un betona kompozītu stiprības rādītājus – spiedi, stiepi, kā arī atbilstošo sprieguma stāvokļu elastības modulus (tās ir konstruktīvo materiālu fizikālās konstantes, kas raksturo materiāla elastīgās īpašības stiepes un spiedes deformāciju gadījumā jeb materiāla stingrību un tā spēju pretoties elastīgām formas un izmēru izmaiņām, kas rodas materiālam pieliekot ārējus spēkus. Betona un cementa kompozītu elastības moduli ir atkarīgi no to sastāvdaļu elastības moduļiem (*ACI 209r-92; Neville et al., 1983 u.c.*)). Cementa un betona kompozīta stiprības rādītāji nepieciešami, lai tālāk noteiktu pareizu slodžu līmeni, kas savukārt nepieciešams otrās apakšdaļas ilgstošajos testos.

[017] Otrajā apakšdaļā nosaka cementa un betona kompozītu ilglaicīgos rādītājus ar un bez slodzes pielikšanas, atbilstoši nosakot šļūdes deformācijas spiedē, stiepē, kā arī žūšanas rukuma deformācijas.

Izgudrojuma mērķis un būtība

[018] Konstrukciju modelēšanai un darbības prognozēšanai ir nepieciešama informācija par materiālu atsevišķo komponentu īpašībām, turklāt betona un cementa kompozītu īpašību raksturojošo parametru noteikšanai ir nepieciešams izstrādāt paņēmieni, kurā ir sniegta informācija, kā noteikt dažādi slogotu – spiedē, stiepē un liecē, betona un cementa kompozītu ilgstošās īpašības. Iegūstamie ilglaicīgo īpašību izpētes dati veicinās arvien racionālāku,

spriegumu laukiem atbilstošāku, jauno betonu un cementa kompozītu izveidošanu, kā arī esošo sastāvu uzlabošanu.

[019] Ar šo paņēmieni var noteikt spiedes, stiepes un lieces stiprību, spiedes, stiepes un lieces elastības moduli un elastīgās deformācijas spiedē, stiepē un liecē, kas ir īslaicīgi noteiktas materiālu īpašības, tāpat ar to nosaka arī ilglaicīgās materiālu īpašības - šļūdes deformācijas spiedes, stiepes un lieces slogojumā. Ar piedāvāto paņēmieni var noskaidrot dažādu ārējo ietekmju, piemēram, gaisa temperatūras un mitruma izmaiņu, paraugu ģeometrijas, slodzes lielumam u.c. un iekšējo ietekmju – sastāva izmaiņu, cietēšanas apstākļu un citu ietekmju iedarbību uz ilglaicīgajām īpašībām.

[020] Paņēmiena ietvaros tiek piedāvāts izmantot šļūdes sviru standus deformāciju noteikšanai dažādos slogojumos, lai noteiktu elastīgās un šļūdes deformācijas, kā arī elastīgos un šļūdes pārvietojumus/izlieces lieces slogojumā. Šie standi ļauj izmantot samazinātu izmēru paraugus, kas vairāk raksturīgi augstas un sevišķi augstas stiprības betonu un cementa kompozītu konstrukciju izmēriem. Izmantojot šos standus, paraugiem iespējams pielikt konstantu slodzi un noturēt to nemainīgu ilgu laiku, turklāt eksperimentu laikā nav nepieciešama spriegumu līmeņa korekcija, kalibrēšanas līknes ir lineāras, iespējams pārbaudīt betona un cementa kompozītus, kam pildvielu maksimālais izmērs ≤ 5 mm, vienlaikus nodrošinot materiālu ietaupījumu.

Izgudrojuma izklāsts

[021] Piedāvātais paņēmiens betonu un cementa kompozītu ilglaicīgo īpašību noteikšanai dažādos sprieguma stāvokļos ietver šādus soļus: materiāla un paraugu sagatavošanu šļūdes deformāciju spiedes, stiepes slogojumos, kā arī žūšanas rukuma deformāciju, šļūdes moduļu dažādos sprieguma stāvokļos noteikšanai, kas ir ilglaicīgi nosakāmie materiālu īpašību parametri; eksperimentālo testu procedūru izveidošanu šļūdes deformāciju spiedes, stiepes slogojumos, žūšanas rukuma deformāciju, šļūdes moduļu spiedē, stiepē noteikšanai; un iegūto datu apstrādi, kā arī betonu un cementa kompozītu ilglaicīgo īpašību noteikšanu, turklāt paņēmiens ir raksturīgs ar to, ka tas papildus ietver paraugu sagatavošanu lieces stiprības un šļūdes deformāciju, šļūdes pārvietojumu/izlieču noteikšanai lieces slogojumā, un papildus testu procedūru izveidošanu lieces stiprības, lieces elastības moduļa un šļūdes deformāciju, šļūdes pārvietojumu/izlieces lieces slogojumā, žūšanas rukuma deformāciju (lieces paraugiem), šļūdes moduļa liecē noteikšanai un iegūto datu apstrādi.

[022] Paņēmiens arī ir raksturīgs ar to, ka betona un cementa kompozītu dažādos sprieguma stāvokļos stiprību nosaka, pārbaudot katram sprieguma stāvoklim atbilstošus, minimums trīs

vienāda izmēra un sastāva paraugus, pakļaujot atbilstošu ģometriju un izmēru paraugus katrā no sprieguma stāvokļiem - spiedes, stiepes un lieces slodzei un, nosakot graužošo dažādos sprieguma stāvokļos stiprību, turklāt nosakot to tāda pat veida paraugiem kādi tiks izmantoti ilglaicīgajos šļūdes un rukuma testos, pieņem vidējo vērtību, bet ar noteikumu, ka atsevišķo lieces stiprību atšķirības nepārsniedz 20% no vidējās vērtības, turklāt papildus nosaka betona un cementa kompozītu stiprības pieaugumu laikā. To nosaka slogotiem un neslogotiem paraugiem pēc ilglaicīgo īpašību testiem. Ilglaicīgo testu - šļūdes deformāciju noteikšanas testu standarta garums kopā ar atslodzi rit 4 mēnešus jeb ~120 dienas. Atslodzes laikā (90 dienas pēc slogošanas) tiek reģistrētas šļūdes atgriezeniskās deformācijas (tās ir materiāla izmaiņas pēc ilgstoša slogojuma noņemšanas vai cementa kompozīta samitrināšanās, kurā izpaužas šļūdes atgriezeniskās – momentānās īpašības (*Neville et al. 1983; Bulavs, Radins, 2006 u.c.*)). Tās reģistrē 30 dienu periodā pēc 90 slogojuma dienām.

[023] Paņēmiens arī ir raksturīgs ar to, ka betona un cementa kompozītu šļūdes deformācijas dažādos sprieguma stāvokļos nosaka, paraugus slogojot ar konstantu, vienmērīgu, statisku slodzi, turklāt paraugus sākotnēji atkārtoti slogo un atslodo divas reizes un katrā slogojumā iegūtos deformāciju rādījumus salīdzina, lai pārbaudītu vai slogojums ir centrisks, lai izpildītos šis nosacījums katra nolasījuma starpības nevar pārsniegt 20 % no vidējās aritmētiskās vērtības, kas iegūta no visiem attiecīgā slogojuma rādījumiem. Ilglaicīgo testu pirmajā slogošanas dienā paraugiem veic indikatoru nolasījumus pirms slodzes pielikšanas un pēc tam pie katras slodzes pakāpes pielikšanas, tālāk, pēc visa, aprēķinātā slodzes lieluma pielikšanas, indikatoru nolasījumus veic ar intervālu ik pēc stundas, to darot pirmās 6 līdz 8 stundas, pēc tam divas nedēļas nolasījumi tiek reģistrēti ar intervālu katru dienu, tad nākošās nedēļas nolasījumus veic ar 2 – 3 dienu intervālu, pēc 30. dienas nolasījumus veic reizi nedēļā, ja tests tiek turpināts arī pēc 90 dienu sasniegšanas, tad turpmāk nolasījumus veic vienu reizi mēnesī, sasniedzot interesējošo slogojuma ilgumu, slodzi pakāpeniski noņem un pie katras slodzes pakāpes, tāpat kā testa sākumā, nolasa deformāciju lielumus, iegūstot tūlītējās jeb acumirklīgās, atgriezeniskās deformācijas, kā arī redzot neatgriezenisko deformāciju daļu.

[024] Pirms eksperimentālajām pārbaudēm un eksperimentālo pārbaudžu laikā, paralēli reģistrē sekojošus datus: uzraksta pārbaudes nosaukumu; pārbaudēs izmantoto iekārtu nosaukumus, to maksimālās slogotspējas, slogošanas diapazonus; mērinstrumentu nosaukumus, to mērīšanas precizitātes, mērinstrumentu bāzes, mērinstrumentu skaitu, rūpnīcas numurus, mērinstrumentu izvietojumu; regulāri reģistrē apkārtējās vides apstākļus (mitrumu; temperatūru); tāpat apraksta materiāla un paraugu raksturojums - materiāla nosaukumu, sastāvdaļas un to raksturojumu; ū/c attiecību; materiāla izgatavošanas procedūru; paraugu sagatavošanu; paraugu cietēšanas

apstākļus (temperatūru un mitrumu) un cietēšanas ilgumu; paraugu atveidņošanas laiku, marķējumu ar šifru, kas satur materiāla apzīmējumu un kārtas skaitli (piem. BS –1 (cementa kompozīts ar stikla piedevu, pirmais paraugs)); paraugu pārbaužu raksturojumus (paraugu formas un ģeometriskos izmērus; paraugu svaru; paraugu izgatavošanas dienas; paraugu testēšanas dienas – betona un cementa kompozītu vecumu; reģistrē dienu, kad paraugi sākuši žūt un šļūdēt; paraugu vecumu testa sākumā un testa beigās); šļūdes testu parametrus (spiedes, stiepes, lieces stiprības; pieņemtās sprieguma līmeņus; noteiktos slodžu lielumus; sloģojuma un atsloģojuma ilgumus; sloģojuma pakāpes; mērierīču nolasījumus; vidējos rādījumus); rukuma testu parametrus - mērierīču nolasījumus; vidējos rādījumus; svāra izmaiņas, mitruma zudumus; aprēķināmos parametrus – betona un cementa kompozītu blīvumus; relatīvās deformācijas spiedes, stiepes un lieces sloģojumos; kopējās, ilglaicīgās deformācijas spiedes, stiepes un lieces sloģojumos; elastīgās un šļūdes deformācijas spiedes, stiepes un lieces sloģojumos; šļūdes pārvietojumu un izlieču lielumus lieces sloģojumā; elastības un šļūdes moduļus spiedes, stiepes un lieces sloģojumos; šļūdes koeficientus spiedē, stiepē un liecē; īpatnējās elastīgās un īpatnējās šļūdes deformācijas spiedē, stiepē un liecē; šļūdes funkcijas spiedē, stiepē un liecē.

Īss zīmējuma apraksts

[025] 1. zīm. parādīta betonu un cementa kompozītu ilglaicīgo īpašību noteikšanas strukturizēta shēma dažādos sprieguma stāvokļos.

Izgudrojuma īstenošanas piemēri

[026] Betonu un cementa kompozītu ilglaicīgo īpašību noteikšanai izgatavo sastāvu, kuru iepilda testiem atbilstošos veidņos. Iegūtos paraugus atveidņo un sagatavo testiem – katram atšķirīgajam sprieguma stāvoklim (sloģojuma testam) ir citi paraugi. Tad veic stiprības testus, kā arī elastīgo deformāciju testus un līdz ar to veic elastības moduļa testus, tad nosaka ilglaicīgās deformācijas dažādos sloģojumos, kā arī bez slodzes – tas ir nosaka rukuma deformācijas. Pēc tam veic datu apstrādi un nosaka ilglaicīgos parametrus – šļūdes koeficientu, šļūdes moduli un īpatnējo šļūdi.

[027] Paraugu sagatavošana. Betona un cementa kompozīta sastāvu izgatavo atbilstoši projektēšanas nosacījumiem, iepilda iepriekš sagatavotos veidņos un ievieto standartā noteiktos cietēšanas apstākļos (20 ± 2 °C, RH > 95 ± 5 %). Pēc 24–48 h paraugus atveidņo, veic paraugu pirmapstrādi un visus paraugus pirms pārbaudēm marķē ar šifru. Tālāk paraugus atkal ievieto

standarta cietēšanas apstākļos (20 ± 2 °C, RH > 95 ± 5 %) līdz atbilstošo pārbaužu veikšanai. Pēc noteiktā betonu un cementa kompozīta paraugu aprūpes laika (cietināšanas) sasniegšanas, tos izņem no ūdens un gatavo eksperimentālajām pārbaudēm. Pirms tam visus paraugus nosver un pārbauda to izmēru atbilstību.

[028] Spiedes stiprības noteikšanai izmanto kubus – 100x100x100 mm; prizmas – 40x40x160 mm; cilindrus ar Ø47x190 mm. Pielietojot pārejas koeficientus, stiprības noteikšanai var tikt izmantoti arī citu izmēru paraugi, būtiski, lai paraugu ģeometrija spiedes testos un ilglaicīgajos testos spiedes slogojumā sakrīt. Slogošanas ātrums paraugiem 0,8 MPa/s (atbilstoši EN 12390–3:2002 standartam). Eksperimentāli kubiskā, cilindriskā vai prizmatiskā spiedes stiprība nosakāma atbilstoši ilglaicīgo slodzes testu sākuma dienai, jo, izejot no graužošās slodzes lieluma, tiek aprēķināts slodzes lielums, kas jāpieliek šļūdei pakļautajiem paraugiem. Paraugus, spiedes iekārtā, novieto maksimāli centriski starp spiedes plaknēm. Lai iegūtu korektus datus, paraugu malām jābūt paralēlām un gludām.

[029] Betona un cementa kompozītu spiedes stiprību nosaka pārbaudot, minimums trīs vienāda izmēra un sastāva paraugus, pakļaujot spiedes testam, kā graužošo spiedes stiprību pieņemot vidējo vērtību, bet ar noteikumu, ka atsevišķo spiedes stiprību atšķirības nedrīkst nepārsniedz 20% no vidējās vērtības.

[030] Nosakot cementa kompozītu stiprības pieaugumu laikā pēc ilglaicīgo testu beigām, šļūdes un rukuma pārbaudēm izmantotos paraugus atkārtoti nosver un sagrauj spiedē.

[031] Betona un cementa kompozīta stiepes stiprību var noteikt, izmantojot koncentrētas stiepes (CT)– 150x150x12mm vai kuponveida paraugus 100x50x12 mm un 150x70x12 mm, būtiski, lai izvēlētajā paraugu ģeometrija stiepes testos un ilglaicīgajos testos stiepes slogojumā sakrīt. Eksperimentāli CT vai kuponveida paraugu stiepes stiprība nosakāma atbilstoši ilglaicīgo slodzes testu sākuma dienai, jo, izejot no graužošās slodzes lieluma, tiek aprēķināts slodzes lielums, kas jāpieliek šļūdei pakļautajiem paraugiem. Paraugus centriski ieliek stiepes iekārtas satvērējzokļos un slogo pakāpeniski līdz sagraušanai ar aptuveno ātrumu ~5 μm/s (Pereira et al., 2011, 2012).

[032] Betona un cementa kompozītu stiepes stiprību nosaka pārbaudot, minimums trīs vienāda izmēra un sastāva paraugus, pakļaujot stiepes testam un, kā graužošo stiepes stiprību pieņem vidējo vērtību, bet ar noteikumu, ka atsevišķo stiepes stiprību atšķirības nepārsniedz 20% no vidējās vērtības.

[033] Nosakot betona un cementa kompozītu stiprības pieaugumu laikā pēc ilglaicīgo testu beigām, šļūdes un rukuma pārbaudēm izmantotos paraugus atkārtoti nosver un sagrauj stiepē.

[034] Lieces stiprības noteikšana. Betona un cementa kompozītu un betona lieces stiprību nosaka, izmantojot plātņveida paraugus 450x75x20mm, kas ir tādi paši kā ilglaicīgajos testos. Eksperimentāli lieces stiprība nosakāma atbilstoši ilglaicīgo slodzes testu sākuma dienai, jo, izejot no graujošās slodzes lieluma, tiek aprēķināts slodzes lielums, kas jāpieliek šļūdei pakļautajiem paraugiem. Paraugu centriski ieliek trīs punktu lieces standā. Paraugu slogo pakāpeniski līdz sagraušanai.

[035] Betona un cementa kompozītu lieces stiprību nosaka pārbaudot, minimums trīs vienāda izmēra un sastāva paraugus, pakļaujot lieces slodzei un, kā graujošo lieces stiprību pieņemot vidējo vērtību, bet ar noteikumu, ka atsevišķo lieces stiprību atšķirības nedrīkst nepārsniedz 20% no vidējās vērtības.

[036] Nosakot cementa kompozītu stiprības pieaugumu laikā pēc ilglaicīgo testu beigām, šļūdes un rukuma pārbaudēm izmantotos paraugus atkārtoti nosver un sagrauj liecē.

[037] Visu sprieguma stāvokļu – spiedē, stiepē un liecē elastības modulūsus nosaka no elastīgajām deformācijām spiedē, stiepē un liecē, kas norisinās šļūdes pārbaužu sākumā. Katra sprieguma stāvokļa šļūdes paraugu slogošanu veic iespējami ātri (15 min laikā), lai precīzi nodalītu elastīgās un šļūdes deformācijas. Nepieciešamo slodzi (betona un cementa kompozīta izmaiņas elastīgajā apgabalā) paraugiem pieliek pakāpeniski piecos piegājienos, katrā pakāpē pieliekot vienādu slodzes lielumu, kas ir vienāda ar 20 % no kopējās slodzes lieluma, un pēc katra posma nosaka acumirklīgās deformācijas vērtības, kuras ievieto Huka likuma vispārējā izteiksmē un nosaka elastības moduli.

[038] Šļūdes deformāciju noteikšanai spiedes slogojumā izmanto cilindriskos paraugus ar izmēriem Ø47x190 mm vai prizmatiskos paraugus ar izmēriem 40x40x160 mm. Lai izslēgtu galu efektu ietekmi uz pārbaudes rezultātiem, paraugu ģeometriskajiem izmēriem jāizpildās nosacījumam

$\frac{b}{l} \leq \frac{1}{4}$, kur b – parauga šķērsriezuma lielākais izmērs; l – parauga garums

(RILEM TC 107-CSP, 1998). Visiem šļūdes paraugiem uz sānu virsmām uzlīmē alumīnija plāksnes (10x15 mm), kas izvietotas centriski un simetriski, lai nodrošinātu deformāciju mērinstrumentu „nažu” stabilitu novietojumu. Līmējot plāksnes, ir jānodrošina, ka „naža” asmens pilnībā saskartos ar plāksni un varēt nolasīt korektus pārvietojumus. Vienam cilindriskam paraugam uzlīmē sešas, bet prizmatiskajam paraugam – četras plāksnes, izmantojot epoksīda līmi. Attālums starp divu alumīnija plāksņu centriem ir 50 mm. Pamatšļūdes (tas ir deformāciju pieaugums laikā zem vienmērīgas, konstantas vai cikliskas, mainīgas slodzes ar ierobežotu, izolētu mitruma apmaiņu paraugos. Tā parāda šļūdes deformāciju lielumu konstantā mitrumā bez mitruma kustības caur materiālu. Deformāciju

pieaugums norit ilgstoši daudzu gadu garumā. Deformāciju lielums salīdzinājumā ar žūšanas šļūdi ir mazāks. Parauga forma un izmēri būtiski neietekmē deformāciju lielumu (*ACI 209.1R-05, 2005; Neville et al., 1983; Neville, 1995 u.c.*) vērtības noteikšanai, daļu paraugu ietin divās kārtās alumīnija folijas, tādējādi nodrošinot, ka neiestāsies žūšanas process un tajos norisināsies tikai pamatšļūde, bet, lai noteiktu žūšanas šļūdi (tā ir deformāciju daļa, kuru ierosina betona un cementa kompozīta žūšana un, kas noteikta paraugiem slogotiem ar vienmērīgu, konstantu vai ciklisku, mainīgu slodzi, kas atrodas apkārtējās vides apstākļos un paraugiem ir pieļaujama žūšanas un mitruma sākotnējā izmaiņa. Deformācijas pieaugums ierobežotā laikā sasniedz gala vērtību. Deformāciju lielums salīdzinājumā ar pamatšļūdi ir lielāks. Parauga forma un izmērs būtiski ietekmē deformāciju lielumu (*ACI 209.1R-05, 2005; Neville, et al., 1983; Neville, 1995 u.c.*), daļu paraugu atstāj neietītus, tādā veidā pieļaujot paraugu žūšanu, ka arī žūšanas rukuma deformācijas.

[039] Visiem paraugiem, pirms tos ievieto spiedes šļūdes sviru stendā, uz sānu virsmām piestiprina deformāciju mērierīces – tenzometrus vai HBM DD1 digitālos deformāciju mēritājus. Prizmiskajiem paraugiem – divus, bet cilindriskajiem paraugiem trīs, kas izvietoti vienādos attālumos cits no cita. Tenzometru „nažus” ievieto uz pielīmētajām plāksnēm, tenzometru bāze – 50 mm. Tenzometrus paraugiem piestiprina ar elastīgām gumijām vai metāla skavām. Šļūdes parādības eksperimentālai pētīšanai paraugus ar tenzometriem ievieto šļūdes sviru stendos maksimāli centriski starp spiedes plaknēm, pa diviem paraugiem katrā stendā. HBM DD1 deformāciju mērījumus caur daudz kanālu reģistrēšanas iekārtu HBM „Spider 8”, reģistrē datorā, izmantojot datorprogrammu HBM „CatMan”. Visus paraugus slogo ar konstantu, vienmērīgu, statisku slodzi (~ 20–40% no graužošajiem spriegumiem, nepārsniedzot betona un cementa kompozīta darbības lineāro posmu). Paraugus atkārtoti slogo un atslogo divas reizes un katra slogojumā iegūtos deformāciju nolasījumus salīdzina, lai pārbaudītu vai slogojums ir centrisks, lai izpildītos šis nosacījums katra nolasījuma starpības nevar pārsniegt 20 % no vidējās aritmētiskās vērtības, kas iegūta no visiem rādījumiem. Pirmajā dienā pēc paraugu noslogošanas, nolasījumus reģistrē ik pēc stundas, tad pirmo nedēļu tos turpina reģistrēt vienu reizi dienā. Pēc pirmās nedēļas nolasījumus reģistrē ar 2–3 dienu intervālu līdz apmēram 30 dienām kopš slogošanas sākuma, pēc pirmā mēneša nolasījumus reģistrē reizi nedēļā. Ja tests tiek turpināts arī, sasniedzot 90 dienas, tad tālāk reģistrēšanu veic vienu reizi mēnesī. Sasniedzot eksperimenta interesējošo slogojuma ilgumu, slodzi pakāpeniski noņem un pie katras slodzes pakāpes, tāpat kā testa sākumā, nolasa deformāciju lielumus, iegūstot tūlītējās jeb acumirklīgās, atgriezeniskās deformācijas. Slodzes noņemšanas pakāpes ir vienādas ar slodzes pielikšanas pakāpēm. Kad paraugs atslogots, to nemainīgi atstāj šļūdes sviru stendā, lai

noteiktu atgriezeniskās deformācijas laikā. Deformāciju atgriezeniskuma mērījumu nolasišanai, datus reģistrē nepieciešami ilgā periodā un reģistrēšanas biežumu veic tāpat, kā noslogojot paraugus.

[040] Žūšanas rukuma deformāciju noteikšanai spiedes formas paraugiem var tikt izmantotas divas metodes. Pirmā, kad rukuma deformācijas mēra parauga garākās malas galos, izmantojot rukuma skavu vai arī, mērot deformācijas paraugu vidusdaļā, tāpat kā mērot šļūdes deformācijas. Izmantojot pirmo pieeju, visiem rukuma paraugiem to galos pielīmē divus pus sfēriskus metāla reperus, kas ir izvietoti pēc iespējas precīzi paraugu galu centrā, lai fiksētu precīzu stāvokli nolasišanas brīdī. Otrajā pieejā paraugus sagatavo tāpat kā šļūdes testam ar sešām vai četrām alumīnijā plāksnēm uz paraugu sānu virsmām. Lai noteiktu korektas šļūdes deformācijas, žūšanas rukuma deformāciju noteikšanai sagatavo identiska sastāva un identisku izmēru paraugus kā šļūdes pārbaudēm. Ja nepieciešams noteikt pamatšļūdi un žūšanas šļūdi, tad atbilstoši jā sagatavo arī daļa rukuma paraugu, ietinot divās kārtās alumīnija folijas, lai nodrošinātu, ka neiestāsies žūšanas process, bet daļu paraugu atstāj neietītus, pieļaujot tajos žūšanas procesu.

[041] Paraugu gatavošana stiepes slodzes un šļūdes deformāciju noteikšanai stiepes slogojumā, izmantojot koncentrētās stiepes paraugus (CT).

[042] Prizmu 150x150x600 mm sazāgē ar dimanta griezējdisku 12 ± 1 mm biezās plāksnēs, izveidojot koncentrētās stiepes paraugus (*Compact Tension (CT)*) (ASTM-E647, 2005) ar gala izmēriem 150x150x12 mm. Stiepes spriegumu intensitātes palielināšanai, stiepes paraugus veido iespējami plānus.

[043] Lai būtu prognozējama un tiktu konkretizēta maksimālo šļūdes deformāciju, tostarp nelineāra slogojuma gadījumā arī mikroplaisu un plaisu parādīšanās, vieta (tas ir apskatāmais laukums), tad paraugam ar „Proxxon 27172 MICRO” MBS 240/E dimanta lentszāģi (lentszāģa izmēri 1065x3,0x0,3 mm) iezāgē 80 mm garu un 0,5 – 2 mm šauru iezāgējumu (*notch*), kura galā stiepes slogojuma laikā koncentrēsies maksimālie spriegumi, šaurais iezāgējums papildus palielina spriegumu intensitāti.

[044] Paraugu gatavošana stiepes slodzes un šļūdes deformāciju noteikšanai stiepes slogojumā, izmantojot kuponveida (*Coupon*) paraugus. Prizmu 150x150x600 mm sazāgē 12 ± 1 mm biezās plāksnēs, izveidojot kuponveida paraugus ar gala izmēriem 100x50x12 mm un 150x70x12 mm. Stiepes spriegumu intensitātes palielināšanai, paraugus veido iespējami plānus.

[045] Lai būtu prognozējama un tiktu konkretizēta maksimālo šļūdes deformāciju, tostarp nelineāra slogojuma gadījumā arī mikroplaisu un plaisu parādīšanās, vieta (tas ir apskatāmais laukums), tad paraugam 100x50x12 mm ar „Proxxon 38070 FKS/E” dimanta zāģi

(Ø50x0,5 mm) paralēli parauga īsākajai malai, pa centrālo ass līnijas perimetru, iezāgē vispirms 2 mm un, tad 10 mm (parauga īsākā šķērsizmēra virzienā) dziļus iezāgējumus, turklāt dziļāko iezāgējumu iegūst, zāģējot rievu aptuveni trīs piegājienos (Paegle, Fischer, 2011, 2013; Pereira *et al.*, 2012).

[046] Savukārt paraugam 150x70x12 mm ar dimanta griezdēdisku iezāgē 20 mm garu un 2 mm šaurus iezāgējumus abās parauga pusēs. Pirms pārbaudēm paraugiem simetriski un centriski iezāgējumam pielīmē četras alumīnija plāksnes.

[047] Pirms testiem abu tipu paraugu virsmas jāapskata, lai atrastu vislabāko deformāciju, kā arī reģistrēšanas un novērošanas vietu, un atbilstoši tai ar dimanta kroņurbi izurbj divus Ø20 mm caurumus. Attālums no parauga malas līdz slodzes pielikšanas caurumu centriem ir 30 mm un attālums starp slodzes pielikšanas caurumu centriem ir 90 mm (Pereira *et al.*, 2010; 2012).

[048] Pirms eksperimentālajām pārbaudēm CT paraugiem simetriski iezāgējumam pielīmē divas alumīnija plāksnes (10x10 mm), bet kuponveida paraugiem simetriski iezāgējumiem pielīmē četras alumīnija plāksnes (10x10 mm), izmantojot epoksīda līmi. Visiem paraugiem, pirms tos ievieto stiepes šļūdes sviru stendā, uz sānu virsmām piestiprina deformāciju mērierīces – tenzometrus vai HBM DD1 digitālos deformāciju mērītājus. CT paraugiem – vienu, bet kuponveida paraugiem divus, kas izvietoti vienādos attālumos cits no cita. Tenzometru „nažus” ievieto uz pielīmētajām plāksnēm, tenzometru bāze – 50 mm. Tenzometrus paraugiem piestiprina ar elastīgām gumijām vai metāla skavām. Šļūdes parādības eksperimentālai pētīšanai paraugus ar tenzometriem ievieto šļūdes sviru stendos maksimāli centriski starp satvērējzokļu elementiem, pa vienam paraugam katrā stendā. HBM DD1 deformāciju mērījumus caur daudz kanālu reģistrēšanas iekārtu HBM „Spider 8”, reģistrē datorā, izmantojot datorprogrammu HBM „CatMan”. Visus paraugus slogo ar konstantu, vienmērīgu, statisku slodzi (~20–40% no graujošajiem spriegumiem, nepārsniedzot betona un cementa kompozīta darbības lineāro posmu). Paraugus atkārtoti slogo un atslogo divas reizes un katra slogojuma iegūtos deformāciju nolasījumus salīdzina, lai pārbaudītu vai slogojums ir centrisks, lai izpildītos šis nosacījums katra nolasījuma starpības nevar pārsniegt 20 % no vidējās aritmētiskās vērtības, kas iegūta no visiem rādījumiem.

[049] Pirmajā dienā pēc paraugu noslogošanas, nolasījumus reģistrē ik pēc stundas, tad pirmo nedēļu tos turpina reģistrēt vienu reizi dienā. Pēc pirmās nedēļas nolasījumus reģistrē ar 2–3 dienu intervālu līdz apmēram 30 dienām kopš slogošanas sākuma, pēc pirmā mēneša nolasījumus reģistrē reizi nedēļā. Ja tests tiek turpināts arī, sasniedzot 90 dienas, tad tālāk reģistrēšanu veic vienu reizi mēnesī. Sasniedzot eksperimenta interesējošo slogojuma ilgumu, slodzi pakāpeniski noņem un pie katras slodzes pakāpes, tāpat kā testa sākumā, nolasa

deformāciju lielums, iegūstot tūlītējās jeb acumirkīgās, atgriezeniskās deformācijas. Slodzes noņemšanas pakāpes ir vienādas ar slodzes pielikšanas pakāpēm. Kad paraugs atslogots, to nemainīgi atstāj šļūdes sviru stendā, lai noteiktu atgriezeniskās deformācijas laikā. Deformāciju atgriezeniskuma mērījumu nolasīšanai, datus reģistrē nepieciešami ilgā periodā un reģistrēšanas biežumu veic tāpat, kā noslogojot paraugus.

[050] Žūšanas rukuma deformāciju noteikšanai stiepes formas paraugiem var tikt izmantota viena metode. Paraugus sagatavo tāpat kā šļūdes testam ar divām vai četrām alumīnija plāksnēm uz paraugu sānu šaurākās virsmas. Lai noteiktu korektas šļūdes deformācijas, tad žūšanas rukuma deformāciju noteikšanai sagatavo identiska sastāva un identisku izmēru paraugus kā šļūdes pārbaudēm.

[051] Šļūdes deformāciju noteikšanai liecē izmanto plātņveida paraugus ar izmēriem 450x75x20mm. Sākotnēji tiek izgatavota plāksne ar izmēriem 500x500x20mm. Svaiga betona vai cementa kompozītu liešanas laikā pārlicinās, ka veidņa virsma ir iespējami gluda. Ja izgatavotā sastāva īpatnību dēļ pēc saistīšanās laika beigām (sacietēšanas) tiek konstatēts, ka plāksnes virsmā ir negludumi, tad tos izmantojot dimanta slīpdisku uzmanīgi un rūpīgi izlīdzina, lai plātnes virsma būtu ar nemainīgu biežumu un gluda. Pēc plātnes atveidošanas un virsmas slīpēšanas plātņi sazāgē sijasveida plātņu elementos ar dimensijām 20x75x450mm (Ranaivomanana *et al.*, 2013)

[052] Katram paraugam centrā, izmantojot epoksīda līmi, tiek pielīmētas alumīnija plāksnītes 1,6x10x15mm. Uz šīs alumīnija plāksnes tiek atspiesta deformāciju mēriekārtas vadītka.

[053] Šļūdes deformāciju noteikšana liecē. Šļūdes deformācijām liecē nosaka iepriekš sagatavotajiem paraugiem. Lieces stendā katram testētajam paraugam tiek kombinēti atsvari, lai sasniegtu nepieciešamo slodzes apjomu. Papildus tiek uzstādīta pasija/as, kur ar sviras skavas ierobežotāj skavu stiprina deformāciju indikatoru.

[054] Pirms paraugu ievietošanas stendā katrs tā indikators tiek pārbaudīts, lai nav mehāniski bojājumi, kas liegtu indikatoram uzrādīt objektīvus mērījumus. Stendā tiek ievietoti paraugi tā, lai parauga centra atzīme būtu pretī pasijai piestiprinātās ierobežotājskavas centram. Pēc tam uz parauga centra tiek uzlikta skava, kurai pievieno asi ar atsvariem, kas složo paraugus.

[055] Paraugiem nepieciešamo slodzi pieliek pakāpeniski – vismaz piecās pakāpēs, pēc katra posma nosakot acumirklīgo deformāciju vērtību, zinot elastīgās deformācijas var aprēķināt elastības moduli liecē. Lai novērtētu deformāciju mērierīču korektu darbību, paraugi stendos atkārtoti tiek slogoti un atslogoti divas reizes un iegūtie nolasījumi tiek salīdzināti, lai to starpības nepārsniedz 20 %. Šļūdes paraugi liecē ilgstoši tiek slogoti ar nemainīgu, statisku

slodzi (~ 20 –40% no graužošajiem spriegumiem, nepārsniedzot betona un cementa kompozīta darbības lineāro posmu).

[056] Pirmajā dienā pēc paraugu noslogošanas nolasījumus veic ik pēc stundas, tad pirmo nedēļu tos reģistrē vienu reizi dienā. Pēc pirmās nedēļas nolasījumus veic ar 2 – 3 dienu intervālu līdz apmēram 30. dienai kopš slogošanas sākuma, pēc tam nolasījumus veic reizi nedēļā. Ja tests tiek turpināts, sasniedzot 90 dienas, tad turpmāk nolasījumus veic vienu reizi mēnesī.

[057] Sasniedzot eksperimentam interesējošo slogojuma ilgumu, slodzi pakāpeniski noņem un pie katras slodzes pakāpes, tāpat kā testa sākumā, nolasa deformāciju lielums, iegūstot tūlītējās jeb acumirkļīgās atgriezeniskās deformācijas. Slodzes noņemšanas pakāpes ir vienādas ar slodzes pielikšanas pakāpēm. Kad paraugs atslogots, to atstāj nemainīgi šļūdes sviru standā, lai noteiktu atgriezeniskās deformācijas laikā. Deformāciju atgriezeniskuma mērījumu nolasīšanai, datus reģistrē nepieciešami ilgā periodā.

[058] Lai izslēgtu žūšanas rukuma deformācijas, tādējādi nosakot tikai pamatšļūdi, tad paraugus ietin vienā kārtā polietilēna (PE) pakošanas plēvē. Otro kārtu paraugiem veido no pašlīmējošas alumīnija lentas, kura tiek uzlīmētā vienā kārtā. Katram paraugam centrā tiek pāršķelts pakojums (PE plēve un alumīnija lenta) un pielīmētas alumīnija plāksnītes izmēros 1,6x10x15mm, izmantojot epoksīda līmi. Uz šīs alumīnija plāksnes tiek atspiesta deformāciju mēriekārtas vadītā.

[059] Pēc tam zonā starp alumīnija plāksnīti un pakojumu tiek pildīta epoksīda līme, lai nenotiktu gaisa, mitruma kustība no parauga un uz paraugu. Uz aplīmētā parauga virsmas perpendikulārā virzienā tiek veidota atzīme ar marķieri, kas apzīmē parauga centrālo asi, kur tiek pielikta slodze.

[060] Cementa kompozītu paraugu vecums visu slogošanu sākumā, spriegumu līmenis, slogošanas ilgums, atslodze atkarīgi no datu tālākās izmantošanas.

[061] Ilgstošo testu laikā reģistrē arī telpas apkārtējās vides mitrumu un temperatūru.

[062] Žūšanas rukuma deformācijas nosaka un izmantoto, lai noteiktu korektas šļūdes deformācijas lielumu. Rukuma testam sagatavo identiska sastāva un identisku izmēru paraugus kā šļūdes pārbaudēm un deformācijas mēra paralēli šļūdes deformāciju nolasījumiem, paraugi tiek turēti identiskos apkārtējās vides apstākļos, vēlams blakus šļūdes paraugiem.

[063] Žūšanas rukuma deformāciju noteikšanai lieces formas paraugiem var tikt izmantot vienu metodi. Paraugus sagatavo tāpat kā šļūdes testam ar divām alumīnijā plāksnēm uz paraugu sānu virsmām. Lai noteiktu korektas šļūdes deformācijas, tad žūšanas rukuma deformāciju noteikšanai sagatavo identiska sastāva un identisku izmēru paraugus kā šļūdes pārbaudēm. Ja

nepieciešams noteikt pamatšļūdi un žūšanas šļūdi, tad atbilstoši jā sagatavo arī daļa rukuma paraugu, ietinot divās kārtās alumīnija folijas, lai nodrošinātu, ka neiestāsies žūšanas process, bet daļu paraugu atstāj neietītus, pieļaujot tajos žūšanas procesu.

[064] Piedāvātais paņēmiens ir pielietojams, izpildoties šādiem nosacījumiem:

- pielietoto cementa un betona kompozītu šļūdes deformāciju spiedē noteikšanas paraugu mazākais izmērs (b) ir ierobežots ar matricas lielākās pildvielas pieckāršu izmēru (\emptyset) – $b_{min} \geq 5 \emptyset$ (RILEM TC 107-CSP, 1998); bet lielākais izmērs (l) ir ierobežots ar standā maksimāli iespējamā, ievotojamā parauga garumu – $l \leq 200$ mm;
- šļūdes defomācijas spiedē un žūšanas rukuma deformācijas spiedes paraugiem noteikt, izvēloties vienotu parauga ģeometriju abām paralēli veicamajām pārbaudēm; ieteicams izmantot paraugus ar ģeometriskajiem izmēriem, kas atbilst nosacījumam $\frac{b}{l} \leq \frac{1}{4}$, kur b – parauga šķērsriezuma lielākais izmērs; l – parauga garums (RILEM TC 107-CSP, 1998);
- stiepes, lieces stiprības un šļūdes deformāciju noteikšanai stiepē un liecē, kā arī rukuma deformāciju noteikšanai stiepes un lieces paraugiem ieteicams izmantot plātņveida paraugus. Stiepes paraugiem papildus veido iezāģējumu vienā vai abās parauga pusēs;
- šļūdes pārbaužu spriegumu līmenis, nosakot deformācijas lineārajā šļūdes posmā, atrodas robežās līdz 40% no graužošo spriegumu lieluma;
- slogojuma sākums un ilgums, kā arī atslodzes ilgums šļūdes pārbaudēs atkarīgs no izvirzītā mērķa un var būt neierobežots;
- ilglaicīgās pārbaudes var tikt veiktas paraugiem divās mitruma koncentrācijās – gaissausiem un mitriem;
- laboratorijā tiek rekomendēts uzturēt pastāvīgus apkārtējās vides apstākļus (temperatūru un gaisa mitrumu).

PRETENZIJAS

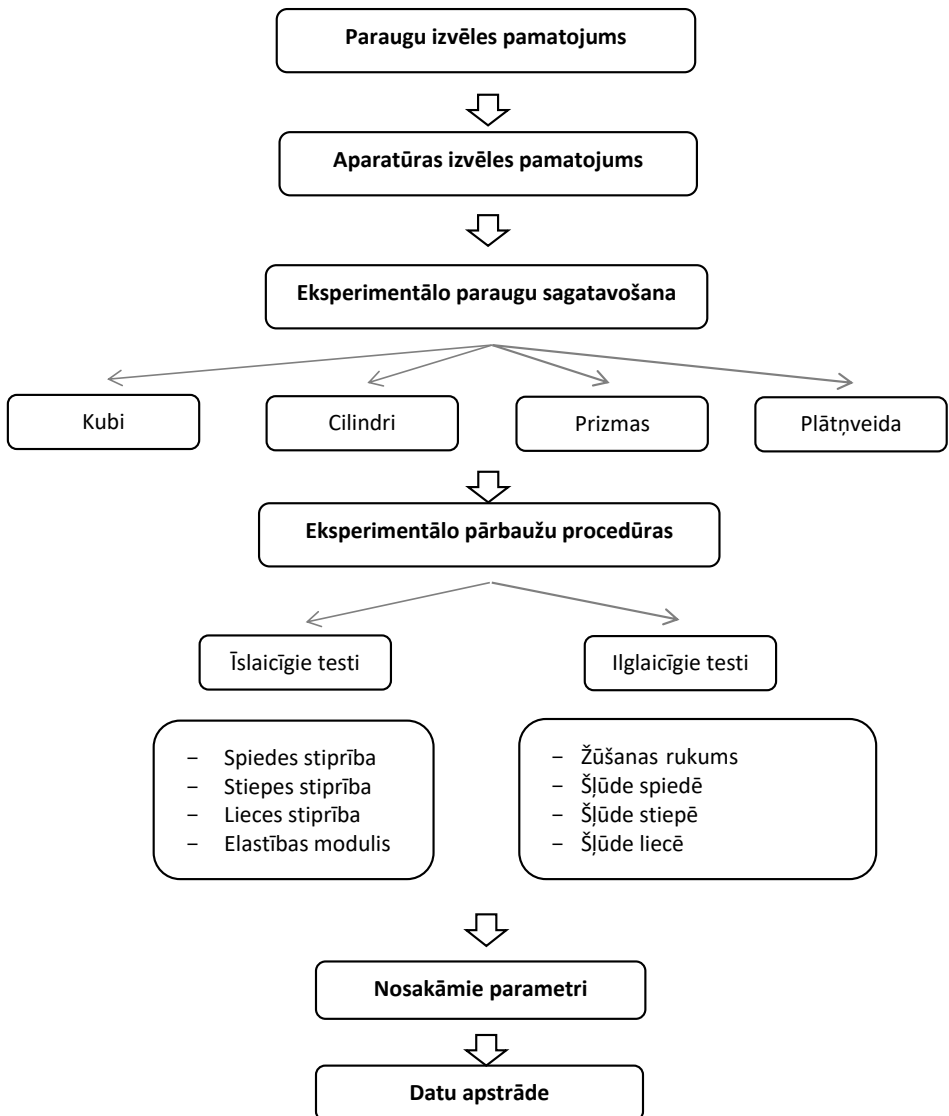
1. Paņēmiens betonu un cementa kompozītu ilglaicīgo īpašību noteikšanai sprieguma stāvokļos, kas ietver šādus soļus:

- i) betona un cementa kompozītu paraugu sagatavošanu kubu, cilindru, prizmas vai plātņveidu formā, iepildot testējamo kompozītu atbilstoši projektēšanas nosacījumiem iepriekš sagatavotos veidņos un atstājot cietēšanai 20 ± 2 °C temperatūrā un $RH > 95 \pm 5$ %, uz 24–48 stundām, pēc kā paraugus atveidņo, veic paraugu pirmapstrādi un, pēc izvēles paraugus atstāj tālākai cietēšanai ūdenī līdz atbilstošajām eksperimentālajām pārbaudēm;
- ii) testējamo paraugu ievietošanu stendā, slogošanu ar slodzi, pēc kā paraugu atslogo;
- iii) parauga atkārtotu slogošanu un atslogošanu vismaz vēl vienu reizi un katra slogojuma iegūtos deformāciju nolasījumu salīdzināšanu, reģistrējot arī apkārtējās vides mitrumu un temperatūru;
- iv) betona un cementa kompozītu ilglaicīgo īpašību noteikšanu, izmantojot iepriekšējos soļos iegūtus datus un kvantitatīvu attēlu analīzi.,

2. Paņēmiens saskaņā ar 1. pretenziju, kas raksturīgs ar to, ka betona un cementa kompozītu stiprību nosaka, pārbaudot minimums trīs vienāda izmēra un sastāva paraugus, pakļaujot stiprības testam, kā graujošo stiprību pieņemot vidējo vērtību, bet ar noteikumu, ka atsevišķo stiprību atšķirības nepārsniedz 20% no vidējās vērtības, turklāt papildus nosaka betona un cementa kompozītu stiprības pieaugumu laikā, slogotiem un neslogotiem paraugiem.

3. Paņēmiens saskaņā ar jebkuru no iepriekšējām pretenzijām, kas raksturīgs ar to, ka šļūdes deformāciju noteikšanai izmanto šļūdes stendus, turklāt paraugu slogošanu veic ar konstantu, vienmērīgu, statisku slodzi 80-100 dienas, pēc kā paraugus atslogo 20-40 dienas.

4. Paņēmiens saskaņā ar jebkuru no iepriekšējām pretenzijām, kas raksturīgs ar to, ka paralēli šļūdes testiem veic paraugu žūšanas rukuma testus, kuru laikā nepārtraukti reģistrē arī apkārtējās vides mitrumu un temperatūru.



Annex IX: Patent II:

Gailitis R., Sprince A., Pakrastins L.

Paņēmiens ārējo iedarbju ietekmes noteikšanai uz betonu un cementa kompozītmateriālu mikrostruktūru dažādos sprieguma stāvokļos/ Technique for Outside Effect Determination on

Concrete and Cement Composite Microstructure in Various Stress-Strain States

Latvian patent application No. LVP2023000039



Latvijas Republikas Patentu valde

Citadeles iela 7/70, Rīga, LV-1010, tālr. 67099600, fakss 67099650, e-pasts lietvediba@lrpv.gov.lv, www.lrpv.gov.lv

Adresāts:

Irīna BOIKO
RĪGAS TEHNISKĀ UNIVERSITĀTE
Āzenes iela 12 - 104
Rīga, LV-1048
patenti@rtu.lv

PAZIŅOJUMS (R2)

Par pieteikuma dokumentu saņemšanu

Jūsu šifrs	Saņemšanas datums	Mūsu šifrs	Mūsu datums
	26.04.2023.	LVP2023000039	26.04.2023.

Patentu valde informē, ka ir saņemts patenta pieteikums:

- | | |
|-----------------------------|--|
| (21) Patenta pieteikuma Nr. | LVP2023000039 |
| (22) Pieteikuma datums | 26.04.2023 |
| (72) Izgudrotāji | Rihards GAILĪTIS, Slokas iela 88B, Jūrmala, LV-2008, LV
Andīna SPRINCE, Varavīksnes iela 9, Ogre, Ogres nov., LV-5001, LV
Leonīds PAKRASTIŅŠ, Lugažu iela 2A - 52, Rīga, LV-1045, LV |
| (71) Pieteicēji | RĪGAS TEHNISKĀ UNIVERSITĀTE, Ķīpsalas iela 6A, Rīga, LV-1048, LV |
| (54) Izgudrojuma nosaukums | PAŅĒMIENS ĀRĒJO IEDARBJU IETEKMES NOTEIKŠANAI UZ BETONU UN CEMENTA KOMPOZĪTMATERIĀLU MIKROSTRUKTŪRU DAŽĀDOS SPRIEGUMA STĀVOKĻOS |

(lūdzam informēt Patentu valdi par pamanītajām kļūdām)

Saistībā ar minēto pieteikumu ir saņemti sekojoši materiāli:

- | | |
|--|--------|
| <input type="checkbox"/> Iesniegums patenta piešķiršanai (2.pielikums MK Not.Nr.224) | 1 eks. |
| <input type="checkbox"/> Izgudrojuma apraksts latviešu valodā | 1 eks. |
| <input type="checkbox"/> Viena vai vairākas izgudrojuma pretenzijas | 1 eks. |
| <input type="checkbox"/> Izgudrojuma zīmējums(-i) | 1 eks. |
| <input type="checkbox"/> Kopsavilkums | 1 eks. |
| <input type="checkbox"/> Kopsavilkuma tulkojums angļu valodā | 1 eks. |

Atgādinām, ka ekspertīze būs iespējama tikai gadījumā, ja pieteikumam tiks pievienoti sekojoši materiāli:

- Maksājums par pieteikuma iesniegšanu, 120,- EUR

Patentu departamenta
eksperte

I.Boiko

PAŅĒMIENS ĀRĒJO IEDARBJU IETEKMES NOTEIKŠANAI UZ BETONU UN
CEMENTA KOMPOZĪTMATERIĀLU MIKROSTRUKTŪRU DAŽĀDOS
SPRIEGUMA STĀVOKĻOS

[001] Izgudrojums attiecas uz būvniecību un būvniecības materiālu testēšanas paņēmieniem, proti uz paņēmieniem ārējo iedarbju ietekmes noteikšanai uz betonu un cementa kompozītmateriālu mikrostruktūru dažādos sprieguma stāvokļos.

Zināmais tehnikas līmenis

[002] Veicot ēku un inženierbūvju projektēšanu, tiek prognozēta un novērtēta konstrukciju un to daļu darbība visā būves ekspluatācijas un dzīves cikla laikā. To veic novērtējot ilglaicīgo īpašību (šķīdes, rukuma u.c.) ietekmi [1; 2]. Iepriekšminētās īpašības noteic eksperimentāli atbilstoši mērījumu veikšanas standartiem (RILEM u.c.) [3] un metodoloģijām [4], un matemātiski pārvērš atbilstošos parcāļajos faktoros atbilstoši konstrukcijas vai konstrukciju kopas darbības raksturam un paredzētās apkārtējās vides ietekmes raksturam. Tomēr ēku un inženierbūvju ekspluatācija mēdz atšķirties no projektēšanā paredzētajiem apstākļiem. Tā rezultātā ilgstošā ekspluatācijas periodā konstrukciju pretestība esošajām ārējām iedarbēm (gan no mehāniskas slodzes, gan apkārtējās vides apstākļiem) var būt samazināta.

[003] Ir zināmi nacionālie standarti, kuri reglamentē ēku un inženierbūvju apsekošanu (LBN 405-21, LVS 190-11:2009), tomēr tie balstās uz kvalitatīvu apsekojumu (vizuālu apsekojumu, kurš balstās uz apsekotāja pieredzi izteikt pieņēmumu par redzētā nolietojuma ietekmi uz konstrukcijas mehāniskajām īpašībām). Šāds apsekojuma veids ir subjektīvs, tas nebalstās skaitliskās, kvantitatīvās, viennozīmīgās vērtībās, bet tiek argumentēts tikai ar apsekotāja empīrisku novērojumu.

[004] Ir zināms zinātnes novirziens petrogrāfija, kur pēta iežu sastāvu, uzbūvi un izcelsmi. Pētniecības paraugu sagatavošana ir adaptējama arī akmeņiem līdzīgiem materiāliem un ļauj veikt mikrostruktūras izpēti betoniem un cementa bāzes materiāliem tos sazāģējot, slīpējot un pulējot, un tālāk izmantojot mikroskopus pētot to mineraloģisko sastāvu un mikrostruktūras raksturu. Pētniecības nozare tiek saukta par betonu petrogrāfiju.

[005] Ir zināmas Gunter Grundmann un Herbert Scholz vadlīnijas „*The preparation of thin sections, polished sections, acetate foil prints, preparation for elutriation analysis, and staining tests for the optical and electron microscopy*” [5], kurā sniegta informācija kā pareizi iegūt un sagatavot plānus pulētos paraugus (no angļu valodas *polished thin section specimens*) dažāda veidu minerālu petrogrāfijas izpētēm gan optiskajā, gan skenējošajā elektronu mikroskopā (no angļu valodas *Scanning Electron Microscope, SEM*). Vadlīnijas nesniedz informāciju par pulētu, biezu paraugu iegūšanas un apstrādes metodēm.

[006] Ir zināmas Donald E. Cadwell un Paul W. Weiblen vadlīnijas „*Diamond disc Preparation of Polished Thin Sections for Electron Microprobe Analysis*” [6], kurā aprakstīta plānu, pulētu paraugu iegūšana, sagatavošana un analīze. Tomēr neparādās nekādi paraugu uzglabāšanas posmu apraksti, kā paraugi, kuri ir trausli vai apkārtējās vides ietekmē var mainīt savas īpašības, ir jāuzglabā vai jāizolē.

[007] Ir zināmi plāno pulēto paraugu sagatavošanas un analīzes paņēmieni [4; 5]. Tie ietver sekojošus secīgu soļus:

- (i) paraugu impregnēšanu un uzglabāšanu līdz apstrādei epoksīda sveķos;
- (ii) liekās epoksīda sveķu kārtas noņemšanu no virsmas, kuru līmēs pie objektstikliņa;
- (iii) paraugu piezāģēšanu līdz 10,0 mm biezos paraugos. Parauga garumam un platumam jāatbilst optiskā mikroskopa paraugu ietvara specifikācijai;
- (iv) paraugu līmēšanu pie objektstikliņa ar epoksīda līmi;
- (v) atkārtotu parauga zāģēšanu līdz biezumam 0,5 mm;
- (vi) paraugu virsmas pulēšanu līdz biezumam 30 μm;
- (vii) pārklājstikliņa līmēšana uz atklātās virsmas ar UV (ultravioleto starojumu) aktivizētu līmi.

[008] Materiālu un eksistējošu konstrukciju un to daļu īpašību novērtēšanai gan slodzes, gan apkārtējās vides ietekmes rezultātā ir nepieciešama ne tikai informācija par mehāniskajām īpašībām (ja tāda ir pieejama), bet arī informācija par to, kas konstrukcijas elementam, materiālam vai konstrukcijai kopumā norisinās iekšienē. Publikācijā „*Geopolymer Microstructure Using Polarization and Fluorescence Microscopy*” [7] ir skaidroti iemesli kāpēc veicama betona un cementa bāzes materiālu mikrostruktūras pētniecība un analīze, un aprakstīta ģeopolimēru un betona mikrostruktūru pētniecība ar optisko mikroskopu, izmantojot

plānus pulētus paraugus. Līdz ar to ir nepieciešams paņēmiens ārējo iedarbju ietekmes noteikšanai uz betonu un cementa kompozītmateriālu mikrostruktūru dažādos sprieguma stāvokļos, kas neapdraudētu tālāku konstrukcijas vai elementa ekspluatāciju un būtu iespējams paraugu izmantot pētniecībai ilgstoši, izslēdzot tā īpašību maiņu ārējo faktoru ietekmē.

Izgudrojuma mērķis un būtība

[009] Šī izgudrojuma paņēmiena mērķis ir precīzi noteikt ekspluatācijā esošajām inženierbūvēm un ēkām ekspertīzes gaitā to konstrukciju materiālu reālo fizisko stāvokli ekspluatācijas rezultātā kā arī ārējo iedarbju rezultātā, tādējādi ļaujot izvairīties no neprecīza konstrukciju stāvokļa un atlikušo resursa novērtēšanas.

[010] Izgudrojuma paņēmiena mērķis ir arī jauniem, eksperimentāliem konstruktīviem būvmateriāliem noteikt mikrostruktūras izmaiņas ilgstoša slogojuma un apkārtējās vides ietekmē.

[011] Izgudrojuma mērķis ir sasniegts ar paņēmienu, kurš ietver šādus secīgus soļus:

- (i) iegūt paraugu daļas vai konstrukciju elementa urbto kodolu parauga sagatavošanai;
- (ii) impregnēt, cietināt un uzglabāt paraugus epoksīda vai līdzvērtīgos sveķos līdz soļa (iii) uzsākšanai;
- (iii) tālāk uzglabātos paraugus piezāģēt 1,0 līdz 2,0 cm (ieteicams 1,0–1,5 cm) biezos paraugos un marķēt. Parauga garumam un platumam jāatbilst skenējošā elektronu mikroskopa ietvara specifikācijai. Paraugus pēc zāģēšanas ievieto žāvskapī un žāvē 40 °C temperatūrā 24 stundas;
- (iv) paraugus slīpēt un pulēt. Pēc katra slīpēšanas un pulēšanas cikla paraugu virsmas skalot un pēc slīpēšanas un pulēšanas cikliem paraugus žāvē (40 °C temperatūrā 24 stundas). Līdz solim (v) – mikrostruktūras pētīšanai – paraugus uzglabā gaisa necaurīdīgā iepakojumā ar silikagēlu vai līdzvērtīgu mitrumu uzsūcošu vielu iekšā ķīmiskā un mehāniskā stāvokļa fiksēšanai, kā arī konturē interesējošās pētāmās zonas parauga šķērsgriezumā. Papildus, atkarībā no mērījumu iekārtas īpatnībām (piemēram, elektronu mikroskopam), pirms konturēšanas un secīgas mikrostruktūras pētīšanas, parauga virsmu pārklāj ar

konduktīvu pārklājumu, piemēram, zeltu vai oglekli, atbilstoši izmantotam skenējošajam elektronu mikroskopam;

- (v) pētīt paraugu mikrostruktūru, izmantojot elektronu mikroskopu vai optisko mikroskopu ar attēlu uzņemšanas funkciju;
- (vi) veikt attēlu kvantitatīvo analīzi, kurā tiek uzskaitīta un analizēta attēlā vai attēlos redzamā parauga virsmas kompozīcija un saturs.

[012] Ar izgudrojuma paņēmieni iespējams noteikt materiāla morfoloģiju – porainību, plaisāšanas izpausmes, to raksturu un apjomu. Iespējams arī noteikt hidratācijas pakāpi, stiegrojuma korozijas pakāpi, ietekmi uz apkārtesošo betona konstrukcijas daļu, pildvielu un saistvielas savstarpējo izkliedi elementa šķērsriezumā un pie liela parauga zonas palielinājuma – kontakta zonu un tās īpašības starp pildvielu un saistvielu un/vai stiegrojumu un saistvielu.

[013] Saskaņā ar izgudrojuma paņēmiena soli (ii) betona un cementa kompozītu materiālu vai konstrukciju paraugus pirms soļa (iii) ievieto epoksīda sveķos un cietina, nodrošinot sveķu un, pēc iespējas, konstrukcijas vai parauga vakuumēšanu un anaerobu vidi, tādējādi nodrošinot deformāciju un ķīmiskā stāvokļa fiksēšanu pēc iespējas tuvāk stāvoklim parauga izņemšanas brīdī no konstrukcijas vai laboratorijas parauga. Epoksīda sveķus iespējams aizstāt ar līdzvērtīgiem sveķiem vai substancēm (piemēram, poliuretāna sveķiem), kuri nodrošina paraugu konservāciju, pilnīgu aizsardzību no apkārtējās vides ietekmes un nemijiedarbojas vai neveido ķīmiskas reakcijas un savienojumus ar parauga materiāliem.

[014] Izgudrojuma paņemiens ir raksturīgs arī ar to, ka laika posmā starp paraugu sagatavošanu mikrostruktūras izpētei skenējošajā elektronu mikroskopā un/vai optiskajā mikroskopā un pašu mikrostruktūru izpēti mikroskopos (starp paņēmiena soļu (iv) un (v) izpildi), paraugus uzglabā gaisa necaurlaidīgā iepakojumā ar mitrumu uzsūcošām vielām (piemēram, plastmasas maisiņā ar rāvējslēdzēja tipa aizdari (pazīstams kā *zip-lock* maisiņš) ar silikagelu iekšā ķīmiskā un mehāniskā stāvokļa fiksēšanai.

[015] Pirms eksperimentālajām pārbaudēm katrs paraugs tiek marķēts un, atkarībā no mērījumu iekārtas īpatnībām (piemēram, elektronu mikroskopam), tiek pārklāts ar konduktīvu pārklājumu, piemēram, zeltu vai oglekli, atbilstoši izmantotam skenējošajam elektronu mikroskopam. Ja paraugs ir ar pētāmās virsmas laukums ir vienāds vai lielāks par 1 cm², tad uz tā tiek atzīmētas raksturīgās, pētāmās zonas.

[016] Papildus, tā kā ar izgudrojuma paņēmieni ir iespējams noteikt mikrostruktūras izmaiņas, piemēram, plaisāšanu, poru deformēšanos un izmēra samazināšanos un citas izmaiņas, kuras notiek materiālam, konstrukcijas elementam vai konstrukcijai kopumā iekšienē, betona un cementa kompozītu mikrostruktūras pētniecībai no konkrētā parauga izgatavo vismaz 3 pulētās virsmas paraugus, kas atrodas viens virs otra pētītā šķērsriezuma pa garenasi.

[017] Uzņemtie mikrostruktūru attēli, ja tie reprezentē virsmas laukumu, kas sastāv no vairākiem attēliem (atbilstoši palielinājumam), tiek apvienoti vienā kopējā attēlā, atbilstoši to uzņemšanas kārtai un atrašanās vietai pētāmajā šķērsriezumu laukumā. Attēlu apvienošanai iespējams izmantot dažādas programmas, piemēram, *Adobe Photoshop* [8] vai patstāvīgi programmētas programmas, kas apvieno attēlus pēc atskaites punktiem (secīgi sekojošu attēlu kopīgajiem punktiem vai attēla īpatnējām zonām). Iegūto attēlu sadala slāņos atbilstoši pētītajiem šķērsriezuma raksturlielumiem (plaisa un šķērsriezuma materiāls vai matrica, pildviela, gaiss, stiegrojums) un/vai veic rentgena staru difrakciju (no angļu valodas *X-ray diffraction, XRD*) analīzi interesējošajām šķērsriezuma zonām.

[018] Atbilstoši attēla zonu kvantitatīvajiem parametriem kā laukumam un to reprezentējošajam zonas pikseļu skaitam veic analīzi un iegūst secinājumus par konkrētā šķērsriezuma īpašībām.

[019] Izgudrojuma izpratnei pievienoti šādi zīmējumi:

1. zīm. Izgudrojuma paņēmiena principālā blokshēma pulētās virsmas paraugu sagatavošanai un pētīšanai.

2a. zīm. Pētāmā parauga virsmas rekomendētā zonu uzņemšanas secvence vertikāli konturētai šķērsriezuma apskatāmai zonai, kur n ir attēla uzņemšanas kārtas skaitlis, kurš norāda uz tā uzņemšanas secību un vēlāk apvienošanas kārtību.

2b. zīm. Pētāmā parauga virsmas rekomendētā zonu uzņemšanas secvence horizontāli konturētai šķērsriezuma apskatāmai zonai, kur n ir attēla uzņemšanas kārtas skaitlis, kurš norāda uz tā uzņemšanas secību un vēlāk apvienošanas kārtību.

3a. zīm. Virsmu konturēšana attēlu uzņemšanai stiepes pārbaudes paraugiem.

3b. zīm. Virsmu konturēšana attēlu uzņemšanai spiedes pārbaudes paraugiem.

Izgudrojuma īstenošanas piemēri

[020] Izgudrojuma paņēmieni, kas ietver paraugu atlasi, iegūšanu, apstrādi un pētīšanu veic saskaņā ar 1. zīmējumā parādīto principiālo blokshēmu.

[021] Betona un cementa kompozītu paraugus, neatkarīgi no ieguves avota (laboratorijā testēti paraugi vai iegūti no ekspluatētas konstrukcijas), nepieciešams ievietot epoksīda vai citos līdzvērtīgu īpašību sveķos un cietināt. Šī darbība veicama nekavējoties pēc parauga ieguves.

[022] Paraugu ievieto traukā vai ietvarā (veidnī), kurā paraugu var pilnībā iegremdēt sveķos un paliek vēl maksimums 5 mm attālums līdz veidņa katrai malai, kur iepildīt sveķus, lai paraugs būtu pilnībā noseigts ar sveķiem un ārējās vides apstākļi kā mitrums, nevarētu to tieši ietekmēt. Sveķus iestrādes laikā, atbilstoši to lietošanas instrukcijai, atgaiso un, ieteicams, pēc iestrādes veidnī arī atgaiso, izmantojot vakuuma kameru.

[023] Pēc iestrādes epoksīda sveķus cietina. Paraugu pēc cietināšanas vai nu uzglabā istabas temperatūrā vēlākai izmantošanai, vai arī sagatavo mikrostruktūras pētījumiem kā pulētos paraugus.

[024] Mikrostruktūras pētniecībai sveķos impregnēto paraugu sazāģē, izmantojot cirkulāro vai lentzāģi ar dimanta griezēj disku, vai lentu un ūdens dzesēšanu. Paraugu sagatavojami tādos izmēros, lai tos būtu iespējams ievietot SEM, piemēram, 4,6 cm diametrā un 1,0 cm biezumā. Paraugi tiek sazāģēti 1,0 līdz 2,0 cm (ieteicams 1,0 līdz 1,5 cm) biezos paraugos. Paraugu sazāģēšanas biezums var atšķirties atkarībā no pulējamās iekārtas specifikas. Paraugu sazāģēšanu veic lēni, lai netiktu izrauti caurumi vai gabali paraugos un zāģētās virsmas paraugiem būtu savstarpēji paralēlas. Paraugu skaits atkarīgs no pētāmās zonas apjoma un paraugu izmēriem. Ja pētāmā zona pieļauj lielu paraugu skaita iegūšanu, tad tie ir jāiegūst un jāpēta. No katra impregnētā parauga iegūst vismaz 3 paraugus, kuri atrodas viens virs otra garenass virzienā.

[025] Paraugus pēc zāģēšanas uzreiz ievieto žāvskapī, kur tos žāvē 40 °C temperatūrā 24 stundas.

[026] Pēc paraugu žāvēšanas to zāģētās virsmas pārklāj ar plānu, iepriekš izmantoto sveķu kārtiņu. Sveķiem jābūt atgaisotiem un uzklātajai sveķu kārtiņai jābūt bez gaisa burbuļiem. Pēc tam paraugus atbilstoši sveķu specifīkacijai cietina.

[027] Pēc zāģēto paraugu virsmu impregnēšanas ar sveķiem un cietināšanas, paraugus slīpē un pulē izmantojot pulējamās mašīnas. Atbilstoši paraugu formai un izmēriem izmanto

automātiskās vai daļēji automātiskās pulēšanas mašīnas, piemēram, *Mecatech 334* [9]. Paraugu pulēšanu veic, lai novāktu lieko sveķu kārtu un pulētu paraugu matricas un pildvielu virsmas, un padarītu parauga virsmu pēc iespējas gludu, vienmērīgu un bez skrāpējumiem vai savādāku virsmas nevienādīgumu. Virsmu slīpēšanu veic ar smilšpapīriem. Slīpēšanas procesā paraugu virsmas un smilšpapīru virsma tiek dzesēta ar ūdeni. Pulēšanu veic ar dimanta emulsijas šķīdumu ar 3 μm dimanta daļiņu izmēru. Smilšpapīru izmēri un pulējamo disku izmēri ir atbilstoši izmantotās pulēšanas mašīnas specifikācijai. Pulēšanas intensitāte un soļi veicami un veidojami atbilstoši materiāla mehāniskajām īpašībām, bet sagatavojot C30/37 klases cementa kompozīta paraugu, izmantojams 1. tabulā parādītais slīpēšanai un pulēšanai rekomendējamo ciklu ilguma, pielietojamo materiālu rekomendētās vērtības.

1. tabula

Slīpēšanai un pulēšanai rekomendējamo ciklu ilguma, pielietojamo materiālu rekomendētās vērtības

Pulēšanas/ slīpēšanas cikla kārtas numurs	Pulēšanas/slīpēšanas sastāva (smilšpapīrs (pēc ISO 6344) vai pulēšanas pastas) tips	Pulēšanas/slīpēšanas cikla ilgums, minūtes	Spiedes spēks pret pulējošo/slīpējošo virsmu, daN
1.	P180	2	2,5
2.	P320	2	2,5
3.	P600	2	2,5
4.	P1000	2	2,5
5.	P1200	2	2,5
6.	3 μm	4	2,5

[028] Pēc katra slīpēšanas/pulēšanas cikla virsmas tiek skalotas un vizuāli pārbaudītas vai virsmas nav bojātas un vai nav ievērojami degradētas. Pēc paraugu virsmas analīzes, atbilstoši 1. tabulā attēlotajai secībai, turpina pulēšanu.

[029] Pēc pulēšanas cikla beigām paraugu virsmas tiek noskalotas un tie tiek ievietoti žāvskapī un žāvēti 24 stundas 40 °C temperatūrā. Pēc žāvēšanas paraugiem veic

mikrostruktūras analīzi vai arī tos uzglabā gaisa necaurīdīgā iepakojumā kopā ar silikagelu un/vai citu mitrumu reducējošu (absorbentu) un uzturošu materiālu. Paraugus tur tumšās, sausās telpās ar nemainīgu temperatūru.

[030] Pulētos paraugus pirms mikrostruktūras pētīšanas pārklāj, ja nepieciešams skenējošajam elektronu mikroskopam (SEM), ar konduktīvu pārklājumu (piemēram, ar zelta vai oglekļa pārklājumu) un konturē interesējošās zonas pētāmajā šķērsgriezumā (atbilstoši 3a. zīmējumam un 3b. zīmējumam).

[031] Paraugu vai paraugus ievieto skenējošajā elektronu mikroskopā, noregulē nepieciešamos parametrus, kā piemēram, attēla asumu, ekspozīcijas pakāpi, gaismas daudzumu u.c. Izvēlas atbilstošu palielinājuma līmeni, piemēram, 25 reižu palielinājumu un uzņem šķērsgriezuma attēlus atbilstošā sekvencē (rekomendēts pēc 2a. un 2b. zīmējuma sekvencēm) ar atbilstošiem atskaites punktiem, pēc kuriem vēlāk būs iespējams attēlus savietot vienā kopējā attēlā tā tālākai analīzei. Attēlu uzņemšanas laikā nedrīkst mainīt nevienu no iepriekš minētajiem attēla parametriem (asums, ekspozīcijas pakāpe u.c.). Tie visu attēlu uzņemšanas laiku paliek konstanti. Ja attēlu uzņemšanas laikā novērojams, ka kādas daļas pētāmajai šķērsgriezuma daļai kļūst tumšākas vai gaišākas, jāpārlicinās vai paraugā nav metāliska stiegrojuma vai kāda cita līdzvērtīga materiāla iespēja atstaroties vairāk kā pārējām šķērsgriezuma sastāvdaļām. Stiegrojuma gadījumā šo attēlu uzņem pie konstantas ekspozīcijas statusa un veic atkārtotu uzņemumu tad, kad visi attēli jau ir uzņemti. Ja tomēr tas nav saistīts ar šķērsgriezuma sastāvdaļas palielināto atstarošanās spēju, tad parauga zāģētās un pulētās virsmas nav savstarpēji paralēlas. Šādu paraugu tālāk neanalizē, bet atkārtoti pulēšanas un slīpēšanas soļus padarot parauga zāģētās virsmas savstarpēji paralēlas. Ja parauga biezums kļūst pārāk mazs, tad šādu paraugu vairs analīzei neizmanto un sagatavo jaunu paraugu.

[032] Iegūtos attēlus, atbilstoši to uzņemšanas kārtībai (sekvencei), apvieno vienā kopīgā attēlā, izmantojot attēlu apstrādes programma, piemēram, *Adobe Photoshop* [8] vai citas.

[033] Iegūto attēlu daļa atbilstošos slāņos, piemēram, poras, plaisas, matrica, pildviela u.c. Šiem slāņiem piešķir katram savu – atšķirīgu krāsas kodu.

[034] Izmantojot attēlu apstrādes programmas veic attēlu kvantitatīvo analīzi pēc vispārpieņemtiem principiem. Saskaista konkrētam slānim piešķirtās krāsas pikseļu skaits un attiecināts pret attēla kopējo pikseļu skaitu. Pēc savstarpējās attiecības nosaka, cik daudz katrā attēlā ir atrodama katrs konkrētais slānis, tā izvietojums un koncentrācija šķērsgriezumā.

[035] Kvantitatīvās analīzes rezultātus apkopo tabulā un veic datu salīdzināšanu un izsaka slēdzienus par paraugu šķērsriezumu veidojošo materiālu, tukšumu kvantitatīvo sastāvu, sadalījumu šķērsgriezumā u.c. novērotajām īpatnībām.

[036] Pēc šķērsriezumu veidojošo materiālu un tukšumu kvantitatīvā daudzuma un izvietojumu iespējams pateikt vai paraugs ir pastiprināti porains, vai ir bijusi neviendabīga cementa kompozīta masa, vai ir notikusi pildvielas segregācija un tā ir nosēdusies parauga apakšā un līdzīgi.

Izmantotie informācijas avoti

1. Neville, A.M. *Creep of plain and structural concrete*. 1983. Pp. 361. Pieejams: https://openlibrary.org/books/OL3488374M/Creep_of_plain_and_structural_concrete.
2. *Report on Factors Affecting Shrinkage and Creep of Hardened Concrete*. Technical Documents 209, A.C.I.C. 209.1R-05.
3. Acker, P., Agullo, L., Auperin, M., Carol, I., J Carreira, D., M R Catarino, J., Chem, J.-C., A Chiorino, M., W Dougill, J., Huet, C., Kanstad, T., Kim, J.-K., Křístek, V., Republic, C., S Muller, H., Byung, G., Oh, H., Ožbolt, J., Reid, S., Wittmann, F. *RILEM TC 107-CSP: CREEP AND SHRINKAGE PREDICTION MODELS: PRINCIPLES OF THEIR FORMATION Recommendation Measurement of time-dependent strains of concrete. Materials and Structures*. 1998. 31. Pp. 507–512.
4. Sprince, A., Kozlovskis, T., Gailītis, R., Radiņa, L., Pakrašiņš, L. *Paņēmiens betonu un cementa kompozītu ilglaicīgo īpašību noteikšanai dažādos sprieguma stāvokļos*. LV15659A. 2022.
5. Grundmann, G., Scholz, H. *The preparation of thin sections, polished sections, acetate foil prints, preparation for elutriation analysis, and staining tests for the optical and electron microscopy*. Chair of Engineering Geology Technische Universität München. 2015. (May). pp. 1–26.
6. Cadwell E. Donald and Wiblen W. Paul. *Diamond disc preparation of polished thin sections for electron microprobe analysis*. *Economic Geology*. 1965. 60. pp. 1520–1525.
7. Valcke, S.L.A., Polder, R.B., Van, H., Henegouwen. *GEOPOLYMER MICROSTRUCTURE USING POLARIZATION AND FLUORESCENCE*

MICROSCOPY. 2012.

8. Adobe Photoshop. [tiešsaiste]. [skatīts 01.02.2023.]. Pieejams:
https://www.adobe.com/lv/products/photoshop/landpb.html?mv=search&s_kwcid=AL!3085!3!601249993831!e!!g!!adobe photoshop!11126299323!109350550059&mv=search&sdid=LZ32SYVR&ef_id=CjwKCAiAuOieBhAIEiwAgjCvcrzPpihbA7oIfdbjWon8t8EpTjchPo-mm_r4RatA1OQrLWdmc0jovBoC5wgQAvD_BwE:G:s&s_kwcid=AL!3085!3!601249993831!e!!g!!adobe photoshop!11126299323!109350550059 (date of application: 1.02.2023).
9. Mecatech 334 - Presi. [tiešsaiste]. [skatīts 26.02.2023.]. Pieejams :
<https://www.presi.com/en/product/mecatech-334/>

PRETENZIJAS

1. Paņēmiens betonu un cementa kompozītu ārējo iedarbju ietekmes noteikšanai uz mikrostruktūru dažādos sprieguma stāvokļos, kas ietver šādus secīgus soļus:

- (i) iegūt paraugu daļas vai konstrukciju elementa urbto kodolu parauga sagatavošanai;
- (ii) impregnēt, cietināt un uzglabāt paraugus epoksīda vai līdzvērtīgos sveķos līdz soļa (iii) uzsākšanai;
- (iii) tālāk uzglabātos paraugus piezāģēt 1,0 līdz 2,0 cm (ieteicams 1,0–1,5 cm) biezus paraugus un marķēt, tad pēc zāģēšanas paraugus ievietot žāvskapī un žāvēt 40 °C temperatūrā 24 stundas;
- (iv) paraugus slīpēt un pulēt, pēc katra slīpēšanas un pulēšanas cikla paraugu virsmas skalot un pēc slīpēšanas un pulēšanas cikliem paraugus žāvēt (40 °C temperatūrā 24 stundas) un uzglabāt gaisa necaurlaidīgā iepakojumā ar silikagēlu vai līdzvērtīgu mitrumu uzsūcošu vielu iekšā ķīmiskā un mehāniskā stāvokļa fiksēšanai līdz solim (v) – mikrostruktūras pētīšanai;
- (v) konturēt pētāmās zonas parauga šķērsgriezumā un pētīt paraugu mikrostruktūru, izmantojot elektronu mikroskopu vai optisko mikroskopu ar attēlu uzņemšanas funkciju;
- (vi) veikt attēlu kvantitatīvo analīzi, uzskaitot un analizējot attēlā vai attēlos redzamā parauga virsmas kompozīcija un saturs.

2. Paņēmiens saskaņā ar 1. pretenziju, kas raksturīgs ar to, ka betona un cementa kompozītu mikrostruktūras pētniecībai no konkrētā parauga iegūta soli (i) izgatavo vismaz 3 pulētās virsmas paraugus, kas atrodas viens virs otra pētītā šķērsgriezuma garenasī.

3. Paņēmiens saskaņā ar 1. vai 2. pretenziju, kas raksturīgs ar to, ka solī (iv) pirms pētīt betona un cementa kompozītu mikrostruktūru, paraugu virsmas pārklāj ar konduktīvu pārklājumu.

4. Paņēmiens saskaņā ar jebkuru no 1. līdz 3. pretenzijai, kas raksturīgs ar to, ka solī (v) pētīt betona un cementa kompozītu mikrostruktūru, paraugu attēlus skenējošā elektronu mikroskopā uzņem noteiktā sekvencē, kur iepriekš uzņemtais attēls daļēji pārklājas ar iepriekš uzņemto.

KOPSAVILKUMS

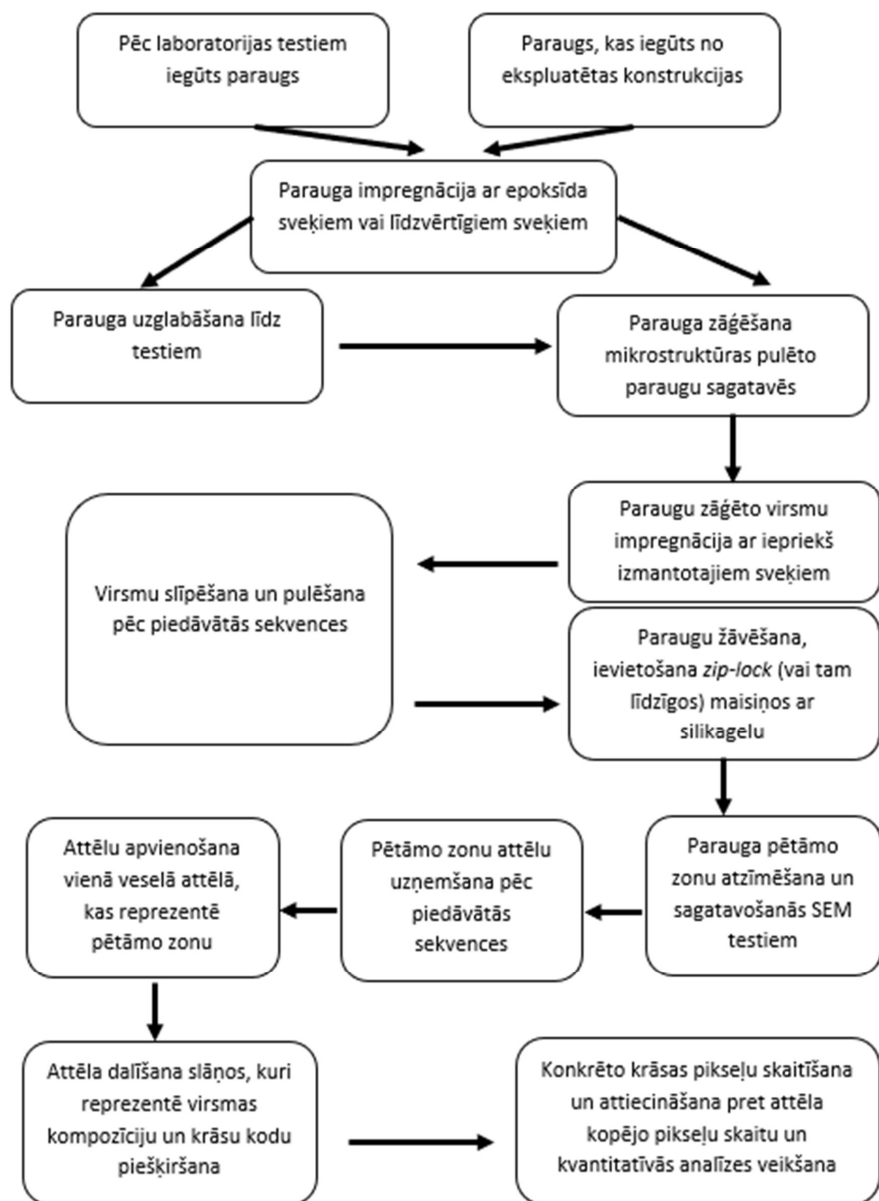
Izgudrojums attiecas uz būvniecību un būvniecības materiālu testēšanas paņēmieniem, proti uz paņēmieniem ārējo iedarbju ietekmes noteikšanai uz betonu un cementa kompozītmateriālu mikrostruktūru dažādos sprieguma stāvokļos.

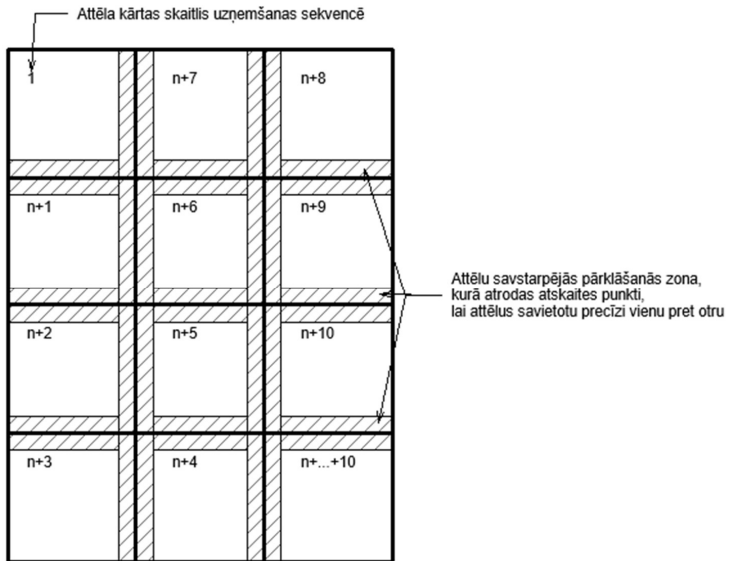
Saskaņā ar zināmiem risinājumiem veicot ēku un inženierbūvju projektēšanu prognozē un novērtē konstrukciju un to daļu darbību visā būves ekspluatācijas un dzīves cikla laikā. To veic novērtējot ilglaicīgo īpašību ietekmi. Tomēr ēku un inženierbūvju ekspluatācija mēdz atšķirties no projektēšanā paredzētajiem, kā rezultātā ilgstošā ekspluatācijas periodā konstrukciju pretestība pret ārējām iedarbēm (gan no mehāniskas slodzes, gan apkārtējās vides apstākļiem) var tikt samazināta. Ar izgudrojuma paņēmieni nosaka konstrukciju un to elementu mikrostruktūru un tās stāvokli. Laboratoriski pārbaudītiem paraugiem ar izgudrojuma paņēmieni nosaka īslaicīgas un ilglaicīgas slodzes ietekmi uz mikrostruktūru un attiecina uz cēloņsakarībām mehānisko īpašību izpausmēm konkrētajā situācijā. Īstenojot izgudrojuma paņēmieni mikrostruktūras analīzei izmanto pulētās virsmas paraugus un tos pēta skenējošajā elektronu mikroskopā (SEM). Paņēmienā norādīts kā sagatavot pulētās virsmas paraugus, kā veikt attēlu uzņemšanu.

TECHNIQUE FOR OUTSIDE EFFECT DETERMINATION ON CONCRETE AND CEMENT COMPOSITE MICROSTRUCTURE IN VARIOUS STRESS-STRAIN STATES

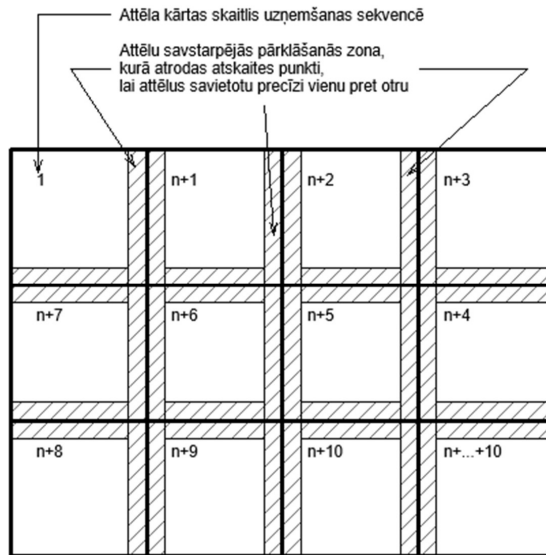
The invention applies to civil engineering and building materials testing techniques. In other words on micro structure disturbance and deuteration assessment of concrete and cement composites that have been subjected to outside effects such as load and environmental impacts.

According to known solutions structures behavior throughout service life is determined in design stage. It is done taking into account the long-term property impact to the structures. Nevertheless, the service life often differs from the anticipated in design stage. Due to this the resistance to the outside effects can be significantly reduced. With the invention technique microstructure and condition of the structure is determined. Also, microstructure change of the short term and long term loaded laboratory specimens is determined with this technique. Polished sections specimens are used to fulfill this technique and they are observed and images acquired in Scanning electron microscope (SEM). In this technique steps for the preparation of the polished section specimens are shown as well as steps for the image acquisition.

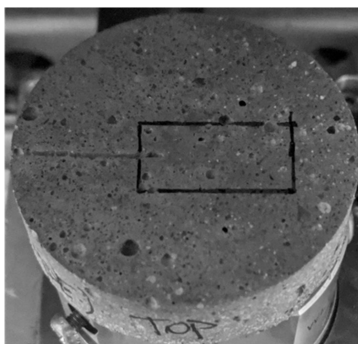




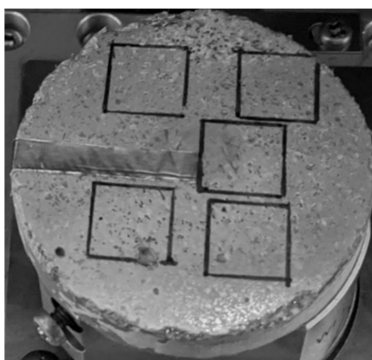
2a. zīm.



2b. zīm.



3a. zīm.



3b. zīm.



Rihards Gailītis was born in 1992 in Riga. He received a Bachelor's degree in 2017 and a Master's degree in 2018 from Riga Technical University (RTU). He is currently an engineer at Husvik Ltd. Since 2019, he has been a researcher at the Institute of Structural Engineering of RTU. He has carried out research in various scientific projects funded by the Latvian Council of Science and the European Regional Development Fund.